Inaugural dissertation

for

obtaining the doctoral degree

of the

Combined Faculty of Mathematics, Engineering and Natural Sciences

of the

Ruprecht - Karls - University

Heidelberg

Presented by

M.Sc. Alexandra Rita Turi da Fonte Dias

born in Cascais, Portugal

Oral examination: 29th of September 2025

The role of E3 ubiquitin ligase complexes in mitotic cell fate decision mechanisms

Referees: Prof. Dr. Ingrid Hoffmann

Prof. Dr. Sylvia Erhardt

Table of contents

Table of contents **5**

Summary **1**

Zusammenfassung **2**

1. Introduction **4**

1.1 The discovery of the ubiquitin system *4*

1.2 The ubiquitylation cascade *5*

1.3 The ubiquitin code *6*

1.4 Non-canonical ubiquitylation *7*

1.5 E3 ligases *8*

1.6 Deubiquitylating enzymes *9*

1.7 Mitotic cell cycle and the Ub-system *10*

1.8 Apoptosis and evasion mechanisms *11*

1.9 Mitotic slippage *12*

1.10 The MYCBP2-FBXO45 E3 ligase complex *15*
1.10.1 MYC-binding protein 2 15
1.10.2 F-Box protein 45 16
1.10.3 MYCBP2-FBXO45 and disease 18

1.11 SPRY-domain containing protein 3 ..... *19*

1.12 X-linked inhibitor of apoptosis protein *19*

1.13 Chromosome alignment-maintaining phosphoprotein 1 ..... *20*

1.14 Ubiquitin specific peptidase 11 ..... *21*

1.15 Ribonucleic acid export 1 ..... *22*

1.16 Objectives *23*

2. Materials and Methods **25**

2.1 Materials *25*
2.1.1 Chemicals and reagents 25
2.1.2 Laboratory equipment 28
2.1.3 Buffers 29
2.1.4 Antibodies 34
2.1.4.1 Primary antibodies 34
2.1.4.2 Secondary antibodies 35
2.1.5 Small interfering RNAs (siRNAs) 35
2.1.6 Primers 36
2.1.7 Plasmids 37
2.1.8 Bacterial strains 40
2.1.9 Cell lines 40
2.1.10 Kits 41
2.1.11 Antibiotics 41

2.2 Methods *41*
2.2.1 Methods in molecular biology 41
2.2.1.1 Polymerase chain reaction (PCR) and site-directed mutagenesis 41
2.2.1.2 Agarose gel electrophoresis 43

2.2.1.3 Extraction of DNA fragments from agarose gels 44
2.2.1.4 Restriction digest of DNA 44
2.2.1.5 Ligation of DNA fragments 44
2.2.1.6 Transformation of chemically competent *E. coli* 44
2.2.1.7 Plasmid DNA preparation from *E. coli* 45
2.2.1.8 Measurement of DNA concentration 45
2.2.2 Methods in cell biology 46
2.2.2.1 Cell culture 46
2.2.2.2 Freezing and harvesting of cells 46
2.2.2.3 Transfection of mammalian cells 47
2.2.2.3.1 Plasmid DNA transfection using polyethylenimine (PEI) 47
2.2.2.3.2 Plasmid DNA and siRNA transfection using Lipofectamine 2000 or RNAiMAX 47
2.2.2.4 Generation of stable U2OS cell lines with inducible MYC-SPRYD3 expression 49
2.2.2.5 Treatment of cells with MG132 and cycloheximide 49
2.2.2.6 Live cell imaging 49
2.2.2.7 Immunofluorescence staining and microscopy 50
2.2.3 Methods in protein biochemistry 51
2.2.3.1 Preparation of protein extracts from cells 51
2.2.3.2 Determination of protein concentration by Bradford assay 51
2.2.3.3 SDS polyacrylamide gel electrophoresis (SDS-PAGE) 52
2.2.3.4 Western blot 52
2.2.3.5 Immunoprecipitation assays 53
2.2.3.5.1 Immunoprecipitation of Flag-tagged proteins using Flag M2 affinity beads with or without λ-phosphatase treatment 53
2.2.3.5.2 Consecutive immunoprecipitation of Flag- and MYC-tagged proteins using Flag M2 affinity beads and MYC-antibody 54
2.2.3.5.3 Immunoprecipitation of GFP-tagged proteins using GFP-trap affinity beads 54
2.2.3.6 *In vivo* ubiquitylation assays 55
2.2.3.7 *In vitro* ubiquitylation assay 56
2.2.3.8 Bacterial expression and purification of recombinant GST-, MBP- and His-tagged proteins 57
2.2.3.9 MBP pull-down assay 58
2.2.3.10 Mass spectrometrical analysis 59
2.2.4 Statistical analysis 61

3. Results 62

3.1 Characterization of SPRYD3 as new specificity factor of the MYCBP2 E3 ligase 62
3.1.1 SPRYD3 promotes mitotic slippage in paclitaxel and nocodazole treated cells 64
3.1.2 SPRYD3 forms a complex with MYCBP2 *in vivo* and *in vitro* 66
3.1.2.1 MYCBP2 and SPRYD3 interact in HEK 293TWT cells 67
3.1.2.2 SPRYD3 binds MYCBP2 independently from FBXO45 68
3.1.2.3 FBXO45 and SPRYD3 bind to different sites of MYCBP2 70
3.1.2.4 SPRYD3 and FBXO45 simultaneously bind to MYCBP2 and MYCBP2 and SPRYD3 interact *in vitro* 71
3.1.3 MYCBP2-SPRYD3 complexes form without SKP1 72
3.1.4 The MYCBP2-SPRYD3 complex 75
3.1.5 Identification of putative SPRYD3-MYCBP2 interaction partners and substrates 75

3.2 Validation of CHAMP1 as a potential SPRYD3 interaction partner 77
3.2.1 CHAMP1 and SPRYD3 interact both in asynchronous and mitotic cells 78
3.2.2 MYCBP2-SPRYD3 deubiquitylates CHAMP1 80

3.3 Validation of XIAP as SPRYD3 interaction partner 81
3.3.1 XIAP interacts with SPRYD3 82
3.3.2 The BIR2-BIR3 of XIAP and the SPRY2-domain of SPRYD3 mediate their interaction 83
3.3.3 MYCBP2-SPRYD3 deubiquitylates XIAP 85

3.4 Characterization of USP11 as a potential substrate of the MYCBP2-SPRYD3 complex 87
3.4.1 USP11 interacts with MYCBP2 and SPRYD3 88
3.4.2 USP11 promotes mitotic slippage in paclitaxel and nocodazole treated cells 88

3.4.3 USP11 interacts with the MYCBP2 RCC1-like and MYC-binding domain 90
3.4.4 USP11 interacts with SPRYD3 *in vitro* 91
3.4.5 USP11 is ubiquitylated by the MYCBP2-SPRYD3 E3 ligase complex 92
3.4.5.1 SPRYD3-MYCBP2 E3 ligase ubiquitylates USP11 92
3.4.5.2 The MYCBP2-SPRYD3 complex ubiquitylates USP11 *in vivo* and *in vitro* 94
3.4.6 MYCBP2-SPRYD3 attaches K63-linked ubiquitin chains to USP11 97
3.4.7 MYCBP2-SPRYD3 mediated ubiquitylation of USP11 is not linked to proteasomal degradation 98
3.4.8 MYCBP2-SPRYD3 targets non-canonical USP11 residues for ubiquitylation 100
3.4.9 MYCBP2-SPRYD3-mediated ubiquitylation of USP11 is essential for bipolar spindle formation 103
3.4.10 MYCBP2-SPRYD3 and USP11 promote mitotic slippage through bipolar spindle formation 109
3.4.11 MYCBP2-SPRYD3-mediated ubiquitylation of $USP11^{C318}$ is required for USP11-RAE1 interaction .. 110
3.4.12 RAE1 promotes mitotic slippage 113

4. Discussion 115

4.1 SPRYD3 is a new MYCBP2-interacting protein 116

4.2 SPRYD3 promotes mitotic slippage after MT-poison treatment 118

4.3 CHAMP1 and XIAP are deubiquitylated upon ectopic SPRYD3 expression 119

4.4 USP11 is a substrate of the MYCBP2-SPRYD3 E3 ligase 121

4.5 MYCBP2-SPRYD3 targets $USP11^{C318}$ for proteasome-independent ubiquitylation 122

4.6 MYCBP2-SPRYD3, USP11 and RAE1 act in the same pathway to regulate bipolar spindle formation 124

4.7 Bipolar spindle formation regulated by the MYCBP2-SPRYD3/USP11/RAE1 axis promotes mitotic slippage in presence of MT-poisons 125

5. Working model 127

6. Future perspectives 129

7. References 130

8. Appendix 148

8.1 Abbreviations 148

8.2 Figures 152

8.3 List of Tables 153

9. Acknowledgements 155

Summary

Ubiquitylation, a conserved post-translational modification, is orchestrated through the interplay of three enzymes referred to as E1, E2 and E3, which activate, relay and ligate the ubiquitin moiety onto a final target protein, respectively. E3 ligases confer specificity to the whole cascade by mediating the last step of substrate ubiquitylation. The implication of E3 ligases in cancer is well-described. MYCBP2 (PAM) forms together with its substrate specificity factor FBXO45 an E3 ligase complex that promotes mitotic slippage. Mitotic slippage enables cancer cells to re-enter interphase after prolonged mitotic arrest caused by microtubule poisons without undergoing cell division, consequently harboring the potential to acquire drug resistance. It is therefore of utmost importance to understand the mechanisms underlying mitotic slippage.

E3 ligase mediated ubiquitylation is antagonized by deubiquitylating enzymes (DUBs) which in turn remove ubiquitin chain moieties from ubiquitylated substrates. Despite their opposing activities, complex formation between DUBs and E3 ligases may occur. Such DUB-E3 complexes can protect E3 ligases from autoubiquitylation, but on the other hand ubiquitylation of DUBs may also enable them to recruit substrates for deubiquitylation.

In the presented thesis, I characterized SPRYD3 as new substrate specificity factor of the MYCBP2 E3 ligase. I show that both SPRYD3 and MYCBP2 promote mitotic slippage in U2OS and RPE1 cells after treatment with nocodazole or paclitaxel, two microtubule poisons. Additionally, I demonstrate that SPRYD3 directly binds to MYCBP2 independently from FBXO45 *in vivo* and *in vitro*, pointing to the existence of a new E3 ligase complex. I identify the deubiquitinase (DUB) USP11 as a binding partner and first ubiquitylation substrate of the MYCBP2-SPRYD3 E3 ligase. MYCBP2-SPRYD3-mediated ubiquitylation of USP11 is linked to proper bipolar spindle formation during mitosis. Interfering with MYCBP2-SPRYD3-mediated ubiquitylation of USP11 increases the number of multipolar spindles, a phenotype that can contribute to mitotic cell death in presence of spindle poisons. Together, this study points to a new mechanism of mitotic cell fate regulation potentially mediated through a DUB/E3 ligase complex consisting of the new E3 ligase complex MYCBP2-SPRYD3 and the DUB USP11.

Zusammenfassung

Die Ubiquitylierung stellt eine konservierte posttranslationale Modifikation dar und wird durch das Zusammenspiel dreier Enzyme ausgeführt, die als E1, E2 und E3 bezeichnet werden. Diese aktivieren das Ubiquitin und binden es an das endgültige Zielprotein. Die E3-Ubiquitin-Ligasen verleihen der gesamten Kaskade Spezifität, indem sie im letzten Schritt die Ubiquitylierung des Substrats katalysieren. E3-Ligasen spielen eine bedeutende Rolle bei Krebserkrankungen. Die E3-Ligase MYCBP2 (PAM) bildet zusammen mit ihrem Substratspezifitätsfaktor FBXO45 einen E3-Ligase-Komplex, der „mitotic slippage“ fördert. „Mitotic slippage“ ermöglicht es Krebszellen, nach einer längeren Blockade während der Mitose, die durch die Behandlung mit Spindelgiften verursacht wird, der Zellteilung zu entkommen und wieder in die Interphase einzutreten. Dieser Prozess kann dazu führen, Resistenzen gegen Spindelgifte zu entwickeln. Es ist daher von größter Bedeutung, die Mechanismen zu entschlüsseln, die dem Prozess von „mitotic slippage“ zugrunde liegen. Die Gegenspieler der durch E3-Ligasen vermittelten Ubiquitylierung sind die deubiquitylierenden Enzyme (DUBs), die ihrerseits Ubiquitin von ubiquitylierten Substraten entfernen. Trotz ihrer gegensätzlichen Aktivitäten ist es nicht ungewöhnlich, dass DUBs und E3-Ligasen Komplexe bilden. Solche DUB-E3-Komplexe können die Autoubiquitylierung von E3-Ligasen verhindern. Andererseits kann die Ubiquitylierung von DUBs durch E3 Ligasen es auch ermöglichen, Substrate für die Deubiquitylierung zu rekrutieren.

In der vorliegenden Arbeit habe ich SPRYD3 als neuen Substratspezifitätsfaktor der MYCBP2 E3-Ligase charakterisiert. Ich zeige, dass sowohl SPRYD3 als auch MYCBP2 „mitotic slippage“ in U2OS- und RPE1-Zellen nach einer Behandlung mit den Spindelgiften Nocodazol oder Paclitaxel fördern. Außerdem zeige ich, dass SPRYD3 unabhängig von FBXO45 direkt an MYCBP2 bindet, was auf die Existenz eines neuen E3-Ligase-Komplexes hindeutet. Ich identifiziere die DUB USP11 als Bindungspartner und erstes bekanntes Substrat der MYCBP2-SPRYD3-E3-Ligase. Die von MYCBP2-SPRYD3 vermittelte Ubiquitylierung von USP11 spielt eine Rolle bei der Ausbildung der bipolaren Spindel während der Mitose. Wenn USP11 nicht durch MYCBP2-SPRYD3 ubiquityliert werden kann, führt dies zu einer Erhöhung der Anzahl der Zellen mit multipolaren Spindeln und somit zum mitotischen Zelltod in Anwesenheit von Spindelgiften. Meine Arbeit beschreibt einen neuen Mechanismus der Regulierung des mitotischen Zellschicksals, der durch einen DUB/E3-Ligase-Komplex bestehend aus

dem neuen E3-Ligase-Komplex MYCBP2-SPRYD3 und der DUB USP11, vermittelt wird.

1. Introduction

1.1 The discovery of the ubiquitin system

In 1942, Schoenheimer proved that cellular protein levels are not static, but undergo turnover due to degradation (Schoenheimer and Clarke, 1942), while the mechanism in question remained elusive. In 1978, Ciechanover, Hershko and colleagues provided the answer by identifying a heat stable polypeptide involved in a process they referred to as lysosome-independent adenosine-triphosphate (ATP)-dependent proteolytic system (Ciehanover et al., 1978). They named this polypeptide ATP-dependent proteolysis factor 1 (APF1) and proposed that APF1 is covalently ligated to exogenous and endogenous protein substrates designating them for protein degradation (Ciechanover et al., 1980; Hershko et al., 1980). It soon became clear that APF1 was in fact Ubiquitin (Ub) (Wilkinson et al., 1980), a 76 amino acid (aa) long protein that had previously been identified as a covalent interactor of histones H2A and H2B (Goldknopf and Busch, 1977). Further investigations revealed that APF1/Ub-mediated degradation of proteins was not only taking place in reticulocytes, where the mechanism had first been identified, but that this process also occurs in nucleated cells (Hershko et al., 1982). In 2004, Aaron Ciechanover, Avram Hershko and Irvin Rose won the 2004 Nobel Prize in Chemistry for their groundbraking research and discovery of protein ubiquitylation.

The mechanism of how protein substrates are conjugated with Ub and consequently degraded was soon unraveled , when all the components of the ubiquitylation cascade were identified: (i) E1, the Ub-activating enzyme which depends on ATP; (ii) E2, the Ub-carrier protein also known as Ub-conjugating enzyme; (iii) E3, the ligase that mediates direct or indirect covalent attachment of Ub to the respective protein substrate (Hershko et al., 1983); and (iv), the 26S proteasome, the protease complex responsible for degradation of ubiquitylated proteins (Hough et al., 1986; Waxman et al., 1987).

For a long time, ubiquitylation was thought to solely regulate proteasomal protein degradation, but growing evidence reveals that covalent fusion of Ub to protein substrates can also have non-proteolytic functions. Ub is a highly conserved protein present across species (Goldstein et al., 1975; Schlesinger et al., 1975; Sharp and Li, 1987) and acts as a post-translational modification implicated in the regulation of a large quantity of cellular processes, such as DNA repair, cell cycle control,

programmed cell death and cellular differentiation. Considering the essential involvement of ubiquitylation in the regulation of almost all cellular processes, it only seems logical that aberrations in the Ub-system can give rise to pathologies such as cancer.

1.2 The ubiquitylation cascade

Post-translational modifications, such as ubiquitylation, acetylation or phosphorylation, are efficient ways to expand the plasticity, but also complexity of a proteome and are present throughout nature (Walsh et al., 2005). Ubiquitylation is orchestrated through the interplay of three distinct enzymes, which ensure that a target protein is covalently modified with Ub. The process consists of three steps that are essential for successful ubiquitylation. First, Ub is activated by attaching its C-terminal carboxy group to a catalytic cysteine residue of a so-called Ub-activating enzyme, referred to as E1. This step is ATP-dependent (Ciechanover et al., 1981). Next, the activated Ub-moiety is transferred through a trans-thiolation reaction onto the active site cysteine of the Ub-conjugating enzyme, E2 (Hershko et al., 1983). And lastly, the E2 enzyme carrying the activated Ub-moiety cooperates with E3 ligases in order to facilitate the transfer of Ub to a substrate (Pickart, 2001). The canonical bond between Ub and substrate is formed by interaction of the C-terminal carboxy group of Ub and the ε-amino group of a lysine (Lys) residue in the target protein, giving rise to an isopeptide bond (Pickart, 2001). E3 ligases confer specificity to the whole ubiquitylation cascade by ensuring correct substrate modification (Figure 1).

The complexity of ubiquitylation was further expanded with the discovery of the ubiquitylation machinery being able to form poly-Ub chains. Substrate-bound Ub can be ubiquitylated itself by linking its internal lysines or N-terminus to another Ub-moiety (Hershko, 1985; Hough et al., 1986), giving rise to polymeric chains that can encode different protein fate outcomes. Interestingly, reports from the past 40 years indicate, that E3 ligases can also mediate non-canonical ubiquitylation on cysteine (Cys), serine (Ser) and threonine (Thr) residues of protein substrates (Kelsall et al., 2019; Pao et al., 2018; Vosper et al., 2009; Williams et al., 2007).

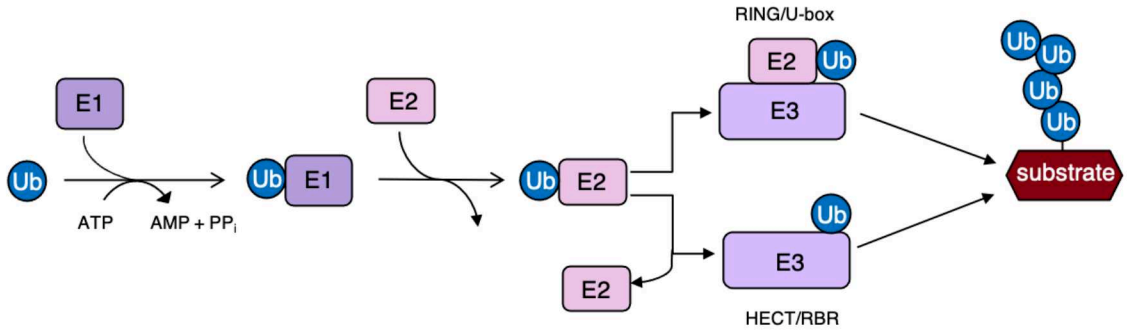


Figure 1: Schematic overview of the ubiquitylation cascade.

1.3 The ubiquitin code

Ub, once attached to a substrate, can be further post-translationally modified. On top of acetylation or phosphorylation, substrate-attached Ub can also be ubiquitylated by linking a donor Ub to one of the seven internal Ub lysine residues (K6, K11, K27, K33, K48 and K63) or its N-terminus (Met1). This gives rise to poly-Ub chains that encode a myriad of different signals with distinct cellular consequences, referred to as the Ub-code. Ubiquitylation on substrates can occur as monoubiquitylation, if only one substrate side chain is modified with Ub. Targeting of multiple substrate side chains with one Ub-moiety is called multi-monoubiquitylation. Polymeric chains arise, when a substrate-attached Ub is further modified with Ub on its N-terminus or one of the seven internal lysine residues.

Chains can vary in length and be characterized according to how the Ub-moieties are linked to each other in order to form polymeric chains (Komander and Rape, 2012). Homogenous chains consist of multiple Ubs linked to each other via the same lysine residue, whereas heterogenous chains contain Ubs linked to each other using distinct lysine residues. Ub within already established polymeric chains can be linked to an additional Ub using a different side chain, giving rise to polymeric branched chains. Chain topologies encode different protein fate outcomes. For example, K48-linked Ub-chains are the most abundant linkage type within cells and were first identified to regulate proteasomal degradation of proteins (Peng et al., 2003; Xu et al., 2009). Nonetheless, ubiquitylation can have non-proteolytic functions as well. K63-linked Ub-chains for example, are involved in immune signaling and DNA-damage repair and can take over scaffolding roles for recruitment of protein complexes to certain locations (Doil et al., 2009; Sobhian et al., 2007; Wu et al., 2016). Ubiquitylation can also

promote or inhibit protein interactions (Dupont et al., 2009; Hoege et al., 2002) and affect protein activity or localization (Komander and Rape, 2012).

1.4 Non-canonical ubiquitylation

Lysine ubiquitylation is widely accepted as canonical ubiquitylation. N-terminal substrate ubiquitylation catalyzed by for example the E2 enzyme UBE2W was long considered to be one of the few exceptions (Tatham et al., 2013). However, a growing body of evidence suggests that internal substrate cysteines, serines and threonines are also modified with Ub, leading to the formation of thioester- or oxyester-bonds, respectively. Even though thioester- or oxyester-bonds between Ub and cysteines, serines or threonines were long neglected, because considered too labile to occur and be stabilized in nature, accumulating evidence has disproved this claim (Kelsall, 2022). When considering that E1, E2 ,and to some extent E3 ligases, use internal cysteines to form a transient thioester-linkage with Ub, it doesn't seem too far-fetched that internal substrate cysteines could be ubiquitylated as well (Kelsall, 2022). Also, studies suggest that thioester- or oxyester-linkages are less labile than previously suggested and that buffer conditions used to determine canonical ubiquitylation are not suited to detect non-canonical ubiquitylation sites (Song et al., 2009; Vosper et al., 2009).

Non-canonical ubiquitylation occurs for example on peroxisomal biogenesis factor 5 (PEX5), where ubiquitylation of a conserved cysteine mediates peroxisomal protein import regulation (Carvalho et al., 2007; Okumoto et al., 2011). The E3 ligase HOIL-1 is another example for non-canonical ubiquitylation. HOIL-1 was shown to not only ubiquitylate itself, but to also modify components of the Myddosome, a complex involved in immune signaling, by targeting serines and threonines for ubiquitylation (Kelsall et al., 2019). Another study pointed out the ability of the bacterial effector protein SdeA from *Legionella pneumophila* to ubiquitylate Golgi tethering proteins on serine residues to induce Golgi disruption and inhibition of the secretory pathway (Liu et al., 2021). And lastly, the MYC-binding protein 2 (MYCBP2) E3 ligase complex ubiquitylates itself *in vivo* and its substrate NMNAT2 *in vitro* via esterification (Pao et al., 2018).

For a long time, proteins were considered as only possible ubiquitylation targets, but recent research was able to prove otherwise: ubiquitylation of non-proteinaceous substrates such as ADP-ribose, bacterial lipopolysaccharides (LPS) and cellular sugars were shown to occur *in vivo* as well, further expanding the scope of Ubiquitin-

mediated regulation (Kelsall et al., 2022; Otten et al., 2021; Perrin et al., 2004; Yang et al., 2017).

1.5 E3 ligases

E3 ligases confer specificity to the ubiquitylation cascade by mediating the direct or indirect transfer of Ub from the E2 enzyme onto the final target. The importance of E3 ligases is reflected in the fact that the human genome contains two genes for E1 enzymes, approximately 30 for different E2 conjugating enzymes, but over 600 genes for E3 ligases. The different conserved domains responsible for catalyzing ubiquitylation allow the division of E3 ligases into different families: Really interesting new gene (RING) or U-box containing E3 ligases, E6-associated protein (E6AP) carboxyl terminus (HECT) E3 ligases and RING-between-RING (RBR) E3 ligases. Recently, the new class of RING-Cys-Relay (RCR) E3 ligases has been identified, with MYCBP2 being its first and so far, only member (Mabbitt et al., 2020; Pao et al., 2018). E3 ligases can mediate direct or indirect transfer of Ub onto the substrate. RING E3 ligases act as scaffolds to bring the E2-conjugated Ub into close proximity of the target to mediate a direct transfer (Deshaies and Joazeiro, 2009). HECT and RBR E3 ligases form a thioester-linked intermediate with Ub by accepting the Ub-moiety from the E2 enzyme through an active-site cysteine, transferring the Ub-moiety onto the target themselves (Lorenz, 2018; Wenzel et al., 2011). Lastly, the RCR E3 ligase MYCBP2 contains two active-site cysteines that undergo transient thioester-linkage formation with Ub through an intramolecular relay mechanism before mediating the transfer onto the final target (Mabbitt et al., 2020; Pao et al., 2018).

E3 ligases can exist as monomers, but can also be composed of multiple subunits that take over different functions within the multi-subunit complex. SKP1-Cullin1-F-Box (SCF) type E3 ligases, a sub-family of RING E3 ligases, are an example for such multimeric E3 ligase complexes. They consist of (i) Cullin 1 (Cul1), the backbone and scaffolding protein that mediates the interaction with other components of the E3 ligase; (ii) a variable F-Box protein (FBP), which is essential for substrate interaction and recruitment to the E3 ligase; (iii) S-phase-kinase-associated protein-1 (SKP1), a linker that anchors the FBP to Cul1; and (iv) RING box protein 1 (RBX1), the subunit with E3 ligase activity (Cardozo and Pagano, 2004). The SCF^{FBXW7} is an example for such an SCF-E3 ligase complex, where F-box/WD repeat-containing protein 7 (FBXW7) is the FBP or substrate specificity factor that recruits substrates for

ubiquitylation. Another important example for a multi-subunit RING E3 ligase is the anaphase-promoting complex / cyclosome (APC/C) that consists of at least 12 different core subunits (Peters, 2006).

Since E3 ligases regulate a wide range of protein substrates, including tumor promotors and suppressors, their deregulation can lead to oncogenic transformation and cancer progression (Wang et al., 2017). Genes coding for E3 ligases are often mutated, deleted or amplified in cancer contexts, consequently resulting in a defective, absent or overexpressed protein product. One of many examples is the E3 ligase MDM2 with elevated expression levels in various cancers such as colorectal or breast cancer. The MDM2 E3 ligase is responsible for negative regulation of p53 protein levels and upon higher MDM2 expression, enhanced degradation of p53 can contribute to cancer formation and progression (Wang et al., 2017).

1.6 Deubiquitylating enzymes

Ubiquitylation is a reversible process and E3 ligase activity is counteracted by deubiquitylases or deubiquitylating enzymes (DUBs), which are proteases that can recognize and remove substrate-bound Ub. By doing so, DUBs change and modulate protein fate outcome, contributing an additional regulatory layer to the whole ubiquitylation cascade (Dewson et al., 2023).

The human genome codes for approximately 100 DUBs (Dewson et al., 2023). Recognition of substrate-conjugated Ub via DUBs can occur in different ways. DUBs can be specialized towards a poly-Ub chain constructed with a specific linkage type, targeting all substrates conjugated with such a chain. An example for such a target-agnostic linkage-specific DUB is the OTU DUB Cezanne, which recognizes K11-linked poly-Ub chains (Dewson et al., 2023). On the other hand, DUBs can act in a Ub-signal agnostic manner by being specialized towards specific substrates, regardless of linkage attributes of the poly-Ub chain. This holds true for most DUBs belonging to the USP DUB family (Dewson et al., 2023).

As for E3 ligases, deregulation of DUB activity or localization can lead to cancer formation and progression, and indeed, a linkage between DUBs and each acknowledged hallmark of cancer has already been established (Hanahan and Weinberg, 2011; Kumari et al., 2017). Depending on the context, DUBs can act as tumor promotors or suppressors, an example being the thoroughly studied USP DUB Ubiquitin-specific protease 7 (USP7). USP7 can act as a tumor suppressor by

regulating the stability of p53 or PTEN, but can also take over the role of a tumor promotor through direct deubiquitylation of MDM2, the E3 ligase complex responsible for p53 degradation (Kumari et al., 2017). USP11 is another example for a context specific DUB. On the one hand, USP11 stabilizes p53 through deubiquitylation. On the other hand it is also involved in stabilization of HPV-16E7, a viral protein involved in cell transformation, and X-linked inhibitor of apoptosis (XIAP), a cellular inhibitor of apoptosis, contributing to tumorigenesis (Ke et al., 2014; Lin et al., 2008; Zhou et al., 2016).

1.7 Mitotic cell cycle and the Ub-system

The cell cycle is a tightly orchestrated process which, if correctly executed, ensures proper DNA replication, chromosome segregation and cell division. The eukaryotic cell cycle comprises four distinct phases, referred to as gap 1- (G1), DNA-synthesis (S), gap 2- (G2) and mitotic-phase (M), and contains three checkpoints for control of correct cell cycle progression. The G1-, S- and G2-phases together form interphase. Progression throughout the cell cycle is regulated by cyclin-dependent kinases (CDKs) and their respective cyclins and cyclin-dependent kinase inhibitors (CKIs). While CDK protein levels remain constant throughout the cell cycle, Cyclin protein levels oscillate and are stabilized only during certain phases, where they interact with their respective CDKs, thus activating them.

CDK1-Cyclin B1 kinase is the main cyclin-CDK complex controlling mitotic progression. Mitosis is divided into five phases. First, the nuclear envelope breaks down and chromatin condensates during prophase. During prometaphase the mitotic spindle forms and spindle microtubules (MTs) start to attach to chromosomal kinetochores. Chromosomes then congress towards the metaphase plate during metaphase, where kinetochore-MT attachment is corrected, if necessary. Only after all kinetochores have attached to respective MTs, the spindle assembly checkpoint (SAC) is inactivated and anaphase onset is promoted. Sister chromatids are pulled towards opposite poles, where two new nuclei can form during telophase. Cytokinesis completes the process by forming two new functional daughter cells that can undergo a new round of cell division at the end of the next interphase (McIntosh, 2016).

Cyclins and CKIs are tightly controlled by the Ub-proteasome system with two main multi-subunit E3 ligase complexes, namely the APC/C and SCF E3 ligase complex, promoting their ubiquitylation (Dang et al., 2021). The APC/C in complex with its co-

factor CDC20 is responsible for degradation of Cyclin B1 and securin during mitosis, thus promoting anaphase onset and mitotic exit. APC/C can recruit CDC20 only after its release from the mitotic checkpoint complex (MCC), consisting of MAD2, BUBR3, BUB1 and CDC20, which accumulates on kinetochores and keeps the SAC active (Musacchio and Salmon, 2007). Only after all spindle MTs have properly attached to respective kinetochores and chromosomes have been bi-oriented, the MCC is depleted from kinetochores and CDC20 can bind to APC/C, thus promoting anaphase onset (Musacchio and Salmon, 2007). Lack of or incorrect kinetochore-MT attachment, but also improper assembly of MT-spindles, leads to sustained SAC and mitotic arrest during prometaphase, and if the delay in mitotic exit is not resolved, the cell will eventually undergo apoptosis (Engeland, 2022; Musacchio and Salmon, 2007; Rieder et al., 1995). The SCF E3 ligase complex regulates cell cycle progression through its interaction with various F-Box proteins such as FBXW7, SKP2 and βTrCP, thus targeting a great variety of key substrates important for cell cycle regulation (Dang et al., 2021).

Any aberrations, such as nutrient deprivation, incorrect DNA-replication, DNA-damage, aberrant spindle-MTs or kinetochore-MT attachments or alteration in MT dynamics can trigger abolishment of cell cycle progression and apoptosis (Engeland, 2022; Musacchio and Salmon, 2007; Rieder et al., 1995).

1.8 Apoptosis and evasion mechanisms

The correct equilibrium between cell proliferation and death is essential to ensure proper cellular homeostasis. Diseases arise when organisms or tissues suffer from deregulated cell death or proliferation (Ergün et al., 2024; Newton et al., 2024). Apoptosis, also known as controlled cell death, is important for controlled elimination of old, dysfunctional, defective, infected or mutated cells that otherwise could give rise to diseases such as cancer or immunological, neurodegenerative and developmental disorders, if not properly removed (Newton et al., 2024). Cells undergoing apoptosis can be morphologically discerned from non-apoptotic cells through nuclear condensation, membrane blebbing and apoptotic body formation and are rapidly eliminated in a controlled manner (Kerr et al., 1972).

The ubiquitylation-system is an important regulator of apoptosis. For example, the E3 ligase Parkin influences apoptosis through direct ubiquitylation of pro-apoptotic BAK and anti-apoptotic MCL-1, therefore acting as an apoptotic suppressor or promotor,

respectively (Bernardini et al., 2019; Cakir et al., 2017; Carroll et al., 2014). MCL-1 is further targeted by the tumor suppressor SCF^{FBXW7} for ubiquitylation-dependent degradation, sensitizing cells towards intrinsic apoptotic stimuli (Inuzuka et al., 2011). This is counteracted by the DUB USP9X, which abolishes MCL-1 degradation through deubiquitylation, consequently inhibiting apoptosis and promoting cell survival (Schwickart et al., 2010). The E3 ligase complex MYCBP2-FBXO45 ubiquitylates the potent tumor suppressor and pro-apoptotic protein PAR-4, leading to its proteasomal degradation and consequent inhibition of apoptosis (Chen et al., 2014). Additionally, MYCBP2-FBXO45 targets FBXW7 for proteasomal degradation during prolonged mitotic arrest caused by MT-poisons, shifting the balance away from mitotic cell death towards mitotic slippage (Richter et al., 2020), an apoptotic evasion mechanism, that can lead to MT-poison resistance (Chan et al., 2012). The E3 ligase X-linked inhibitor of apoptosis protein (XIAP) does not only inhibit apoptosis through direct binding of caspases-3, -7 and -9 (Eckelman et al., 2006; Vucic, 2018), but also plays an important role in mitotic slippage, similar to MYCBP2-FBXO45 (Ergün et al., 2024; Hou et al., 2017; Richter et al., 2020).

Certain circumstances, like genomic instability or treatment with cytotoxic agents amongst others, can lead to the acquisition of evasion mechanisms, which help cells to evade and become resistant towards apoptosis (Chan et al., 2012; Hanahan and Weinberg, 2011, 2000). Often, ubiquitylation, deregulated or not, is involved in acquisition of evasion mechanisms (Balachandran et al., 2016; Brito and Rieder, 2006; Richter et al., 2020). Especially in diseases such as cancer, evasion of apoptosis is implicated in disease progression, survival and resistance (Chan et al., 2012; Hanahan and Weinberg, 2011, 2000), endangering the application of chemotherapeutic agents aiming at killing cancer cells through apoptosis. The elucidation of these evasion mechanisms is of great importance, in order to re-establish apoptosis in those cells, where resistance development has disrupted the apoptotic response.

Mitotic slippage is one of many examples for apoptotic evasion mechanisms, that contributes to resistance acquisition in cancer.

1.9 Mitotic slippage

The SAC is constitutively active in higher animals and its satisfaction is only reached when and if all kinetochores have attached correctly to their respective MTs (Rieder and Maiato, 2004). Thus, absence or incorrect kinetochore-MT attachment can delay

anaphase onset and mitotic exit due to unsatisfied SAC (Rieder and Maiato, 2004). This is referred to as mitotic arrest, and can be induced by extensive DNA damage, ionizing radiation or anti-mitotic agents, such as MT-poisons, also known as spindle poisons (Musacchio and Salmon, 2007; Rieder and Maiato, 2004).

Sustained mitotic arrest is an unnatural state that can evoke apoptosis to avoid aberrant mitosis (Jordan and Wilson, 2004). MT-poisons, such as taxanes and vinca alkaloids, are important therapeutic agents used extensively in chemotherapy due to their great efficacy in treatment of solid and hematological cancers through induction of apoptosis (Jordan and Wilson, 2004).

MT-poisons interfere with the high dynamicity of spindle-MTs (Jordan and Wilson, 2004). Consequently, correct kinetochore-MT attachments cannot be achieved, leading to non-satisfaction of the SAC and a robust and sustained mitotic arrest (Brito and Rieder, 2006; Musacchio and Salmon, 2007). Nonetheless, response to MT-poisons differs in between individual cancer cells and cell lines and mitotic arrest with consequent apoptosis can be evaded (Brito and Rieder, 2009; Gascoigne and Taylor, 2008). Despite of an active and robust SAC induced after MT-poison treatment, Cyclin B1 degradation can still occur (Brito and Rieder, 2006) and when reaching a certain threshold of Cyclin B1 protein levels, cancer cells might evade mitotic arrest without completing mitosis (Brito and Rieder, 2009; Gascoigne and Taylor, 2008). This is referred to as mitotic slippage and results in interphasic tetraploid cancer cells that can undergo different post-mitotic cell fates depending on their genomic content (Cheng and Crasta, 2017) (Figure 2). The phenomenon of continued gradual Cyclin B1 degradation and mitotic exit can be explained with the hypothesis that the SAC might not be 100% effective in preventing APC/C-mediated degradation of Cyclin B1 (Brito and Rieder, 2006). Another study performed by Balachandran et al., 2016 served an additional explanation by identifying the E3 Ligase $CRL2^{ZYG11}$ responsible for Cyclin B1 degradation during mitotic arrest (Balachandran et al., 2016).

To explain the intra- and interline variation in cancer cells leading to different responses to MT-poisons, Gascoigne and Taylor presented the “competing threshold model” of two independent pathways that determines, whether a cell tends to commit mitotic slippage or mitotic cell death (Gascoigne and Taylor, 2008). On the one hand, gradual degradation of Cyclin B1 needs to reach a certain threshold, below which the cell cannot maintain the mitotic state anymore, consequently committing mitotic slippage. On the other hand, mitotic arrest and the inability to satisfy the SAC leads to activation

of the apoptotic response and accumulation of apoptotic signals in order to avoid aberrant mitosis. Depending on which threshold is breached first, the cell either commits mitotic slippage or mitotic cell death (Gascoigne and Taylor, 2008). Since individual cancer cells or cancer cell lines differ in their proteomic makeup at any given time, different cell lines or individual cells tend to be more efficient in breaching a certain threshold first (Gascoigne and Taylor, 2008).

Another study revealed, that the competing networks of Cyclin B1 degradation and accumulation of death signals might not be that independent after all (Sakurikar et al., 2012). CDK1-Cyclin B1 was shown to control MCL-1 degradation and BCL-X_L phosphorylation status during prolonged mitotic arrest, leading to the abolishment of their anti-apoptotic functions, thus promoting mitotic cell death (Sakurikar et al., 2012).

Mitotic slippage generates tetraploid cells due to skipping of anaphase and consequent cytokinesis. According to the genomic make-up of these tetraploid cells, they either undergo post-slippage cell death, senescence or continued proliferation in case of p53 loss (Cheng and Crasta, 2017) (Figure 2). Genomic instability, as it is given in tetraploidy, is a hallmark of solid tumors and known to promote tumorigenesis, but also resistance acquisition against MT-poisons (Chan et al., 2012; Cheng and Crasta, 2017; Ganem et al., 2007; McGranahan et al., 2012). Thus, mitotic slippage endangers the application of MT-poisons as cancer therapeutic agents, because of its potential to promote MT-poison resistance. It is therefore of utmost importance to understand and elucidate the mechanisms leading up to mitotic slippage in order to re-establish the efficacy of MT-poisons and avoid the generation of more aggressive and resistant tumors.

Various studies have demonstrated the involvement of the ubiquitylation system in mitotic cell fate regulation after MT-poison treatment. For example, the E3 ligase and potent tumor promotor XIAP promotes mitotic slippage (Hou et al., 2017), whereas the SCF-E3 ligase component and tumor suppressor FBXW7 promotes mitotic cell death through WDR5 and MCL-1 degradation (Hänle-Kreidler et al., 2022; Wertz et al., 2011). This is counteracted by the RCR E3 ligase complex MYCBP2-FBXO45, which promotes mitotic slippage by Ub-mediated degradation of FBXW7 and PAR-4 after MT-poison treatment (Chen et al., 2014; Richter et al., 2020).

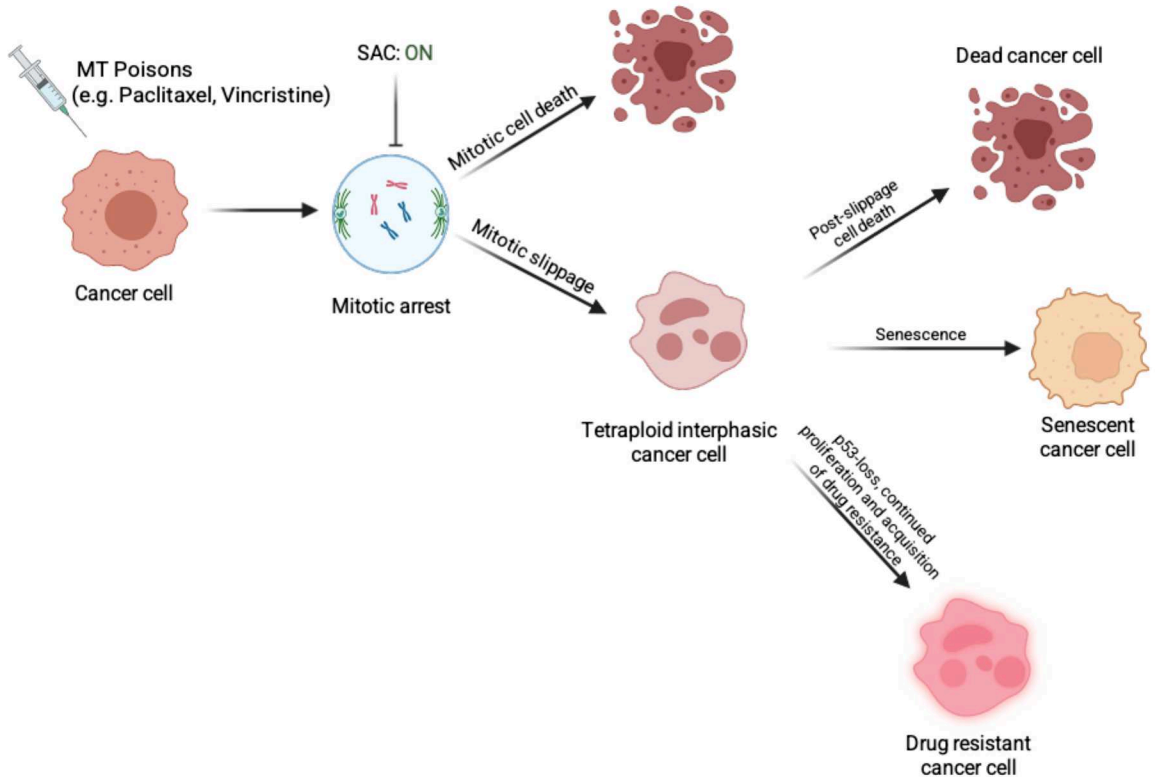


Figure 2: Schematic overview of mitotic cell fates after MT-poison treatment.
Adapted from Cheng and Crasta, 2017. Created with BioRender.

1.10 The MYCBP2-FBXO45 E3 ligase complex

1.10.1 MYC-binding protein 2

MYCBP2, also known as protein associated with MYC (PAM), was firstly identified as a MYC-binding protein and forms part of the conserved PHR protein family comprising human PAM/MYCBP2, mouse Phr1, *Drosophila melanogaster* highwire (HIW), *Caenorhabditis elegans* regulator of presynaptic morphology 1 (RPM-1) and zebrafish Esrom/Phr1 (Grill et al., 2016; Guo et al., 1998). PHR proteins are large proteins with a molecular weight of >400 kDa and conserved regulators of axon and synapse development as well as axon degeneration (Desbois et al., 2018; Grill et al., 2016). Due to the expression of a RING zinc-finger domain on their C-terminus, PHR proteins possess E3 ligase activity and partly mediate their downstream functions in a ubiquitylation-dependent manner. However, their capability of ubiquitylation-independent regulation and binding of several conserved non-target proteins (Baker et al., 2014; Grill et al., 2016, 2012), transforms PHR proteins into signaling hubs that regulate numerous downstream pathways in neuronal development in various ways (Grill et al., 2016).

Interestingly, several important links between PHR protein function and the MT cytoskeleton exist. Mouse Phr1 associates with MTs in neurons and promotes their stability and cytoskeletal polarization during neurite growth by mediating ubiquitylation-dependent degradation of the mitogen-activated protein kinase-kinase-kinase dual leucine zipper-bearing kinase (DLK) (Lewcock et al., 2007). Furthermore, PHR proteins were shown to bind with and function through the MT-binding protein mRNA export factor 1 (RAE1) in invertebrate cells (Tian et al., 2011).

The mammalian *MYCBP2* gene is located on chromosome 13q22.31 and is expressed in almost all tissues, with especially high abundance in the brain and thymus (Guo et al., 1998). MYCBP2 comprises a predicted molecular weight of 510 kDa and contains a RCC1-like domain, two PHR domains, a MYC-binding domain and a RING zinc finger domain on its C-terminus with E3 ligase activity (Figure 4A). The RCC1-like domain is significantly homologous to the protein regulator of chromosome condensation 1 (RCC1) (Guo et al., 1998). This domain mediates ubiquitylation-independent processes, like regulation of KCC2 ion channels and adenylyl cyclases, and also functions as a guanine exchange factor (GEF) for Ran, a protein important in nuclear transport, MT-assembly and nuclear envelope and pore complex formation (Dörr et al., 2015; Guo et al., 1998). The MYCBP2 MYC-binding domain was identified as the binding site of the transcription factor (TF) MYC (Guo et al., 1998).

1.10.2 F-Box protein 45

In mammals, MYCBP2 binds the highly conserved substrate specificity factor and FBP F-box protein 45 (FBXO45), forming an active E3 ligase complex (Desbois et al., 2018; Saiga et al., 2009). FBXO45 binds and recruits substrates to MYCBP2 for consequent ubiquitylation (Chen et al., 2014; Desbois et al., 2018; Lin et al., 2021; Richter et al., 2020; Saiga et al., 2009). FBXO45 is required for normal development of central and peripheral neurons and its physical association with MYCBP2 is evolutionary conserved (Saiga et al., 2009). On top of its function in neuronal development, FBXO45 is also involved in promoting proteolysis of molecules implicated in cell survival and DNA damage, such as FBXW7, PAR-4 and p73 (Chen et al., 2014; Richter et al., 2020).

The *FBXO45* gene resides on chromosome 3q29 and the expressed protein forms part of the SPRY/B30.2 protein family, which comprises proteins expressing SPRY-domains important for mediation of protein-protein interactions (D'Cruz et al., 2013). The eukaryotic genome encodes hundreds of FBPs, but so far, FBXO45 is the only

identified FBP expressing a SPRY-domain (Jin et al., 2004). N-terminally, FBXO45 expresses an F-box domain (Jin et al., 2004).

Interestingly, MYCBP2-FBXO45 forms an atypical E3 ligase complex in mammals, unlike its counterpart in *Caenorhabditis elegans*, where respective orthologs FSN-1 and RPM-1 form a canonical SCF complex containing CUL-1 and SKR-1, orthologs of mammalian Cul1 and SKP1 (Saiga et al., 2009). Due to the absence of Cul1, but the presence of SKP1, the E3 ligase MYCBP2-FBXO45 was long considered an atypical SCF E3 ligase complex (Desbois et al., 2018; Saiga et al., 2009). However, SKP1 does not serve as linker between FBXO45 and MYCBP2 as it is the case for canonical SCF E3 ligases (Figure 3A) (Desbois et al., 2018; Saiga et al., 2009). Instead, FBXO45 binds the MYCBP2 MYC-binding domain directly via its SPRY-domain and SKP1 serves as an auxiliary protein that contributes to target recognition by binding to the FBXO45 F-Box domain (Desbois et al., 2018; Saiga et al., 2009). Interestingly, the FBXO45 SPRY-domain is also used for substrate binding and recruitment (Desbois et al., 2018; Richter et al., 2020; Saiga et al., 2009). Additionally, the ubiquitylation mechanism of MYCBP2-FBXO45 does not resemble the mechanism of RING E3 ligases (Mabbitt et al., 2020; Pao et al., 2018). In fact, MYCBP2 was later characterized as the first and so far only member of the novel RCR E3 ligase family that mediates ubiquitylation of substrates via two internal cysteines (cysteines 4520 and 4572), which relay the Ub-moiety intramolecularly, before discharging the Ub onto substrates, preferentially targeting serines and threonines (Figure 3B) (Mabbitt et al., 2020; Pao et al., 2018).

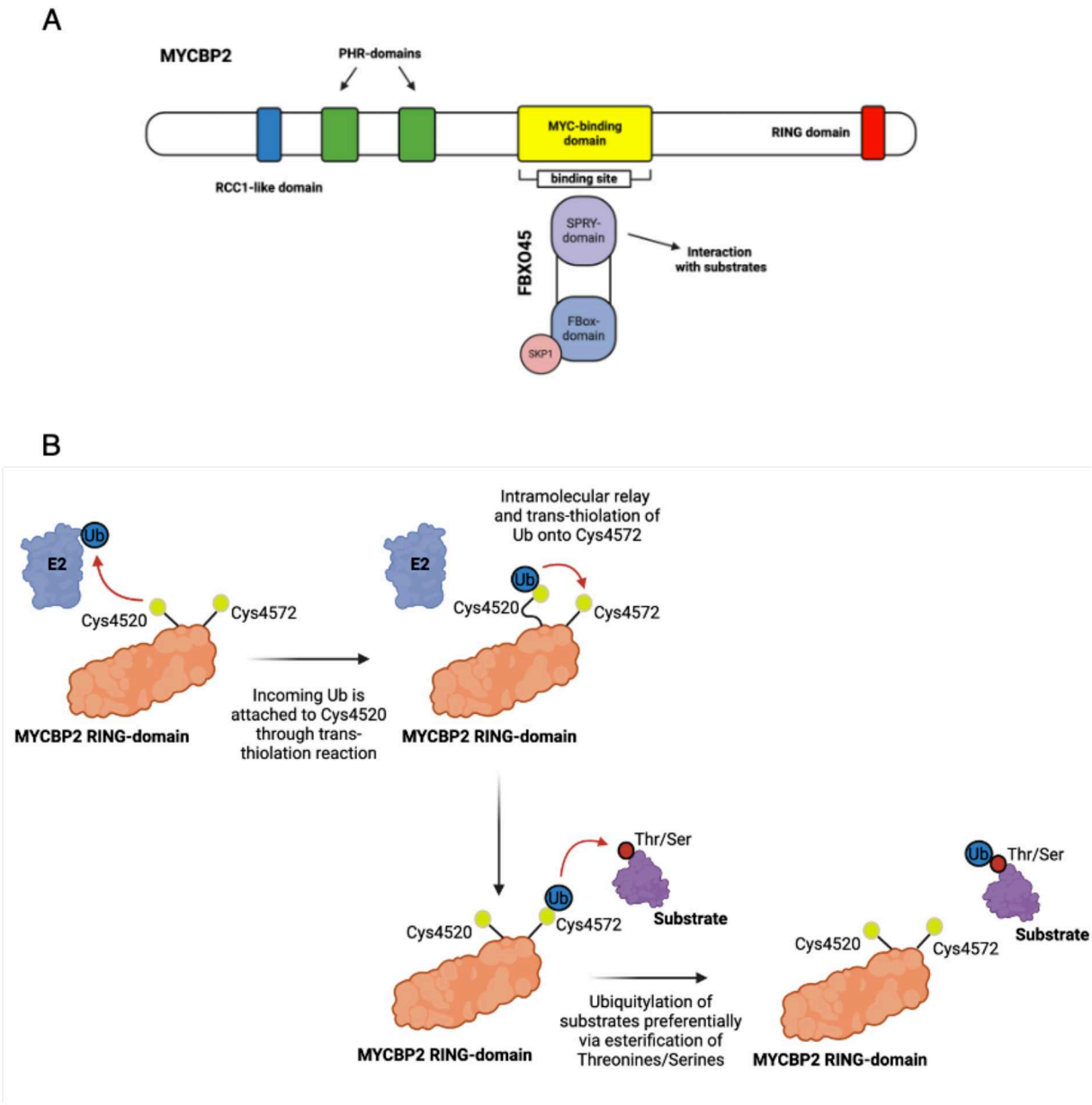


Figure 3: Schematic overview of MYCBP2-FBXO45 E3 ligase complex and its underlying ubiquitylation mechanism.
(A) Schematic overview of the MYCBP2-FBXO45 E3 ligase complex (adapted from Desbois et al. 2018). Created with BioRender. **(B)** Schematic overview of the RING-Cys-Relay mechanism of MYCBP2 (adapted from Pao et al. 2018). Cysteine 4520 (Cys4520) accepts the incoming Ubiquitin (Ub) via a trans-thiolation reaction and consequently relays it intramolecularly onto Cysteine 4572 (Cys4572). The Ubiquitin (Ub) moiety is than discharged preferentially on substrate threonine (Thr) or serine (Ser) residues via esterification. Created with BioRender.

1.10.3 MYCBP2-FBXO45 and disease

Numerous studies have linked alterations in PHR- and FBXO45 protein function to neurodevelopmental disorders. The *FBXO45* gene for example, is one of several deleted genes involved in the so-called 3q29 microdeletion syndrome, which can result in autism, intellectual disability and schizophrenia (Mulle et al., 2010; Quintero-Rivera et al., 2010; Willatt et al., 2005). *De novo* and loss-of-function variants of MYCBP2

affect corpus callosum development and are the cause of a novel neurodevelopmental disorder referred to as MYCBP2-related developmental delay with corpus callosum defects (MDCD) (AlAbdi et al., 2023). Corpus callosum defects can contribute to developmental delay, intellectual disability, epilepsy and autism (AlAbdi et al., 2023).
On top of their conserved function in neurodevelopment, PHR proteins and FBXO45 also play an important role in oncogenesis (Chen et al., 2014; Lin et al., 2021; Richter et al., 2020; Tricoli et al., 2018; Xu et al., 2015). For example, MYCBP2 was identified as a frequently mutated gene in colon cancers of adolescents and young adults (Tricoli et al., 2018). Furthermore, MYCBP2-FBXO45 is implicated in hepatocellular tumorigenesis through K63-ubiquitylation-dependent activation of IGF2BP1 and consequent stabilization of PLK1 (Lin et al., 2021). MYCBP2-FBXO45 also controls turnover of epithelial-to-mesenchymal (EMT) TFs and thus directly influences EMT in mammalian cells (Xu et al., 2015). Lastly, MYCBP2-FBXO45 promotes mitotic slippage and cell survival through ubiquitylation-mediated degradation of potent tumor suppressors PAR-4 and FBXW7, consequently contributing to apoptosis evasion and tumorigenesis (Chen et al., 2014; Richter et al., 2020).

1.11 SPRY-domain containing protein 3

The *SPRYD3* gene is located on chromosome 12q13 (Ensembl) and encodes an approximately 55 kDa protein referred to as SPRY-domain containing protein 3 (SPRYD3). SPRYD3 is so far poorly characterized, with some predicted functions in cell surface receptor signaling pathways and cytoskeleton organization (Alliance of Genome Resources). Furthermore, it was shown to be upregulated together with MYCBP2 and FBXO45 in mice lacking F506 binding protein 5 (FKBP5), a molecular chaperone involved in regulation of hormone signaling and stress response (Gebru et al., 2024). According to the Human Protein Atlas, SPRYD3 is expressed in multiple tissues such as the brain, liver, thyroid gland and kidneys.
SPRYD3 contains two SPRY-domains and together with FBXO45, it forms part of the SPRY/B30.2 protein family (D'Cruz et al., 2013; Stockum et al., 2018).

1.12 X-linked inhibitor of apoptosis protein

X-linked inhibitor of apoptosis protein (XIAP) resides on chromosome Xq25 (National Institutes of Health, NIH) and belongs to the family of inhibitors of apoptosis (IAPs) (Abbas and Larisch, 2020; Galbán and Duckett, 2010; Vucic, 2018).

The XIAP BIR-domains are essential for direct binding and inhibition of enzymatic activity of caspases-3, -7 and -9, the initiator and executioner proteases of the apoptotic downstream response (Abbas and Larisch, 2020; Galbán and Duckett, 2010; Thornberry and Lazebnik, 1998). Due to its ability to directly bind and inhibit those caspases, XIAP is the most potent apoptotic inhibitor within the mammalian IAP family (Abbas and Larisch, 2020; Eckelman et al., 2006; Schimmer, 2004; Vucic, 2018). Additionally, XIAP contains a Ubiquitin-associated domain (UBA), which enables poly-Ub chain-binding, and a RING domain, that confers E3 ligase activity (Abbas and Larisch, 2020).

Due to its cell death protective function, XIAP is a potent tumor promotor and its expression is de-regulated in various cancers, such as leukemia, colon, melanoma and breast cancer (Abbas and Larisch, 2020). Hou et al. demonstrated that XIAP is inhibited by CDK1-Cyclin B1 mediated phosphorylation during mitosis, leading to promotion of mitotic cell death after MT-poison treatment (Hou et al., 2017). Conversely, a non-phosphorylatable version of XIAP helps the cells to evade mitotic cell death after MT-poison treatment by undergoing mitotic slippage (Hou et al., 2017). Furthermore, XIAP was shown to inhibit anoikis and promote tumor transformation and drug resistance through USP11-mediated deubiquitylation and consequent stabilization (Zhou et al., 2016).

Its influential roles in apoptosis inhibition, cell cycle regulation and tumorigenesis render XIAP as an important target for cancer therapies. Therefore, it will be necessary that more about its upstream regulation is elucidated.

1.13 Chromosome alignment-maintaining phosphoprotein 1

The *CHAMP1* gene resides on chromosome 13q34 and encodes an 812 aa long zinc-finger protein called chromosome alignment-maintaining phosphoprotein 1 (CHAMP1), also known as CAMP, C13orf8 or ZNF929 (Hempel et al., 2015; Hino et al., 2021; Itoh et al., 2011). It localizes to chromosomes, mitotic spindles and is phosphorylated during mitosis (Itoh et al., 2011).

CHAMP1 contains two C2H2 zinc-finger domains on its N-terminus and three CH2H2 zinc-finger domains on its C-terminus, and expresses several repeat motifs referred to as SPE- (PxxSPExxK), WK- (SPxxWKxxP) and FPE- (FPExxK) (Itoh et al., 2011). CHAMP1 interacts with MAD2L2, also known as REV7, to mediate double-strand break (DSB) end resection and homologous repair (HR) (Li et al., 2022) or to position

MAD2L2 to mitotic spindles (Itoh et al., 2011). Additional to its role in HR, CHAMP1 regulates kinetochore-MT attachment and maintenance of chromosomes at the metaphase plate (Itoh et al., 2011). Depletion of CHAMP1 results in severe chromosome misalignments at the metaphase plate and multipolar spindle formation (Itoh et al., 2011).
Independently from its function in kinetochore-MT attachment, CHAMP1 also promotes mitotic slippage in presence of MT-poisons and apoptosis evasion through stabilization of anti-apoptotic factor MCL-1 (Hino et al., 2021).
Many cancer types, such as breast and ovarian cancer, manifest amplification of the *CHAMP1* gene and CHAMP1 upregulation has been linked to tumor cell proliferation (Sack et al., 2018).

1.14 Ubiquitin specific peptidase 11

Ubiquitin-specific peptidase USP11 belongs to the family of USPs and its coding gene was first identified and subcloned by Swanson et al. in 1996. The USP11 gene resides on the X-chromosome, precisely on Xp21.2 (Guo et al., 2022; Swanson et al., 1996), and codes for a 963 aa long polypeptide.
USP11 forms together with USP4 and USP15 the so-called DUSP-UBL family of USPs due to the presence of an N-terminal domain present in ubiquitin-specific protease (DUSP) and two Ubiquitin-like domains (UBLs) (Harper et al., 2014; Zhu et al., 2007). For all three enzymes, the first UBL domain resides within the N-terminus, following the DUSP domain, whereas the second UBL domain is placed within the catalytic core (Harper et al., 2014; Zhu et al., 2007). UBL domains share similarity with the Ub superfold and are the most common domain present in the human USP family. It is hypothesized, that UBL domains regulate enzymatic activity, specificity towards substrates or poly-Ub chain linkages, but also recruitment and interaction with non-substrate partners (Harper et al., 2014; Zhu et al., 2007). Furthermore, other non-catalytic properties such as cellular and subcellular localization and trafficking might also be regulated by UBL domains.
Due to its localization on the X-chromosome, USP11 was first named Ubiquitin hydrolase on the X chromosome (UHX1) and linked to X-chromosome dependent retinal disorders (Swanson et al., 1996). Ongoing research reveals that the cellular role of USP11 is more intricate and not only limited to X-chromosome related processes. A myriad of cellular mechanisms, such as cell division, DNA repair, translation, apoptosis

and maintenance of genome stability through chromatin remodeling are mediated by USP11 deubiquitylation activity (Ideguchi et al., 2002; Lee et al., 2015; Schoenfeld et al., 2004; Stockum et al., 2018; Ting et al., 2019; Zhou et al., 2016). For example, USP11 is crucial for cell division, where direct USP11-mediated deubiquitylation of RanBPM and RAE1 ensures correct MT-nucleation and bipolar spindle formation, respectively (Ideguchi et al., 2002; Stockum et al., 2018). DUB deregulation is involved in cancer formation and progression and indeed, altered USP11 expression levels in different cancer types such as colorectal, breast or lung cancer have been observed (Dewson et al., 2023; Hanahan and Weinberg, 2011; Zhu et al., 2007).

Interestingly, depending on the cancer context and substrates targeted for deubiquitylation, USP11 can act as either tumor suppressor or promotor. For example, in colorectal cancer (CRC), USP11 acts as an oncogene by stabilizing the phosphatase protein phosphatase 1 catalytic subunit α (PPP1CA). Consequently, this activates the ERK/MAPK signaling pathway leading to growth and metastasis of CRC (Sun et al., 2019). In another example, USP11 promotes tumorigenesis by deubiquitylating and stabilizing XIAP, a well-known tumor promotor and inhibitor of apoptosis (Zhou et al., 2016).

Notably, USP11 is able to form complexes and collaborate with another DUB, USP7, in the regulation of downstream substrates. For example, USP11 was reported to collaborate with USP7 in the transcriptional regulation of the INK4a tumor suppressor gene through interaction with the Polycomb repressive complex 1 (PRC1) (Maertens et al., 2010). Additionally, USP11 deubiquitylates the oncogenic tyrosine kinase LCK by forming a complex with USP7 (Jin et al., 2022).

1.15 Ribonucleic acid export 1

The gene encoding ribonucleic acid export 1 (RAE1) resides on chromosome 20q13.31 (NIH) and codes for a protein of approximately 41 kDa. RAE1 forms part of the WD-repeat superfamily of proteins, which mostly fold into a globular propeller structure and commonly form part of large macromolecular assemblies (Pritchard et al., 1999).

In *Drosophila melanogaster*, RAE1 is a conserved interactor of the MYCBP2 homolog HIW and promotes its abundance in post-mitotic neurons (Tian et al., 2011). In *S. pombe* and *S. cerevisiae*, various studies have suggested a role of RAE1 homologs in mRNA export, since its ablation leads to accumulation of poly(A)+ RNA in the nucleus

(Brown et al., 1995; Murphy et al., 1996). In humans, RAE1 interacts with NUP98 at the nuclear pore complex and directly mediates mRNA export out of the nucleus (Pritchard et al., 1999). However, experiments carried out in mice suggest that the primary function of RAE1 is not connected to mRNA export, and that it is compensated by other shuttling factors (Babu et al., 2003). In higher eukaryotes, the involvement of RAE1 in mitotic check point regulation and bipolar spindle formation seems to play a bigger role. RAE1 was reported to interact with structural maintenance of chromosomes 1 (SMC1) and nuclear mitotic apparatus protein (NuMa) on mitotic spindles, and to contribute to correct spindle bundling at the poles and promotion of bipolar spindles (Wong, 2010; Wong et al., 2006). The function of RAE1 in bipolar spindle formation is further regulated through USP11-mediated deubiquitylation (Stockum et al., 2018). Additionally, RAE1 cooperates with mitotic checkpoint protein BUB3 in mitotic checkpoint regulation (Babu et al., 2003). Similar to BUB3 haplo-insufficiency, RAE1 haplo-insufficiency leads to severe mitotic checkpoint and chromosome segregation defects, while complete RAE1 loss is embryonically lethal in mice (Babu et al., 2003).

Interestingly, RAE1 mRNA is upregulated in various cancers and RAE1 was reported to promote chemoresistance and apoptosis evasion in presence of paclitaxel, most probably due to its function in promoting bipolar spindle formation (Kobayashi et al., 2021).

1.16 Objectives

Apoptosis evasion in form of mitotic slippage constitutes a serious problem in chemotherapy which is due to its considerable contribution to MT-poison resistance development (Chan et al., 2012). MT-poisons like taxanes and vinca alkaloids alter MT-dynamics and interfere with proper spindle formation, inducing sustained mitotic arrest and eventual cell death (Brito and Rieder, 2006; Musacchio and Salmon, 2007). While MT-poisons were proven efficacious in the treatment of solid and hematological cancers (Jordan and Wilson, 2004), targeting mitotic non-MT proteins for cancer killing has so far been unsuccessful in clinical trials (Chan et al., 2012; Huszar et al., 2009; Manchado et al., 2012; Salmela and Kallio, 2013).

In order to re-establish a proper apoptotic response, mechanisms leading up to mitotic slippage need to be elucidated. MYCBP2 is postulated to be a signaling hub that interacts with conserved non-target proteins to mediate ubiquitylation-independent

functions (Baker et al., 2014; Grill et al., 2016, 2012). Due to its involvement in oncogenesis and mitotic slippage, I hypothesized that other than targeting the already characterized substrates FBXW7 and PAR-4 (Chen et al., 2014; Richter et al., 2020), MYCBP2-FBXO45 might additionally regulate mitotic slippage through ubiquitylation of so far unidentified substrates. Thus, identifying new MYCBP2-FBXO45 ubiquitylation targets involved in mitotic slippage regulation would provide valuable information and broaden our understanding as to how mitotic slippage and consequent chemoresistance arises.

In the presented thesis, I utilized a combined Immunoprecipitation (IP) – Mass spectrometry (MS) approach to identify new FBXO45 interactors and/or substrates. However, during the validation process of candidate hits, I identified a potentially new substrate specificity factor of the MYCBP2 E3 ligase, SPRYD3. I hypothesized that MYCBP2 could form an E3 ligase complex with SPRYD3 acting as a substrate specificity factor, regulating mitotic cell fate. In order to validate this hypothesis, I performed *in vivo* and *in vitro* IP experiments to confirm a direct and FBXO45-independent interaction between MYCBP2 and SPRYD3. Additionally, I performed live cell imaging experiments in U2OS and RPE1 cell lines using RNA interference (RNAi) to assess the involvement of SPRYD3 in mitotic cell fate regulation in presence of MT-poisons nocodazole and paclitaxel. To assess the E3 ligase activity of the new complex consisting of MYCBP2-SPRYD3, I performed an additional combined IP-MS analysis approach to specifically identify SPRYD3 interactors. To validate potential candidate hits, I performed both *in vivo* and *in vitro* IP experiments to confirm a physical interaction between SPRYD3 and putative substrates. In order to assess whether putative substrates are targeted by MYCBP2-SPRYD3 in a ubiquitylation-dependent manner, I carried out RNAi and ubiquitylation assays, as well as a combined IP-MS analysis approach to identify putative substrate ubiquitylation sites. Lastly, to understand the underlying mechanism leading to mitotic slippage, I performed immunofluorescence experiments combined with RNAi or plasmid overexpression.

2. Materials and Methods

2.1 Materials

2.1.1 Chemicals and reagents

Table 1: Chemicals and reagents

Chemicals/ Reagents	Source
λ-phosphatase	New England BioLabs
Acrylamide solution	Sigma-Aldrich
Agarose	VWR Chemicals
Ammonium persulfate (APS)	Carl Roth
Ampicillin	AppliChem
Aprotinin	Roche
Bicine	Carl Roth
Bio-Rad Protein Assay Dye Reagent Concentrate, 5x	Bio-Rad
BIS-TRIS	Sigma-Aldrich
Bovine Serum Albumin (BSA)	Sigma-Aldrich
Cycloheximide	Santa Cruz Biotechnology
Dimethylsulfoxide (DMSO)	Sigma-Aldrich
Dithiothreitol (DTT)	Carl Roth
1 kb ladder	Thermo Fisher Scientific
100 bp ladder	Thermo Fisher Scientific
Doxycycline	Sigma-Aldrich
DPBS	Gibco
Dulbecco's Modified Eagle's Medium (DMEM)	Gibco
Dulbecco's Modified Eagle's Medium/Nutrient Mixture F-12 Ham	Sigma-Aldrich
Ethanol	Sigma-Aldrich
Ethylenediaminetetraacetic acid (EDTA)	Carl Roth
Fetal bovine serum (FBS)	Gibco
Flag M2 affinity gel	Sigma-Aldrich
3x Flag peptide	Thermo Fisher Scientific

Formaldehyde solution	Sigma-Aldrich
GFP-trap agarose	I. Hoffmann, DKFZ
Glutathione, reduced	Sigma-Aldrich
Glycerol	Thermo Fisher Scientific
β-Glycerophosphate	Sigma-Aldrich
Glycine	Carl Roth
Imidazole	Sigma-Aldrich
Immobilized reduced Glutathione Sepharose^{Tm} 4B	Cytiva
IPTG (Isopropyl-ß-D-thiogalactopyranoside)	Biomol
Isopropanol	VWR Chemicals
Kanamycin	AppliChem
LB medium	Carl Roth
LB-Agar	Carl Roth
Leupeptin	Roche
Lipofectamine 2000	Invitrogen
Lipofectamine RNAiMAX	Invitrogen
Lysozyme	Carl Roth
Magnesium chloride	Merck
Maltose	Sigma-Aldrich
β-Mercaptoethanol	Sigma-Aldrich
Methanol	Sigma-Aldrich
MG132 (Z-Leu-Leu-Leu-Al)	Sigma-Aldrich
Milk powder	Gerbu
N-ethylmaleimide (NEM)	Sigma-Aldrich
Ni-NTA agarose	Qiagen
Nocodazole	Merck
Nonidet NP40 (Igepal)	MP Biochemicals
Nuclease-free water	Dharmacon
Oligonucleotides/primers	Merck
OptiMEM	Gibco

Paclitaxel	Merck
Penicillin-Streptomycin	Sigma-Aldrich
PIN	Roche
PIPES	Sigma-Aldrich
Platinum™ SuperFi™ PCR Master Mix	Invitrogen
Platinum™ SuperFi™ DNA-Polymerase	Invitrogen
Polyethylenimine, Linear, MW 25000	Polysciences
Ponceau S Solution	Serva
ProLong Gold Antifade Mountant	Invitrogen
Protein G sepharose	GE Healthcare
Protein ladder prestained	neoLab
Restriction enzymes	New England Biolabs
Rotiphorese Gel 30 acrylamide/bisacrylamide 37.5:1	Carl Roth
Sodium azide	Merck
Sodium chloride	Sigma-Aldrich
Sodium dodecyl sulfate (SDS)	Carl Roth
Sodium fluoride	Merck
Sodium hydroxide	J. T. Baker
Sodium vanadate	Sigma-Aldrich
StainIN RED Nucleic Acid Stain	HighQu
T4 IHRES ligase	Thermo Fisher Scientific
N,N,N',N'-Tetramethylethylenediamine (TEMED)	Carl Roth
TLCK (1-Chloro-3-tosylamido-7-amino-2-butanon)	Roche
TPCK (1-Chloro-3-tosylamido7-amino-2-heptanon)	Roche
Trans-Blot Turbo 5x Transfer Buffer	Bio-Rad
Tricine	Carl Roth
TRIS base	Serva
Triton X-100	Sigma-Aldrich
0.05% Trypsin-EDTA	Thermo-Scientific
Tween 20	Sigma-Aldrich

Urea	Thermo Fisher Scientific
Western Chemiluminescence HRP-substrate	Merck

2.1.2 Laboratory equipment

Table 2: Laboratory equipment

Name	Specification	Source
Cell culture dishes	Cellstar	Greiner Bio-One
Cell culture incubator	CO_2 Incubator	Sanyo
Centrifuges	5415 R 5810 R RC5C	Eppendorf Eppendorf Sorvall
Coverslips		NeoLab
DNA gel electrophoresis	Mini-Sub Cell	Bio-Rad
Electrotransfer unit	Transblot Turbo	Bio-Rad
Fluorescence microscope	Cell Observer Z1	Zeiss
Freezer (- 20 °C)	MEDLine	Liebherr
Freezer (- 80 °C)	Ultralow	Sanyo
Fridge (4 °C)	ProfiLine	Liebherr
Gel documentation	Gelstick	Intas
Glassware	Glass pipettes, measuring cylinders, flasks, bottles	Brand, Schott
Heat block	Thermomixer comfort Digital Heatblock	Eppendorf VWR
Incubation shaker	Minitron	Infors IHRES
Laboratory balance	Extend	Sartorius
Light microscope	Axio Vert.A1	Zeiss
Live-cell imaging dish	x-well cell culture chamber	Sarstedt
Luminescent image analyzer	ImageQuant LAS 4000	GE Healthcare
Magnet stirrers	Ikamag RTC	IKA-Labortechnik
Microplate absorbance reader	SPECTROstar Nano	BGM Labtech
Microscope slides	Cut frosted	Epredia
Microwave		Sharp
Mini Trans-Blot Cell	Mini-PROTEAN® 3 Cell	Bio-Rad

NanoDrop spectrophotometer	ND-1000	Peqlab
Nitrocellulose membrane	Amersham Protran 0.45 µM	GE Healthcare
PAGE system	Mini Protean III	Bio-Rad
Parafilm	Laboratory film M	Bemis
PCR thermocycler	Mastercycler nexus GX2	Eppendorf
pH meter	Seven Easy	Mettler Toledo
Pipettes	Pipetman	Gilson
Pipettor	Pipetboy	Integra
Plasticware	Reaction tubes, falcon tubes, pipette tips, PCR tubes, petri dishes	Eppendorf, Nerbe, Falcon, Biozym, Greiner Bio-One, TPP
Power supply	PowerPac 200	Bio-Rad
Rocking platform shaker	Rocker 25	Labnet
Rotating wheel	Test tube rotator	Snijders
Sonifier	Sonifier 250	Branson
Sterile workbench	SterilGARD Hood	Baker Company
Vortex shaker	Vortex-Genie 2	Scientific Industries
Water bath	12B	Julabo EM

2.1.3 Buffers

Table 3: Buffers

Name	Composition
4x Laemmli buffer	0.1 M Tris-HCl pH 6.8 4 % SDS 20 % glycerol 0.02 % bromophenol blue Added before use: Add freshly: 0.1 M DTT

In vitro ubiquitylation assay buffer	50 mM Tris-HCl pH 7.5 100 mM NaCl 10 mM $MgCl_2$ 0.05 % NP-40 Added before use: 1 mM DTT 0.1 mM Na_3VO_4 1 µg/ml Aprotinin 1 µg/ml Leupeptin 10 µg/ml Trypsin inhibitor from soybean
NP-40 buffer	40 mM Tris-HCl pH 7.5 150 mM NaCl 5 mM EDTA 10 mM β-Glycerophosphate 5 mM NaF 0.5 % NP-40 Added before use: 1 mM DTT 10 µg/ml TPCK 5 µg/ml TLCK 0.1 mM Na_3VO_4 1 µg/ml Aprotinin 1 µg/ml Leupeptin 10 µg/ml Trypsin inhibitor from soybean
PBS	137 mM NaCl 2.7 mM KCl 1.8 mM KH_2PO_4 10 mM Na_2HPO_4 pH 7.4
PBS-T	0.1 % Tween-20 in PBS
PBS-BT	3 % BSA 0.1% Triton X-100

	1:500 NaN_3 (stock: 10 %) in PBS
GST protein purification lysis buffer	50 mM Tris-HCl 300 mM NaCl 0.1% NP40 5% Glycerol 5mM EDTA Added before use: 1mg/ml Lysozyme 5 mM β-Mercaptoethanol 10 µg/ml TPCK 5 µg/ml TLCK 0.1 mM Na_3VO_4 1 µg/ml Aprotinin 2 µg/ml Leupeptin 10 µg/ml Trypsin inhibitor from soybean
GST protein purification dialysis buffer	GST protein purification lysis buffer without Lysozyme 1 mM DTT
GST protein purification elution buffer	GST protein purification lysis buffer without Lysozyme 10 mM reduced glutathione
GST protein purification washing buffer	GST protein purification lysis buffer without lysozyme
MBP protein purification column buffer	20 mM Tris-HCl pH 7.4 200 NaCl 5 mM EDTA Added before use: 1 mM DTT 10 µg/ml TPCK 5 µg/ml TLCK 0.1 mM Na_3VO_4 1 µg/ml Aprotinin 1 µg/ml Leupeptin

	10 µg/ml Trypsin inhibitor from soybean
MBP protein purification elution buffer	MBP protein purification column buffer 10 mM maltose
HIS protein purification lysis buffer	50 mM Tris pH 8.0 500 mM NaCl Added before use: 30 mM Imidazole 10 µg/ml Trypsin inhibitor from soybean 1 mg/ml Lysozyme
HIS protein purification elution buffer	HIS protein purification lysis buffer 300 mM Imidazole
RIPA buffer	50 mM Tris-HCl pH 7.4 150 mM NaCl 2 mM EDTA 50 mM NaF 1 % NP-40 0.5 % Na-deoxycholate 0.1 % SDS Added before use: 5 mM DTT 10 µg/ml TPCK 5 µg/ml TLCK 0.1 mM Na_3VO_4 1 µg/ml Aprotinin 1 µg/ml Leupeptin 10 µg/ml Trypsin inhibitor from soybean
SDS running buffer	25 mM Tris-HCl pH 8.3 190 mM glycine 0.1 % SDS

Gel buffer for TRIS-acetate gels, 10x	3 M Tris pH 7.0
Running buffer for TRIS-acetate gels, 10x	1L: 179 g Tricine 121.2 g Tris-Base 20 g SDS
Transfer Buffer for TRIS-acetate gels, 20x	1L: 81.6 g Bicine 104.8 g Bis-Tris 6 g EDTA
TAE buffer	40 mM Tris-HCl pH 7.6 20 mM acetic acid 1 mM EDTA
TBS	50 mM Tris-HCl pH 7.4 150 mM NaCl
TBS-T	0.05 % Tween-20 in TBS
Urea buffer	8 M Urea 0.1 M potassium phosphate pH 8.0 Added before use: 30 mM imidazole 20 mM N-ethylmaleimide 1 mM DTT 10 µg/ml TPCK 5 µg/ml TLCK 0.1 mM Na_3VO_4 1 µg/ml Aprotinin 1 µg/ml Leupeptin 10 µg/ml Trypsin inhibitor from soybean
Western blot blocking solution	5 % Milk powder in PBS-T

2.1.4 Antibodies

2.1.4.1 Primary antibodies

Table 4: Primary antibodies

Target protein	Origin	Dilution	Clone	Source
Centrin	Mouse (IgG_{2a})	1:500 (IF)	20H5	Merck
CHAMP1	rabbit	1:1000 (WB)	-	Atlas Antibodies
FBXO45	rabbit	1:1000 (WB)	-	I. Hoffmann, DKFZ Heidelberg
FBXW7	rabbit	1:1000 (WB)	A301-720A	Bethyl
Flag	mouse	1:1000 (WB) 1:500 (IF)	M2 (F3165)	Sigma-Aldrich
GFP	rabbit	1:1000 (WB)	-	I. Hoffmann, DKFZ Heidelberg
GST	rabbit	1:1000 (WB)	Z-5	Santa Cruz
HA	mouse	1:1000 (WB)	16B12	Babco
MBP	mouse	1:1000	F-6	Santa Cruz
MYCBP2	rabbit	1:1000 (WB)	-	Abcam
MYC (tag)	mouse	1:1000 (IF) 1:100 (WB)	9E10	Santa Cruz
RAE1	rabbit	1:1000 (WB)	-	Blower et al. 2005
SKP1 p19	rabbit	1:1000 (WB)	H-163	Santa Cruz
SPRYD3	rabbit	1:500 (WB)	NBP1-74270	Novus
α-tubulin	Mouse (IgG_1)	1:1000 (WB) 1:2000 (IF)	B-5-1-2	Sigma-Aldrich
USP11	mouse	1:1000 (WB)	-	Santa Cruz
XIAP	mouse	1:1000 (WB)	610763	BD Biosciences
vinculin	mouse	1:1000 (WB)	hVIN-1	Sigma-Aldrich

2.1.4.2 Secondary antibodies

Table 5: Secondary antibodies

Antibody	Origin	Dilution	Source
Anti-mouse IgG HRP	goat	1:5000 (WB)	Novus
Anti-rabbit IgG HRP	donkey	1:5000 (WB)	Jackson Laboratories
Anti-mouse IgG_{2a} Alexa 594	goat	1:2000 (IF)	Invitrogen
Anti-mouse IgG_1 Alexa 488	goat	1:2000 (IF)	Invitrogen

2.1.5 Small interfering RNAs (siRNAs)

Table 6: Small interfering RNAs

Name	Sequence sense (5' – 3')	Source
siGL2	CGUACGCGGAAUACUUCGAdTdT	Wang et al., 2006
siSPRYD3 #1	AUGGAGAUACUUUAAGUUA	Ambion, Silencer Select
siSPRYD3 #2	UCAUGAUGGUGGACAGUUA	Ambion, Silencer Select
siSPRYD3 #3	CGAUAUCAGGAGAGGUUCAtt	Ambion, Silencer Select
siMYCBP2 #1	CCCGAGAUCUUGGGAAUAAtt	Eurofins
siMYCBP2 SMART	GGAAGUAGUUCUGUUAUUU GCAGAAAUGCCCACACUUU GAAUAGUUGUGGUUGGUUU GCAAGGAUUUGGUGUGUGU	Dharmacon, SMARTpool
siMYCBP2 #2	GGAAGUAGUUCUGUUAUUUtt	Taken from SMARTpool
siMYCBP2 #3	GCAGAAAUGCCCACACUUUtt	Taken from SMARTpool
siUSP11 #1	GGACCGUGAUGAUAUCUUC	Jurga et al. 2021
siUSP11 #2	GAAGAAGCGUUACUAUGAC	Jurga et al. 2021
siCHAMP1	CCGGCAUAAUGAAGAGGCAAAUAAA	Itoh et al. 2010

2.1.6 Primers

Table 7: Primers

Name	Sequence (5' – 3')	No.
SPRYD3_FL_EcoRI_FW	ATGCGAATTCATGAGGAGGACGCGGC	1
SPRYD3FLHINDIIIRev	ATGCAAGCTTCTAGCCACTCAAGGGGTGCA	2
SPRYD3_bdSPRY1_rev	GTCCTCACGGCCCAGCTCACCAGAGTTTCCATGATAA	3
SPRYD3_cdSPRY1_fw	AGTTATCATGGAAACTCTGGTGAGCTGGGCCGTGAGGACGA	4
SPRYD3_dSPRY2_rev	ATGCAAGCTTCTAGCTGAGTGGGTGCCGGGCCT	5
MBD_EcoRI_fwFL	ATGCGAATTCTCTTCTAATACTGACATGACT	6
MBD_HINDIII_RevFL	TGCAAGCTTCTACTGATCCAGTTGCACC	7
MBD_HINDIII_RevF1	ATGCAAGCTTCTACTGCTCACTCTGAAGGGA	8
MBD_EcoRI_fwF2	ATGCGAATTCATAGGCATAGTGAAAGTCAA	9
MBD_BamHI_fw_2400	ATGCGGATCCTCTTCTAATACTGACAT	10
MBD_XhoI_rev	ATGCCTCGAGCTATATTTTGGGAGATGCTC	11
MBD_BamHI_fw	ATGCGGATCCAACAGCATGGTAGAGTTC	12
MBD_BamHI_fw28	ATGCGGATCCATAGGCATAGTGAAAGTCAA	13
MBD_XhoI_Rev28	ATGCCTCGAGCTAACTGTGGGAATCTGACC	14
USP11_EcoRI_fw	ATGCGAATTCATGGCAGTAGCCCCGCGA	15
USP11-XhoI_rev	ATGCCTCGAGTCAATTAACATCCATGAACT	16
USP11_HINDIII_Rev	ATGCAAGCTTTCAATTAACATCCATGAACTCAGAGCT	17
C318S FW	CAACACGTCCTTCATGAACTC	18
C318S REV	GAGTTCATGAAGGACGTGTTG	19
FRT-SPRY_HINDIIIfw	ATGCAAGCTTATGGATTACAAGGATGACGACGAT	20

FRT-SPRY_XhoI_rev	ATGCCTCGAGCTAGCCACTCAAGGGGTGCA	21

2.1.7 Plasmids

Plasmids that were provided are listed below.

Table 8: Provided plasmids

Plasmid name	Source
pCMV-3Tag2A-MYC	Agilent Technologies
pCMV-3Tag1A-Flag	Agilent Technologies
pPK-CMV-HA-UbiquitinC	F. Rösl, DKFZ Heidelberg
pSG5-His-Myc-Ubiquitin	M. Scheffner, University of Konstanz
pGM-Flag-SPRYD3	G. Maertens, Imperial College London, UK
pCMV-MYC-MYCBP2	Addgene (plasmid #42570)
pCMV-3Tag1A-Flag MYCBP2 1-1050	Richter et al. 2020
pCMV-3Tag1A-Flag MYCBP2 1051-1950	Richter et al. 2020
pCMV-3Tag1A-Flag MYCBP2 1951-2950	Richter et al. 2020
pCMV-3Tag1A-Flag MYCBP2 2951-3600	Richter et al. 2020
pCMV-3Tag1A-Flag MYCBP2 3601-4640	Richter et al. 2020
pCMV-3Tag-1A-Flag-MYCBP2 1951-2400	I. Hoffmann, DKFZ Heidelberg
pCMV-3Tag-1A-Flag-MYCBP2 C4520S	I. Hoffmann, DKFZ Heidelberg
pQCXIZ-Flag-MYCBP2	I. Hoffmann, DKFZ Heidelberg
pDEST-LTR-N-Flag-HA-IHRES-puro-USP11	Addgene (plasmid #22566)
pCMV-3Tag-2A-MYC-FBXO45	Richter et al. 2020
pCMV-3Tag-1A-Flag-FBXO45	Richter et al. 2020
pcDNA5-FRT-TO	Invitrogen
pET28a(+)-HIS	M. Müller, DKFZ Heidelberg
pGEX4T1-GST	GE Healthcare
pOG44	Invitrogen
HA-mRAE1	D. Lyles, Wake Forest Bapt. Health

pEGFP-C1-mRAE1	Kai Richter, Hoffmann lab
pMAl-c2-MBP	NEB
pEGFP-C1-CHAMP1	Addgene (plasmid #159892
USP11_AllMut_pUC57-Mini	GenScript
pUC57-USP11^{WT} fragment siRNA-resistant	GenScript
pUC57-USP11^{C318S} fragment siRNA-resistant	GenScript
pCMV-3Tag-1A-Flag-XIAP	I. Hoffmann, DKFZ Heidelberg
pCMV-3Tag-1A-Flag-XIAP ΔRING	I. Hoffmann, DKFZ Heidelberg
pCMV-3Tag-1A-Flag-XIAP ΔUBA-RING	I. Hoffmann, DKFZ Heidelberg
pCMV-3Tag-1A-Flag-XIAP ΔBIR3-RING	I. Hoffmann, DKFZ Heidelberg
pCMV-3Tag-1A-Flag-XIAP ΔBIR1	I. Hoffmann, DKFZ Heidelberg
pCMV-3Tag-1A-Flag-XIAP ΔBIR1-BIR2	I. Hoffmann, DKFZ Heidelberg
pCMV-3Tag-1A-Flag-XIAP ΔBIR2	I. Hoffmann, DKFZ Heidelberg
pCMV-3Tag-1A-Flag-XIAP ΔBIR3-UBA	I. Hoffmann, DKFZ Heidelberg
pCMV-3Tag-1A-Flag-XIAP ΔUBA	I. Hoffmann, DKFZ Heidelberg
pCMV-3Tag-1A-Flag-XIAP ΔBIR2-BIR3	I. Hoffmann, DKFZ Heidelberg
pCMV-3Tag-1A-Flag-XIAP ΔBIR1-BIR3	I. Hoffmann, DKFZ Heidelberg
pCMV-3Tag-1A-Flag-XIAP ΔBIR3	I. Hoffmann, DKFZ Heidelberg

Plasmids that were generated during this thesis are listed below.

Table 9: Plasmids generated during this thesis

Plasmid name	Template	Primers	Enzymes
pCMV-3Tag-1A-Flag-SPRYD3	pGM-Flag-SPRYD3	1, 2	EcoRI, HINDIII
pCMV-3Tag-1A-Flag-SPRYD3ΔSPRY1	pCMV-3Tag-1A-Flag-SPRYD3	1-4	EcoRI, HINDIII
pCMV-3Tag-1A-Flag-SPRYD3ΔSPRY2	pCMV-3Tag-1A-Flag-SPRYD3	1, 5	EcoRI, HINDIII
pCMV-3Tag-2A-MYC-SPRYD3	pCMV-3Tag-1A-Flag-SPRYD3	1, 2	EcoRI, HINDIII

pCMV-3Tag-2A-MYC-SPRYD3ΔSPRY1	pCMV-3Tag-1A-Flag-SPRYD3	1-4	EcoRI, HINDIII
pCMV-3Tag-2A-MYC-SPRYD3ΔSPRY2	pCMV-3Tag-1A-Flag-SPRYD3	1, 5	EcoRI, HINDIII
pCMV-3Tag-1A-Flag-MYCBP2 2400-2700	pCMV-3Tag-1A-Flag-MYCBP2 1951-2950	6, 7	EcoRI, HINDIII
pCMV-3Tag-1A-Flag-MYCBP2 2400-2550	pCMV-3Tag-1A-Flag-MYCBP2 1951-2950	6, 8	EcoRI, HINDIII
pCMV-3Tag-1A-Flag-MYCBP2 2551-2700	pCMV-3Tag-1A-Flag-MYCBP2 1951-2950	7, 9	EcoRI, HINDIII
pCMV-3Tag-1A-Flag-MYCBP2 2400-2950	pCMV-3Tag-1A-Flag-MYCBP2 1951-2950	10, 11	BamHI, XhoI
pCMV-3Tag-1A-Flag-MYCBP2 2700-2950	pCMV-3Tag-1A-Flag-MYCBP2 1951-2950	11, 12	BamHI, XhoI
pCMV-3Tag-1A-Flag-MYCBP2 2550-2825	pCMV-3Tag-1A-Flag-MYCBP2 1951-2950	13, 14	BamHI, XhoI
pCMV-3Tag-2A-MYC-USP11	pDEST-LTR-N-Flag-HA-IHRES-puro-USP11	15, 16	EcoRI, XhoI
pCMV-3Tag-1A-Flag-$USP11^{WT}$	pCMV- pCMV-3Tag-2A-MYC-USP11		EcoRI, XhoI
pCMV-3Tag-1A-Flag-$USP11^{6A}$	USP11 AllMut_pUC57-Mini		EcoRI, HINDIII
pCMV-3Tag-1A-Flag-$USP11^{C318S}$	pDEST-LTR-N-Flag-HA-IHRES-puro-USP11	15, 17, 18, 19	EcoRI, HINDIII
pCMV-3Tag-1A-Flag-$USP11^{WT\ siRes}$	pCMV-3Tag-1A-Flag-$USP11^{WT}$ and pUC57-$USP11^{WT}$ fragment siRNA-resistant		ScaI, XhoI
pCMV-3Tag-1A-Flag-$USP11^{C318S\ siRes}$	pCMV-3Tag-1A-Flag-$USP11^{C318S}$ and pUC57-$USP11^{C318S}$ fragment siRNA-resistant		ScaI, HINDIII
pMAl-c2-MBP-SPRYD3	pCMV-3Tag-1A-Flag-SPRYD3		EcoRI, HINDIII

pGEX4T1-GST-MYCBP2 2550-2825	pCMV-3Tag-1A-Flag-MYCBP2 2550-2825		BamHI, XhoI
pET28a(+)-HIS-MYCBP2 2550-2825	pCMV-3Tag-1A-Flag-MYCBP2 2550-2825		HINDIII, BamHI
pET28a(+)-HIS-USP11	pDEST-LTR-N-Flag-HA-IHRES-puro-USP11		EcoRI, XhoI
pGEX4T1-GST-USP11	pCMV- pCMV-3Tag-2A-MYC-USP11		EcoRI, XhoI
pcDNA5-FRT-TO-MYC-SPRYD3	pCMV-3Tag-2A-MYC-SPRYD3	20, 21	HINDIII, XhoI

2.1.8 Bacterial strains

Table 10: Bacterial strains

Strain	Genotype	Source
E. coli Top10 One Shot	F-*mcrA* Δ(*mrr-hsd*RMS-*mcr*BC) Φ80*Lac*ZΔM15 Δ *Lac*X74 *rec*A1 *ara*D139 Δ(*araleu*) 7697 *gal*U *gal*K *rps*L (StrR) *end*A1 *nup*G	Thermo Fisher Scientific
E. coli Rosetta (DE3)	F^-*ompT hsDS*$_B$($r_B^-m_B^-$) *gal dcm* (DE3= pRARE2 (Cam^R)	Merck

2.1.9 Cell lines

Table 11: Cell lines

Name	Cell type	Source
HEK 293T	Human epithelial embryonic kidney cells expressing the SV-40 large T-antigen	DSMZ, Braunschweig
HEK 293T ΔFBXO45	Human epithelial embryonic kidney cells expressing the SV-40 large T-antigen with knock out in the FBXO45 gene	I. Hoffmann, DKFZ Heidelberg
hTERT RPE1	Retinal pigment epithelial cells immortalized through human telomerase reverse transcriptase (=hTERT).	ATCC

HeLa	Human epithelial cervix adenocarcinoma cells transformed by HPV18	ATCC
HeLa ΔFBXO45	Human epithelial cervix adenocarcinoma cells transformed by HPV18 with knock out in the FBXO45 gene	I. Hoffmann, DKFZ Heidelberg
U2OS	Human osteosarcoma cells	ATCC
U2OS Flp-In-T-REX MYC-SPRYD3	Stable U2OS cell line homogenously expressing MYC-SPRYD3 after doxycycline addition	This work

2.1.10 Kits

Table 12: Kits

Name	Source
GeneJET Plasmid Miniprep Kit	Thermo Fisher Scientific
PureLink HiPure Plasmid Maxiprep Kit	Invitrogen by Thermo Scientific
NucleoSpin Gel and PCR Clean-up Kit	Macherey-Nagel

2.1.11 Antibiotics

Table 13: Antibiotics

Antibiotic	Stock concentration	Working concentration
Ampicillin	100 mg/ml	100 µg/ml
Kanamycin	50 mg/ml	50 µg/ml
Hygromycin	41 µg/ml	400 µg/ml; 1000 µg/ml
Doxycycline	2 mg/ml	2 µg/ml

2.2 Methods

2.2.1 Methods in molecular biology

2.2.1.1 Polymerase chain reaction (PCR) and site-directed mutagenesis

To perform site directed mutagenesis or cloning, the polymerase chain reaction (PCR) method was applied for DNA amplification. DNA was amplified with forward and

reverse primers containing specific restriction enzymes sequences. This allowed for the insertion of the DNA sequence into a new backbone after digestion with respective enzymes. For DNA sequences that already carried correct restriction enzyme sites, the plasmid containing the DNA sequence was digested with respective enzymes and cloned into a new backbone. Site-directed mutagenesis for insertion of point mutations or generation of deletion constructs was performed via the protocol described in (Heckman and Pease, 2007). To generate siRNA-resistant plasmids Flag-USP11^{WT} siRes and Flag-USP11^{C318S} siRes, the siUSP11 #1 target sequence (Jurga et al., 2021) in the original Flag-USP11^{WT} and Flag-USP11^{C318S} plasmids was mutated by introducing synonymous substitutions at every third base pair to preserve the amino acid sequence. Specifically, the original siUSP11 #1 target sequence, GGACCGTGATGATATCTTC, was altered to AGATCGAGACGACATATTT. A DNA fragment containing this siRNA-resistant sequence was synthesized by GenScript and cloned into the original plasmids using ScaI/XhoI restriction sites for Flag-USP11$^{WT\ siRes}$ and ScaI/HindIII sites for Flag-USP11$^{C318S\ siRes}$.

PCR reactions were carried out using Platinum™ SuperFi II DNA Polymerase (Thermo Fisher Scientific; Cat#: 12361250) or Platinum™ SuperFi™ PCR Master Mix (Thermo Fisher Scientific; Cat#: 12358010) according to manufacturer's orders. Briefly, reactions were set-up as described below:

For Platinum™ SuperFi™ DNA Polymerase:	
Platinum™ SuperFi™ DNA Polymerase	1x
Template DNA	100-200 ng
Forward primer	0.5 µM
Reverse primer	0.5 µM
5x SuperFi™ II Buffer	1x
Nuclease-free H_2O	ad to desired end volume

For Platinum™ SuperFi™ PCR Master Mix:	
2x Platinum™ SuperFi™ PCR Master Mix	1x
Forward primer	0.5 µM
Reverse primer	0.5 µM
Nuclease-free H_2O	ad to desired end volume

PCR reactions were carried out in a thermocycler (Eppendorf) with settings as described below:

Initial denaturation	98 °C	4 min	
Denaturation	98 °C	1 min	x 35
Annealing	60 °C	1 min	
Elongation	72 °C	1 min/ kb	
Final elongation	72 °C	10 min	
Cooling	4 °C		

Platinum™ SuperFi II DNA Polymerase or Platinum™ SuperFi™ PCR Master Mix allows for a constant annealing temperature of 60 °C regardless of the primers' melting temperatures. Depending on the length of the final PCR product, the elongation time was adjusted accordingly. For analysis of the final PCR products, agarose gel electrophoresis was performed as described in 2.2.1.2. PCR products were purified using the NucleoSpin Gel and PCR Clean-up Kit (Macherey-Nagel) as described in 2.2.1.3.

2.2.1.2 Agarose gel electrophoresis

To separate DNA fragments according to their size, agarose gel electrophoresis was performed. To prepare 0.5 – 1.5 % agarose gels, the respective amount of agarose was boiled in 1x TAE buffer until completely dissolved. After cooling down of the agarose solution to around 50 °C, 0.05 % StainIN RED Nucleic Acid Stain was added to visualize DNA fragments. The agarose solution was poured into a gel chamber, left to polymerize and transferred into an electrophoresis chamber (Bio-Rad). The gel was covered with 1x TAE buffer and DNA samples were prepared for loading. Briefly, DNA samples were mixed with 6x DNA sample buffer (final concentration: 1x) and loaded into gel-wells. According to the DNA fragment size, a 100 bp or 1 kb DNA ladder was added as a size reference in a separate well. Agarose gels were run at 100-120 V until desired band separation was achieved. For visualization of separated DNA bands, the agarose gel was placed under UV light at 366 nm wavelength.

2.2.1.3 Extraction of DNA fragments from agarose gels

After visualization of DNA fragments in agarose gel using UV light at 366 nM, correct DNA fragments were cut out with a scalpel and transferred to a reaction tube. The NucleoSpin Gel and PCR Clean-up Kit (Macherey-Nagel) was used according to the manufacturer´s instructions to extract the DNA fragments from cut-out gel pieces. DNA was eluted with 20-50 µl ddH_2O and DNA concentration was determined using a NanoDrop spectrophotometer as described in 2.2.1.7.

2.2.1.4 Restriction digest of DNA

If required, DNA or purified PCR products were digested with respective pairs of restriction enzymes (NEB) depending on the available restriction sites. 1 – 5 µg of plasmid DNA or PCR product was digested using 1 – 3 µl of each restriction enzyme in a total reaction volume of 20 – 50 µl. The volume of restriction enzyme never exceeded 10% of the final volume. For successful digestion, reactions were incubated for 2 hours at 37 °C and enzymes were heat-inactivated at 65 °C for 10 minutes. If required, digested DNA fragments were separated by agarose gel electrophoresis as described in 2.2.1.2 and correct fragments were extracted from the agarose gel as described in 2.2.1.3.

2.2.1.5 Ligation of DNA fragments

For cloning purposes, digested and purified DNA fragments were combined with desired backbone DNA for ligation. 100-200 ng of linearized backbone and threefold molar amount of digested insert were mixed with 10x T4 DNA ligase buffer (Thermo Fisher Scientific, final concentration 1x) and 1U of T4 DNA ligase (Thermo Fisher Scientific) at a final volume of 20 µl. The ligation reaction took place at 22 °C for 1h. For heat-inactivation of enzymes, the reaction was additionally incubated for 10 minutes at 65 °C. Chemically competent *E. coli* Top 10 or Rosetta (DE3) were transformed using 10 µl of the final ligation reactions as described in 2.2.1.6.

2.2.1.6 Transformation of chemically competent *E. coli*

Plasmid DNA or ligations were transformed into chemically competent *E. coli* Top 10 or Rosetta (DE3) for plasmid amplification or cloning purposes. Briefly, bacteria were

thawed on ice and 50 µl of competent *E. coli* were gently mixed with 100 ng of plasmid DNA or 10 µl of ligation reaction. Bacteria were incubated on ice for 20 minutes and heat-shocked for 45 seconds at 42 °C. Bacteria were immediately placed back on ice and incubated for further 5 minutes. 950 µl of LB medium was added to bacteria and an incubation period of 1 hour at 37 °C with constant shaking at 500-650 rpm followed. For plasmid amplification, 100 µl of bacterial suspension was spread on an LB agar plate containing the respective antibiotic for selection. For cloning purposes, bacteria in solution were first pelleted at 5000 g for 2 minutes and the pellet was resuspended in 100 µl of LB medium before being spread onto an LB agar plate with appropriate antibiotic for selection. LB plates were incubated overnight at 37 °C top-down. On the next day, single colonies were picked and inoculated in LB medium with respective antibiotic to grow overnight cultures.

2.2.1.7 Plasmid DNA preparation from *E. coli*

Overnight cultures of *E. coli* Top 10 or Rosetta (DE3) previously transformed with plasmid DNA were grown in LB medium containing the appropriate antibiotic at 37 °C and 180 rpm. Bacterial cells were pelleted at 5000 g and 4 °C for 25-30 min. According to the culture volume, plasmid DNA was isolated from *E. coli* using the GeneJET Plasmid Miniprep Kit (Thermo Fisher Scientific) or PureLink HiPure Plasmid Maxiprep Kit (Invitrogen) according to the manufacturer´s instructions. Elutions were performed with ddH_2O.

2.2.1.8 Measurement of DNA concentration

A NanoDrop ND-1000 spectrophotometer (Peqlab) was used to determine DNA concentration and purity. The optical density of the sample was measured at 230 nm, 260 nm and 280 nm wavelength after previously using ddH_2O as a blank. The DNA concentration was determined based on the absorbance at 260 nm, while $OD_{260\ nm} = 1$ corresponds to a DNA concentration of 50 µg/ml. Ratios of $OD_{260\ nm}$ /$OD_{280\ nm} \sim 1.8$ and $OD_{260\ nm}$ /$OD_{230\ nm}$ between 1.8 and 2.2 indicated high purity of the DNA solution. To make sure that plasmid DNA was cloned correctly, samples of cloned DNA plasmids were sequenced at LGC Genomics, Berlin, Germany.

2.2.2 Methods in cell biology

2.2.2.1 Cell culture

HEK 293T, HEK 293T ΔFBXO45, HeLa, U2OS, and U2OS Flp-In-T-REX MYC-SPRYD3 cells were cultured in Dulbecco's Modified Eagle's Medium (DMEM) with 4.5 g/L glucose (Gibco; Cat# 41965-039), supplemented with 10% fetal bovine serum (FBS) (Gibco; Cat# 10270-106) and 1% Penicillin-Streptomycin (Sigma-Aldrich; Cat# P0781). Cells were maintained at 37 °C in a humidified atmosphere with 5% CO_2.
hTERT RPE1 cells were cultured in Dulbecco's Modified Eagle's Medium/Nutrient Mixture F-12 Ham (Sigma-Aldrich; Cat# D8900) supplemented with 15 mM HEPES, sodium bicarbonate, 10% FBS, and 1% Penicillin-Streptomycin under the same incubation conditions.
For passaging, culture medium was removed and cells were washed once with 1× PBS. Cells were detached by incubation with 0.05% Trypsin-EDTA at 37 °C for 3–5 minutes, depending on the cell line. Detached cells were resuspended in fresh growth medium and diluted to the desired density in new culture dishes. All cell culture procedures were conducted under sterile conditions. Cell line identities were regularly verified by authentication (Multiplexion, Heidelberg).

2.2.2.2 Freezing and harvesting of cells

For long term storage, cells were frozen in cryo-vials. In order to do so, medium was removed from cell culture dishes and cells were washed one time with 1x PBS. To detach them from the cell culture dish surface, cells were incubated with 0.05% Trypsin-EDTA at 37 °C for 3-5 minutes according to the cell line. Trypsinization was stopped by resuspending cells in fresh growth medium. Resuspended cells were pelleted by centrifugation at 330 g for 3 min. Pellets were resuspended in growth medium and supplemented with additional 10% FBS and 10% DMSO. Cell suspensions were transferred to 1.5 ml cryo-vials and frozen in a freezing container (Nalgene by Thermo Fisher Scientific) at – 80 °C, where they were also kept for short term storage; for long term storage they were transferred to liquid nitrogen tanks.
For cell harvest, medium was removed from cell culture dishes and cells were washed one time with 1x PBS. 0.05% Trypsin-EDTA was used to detach cells from cell culture dish surfaces as described above. All cell lines, except HEK 293T and HEK 293T ΔFBXO45, were resuspended in fresh growth medium and transferred to tubes. HEK

293T and HEK 293T ΔFBXO45 cells were harvested by gentle scraping in 1x PBS. Cells were pelleted by centrifugation at 330 g for 5 min. Cell pellets were used for preparation of protein lysates immediately or stored at -20 °C for short-term storage or at – 80 °C for long-term storage.

2.2.2.3 Transfection of mammalian cells

2.2.2.3.1 Plasmid DNA transfection using polyethylenimine (PEI)

HEK 293T or HEK 293TΔFBXO45 cells were transiently transfected with plasmid DNA in 10 cm or 15 cm cell culture dishes using polyethylenimine (PEI, Polysciences). Cells were seeded one day prior to transfection so that a confluency of 60-70% was reached on the next day. For preparation of transfection mixtures, 5-15 µg of plasmid DNA was diluted in 1 ml DMEM (w/o FBS, w/o Penicillin-Streptomycin) containing 30 µl (10 cm dish) or 92.5 µl (15 cm dish) of PEI (1mg/ml stock solution). The mixtures were incubated for 10 min at room temperature (RT). Meanwhile, old growth medium was removed from cells and 9 ml or 15 ml of fresh DMEM (+5% FBS, w/o Penicillin-Streptomycin) was added. The transfection mixtures were added to cells and incubated for 24h or 48 hours at 37 °C and 5% CO_2. If cells were incubated for longer than 24h, transfection mixtures were replaced with fresh growth medium 24h after transfection. Cells were then either harvested or treated with 10 µM MG132 for 5h prior to harvest.

2.2.2.3.2 Plasmid DNA and siRNA transfection using Lipofectamine 2000 or RNAiMAX

U2OS and HeLa cells were transfected with plasmid DNA using Lipofectamine 2000 (Invitrogen; Cat#: 11668019) according to manufacturer's orders. Briefly, cells were seeded on cover slips in 6-well plates, 6-well plates without cover slips or in 10 cm culture dishes one day prior to transfection so that a confluency of 70-80 % was reached on the next day. For preparation of transfection mixtures, 2 or 6 µg of DNA and 4 or 12 µl of Lipofectamine 2000 were diluted separately in 100 µl Opti-MEM (Gibco; Cat#: 31985070). Both mixtures were combined and incubated for 10 minutes at room temperature. Meanwhile, old growth medium was removed from cell culture dishes containing cells and replaced with 1,8 ml (6-well plates) or 4,8 ml (10 cm dishes) DMEM (+5 % FBS, w/o Penicillin-Streptomycin). The transfection mix was added

droplet-wise. 6h after transfection, the medium containing transfection mixture was replaced by fresh complete DMEM. For transfection of U2OS with siRNA and siRNA-resistant DNA plasmids, cells were seeded on cover slips in 6-well plates at a confluency of 60-70%. siRNAs targeting GL2 or USP11 were transfected at a concentration of 50 nM using Lipofectamine RNAiMAX as described above. 6h after the first transfection, a second round of siRNA transfection followed. 24h after the first siRNA-transfection, cells were transfected with 2µg of siRNA-resistant plasmids using Lipofectamine 2000 as described above and left incubating for further 24h. U2OS cells were then harvested or underwent the IF protocol as described in section 2.2.2.7. HeLa cells were harvested 24h after transfection.

HeLa, U2OS, HEK 293T and RPE1 cells were transfected with siRNA using Lipofectamine RNAiMAX (Invitrogen; Cat#: 13778150) and Opti-MEM according to manufacturer's orders. Briefly, cells were seeded on cover slips in 6-well plates, in 6-well plates without cover slips or 10 cm culture dishes one day prior to transfection so that a confluency of 60-70 % was reached on the next day. 2, 4 or 5 µl of siRNA from 20 µM stocks and 2 or 4 µl of Lipofectamine RNAiMAX were diluted separately in 100 µl Opti-MEM (w/o FBS, w/o Penicillin-Streptomycin). Mixtures were combined and incubated at room temperature for 10 minutes. Meanwhile, old growth medium was removed from cell culture dishes containing cells and replaced with 1,8 ml (6-well plates) or 4,8 ml (10 cm plates) DMEM (+ 5% FBS, w/o Penicillin-Streptomycin). The transfection mixture was added droplet-wise, giving rise to a final siRNA concentration of 20, 40 or 50 nM. siRNA transfection was repeated again 6h or 24h after the first siRNA transfection. If the second transfection was carried out after 24h, transfection medium was replaced with fresh growth medium 6h after the first transfection. In case of RPE1 and U2OS cells, cells were either harvested 72h after the first siRNA transfection for cell lysate preparation as described in 2.2.3.1 or further used for immunofluorescence purposes as described in section 2.2.2.7 In case of HEK 293T cells, cells were transfected with DNA 6h after the second siRNA transfection as described in 2.2.2.3.1 and incubated in total for 72h after the first siRNA transfection. Cells were then either harvested or treated with 10 µM MG132 (Sigma-Aldrich; CAS#: 133407-82-6 for 5h prior to harvest. HeLa cells were harvested for protein lysate preparation as described in 2.2.3.1.

2.2.2.4 Generation of stable U2OS cell lines with inducible MYC-SPRYD3 expression

U2OS T-Rex inducible cell lines were generated following the manufacturer's instructions (Thermo Fisher Scientific). U2OS Flp-In-T-Rex (J.D. Pravin, Ohio State University) were seeded in 6-well plates one day prior to transfection so that they reached a confluency of 60-70% on the next day. Cells were transfected with 1.8 µg pOG44 Flp-Recombinase and 0.2 µg pcDNA5-FRT-TO-MYC-SPRYD3 using Lipofectamine 2000 as described in 2.2.2.3.2. Transfection mixtures were prepared by diluting plasmid DNA and Lipofectamine 2000 in 125 µl fresh DMEM (w/o FBS, w/o Penicillin-Streptomycin). 1.75 ml of fresh DMEM (+ 5% FBS, w/o penicillin-streptomycin) was added to cells prior to addition of the transfection mix. Cells were incubated with transfection mixtures for 24h and passaged to 10 cm dishes. After 48h, antibiotic selection was carried out with 400 µg/ml Hygromycin B for three days. This was followed by two antibiotic selection rounds with 1000 µg/ml Hygromycin B for two days each. Remaining cells were cultured in fresh complete growth medium for seven days and single colonies were picked by scraping with 10 µl pipette tips. Picked colonies were transferred to 24-well plates and passaged to larger dishes before reaching confluency. The expression of MYC-SPRYD3 was tested by incubation with 2 µg/ml Doxycycline (Sigma-Aldrich; CAS#: 10592-13-9) for 48-72h and consequent SDS-PAGE and western blot analysis.

2.2.2.5 Treatment of cells with MG132 and cycloheximide

HEK 293T WT or HEK 293T ΔFBXO45 cells were treated with 10 µM proteasome inhibitor MG132 for 5 h previous to harvest. U2OS and RPE1 cells were treated with 5 µM MG132 90 minutes prior to methanol fixation and immunofluorescence staining. Cycloheximide chases were performed in U2OS or U2OS Flp-In-T-REX MYC-SPRYD3 cells using 100 µg/ml cycloheximide for the indicated time periods.

2.2.2.6 Live cell imaging

Normal cell division, mitotic slippage or mitotic cell death of U2OS or RPE1 cells was analyzed by live cell imaging. For mitotic slippage or cell death analysis, U2OS and RPE1 cells were transfected 24h and 48h after seeding with 20 nM siRNA targeting GL2, SPRYD3, MYCBP2 or USP11 as described in 2.2.2.3.2. 48h after the first siRNA

transfection, cells were seeded into 8-well imaging dishes (Sarstedt) at around 50-70% confluency. 72h after the first transfection, cells were treated with nocodazole (Merck; CAS#: 31430-18-9) (250 ng/ml for U2OS; 3.1 µM for RPE1) or paclitaxel (1 µM for U2OS; 5 µM for RPE1) and consequently placed in a microscopy incubation chamber at 5% CO_2 and 37 °C. For analysis of normal cell division, the same procedure as described above was applied, but microtubule poison treatment was left out.
Cells were imaged using a 10×/0.3 EC PlnN Ph1 DIC objective on a Zeiss Cell Observer Z1 inverted microscope equipped with an AxioCam MRm camera system. Phase-contrast images of multiple fields were captured every 10 minutes for up to 60h using Zeiss ZEN Blue software. Mitotic cell fates and unperturbed mitosis were analyzed with ImageJ Fiji. Cell death was identified based on morphological changes, while mitotic slippage was defined as mitotic exit without preceding cell division. Normal cell division was classified as unperturbed mitosis. To measure mitotic timing in untreated dividing cells, the onset of mitosis was determined by the appearance of rounded cell morphology, and cytokinesis was designated as the endpoint of mitosis.

2.2.2.7 Immunofluorescence staining and microscopy

For analysis of aberrant spindles, U2OS and RPE1 cells were seeded and grown on glass coverslips and transfected with either 50 nM siRNA or 2 µg of DNA or both as described in 2.2.2.3.2. In case of siRNA transfection and combined siRNA and DNA transfection, cells were treated with 200 ng/ml nocodazole 48h after the first siRNA transfection for additional 24h. In case of DNA transfection only, cells were treated 24h with the same amount of nocodazole 24h after DNA transfection. Cells were released from mitotic arrest by careful washing with 1x PBS for three times and a 90-minute treatment step with 5 µM MG132 followed (Stockum et al., 2018). Afterwards, cells were washed one time with 1x PBS and fixed with ice-cold methanol for 10 minutes at – 20 °C. Ice-cold methanol was added slowly and droplet-wise in order not to lose mitotic cells on cover slips. After fixation, cells were washed two times with 1x PBS. Incubation with respective primary and secondary antibodies previously diluted in PBS-BT was performed for 1h at room temperature. Three washing steps with 1x PBS-BT were carried out in between each incubation. After staining with secondary antibodies, coverslips were washed again with 1x PBS-BT and mounted onto microscope slides using ProLong™ Gold Antifade (Molecular Probes by Life Technologies) containing DAPI. Z-stack images of cells on cover slips were imaged using a 63x/1.4 Oil Pln Apo

DICII objective of the Zeiss Observer.Z1 inverted motorized microscope and images were processed using Fiji software with maximum intensity projection of Z-stack images (Schindelin et al., 2012).

2.2.3 Methods in protein biochemistry

2.2.3.1 Preparation of protein extracts from cells

In order to prepare protein extracts from cell pellets, cells were harvested as described in 2.2.2.2. For immunoprecipitations, cell pellets were resuspended in 1 ml NP-40 buffer. For direct SDS-PAGE and western blot analysis, 3-5 volumes of RIPA buffer were used for cell pellet resuspension. Cell lysis was performed by incubating pellet resuspensions for 30 min on ice. A centrifugation step at 16000 g and 4 °C for 15 minutes followed and supernatants were transferred to fresh tubes. For pull-down assays using Ni-NTA beads (Qiagen; Cat#: 30210), 8 M urea buffer was used to resuspend cell pellets. Lysis was achieved by sonication using a Branson Sonifier 250 at output 3 and 50 % cycle duty for 10-20 pulses. Lysates were centrifuged and cleared for 20 min at 16000 g and 4 °C. Bradford assay was performed to determine protein concentrations from obtained protein extracts as described in 2.2.3.2. Protein extracts were mixed with 2x Laemmli buffer and denatured for 5 minutes at 95 °C. Protein extracts were then analyzed by SDS-PAGE and western blot.

2.2.3.2 Determination of protein concentration by Bradford assay

To determine protein concentrations of protein extracts the Bradford method using the Bio-Rad Protein Assay was performed. 800 µl ddH_2O and 200 µl of assay dye were combined and 1 µl of protein extract was diluted in the resulting 1 ml solution. For generation of the standard curve, different amounts of BSA (stock: 1 mg/ml) were also diluted in 800 µl ddH_2O combined with 200 µl assay dye. Tubes containing solutions were inverted to allow for proper mixing and incubated for 5 minutes at RT. In order to determine the $OD_{595\ nm}$, 200 µl of each sample were transferred to a 96-well plate, which was inserted into a SPECTROstar nano microplate reader (BMG Labtech). To ensure exact measurements, all samples were prepared and measured in triplicates. The BSA standard curve was used to calculate protein concentrations of the protein extracts.

2.2.3.3 SDS polyacrylamide gel electrophoresis (SDS-PAGE)

In order to separate proteins according to their molecular weight (MW), SDS polyacrylamide gel electrophoresis (SDS-PAGE) was performed. For proteins with a MW under 300 kDa, polyacrylamide gels were prepared using the Mini-Protean vertical electrophoresis system (Bio-Rad). Gels consisted of a separating gel and a stacking gel on top. Depending on protein sizes, the separating gel contained 6 – 12 % acrylamide/bisacrylamide, 375 mM Tris-HCl pH 8.8, 0.1 % SDS, 0.1 % APS and 0.1 % TEMED. Stacking gels contained 5 % acrylamide/bisacrylamide, 125 mM Tris-HCl pH 6.8, 0.1 % SDS, 0.1 % APS and 0.1 % TEMED.

For the analysis of large proteins such as MYCBP2 (>500 kDa), Tris-acetate gels were prepared according to (Cubillos-Rojas et al., 2010). Separating gels contained a gradient and were prepared by mixing separating gel solutions containing 4 % or 8 % acrylamide/bisacrylamide, 200 mM Tris-acetate pH 7.0, 0.1% APS and 0.1% TEMED. After completion of polymerization, gels were transferred to SDS-PAGE chambers and filled with 1x SDS running buffer. Protein samples were loaded into gel-wells and a MW marker (neoLab) was loaded in a separate well serving as a size reference. Gels were run at a constant voltage of 50 – 120 V until desired molecular weight separation was achieved.

2.2.3.4 Western blot

After separation by SDS-PAGE, proteins were transferred to nitrocellulose membranes by western blotting using the Trans-Blot Turbo semi-dry system (Bio-Rad). Transfer of MYCBP2 from Tris-acetate gels was performed using a wet blot chamber (Mini Trans-Blot Cell, Bio-Rad) and wet blot buffer. Semi-dry blots were run at 2.5 A for 15 minutes and wet blots were run at 200 mA for two hours at 4 °C in Tris-Bicine buffer.

In order to assess transfer quality, nitrocellulose membranes containing transferred proteins were stained using Ponceau S solution. If transfer was successful, membranes were blocked in 5% milk powder in PBS-T at RT for approximately 15-30 minutes, shaking. Proteins of interest were detected by incubation with primary antibodies at desired dilutions overnight at 4 °C, shaking. Membranes were washed three times with 1x PBS-T at RT for 5-10 minutes. Species-specific HRP-conjugated secondary antibodies were diluted in fresh blocking buffer and membranes were

incubated for further 1-2h at RT, shaking. For removal of excess secondary antibodies, membranes were washed three times with 1x PBS-T for 5-10 minutes. Signal detection was achieved with Immobilon Western Chemiluminescence HRP-substrate (Merck) according to the manufacturer's instructions. Signals were detected in an ImageQuant LAS 4000 (GE) and image processing and quantifications were performed using ImageJ Fiji (Schindelin et al., 2012).

2.2.3.5 Immunoprecipitation assays

2.2.3.5.1 Immunoprecipitation of Flag-tagged proteins using Flag M2 affinity beads with or without λ-phosphatase treatment

Flag-tagged proteins were immunoprecipitated using α-Flag M2 beads (Sigma-Aldrich; Cat#: A2220*).* Cell lysates were prepared with NP-40 buffer as described in 2.2.3.1. 20-25 µl of Flag M2 affinity gel (Sigma-Aldrich; Cat#: A2220) was used for each sample and equilibrated in batch by washing two times with 1xTBS*,* one time with glycine-HCl (0.1 M, pH 3.5) and again two times with 1xTBS. Centrifugation steps at 5000 g and 4 °C for 2 minutes were performed in between each washing step. After resuspension in NP-40 buffer, beads were added to 5-15 mg of protein extract. If needed, sample volumes were equalized by adding NP-40 buffer. Immunoprecipitations (IPs) were incubated for at least 3h or overnight at 4 °C on a rotating wheel. Flag-M2 beads were washed 3 times with NP-40 buffer. For elution of bound proteins, beads were incubated for 30 minutes on ice with 50 µl of NP-40 buffer containing 200 ng/µl 3x Flag peptide (Thermo Fisher Scientific; Cat#: A35805). Beads were pelleted by centrifugation for 2 min at 5000 g and 4 °C and supernatants were transferred to fresh tubes. Supernatants were mixed with 2x Laemmli buffer and denatured at 95 °C for 5 minutes followed. IP samples were analyzed by SDS-PAGE and western blot.

For dephosphorylation of Flag-SPRYD3-XIAP complexes, Flag-IPs were performed as described above, but treated with λ-phosphatase previous to elution from Flag-M2 beads. Briefly, IP samples were washed 3 times with NP40 special buffer and incubated with λ-phosphatase in presence of 10x PMP (final conc.: 1x) buffer and 10x MnCl2 (final conc.:1x) for 30 minutes at 30 °C. IP samples were then washed 3 times with normal NP40 buffer, followed by the elution steps described above.

2.2.3.5.2 Consecutive immunoprecipitation of Flag- and MYC-tagged proteins using Flag M2 affinity beads and MYC-antibody

In order to analyze if MYCBP2, SPRYD3 and FBXO45 were part of the same complex, consecutive IPs were performed. Previous to harvest, 10 µM MG132 was added to cells for 5 hours in order to stabilize a potential complex between the afore-mentioned proteins. Flag-tagged proteins were immunoprecipitated using α-Flag M2 beads as described previously in section 2.2.3.5.1. Bound proteins were eluted in 100 µl NP40-buffer containing 200 ng/µl 3x Flag peptide. NP-40 buffer was added to reach a final volume of 400 µl and eluates were subjected to a consecutive IP using α-MYC-tag antibody (Santa Cruz Biotechnologies) in order to precipitate MYC-tagged proteins. 15 µg of α-MYC-tag antibody was added to each of the eluates and left incubating over-night on a rotating wheel at 4 °C. At the same time, 20 µl of protein G sepharose beads (GE Healthcare) per IP were equilibrated in batch by washing two times in 1x PBS and with centrifugation at 4000 g for two minutes at 4 °C between each washing step. They were incubated overnight in 1 ml 0.1 % BSA in 1xPBS on a rotating wheel at 4 °C. On the next day, protein G sepharose beads were washed two times in 1x PBS with centrifugation steps in between at 4000 g for 2 minutes at 4 °C. Beads were resuspended in NP-40 buffer and added to α-MYC-tag IPs, which were incubated for further 2-3 hours on a rotating wheel at 4 °C. Bound complexes were eluted through addition of 50 µl of 2x Laemmli buffer with following denaturation at 95 °C for 5 minutes. Beads were pelleted and supernatants were transferred to fresh tubes and consequently analyzed by SDS-PAGE and western blot.

2.2.3.5.3 Immunoprecipitation of GFP-tagged proteins using GFP-trap affinity beads

GFP-tagged proteins were pulled down using GFP-trap affinity beads. Protein lysates were prepared using NP-40 buffer as described previously in section 2.2.3.1. 15-20 µl bead slurry was used for each sample and equilibrated in batch by washing one time with ddH_2O and two times with NP-40 buffer. A centrifugation step at 5000 g and 4 °C for 2 minutes was performed in between each equilibration step. Equilibrated beads were resuspended in NP-40 buffer and added to 5-15 mg of protein lysate. If necessary, sample volumes were equalized by adding NP-40 buffer. IPs were

incubated for at least 3h or over-night at 4 °C on a rotating wheel. After incubation, beads were washed three times with NP-40 buffer. Bound proteins were eluted by incubation with 50 µl 2x Laemmli buffer for 10 min at 95 °C. Beads were pelleted and supernatants were transferred to fresh tubes. Supernatants were analyzed by SDS-PAGE and western blot.

2.2.3.6 *In vivo* ubiquitylation assays

Flag-IP or Ni-NTA pulldown assays with subsequent western blot analysis were performed for analysis of USP11, XIAP, CHAMP1 or RAE1 ubiquitylation by MYCBP2-SPRYD3. For the Flag-IP assay, Flag-USP11 or point mutants, MYC-MYCBP2 WT / MYC-MYCBP2 C4520S / MYC-MYCBP2 3601-4640 or MYC-SPRYD3 / MYC-SPRYD3ΔSPRY1 / MYC-SPRYD3ΔSPRY2 and HA-tagged Ubiquitin WT or point mutants K48R/K63R were co-expressed in HEK 293T WT or ΔFBXO45 cells for 24h or 48h. Flag-XIAP was co-expressed with MYC-SPRYD3 or MYC-MYCBP2 and HA-Ubiquitin in HEK 293T WT or ΔFBXO45 cells for 24h or 48h. For GFP-pulldown assays, GFP-CHAMP1 was co-transfected with Flag-SPRYD3 and HA-Ubiquitin in HEK 293T WT or ΔFBXO45 cells for 24h. GFP-RAE1 was co-transfected with MYC-SPRYD3 or MYC-MYCBP2 WT and HA-Ubiquitin for 24h or 48h.

If cells were incubated for longer than 24h, transfection mixtures were replaced with fresh growth medium after 24h of transfection. Cells were transfected as described in 2.2.2.3.1 and treated with 10 µM MG132 (Sigma-Aldrich) 5 h previous to harvest. Protein extracts were prepared as described in 2.2.3.1 using NP-40 buffer additionally supplemented with 20 mM N-ethylmaleimide (NEM). Flag-USP11, Flag-XIAP, GFP-CHAMP1 or GFP-RAE1 were pulled down as described in 2.2.3.5.1 and 2.2.3.5.3. For all washing steps, NP-40 buffer supplemented with 20 mM NEM was used. Eluted proteins were mixed with 2x Laemmli buffer +/- 1 M DTT and denatured for 5 min at 95 °C. Sample analysis was performed via SDS-PAGE and western blot.

For the Ni-NTA pulldown assays, MYC-USP11, Flag- MYCBP2 3601-4640 or Flag-SPRYD3 and His-Ubiquitin were co-expressed in HEK 293T cells for 24h after previous siRNA treatment as described in sections 2.2.2.3.1 and 2.2.2.3.2. 5h previous to harvest, cells were treated with 10 µM MG132 and protein extracts were prepared as described in 2.2.3.1 using 8 M Urea buffer supplemented with 20 mM NEM and sonication. Per sample, 40 µl suspension of Ni-NTA beads (Qiagen; Cat#: 30210) was used. For equilibration, beads were washed in batch one time with ddH_2O and two

times with 8 M Urea buffer supplemented with 20 mM NEM. Centrifugation steps at 7000 g and 4 °C for 2 min were carried out in between each equilibration step. Equilibrated Ni-NTA beads were resuspended in Urea buffer and added to 5-15 mg of each protein extract. Samples containing Ni-NTA beads were incubated for 3-4h at room temperature on a rotating wheel. Afterwards, beads were washed three times in 8 M Urea buffer supplemented with 0.1 % Triton X-100. For elution, 50 µl of 2x Laemmli buffer supplemented with 200 mM imidazole was added to beads and incubated for 10 min at RT. After centrifugation, supernatants containing precipitated proteins were taken off, transferred to fresh tubes and denatured at 95 °C for 5 minutes. Samples were analyzed by SDS-PAGE and western blot.

2.2.3.7 *In vitro* ubiquitylation assay

To analyze direct ubiquitylation of recombinantly expressed HIS-USP11 by MYCBP2-SPRYD3, *in vitro* ubiquitylation assays with purified recombinant proteins and SPRYD3-MYCBP2 E3 ligase complex precipitated from HEK 293T cells were performed. Flag-SPRYD3 or Flag-SPRYD3ΔSPRY2 were co-expressed with MYC-MYCBP2 WT or MYC-MYCBP2 C4520S for 48h as described in 2.2.2.3.1. Protein extracts were prepared as described in 2.2.3.1 and Flag-SPRYD3 or Flag-SPRYD3ΔSPRY2 was immunoprecipitated as described in 2.2.3.5.1. Bound protein complexes were washed four times with NP-40 buffer and equilibrated two times in ubiquitin assay reaction buffer (50 mM Tris-HCl, pH 7.5, 100 mM NaCl, 10 mM $MgCl_2$, 0.05%, 1 mM DTT, 0.1 mM Na_3VO_4, 1 µg/ml aprotinin, 1 µg/ml leupeptin,10 µg/ml trypsin inhibitor from soybean and 1 mg/ml BSA with final concentration of 1:20). Bound protein complexes were washed four times with NP-40 buffer and subsequently equilibrated twice in ubiquitin assay reaction buffer (50 mM Tris-HCl, pH 7.5; 100 mM NaCl; 10 mM $MgCl_2$; 0.05% NP-40; 1 mM DTT; 0.1 mM Na_3VO_4; 1 µg/ml aprotinin; 1 µg/ml leupeptin; 10 µg/ml soybean trypsin inhibitor; and 1 mg/ml BSA at a final dilution of 1:20). Bound E3 ligase complexes were eluted from beads in 100 µl ubiquitin assay buffer containing 200 ng/µl 3x Flag peptide. HIS-UBA1, ubiquitin, GST-UBCH5b, and ATP were kindly provided by Frauke Melchior (University of Heidelberg).

For the *in vitro* ubiquitylation reactions, 10 µl of the eluted E3 ligase complex was combined with 200 nM HIS-USP11, 170 nM HIS-UBA1, 80 µM ubiquitin, 250 nM GST-UBCH5b, and 5 mM ATP in a total volume of 20 µl ubiquitin assay buffer. Samples were incubated at 37 °C with shaking at 550 rpm for either 0 or 60 minutes using an

Eppendorf Thermomixer Comfort 5355. Reactions were terminated by adding 2× Laemmli buffer and denaturing the samples at 95 °C for 5 minutes. Proteins were then resolved by SDS-PAGE and analyzed by western blotting.

2.2.3.8 Bacterial expression and purification of recombinant GST-, MBP- and His-tagged proteins

The plasmids pGEX4T1-GST-MYCBP2 2550–2825 and pGEX4T1-GST-USP11 were transformed into competent *E. coli* Rosetta (DE3) cells as described in section 2.2.1.6. A single colony from each transformation was used to inoculate 10 ml LB medium supplemented with 100 µg/ml ampicillin. Cultures were incubated overnight at 37 °C with shaking at 180 rpm. Subsequently, 4 ml of the overnight culture was used to inoculate 400 ml LB medium containing 100 µg/ml ampicillin. When the culture reached an OD600 of 0.5, it was cooled on ice for 10 minutes and protein expression was induced by adding 400 µM isopropyl β-D-1-thiogalactopyranoside (IPTG). Cultures were incubated overnight at 18 °C with shaking at 180 rpm. Bacterial cells were harvested by centrifugation at 5000 rpm and 4 °C for 30 minutes (F10-6 x 500Y rotor, Piramoon), and pellets were stored at –80 °C for at least 4 hours. Thawed pellets were resuspended in protein purification buffer and lysed by sonication. Lysates were cleared by centrifugation at 1300 rpm and 4 °C for 30 minutes (F28/50 rotor, Sorvall, DuPont). Glutathione Sepharose™ 4B beads (Cytiva) equilibrated in 10 ml lysis buffer were added to the cleared lysates containing GST-MYCBP2 2550–2825 or GST-USP11 and incubated with rotation at 4 °C for 2 hours. Beads with bound GST-fusion proteins were washed three times with 10 ml washing buffer. Proteins were eluted by incubation with elution buffer, collecting nine fractions of 600 µl each. Protein-containing fractions were identified by spotting 1 µl on nitrocellulose membranes followed by Amido Black staining. Positive fractions were pooled and dialyzed overnight in 1 L dialysis buffer with gentle stirring at 4 °C. Dialyzed proteins were analyzed by SDS-PAGE and colloidal Coomassie staining, aliquoted, snap-frozen in liquid nitrogen, and stored at –80 °C.

The pMal-c2-MBP-SPRYD3 plasmid was transformed into competent *E. coli* Rosetta (DE3) cells as described in section 2.2.1.6. A single colony was inoculated into 10 ml LB medium with 100 µg/ml ampicillin. Protein expression was induced with IPTG, and cultures were incubated overnight at 18 °C with shaking at 180 rpm. Cells were harvested by centrifugation at 5000 rpm and 4 °C for 30 minutes, and pellets were

frozen at –80 °C for at least 2 hours. Pellets were resuspended in 20 ml cold column buffer and lysed by sonication using a Branson Sonifier 250. Lysates were cleared by centrifugation at 1300 rpm and 4 °C for 30 minutes. Amylose resin (New England BioLabs) was equilibrated by washing twice with cold column buffer and then incubated with the cleared lysate containing MBP-SPRYD3 for 2 hours at 4 °C with rotation. Resin-bound MBP-SPRYD3 was washed three times with 5–10 ml cold column buffer and eluted with elution buffer in nine fractions of 500 µl each. Protein-containing fractions were pooled and dialyzed overnight at 4 °C in cold 1× PBS containing 5 mM β-mercaptoethanol with gentle stirring. The dialyzed protein was analyzed by SDS-PAGE and colloidal Coomassie staining, aliquoted, snap-frozen in liquid nitrogen, and stored at –80 °C.

pET28a(+)-HIS-USP11 and pET28a(+)-HIS-MYCBP2 2550-2825 plasmids were transformed into competent *E. coli* Rosetta (DE3) as described in 2.2.1.6 and one clone of each transformation was used to inoculate 10 ml LB containing 100 µg/ml kanamycin. Protein production was induced with IPTG and cultures were incubated overnight at 18 °C shaking at 180 rpm. Cells were harvested as described above and cell pellets were resuspended in 20 ml lysis buffer. The lysis solution was rotated at 4 °C for 30 minutes. Lysis was performed by sonication. Samples were centrifuged and cleared at 13000 rpm at 4 °C for 20 minutes. Ni-NTA agarose was equilibrated two times with lysis buffer and added to supernatants containing HIS-USP11 or HIS-MYCBP2 2550-2825. Mixtures were rotated for 2h at 4 °C. Beads with bound HIS-USP11 or HIS-MYCBP2 2550-2825 were washed two times with lysis buffer and elution was performed by adding elution buffer. 9 fractions of 500 µl each were collected. Protein containing fractions were pooled and dialyzed three times in 1 l cold 1x PBS for 1 hour each with gentle stirring at 4 °C. Dialyzed HIS-USP11 or HIS-MYCBP2 2550-2825 was analyzed by SDS-PAGE and colloidal Coomassie staining, aliquoted, frozen in liquid nitrogen and consequently stored at -80 °C.

2.2.3.9 MBP pull-down assay

To demonstrate a direct interaction between SPRYD3 and MYCBP2 or between SPRYD3 and USP11, 10 µg of MBP-SPRYD3 or an equimolar amount of empty MBP was mixed with 10 µg of HIS-MYCBP2 2550–2825, GST-MYCBP2 2550–2825, or GST-USP11 in 500 µl NP-40 buffer. The recombinant protein mixtures were incubated with rotation at 4 °C for 1h. Meanwhile, 10 µl of amylose resin per sample were

equilibrated by washing twice with NP-40 buffer. The resin was then resuspended in NP-40 buffer and added to the protein mixtures. These mixtures were rotated at 4°C for 2h, followed by five washes with NP-40 buffer. Protein complexes bound to the amylose resin were eluted by incubation with 30 µl of 2× Laemmli buffer for 5 minutes at 95 °C. Samples were subsequently analyzed by SDS-PAGE and western blotting.

2.2.3.10 Mass spectrometrical analysis

To identify potential interactors and/or substrates of FBXO45 or SPRYD3, 10 µg of Flag-tagged empty vector (EV, control), Flag-FBXO45, or Flag-SPRYD3 plasmids were transfected into HEK 293T WT cells, cultured in 3–4 15-cm dishes per condition. Expression was carried out for 24–30h prior to harvest. Cells were pooled and lysed using NP-40 lysis buffer. Immunoprecipitation (IP) of Flag-tagged proteins was performed as previously described, with the following modifications: 20–25 mg/ml of protein lysate was incubated with 80 µl of Flag-M2 affinity beads overnight at 4 °C. Bound proteins were eluted using 70 µl of 3x Flag peptide (0.5 mg/ml) for 30 minutes on ice. Eluted samples were subsequently boiled in 2x Laemmli buffer at 95 °C for 5 minutes. A total of four biological replicates per condition were processed and submitted to the DKFZ proteomics facility (Heidelberg). The facility carried out mass spectrometry (MS) and data analysis, following their in-house protocol, which is described in the following paragraphs. They kindly provided the protocol Specifically, 35 µl of each eluate was loaded onto an SDS-PAGE gel and electrophoresed approximately 0.5 cm into the gel. The corresponding gel region was excised and subjected to in-gel tryptic digestion (Shevchenko et al., 2006), adapted for use with the DigestPro MSi robotic platform (INTAVIS Bioanalytical Instruments AG). Liquid chromatography-tandem mass spectrometry (LC-MS/MS) was performed using an Ultimate 3000 UPLC system (Thermo Fisher Scientific) coupled directly to an Orbitrap Exploris 480 mass spectrometer. Peptides were desalted online using a trapping cartridge (Acclaim PepMap300 C18, 5 µm, 300 Å) with a flow rate of 30 µl/min of 0.05% trifluoroacetic acid (TFA) in water for 3 minutes. Analytical separation was achieved with a nanoEase MZ Peptide C18 column (300 Å, 1.7 µm, 75 µm × 200 mm, Waters) at 300 nl/min using a multi-step gradient: solvent B (0.1% formic acid in acetonitrile) was increased linearly from 4% to 30% over 102 minutes, ramped quickly to 78%, reduced to 2% after 2 minutes, followed by a 10-minute re-equilibration. Peptides were analyzed in data-dependent acquisition (DDA) mode. Full MS scans were acquired at

a resolution of 120,000 (m/z 380–1400; AGC target: 300%; max injection time: 45 ms), followed by MS/MS scans for up to 2 seconds. Precursors were isolated with a 1.4 m/z window and fragmented with 26% normalized collision energy (NCE). Fragment ions were analyzed at a resolution of 15,000 (AGC target: 100%; max IT: 54 ms). Singly charged and unassigned precursors were excluded, with dynamic exclusion set to 30 seconds. Wash runs (40 min) were included between samples to reduce carry-over. Instrument performance was monitored by routine injections of a standard sample and tracked via a custom Shiny application.

Data analysis was conducted using MaxQuant (v1.6.14.0) (Tyanova et al., 2016) with the human reference proteome (UniProt, 74,811 entries; release: February 27, 2020). Default settings were used with the following modifications: "Match between runs" (MBR) was enabled, restricted to within replicates. Label-free quantification (LFQ) was also enabled, and separate parameter groups were defined for the EV and experimental conditions to allow independent normalization. LFQ values were used for statistical comparisons: Flag-FBXO45, Flag-FBXO45ΔSPRY, and Flag-SPRYD3 conditions were each compared to Flag-EV using unpaired, two-tailed Student's t-tests. Additionally, enriched proteins from the Flag-FBXO45 and Flag-FBXO45ΔSPRY conditions were directly compared using another unpaired, two-tailed Student's t-test. Statistical significance was defined as $p < 0.05$ (n = 4).

For identification of USP11 ubiquitylation sites, 3-4 15 cm dishes of HEK 293T cells were transfected with Flag-USP11 and MYC-EV or MYC-MYCBP2 or MYC-SPRYD3 and HA-Ubiquitin. MYC-MYCBP2 co-expressing cells were incubated for 48h and MYC-SPRYD3 co-expressing cells were incubated for 24h. 5h prior to harvest, 10 µM of MG132 was added to inhibit the proteasome. Flag-immunoprecipitation was performed and IP samples were denatured with 2x Laemmli buffer with or without DTT. All samples were prepared in triplicates and submitted to the DKFZ Proteomics Facility, Heidelberg for execution of MS and data analysis of USP11 ubiquitylation sites. Briefly, IP eluates (40 µl) were run for 0.5 cm into an SDS-PAGE and the entire piece was cut out and digested using trypsin (Shevchenko et al., 2006)(Shevchenko, Andrej, et al. "In-gel digestion for mass spectrometric characterization of proteins and proteomes." *Nature protocols* 1.6 (2006): 2856.) adapted to on a DigestPro MSi robotic system (INTAVIS Bioanalytical Instruments AG). The LC-MS/MS analysis was carried out as described previously, with minimal alterations. Briefly, the LC-MS/MS analysis was carried out for a total of 60 min. Concentration of solved B was linearly ramped from

4% to 30% for 43 min, with a quick ramp to 80%. Full scan was performed at 60k resolution instead of 120k. Unassigned and singly charged eluting features were excluded from fragmentation and dynamic exclusion was set to 20 s.

Data analysis was carried out by MaxQuant (Tyanova et al., 2016) using an organism specific database extracted from Uniprot.org (human reference database with one protein sequence per gene, containing 20,597 unique entries from 9th of February 2024). Settings were left at default with the following adaptions. Match between runs (MBR) was enabled to transfer peptide identifications across RAW files based on accurate retention time and m/z. Fractions were set in a way that MBR was only performed within replicates. Label free quantification (LFQ) was enabled with default settings. The iBAQ-value (Schwanhäusser et al., 2011) generation was enabled. GlyGly(KST) was added as variable modification.

2.2.4 Statistical analysis

All statistical analyses were conducted using GraphPad Prism version 10 (GraphPad Software, Inc.). Each dataset was derived from at least three independent experiments, with individual replicates presented as either single values or mean ± standard deviation (SD). Fold change data were normalized to the control group, and the resulting values were log-transformed to ensure normal distribution. Statistical significance of the log-transformed values was assessed using two-tailed one-sample t-tests and Wilcoxon tests against the control group mean, set at 1.0. While log-transformed data were used for significance testing, non-transformed values were displayed in the fold-change quantification graphs. Normally distributed data not normalized to a control group were analyzed for significance using unpaired, two-tailed Student's t-tests with Welch's correction or ordinary one-way ANOVA for multiple group comparisons. A p-value threshold of 0.05 was used to determine statistical significance (ns > 0.05; * $p < 0.05$; ** $p < 0.01$; *** $p < 0.001$; **** $p < 0.0001$).

3. Results

3.1 Characterization of SPRYD3 as new specificity factor of the MYCBP2 E3 ligase

The E3 ligase complex MYCBP2-FBXO45 promotes mitotic slippage and cell survival through ubiquitin-mediated proteasomal degradation of the tumor suppressor FBXW7 (Richter et al., 2020). MYCBP2, with an approximate molecular weight of 500 kDa, is an E3 ligase complex and postulated signaling hub interacting with multiple proteins (Grill et al., 2016). I wondered whether MYCBP2-FBXO45 exerted a major function in mitotic cell fate regulation by targeting additional substrates for ubiquitin-mediated degradation. In order to identify additional MYCBP2-FBXO45 interactors and/or substrates that could play a role in mitotic cell fate regulation, I performed a combined IP-MS analysis approach. I ectopically expressed Flag-FBXO45 or Flag-FBXO45ΔSPRY in HEK 293T WT cells, and performed Flag-immunoprecipitation. Flag-FBXO45ΔSPRY served as negative control to specifically determine proteins interacting with the FBXO45 SPRY-domain, hence potential substrates. The DKFZ proteomics facility carried out the MS-analysis. Amongst already known interactors of the MYCBP2-FBXO45 E3 ligase complex, such as SKP1, FBXW7 and RAE1 (Desbois et al., 2018; Grill et al., 2012; Richter et al., 2020; Saiga et al., 2009), SPRYD3, a so far uncharacterized protein, was enriched in the MS-screen and interacted with FBXO45 in HEK 293T cells (Figure 4A, B). SPRYD3 comprises a molecular weight of approximately 55 kDa (Figure 4B, D) and is predicted to function in surface receptor signaling and cytoskeleton organization (Alliance of Genome Resources). Additionally, it is reported to be upregulated together with MYCBP2 and FBXO45 in mice lacking FKBP5 expression, a chaperone involved in hormone signaling and stress response regulation (Gebru et al., 2024). Both SPRYD3 and FBXO45 belong to the SPRY/B30.2 protein family and contain SPRY-domains (D'Cruz et al., 2013) (Figure 4C). SPRY-domains are postulated to mediate protein-protein interactions and are contained in many E3 ligases, such as TRIM E3 ligases (D'Cruz et al., 2013). While FBXO45 has one SPRY-domain, which mediates substrate recruitment and MYCBP2-binding (Desbois et al., 2018; Saiga et al., 2009), SPRYD3 contains two such SPRY-domains, denoted SPRY1 and SPRY2 (Figure 4C). SPRYD3 is present in U2OS, HeLa and RPE1 cells, with mostly one band being detectable (Figure 4D, U2OS and HeLa WB),

while a second higher molecular weight isoform is visible in RPE1 cells (Figure 4D, RPE1 WB).

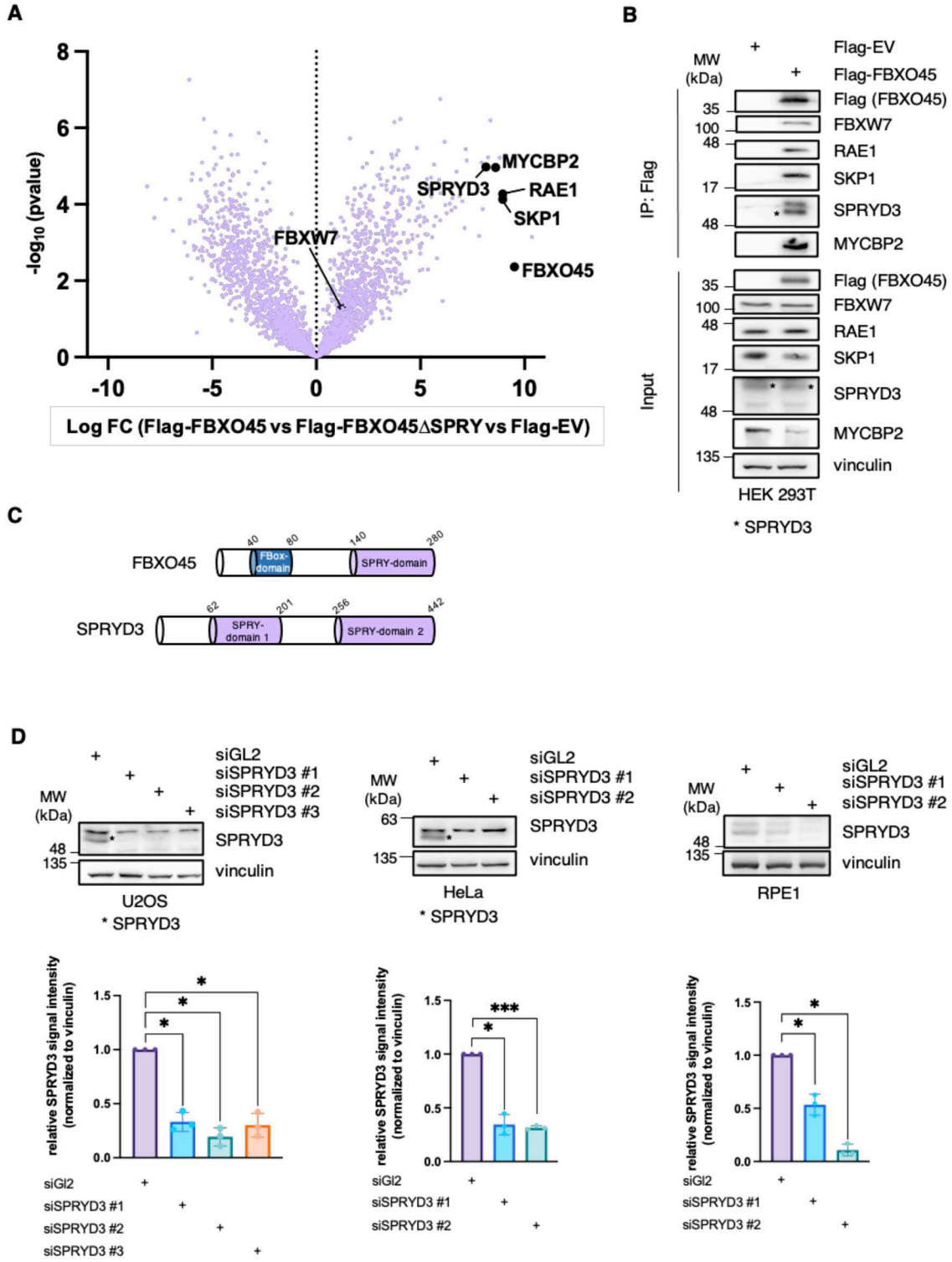


Figure 4: SPRYD3 is a new interactor of FBXO45.
(A) Volcano plot of putative FBXO45 interaction partners identified by a combined IP-MS approach. Flag-FBXO45, Flag-FBXO45ΔSPRY or Flag-EV were overexpressed in HEK 293T WT cells for 24h. Cells were harvested for IP. IP samples were applied to MS analysis, n=4. **(B)** HEK 293T WT cells were transfected with Flag-FBXO45 and incubated for 24h. Cells were harvested for Flag-IP. IPs and inputs were subjected to western blot analysis. **(C)** Schematic overview of FBXO45 and SPRYD3 with respective protein domains. **(D)** U2OS, HeLa or RPE1 cells were transfected twice with 20 nM siRNA targeting GL2 (control) or SPRYD3 and incubated for 72h after the first

transfection. Cells were harvested and protein extracts were subjected to western blot analysis. Absolute SPRYD3 western blot signals were normalized to respective vinculin signal and siGL2 was used as 100% reference. Quantification graphs depict relative values in relation to siGL2 control. Relative values were log-transformed to obtain parametric distribution for statistical analysis. Log-transformed values were applied to one sample t and Wilcoxon test, n=3 independent experiments. *$p < 0.05$, ***$p < 0.001$.

Due to the presence of SPRY-domains and their affiliation to the SPRY/B30.2 protein family (D'Cruz et al., 2013), I assumed that SPRYD3 and FBXO45 could exert similar functions. I hypothesized that SPRYD3 could be a substrate specificity factor forming a new E3 ligase complex with MYCBP2 and decided to follow up on this idea. I set out to explore whether the formation of a new E3 ligase complex consisting of MYCBP2 and SPRYD3 is present, and whether this complex is involved in mitotic slippage regulation after MT-poison treatment through ubiquitylation of a substrate.

3.1.1 SPRYD3 promotes mitotic slippage in paclitaxel and nocodazole treated cells

I wanted to investigate the role of a potential E3 ligase complex consisting of MYCBP2 and SPRYD3 as new specificity factor in context of mitotic cell fate decision. Thus, before characterizing a potential complex formation between those two proteins, I investigated the role of SPRYD3 in mitotic cell fate regulation in response to MT-poison treatment. Therefore, I performed live cell imaging combined with RNA interference and MT-poison treatment using either nocodazole or paclitaxel. Nocodazole and paclitaxel are both MT-poisons that interfere with MT-dynamics and induce mitotic arrest (Musacchio and Salmon, 2007; Rieder and Maiato, 2004). I transfected U2OS and RPE1 cells with siRNA targeting either GL2 (control), SPRYD3 and/or MYCBP2, which served as a control, since its function in mitotic slippage is already reported (Richter et al., 2020). After 72h of siRNA-mediated downregulation, I treated cells with nocodazole or paclitaxel and performed live cell imaging. I analyzed mitotic cell fate of 60 cells, discerning between mitotic slippage or mitotic cell death. Ablation of either SPRYD3 and/or MYCBP2 resulted in a significant decrease of cells committing mitotic slippage after nocodazole or paclitaxel treatment in both U2OS and RPE1 cells compared to a siGL2-treated control (Figure 5). Interestingly, simultaneous knockdown of MYCBP2 and SPRYD3 showed no significant increase in mitotic cell death commitment compared to knockdown of MYCBP2 alone in both U2OS and RPE1 cells (Figure 5). This suggests that SPRYD3 and MYCBP2 might function in the same pathway in promoting mitotic slippage in presence of MT-poisons.

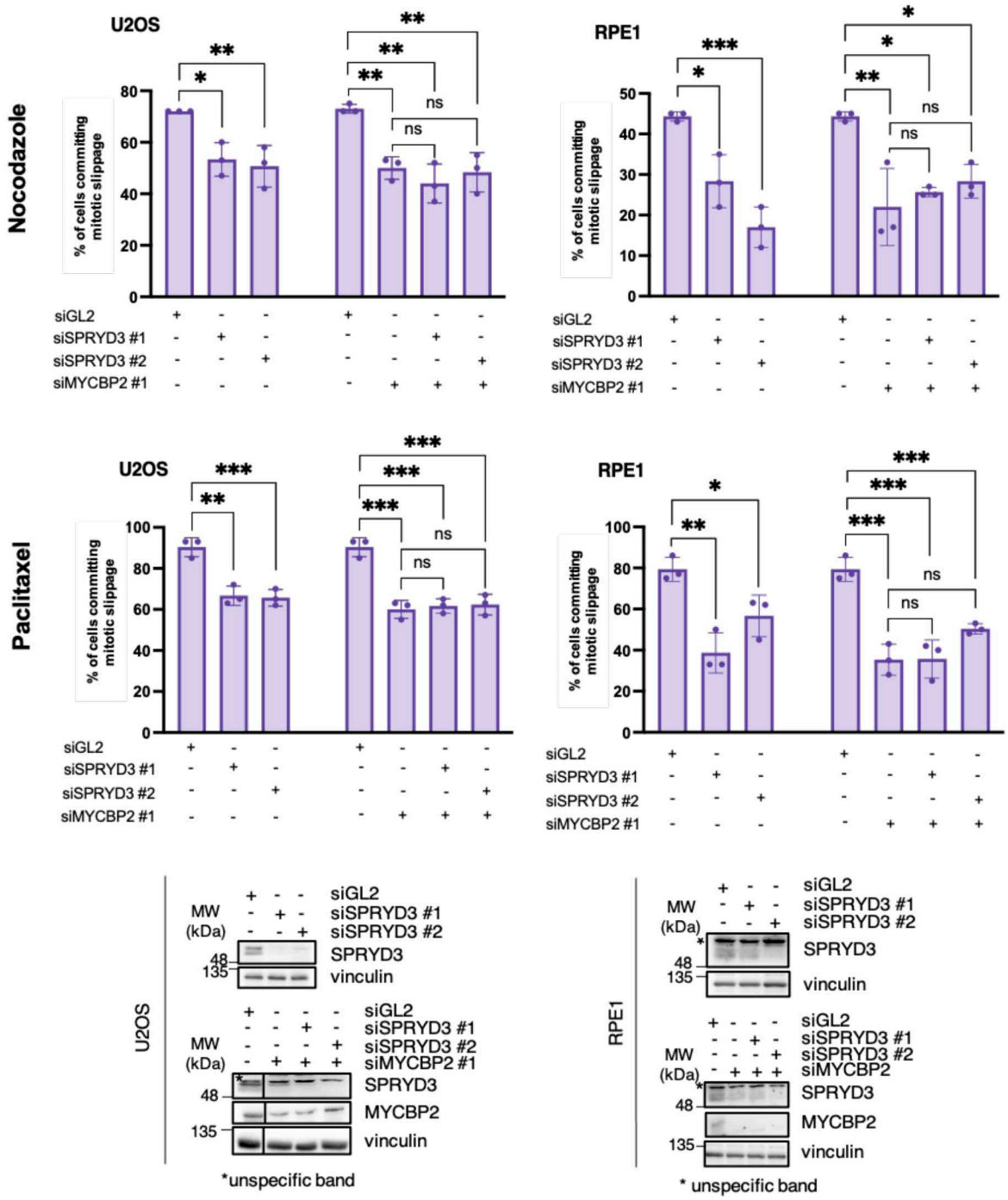


Figure 5: SPRYD3 mediates mitotic slippage in nocodazole or paclitaxel treated U2OS and RPE1 cells. U2OS or RPE1 cells were transfected twice with 20 nM siRNA targeting GL2 (control), SPRYD3 and/or MYCBP2. 72h after the first transfection, cells were treated with nocodazole or paclitaxel. Live cell imaging was performed and mitotic cell fate of n=60 cells was determined for each experiment. ns > 0.05, *p < 0.05, **p < 0.01, ***p < 0.001, one-way ANOVA with Dunette post hoc test, n=3 independent experiments for each cell line and drug treatment.

Next, I explored whether the function of MYCBP2 and SPRYD3 in mitotic slippage regulation is specific for MT-poison treatment or also occurs in non-treated cells. I transfected U2OS and RPE1 cells with siRNA targeting GL2, SPRYD3 or MYCBP2 and performed live cell imaging without prior MT-poison treatment. Interestingly,

knock-down of SPRYD3 or MYCBP2 did have no effect on cell division in both cell lines. Almost 100% of cells divided normally throughout all conditions (Figure 6A). Additionally, mitotic timings of SPRYD3- or MYCBP2-depleted cells were not altered compared to siGL2-treated cells (Figure 6B). Taken together, these results indicate that MYCBP2 and SPRYD3 specifically regulate mitotic cell fate decision upon MT-poison treatment.

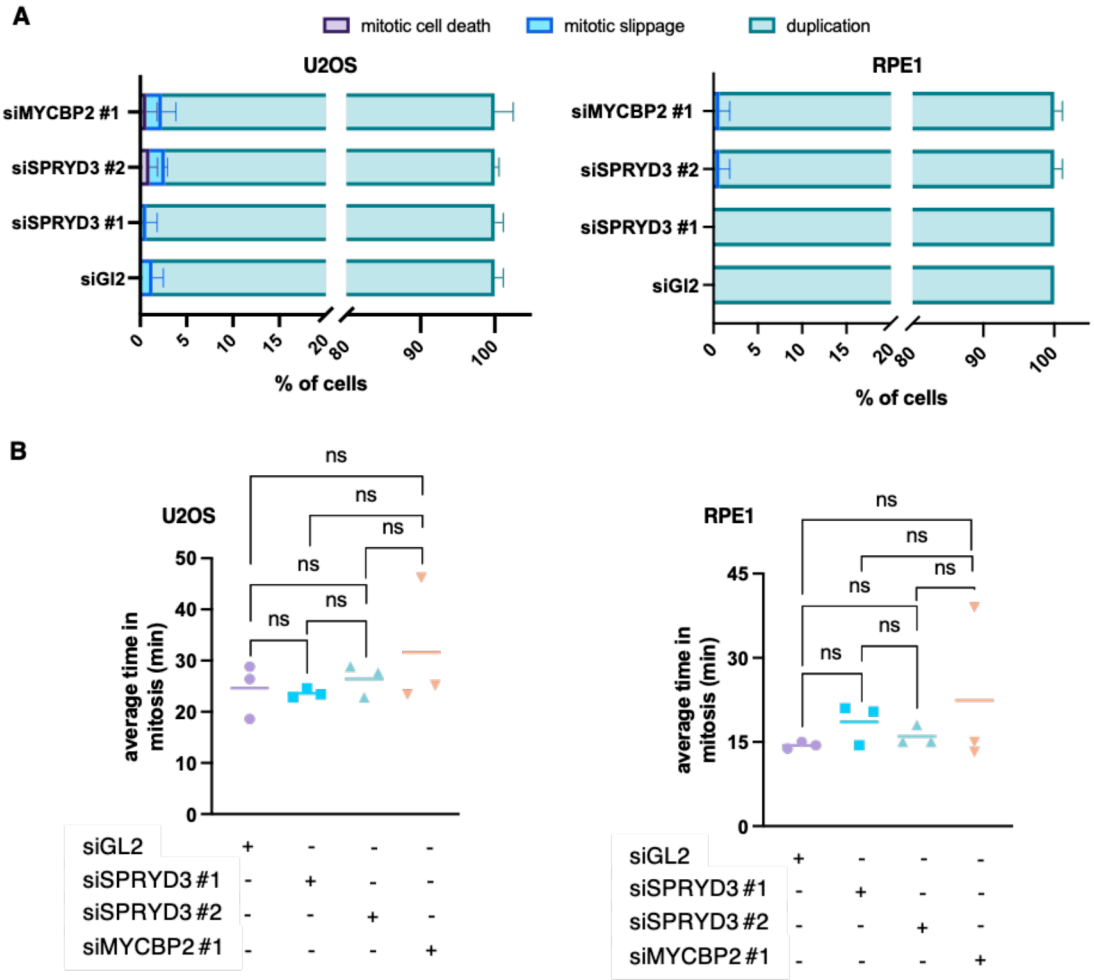


Figure 6: Depletion of SPRYD3 or MYCBP2 in untreated cells does not alter mitotic cell fate or timing.
(A) U2OS or RPE1 cells were transfected twice with 20 nM siRNA either targeting GL2 (control), SPRYD3 or MYCBP2. 72h after the first transfection, live cell imaging was performed and mitotic cell fate of n=60 cells was determined for each experiment. ns > 0.05, one-way ANOVA with Dunette post hoc test, n=3 independent experiments for each cell line. **(B)** U2OS or RPE1 cells were transfected twice with 20 nM siRNA targeting either GL2 (control), SPRYD3 or MYCBP2. 72 hours after the first transfection, live cell imaging was performed and time in mitosis for n=60 cells was determined for each experiment. Mitotic timing was determined by visually following cells from roundup (=beginning of mitosis) until cytokinesis (=end of mitosis). ns > 0.05, one-way ANOVA with Dunette post hoc test, n=3 independent experiments for each cell line.

3.1.2 SPRYD3 forms a complex with MYCBP2 *in vivo* and *in vitro*

After having proven an involvement of SPRYD3 in mitotic slippage regulation, I aimed at characterizing the relationship between MYCBP2 and SPRYD3. I performed various

interaction experiments in cells and *in vitro* to find out whether they bind to each other. Furthermore, I performed siRNA experiments to investigate their relation to each other.

3.1.2.1 MYCBP2 and SPRYD3 interact in HEK 293TWT cells

I ectopically co-expressed Flag-MYCBP2 and MYC-SPRYD3 or Flag-SPRYD3 and MYC-MYCBP2 in HEK 293T WT cells and immunoprecipitated Flag-tagged proteins. Both MYCBP2 and SPRYD3 interacted reciprocally after overexpression (Figure 7A). To exclude SPRYD3 being a ubiquitylation-substrate of the MYCBP2 E3 ligase destined for proteasomal destruction, I performed siRNA experiments in U2OS and RPE1 cells to investigate SPRYD3 protein levels after MYCBP2 knock-down. Interestingly, siRNA-mediated depletion of MYCBP2 lead to a significant destabilization of SPRYD3 protein levels in both U2OS and RPE1 cells compared to a siGL2-treated control, proving that MYCBP2 stabilizes SPRYD3 protein levels (Figure 7B). This suggests that SPRYD3 is probably not marked by MYCBP2 for proteasomal destruction, but does not exclude its ubiquitylation by MYCBP2 with different protein fate outcomes as a consequence.

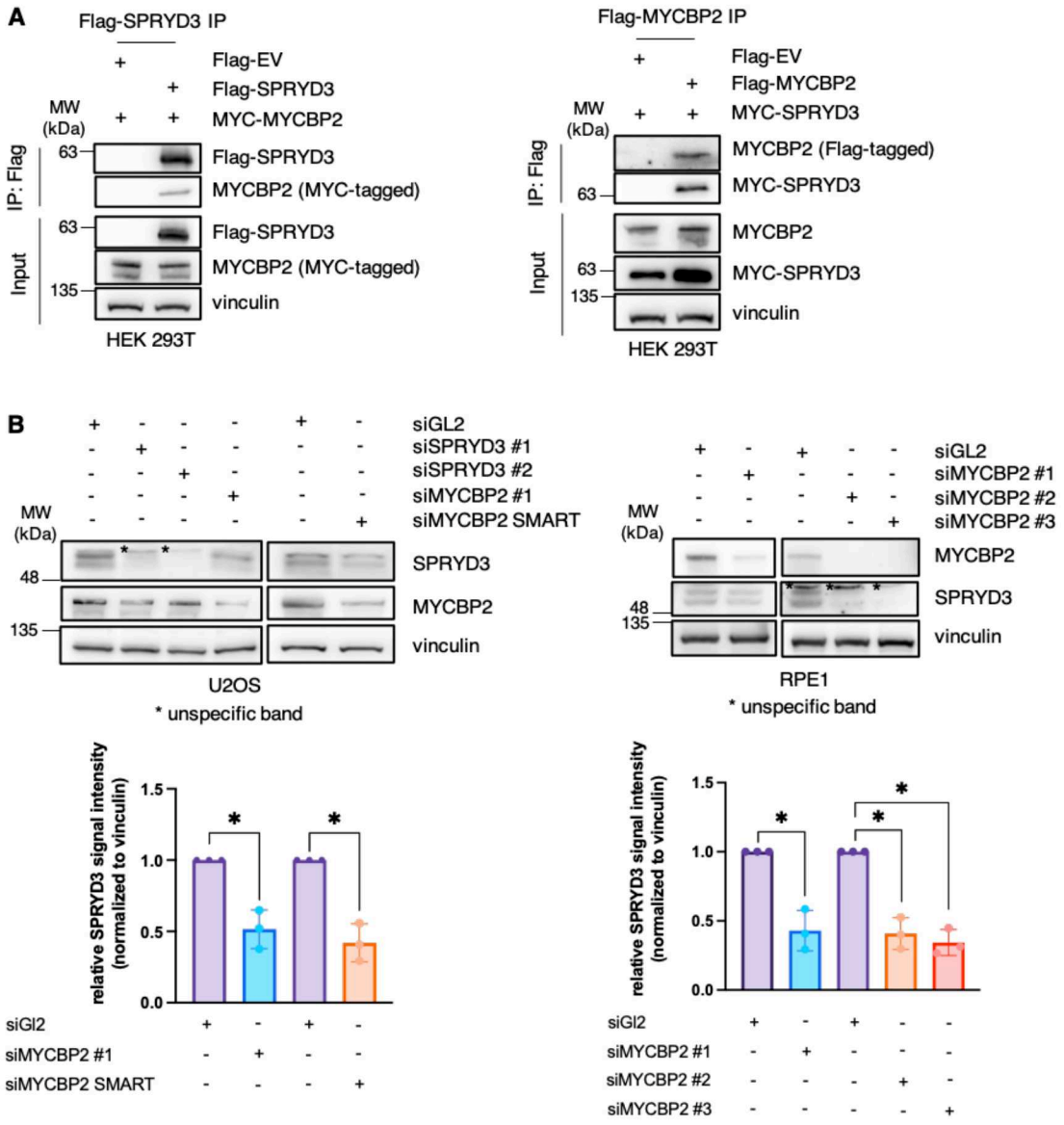


Figure 7: SPRYD3 interacts with and is stabilized by MYCBP2.
(A) Flag-SPRYD3 and MYC-MYCBP2 or MYC-SPRYD3 and Flag-MYCBP2 were co-transfected as indicated into HEK 293T WT cells and overexpressed for 48h. Cells were harvested for Flag-IP. IPs and inputs were subjected to western blot analysis. **(B)** U2OS and RPE1 cells were transfected twice with 20 nM siRNA targeting GL2 (control), SPRYD3 or MYCBP2. 72h after the first transfection, cells were harvested and protein lysates were subjected to western blot analysis. Absolute SPRYD3 western blot signals were normalized to respective vinculin signals and siGL2 was used as a 100% reference. Quantification graphs depict relative values in relation to siGL2 control. For statistical analysis, relative values were log-transformed to obtain parametric distribution. Log-transformed values were applied to one sample t and Wilcoxon test, n=3 independent experiments. *$p < 0.05$, * unspecific band.

3.1.2.2 SPRYD3 binds MYCBP2 independently from FBXO45

Next, I aimed at characterizing the interaction between SPRYD3 and MYCBP2 more in detail. I ectopically expressed Flag-tagged truncations of MYCBP2 harboring its different characterized domains in HEK 293T WT cells (Figure 8A). Similar to FBXO45, endogenous SPRYD3 co-precipitated with the truncation harboring the MYC-binding domain of MYCBP2 (Flag-MYCBP2 1951-2950) (Figure 8A). Interestingly, both

FBXO45 and SPRYD3 also co-precipitated with the construct harboring the MYCBP2 RING-domain, but to a far lesser extent (Figure 8A). To exclude the canonical MYCBP2-specifity factor FBXO45 as a potential mediator of interaction between SPRYD3 and MYCBP2, I transfected HEK 293T ΔFBXO45 cells with Flag-MYCBP2 1951-2950, the construct shown to interact with both FBXO45 and SPRYD3 (Figure 8B, left). In absence of FBXO45, Flag-MYCBP2 1951-2950 was able to co-precipitate endogenous SPRYD3. On the other hand, ectopically expressed Flag-MYCBP2 1951-2950 interacted with endogenous FBXO45 in SPRYD3-depleted HEK 293T WT cells (Figure 8B, right). Even though complex formation seems to be possible, Flag-MYCBP2 1951-2950 precipitates less endogenous SPRYD3 or FBXO45 in both SPRYD3-depleted HEK 293T or ΔFBXO45 cells, respectively (Figure 8B). This suggests that SPRYD3, FBXO45 and MYCBP2 reciprocally stabilize each other.

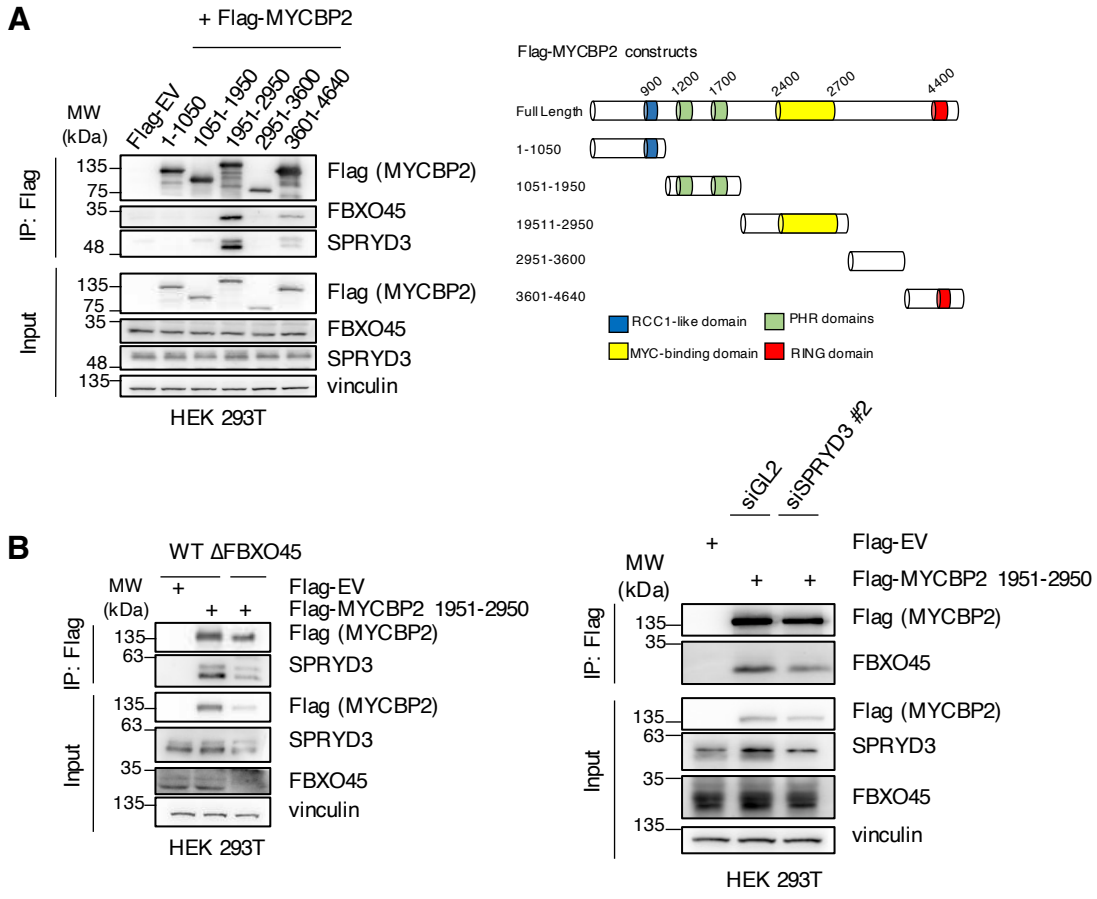


Figure 8: SPRYD3 interacts with the MYCBP2 MYC-binding domain independently of FBXO45.
(A) Flag-MYCBP2 constructs were transfected into HEK 293T WT cells and overexpressed for 24h. Cells were harvested for Flag-IPs. IPs and inputs were subjected to western blot analysis. **(B)** Left: Flag- Flag-MYCBP2 1951-2950 was transfected into HEK 293T WT/ΔFBXO45 cells and incubated for 24h. Cells were harvested for Flag-IP. IPs and inputs were subjected to western blot. Right: HEK 293T WT cells were transfected twice with 20 nM siRNA targeting GL2 (control) or SPRYD3. 48h after the first transfection, Flag-MYCBP2 1951-2950 was transfected and cells were incubated for further 24h. Follow-up procedures were executed as described in (B, left).

3.1.2.3 FBXO45 and SPRYD3 bind to different sites of MYCBP2

Since both FBXO45 and SPRYD3 bind to the MYCBP2 construct harboring the MYC-binding domain (Figure 8A), I aimed at mapping the exact binding site of SPRYD3 on MYCBP2. I generated smaller truncations of Flag-MYCBP2 1951-2950, and performed interaction experiments by ectopically expressing these in HEK 293 WT cells (Figure 9A). Interestingly, FBXO45 and SPRYD3 did not bind the same region on MYCBP2. While endogenous FBXO45 precipitated with Flag-MYCBP2 2400-2700, which expresses the MYCBP2 MYC-binding domain only, SPRYD3 interacted with Flag-MYCBP2 2550-2825, which expresses half of the MYC-binding domain and the following 125 aas (Figure 9A). This suggests a partial overlap of FBXO45- and SPRYD3-binding sites on MYCBP2 and supports the finding that both FBXO45 and SPRYD3 can bind MYCBP2 independently from each other (Figure 8B), since they do not fully occupy the same binding-site. To assess the MYCBP2-binding site on SPRYD3, I generated MYC-tagged SPRYD3 constructs lacking either the first or second SPRY-domain (Figure 9B) and co-transfected them with Flag-MYCBP2 2550-2825, the minimal SPRYD3-binding site on MYCBP2 identified earlier, into HEK 293T WT cells. The interaction between MYC-SPRYD3 and Flag-MYCBP2 2550-2825 occurred through the SPRYD3 SPRY2-domain (Figure 9B).

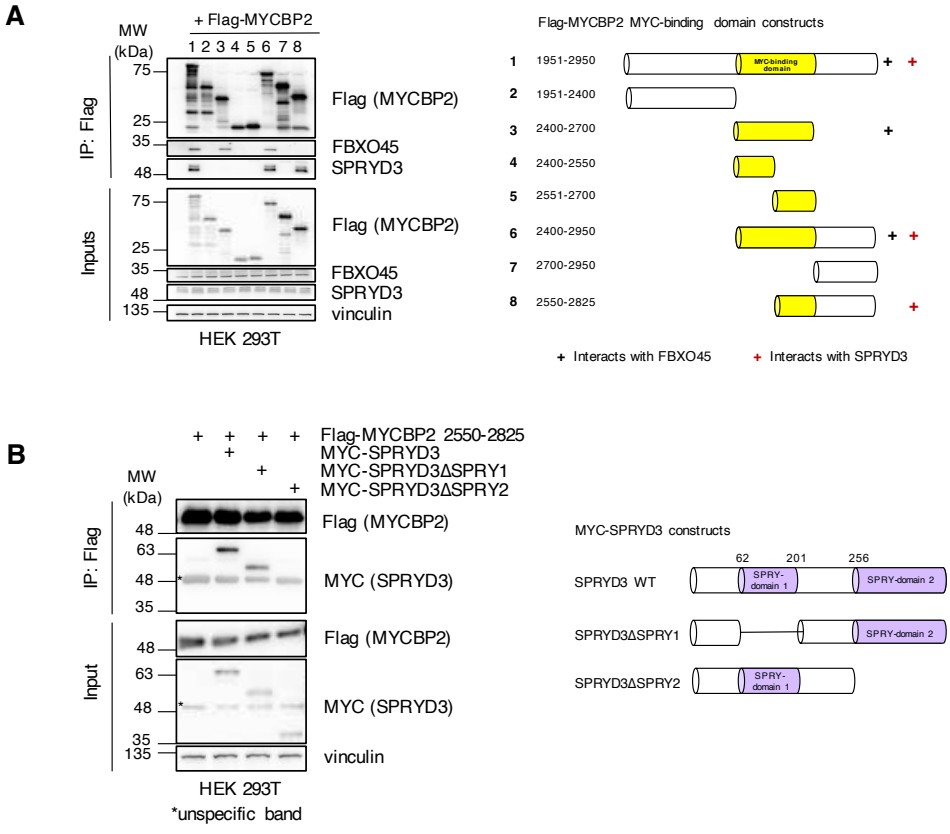


Figure 9: SPRYD3 binds to MYCBP2 via its SPRY2-domain.

(A) Flag-MYCBP2 constructs were ectopically expressed in HEK 293T WT cells for 24h. Cells were harvested for Flag-IP. IPs and inputs were subjected to western blot analysis. **(B)** Flag-MYCBP2 2550-2825 and MYC-SPRYD3 constructs were co-transfected into HEK 293T WT cells and overexpressed for 24h. Cells were harvested for Flag-IP. IPs and inputs were subjected to western blot analysis.

3.1.2.4 SPRYD3 and FBXO45 simultaneously bind to MYCBP2 and MYCBP2 and SPRYD3 interact *in vitro*

SPRYD3 and FBXO45 can interact with MYCBP2 independently from each other (Figure 8B). I wondered how the MYCBP2 complex is expressed within the cell and thus wanted to assess whether SPRYD3 and FBXO45 are bound simultaneously or not. To assess this, I ectopically co-expressed Flag-MYCBP2 1951-2950 with either MYC-SPRYD3 or MYC-FBXO45 in HEK 293T WT cells, since Flag-MYCBP2 is able to interact with both FBXO45 and SPRYD3. Flag-MYCBP2 1951-2950 was immunoprecipitated with Flag-M2 beads and the IPs were subjected to a consecutive immunoprecipitation against either MYC-SPRYD3 or MYC-FBXO45 using a MYC-tag antibody. In both cases, endogenous SPRYD3 or FBXO45 co-precipitated respectively (Figure 10A), suggesting that complexes of MYCBP2 binding both FBXO45 and SPRYD3 may simultaneously form in the cell. However, this result cannot exclude the existence of a MYCBP2 complex binding either SPRYD3 or FBXO45 alone.

Finally, to assess whether MYCBP2 and SPRYD3 directly interact with each other, I performed *in vitro* pull-down assays. I recombinantly expressed and purified MBP-SPRYD3 and GST- or HIS-tagged MYCBP2 2550-2825 in *E. coli* Rosetta (DE3). I decided to purify the minimal SPRYD3-binding site, MYCBP2 2550-2825, because it is difficult to recombinantly express and purify a protein of approximately 500 kDa, as it is the case for MYCBP2. I combined MBP-SPRYD3 or an equimolar amount of MBP-Empty vector (EV) with either GST-MYCBP2 2550-2825 or HIS-MYCBP2 2550-2825 and performed MBP-pull down assays. In both cases, MBP-SPRYD3 was able to bind and precipitate GST- or HIS-tagged MYCBP2 2550-2825, confirming a direct physical interaction between MYCBP2 and SPRYD3 (Figure 10B). Thus, the existence of an interaction-mediator of any kind between MYCBP2 and SPRYD3 can be excluded.

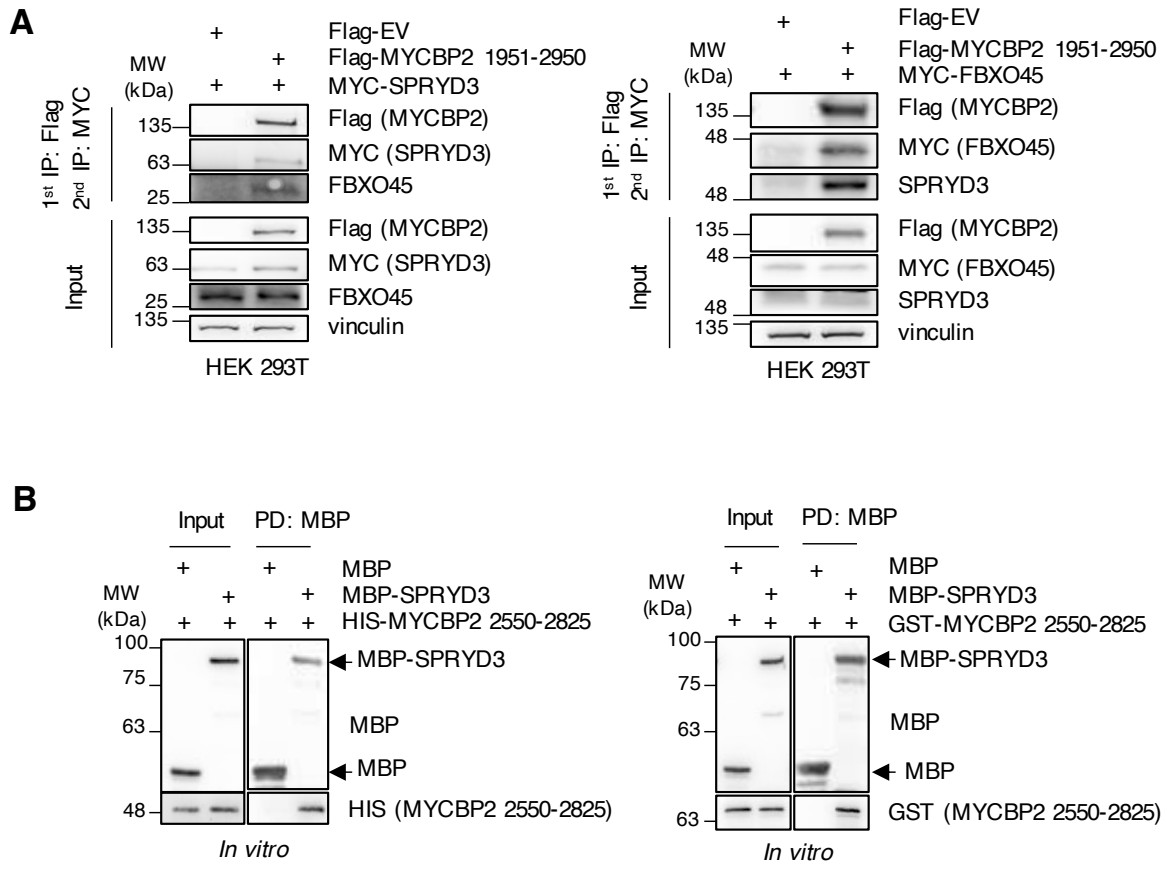


Figure 10: SPRYD3 directly interacts with MYCBP2.
(A) Flag-MYCBP2 1951-2950 was co-transfected with MYC-SPRYD3 or MYC-FBXO45 into HEK 293T WT cells and overexpressed for 24h. Cells were harvested for Flag-IP. IPs were subjected to a second immunoprecipitation against MYC-SPRYD3 or MYC-FBXO45 using a MYC-antibody. Resulting IPs and inputs were subjected to western blot analysis. **(B)** Purified recombinant MBP or MBP-SPRYD3 was combined with HIS-MYCBP2 2550-2825 or GST-MYCBP2 2550-2825 and MBP pull-downs were performed.

3.1.3 MYCBP2-SPRYD3 complexes form without SKP1

As shown in previous chapters, MYCBP2 and SPRYD3 directly associate with each other and can form a complex independent from FBXO45 (Figure 8B and 10B). SKP1 is a reported member of the MYCBP2-FBXO45 complex (Desbois et al., 2018; Saiga et al., 2009) and I wondered whether it also played a role in regard to the new MYCBP2-SPRYD3 complex. In canonical SCF E3 ligase complexes, SKP1 serves as a linker between the substrate specificity factor and the Cullin backbone of the E3 ligase (Cardozo and Pagano, 2004). However, in case of MYCBP2-FBXO45, member of the novel RCR family of E3 ligases (Pao et al., 2018), SKP1 does not serve as a linker, but binds to the FBXO45 F-Box domain and exerts the role of an auxiliary protein contributing to target recognition (Desbois et al., 2018). Furthermore, SKP1 stabilizes FBXO45 protein levels (Desbois et al., 2018). I wondered whether SKP1 might play a similar role in regard to SPRYD3. Therefore, I performed various interaction and siRNA

experiments to assess the relationship between SPRYD3 and SKP1. I ectopically expressed Flag-SPRYD3 in HEK 293T WT/ΔFBXO45 cells and performed Flag-immunoprecipitation. While SKP1 co-precipitated with Flag-SPRYD3 in HEK 293T WT cells, the interaction was abolished in HEK 293T ΔFBXO45 cells (Figure 11A), suggesting that SKP1 interacts with SPRYD3 indirectly through FBXO45. The same result was obtained in HeLa ΔFBXO45 cells (Figure 11B).

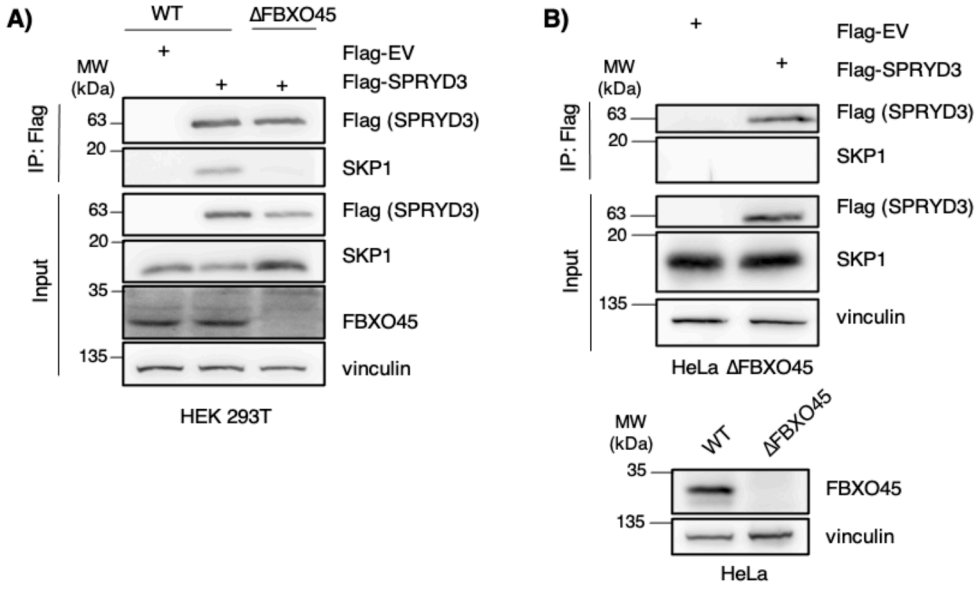


Figure 11: SPRYD3 and SKP1 do not interact directly.
(A) Flag-SPRYD3 was ectopically expressed in HEK 293T WT/ΔFBXO45 cells for 24h. Cells were harvested for Flag-IP. IPs and inputs were subjected to western blot analysis. **(B)** Flag-SPRYD3 was transfected into HeLa ΔFBXO45 cells using Lipofectamine 2000 and overexpressed for 24h. Follow-up procedures were executed as described in (A).

To explore whether SKP1 might regulate SPRYD3 protein levels as it was shown to do for FBXO45 (Desbois et al., 2018), I analyzed SPRYD3 and FBXO45 protein levels in SKP1-depleted U2OS, HeLa and RPE1 cells. While FBXO45 protein levels dropped significantly in all three SKP1-depleted cell lines compared to a siGL2-treated control, SPRYD3 protein levels remained unchanged (Figure 12A). Additionally, when I transfected Flag-MYCBP2 1951-2950 into SKP1-depleted HEK 293T WT cells and performed immunoprecipitation, co-precipitation of endogenous FBXO45 with Flag-MYCBP2 1951-2950 decreased significantly (Figure 12B). This can be explained with the fact that FBXO45 protein levels decrease overall in the cell as shown in Figure 12A, and therefore less FBXO45 is available for MYCBP2-binding. Endogenous co-precipitation of SPRYD3 with Flag-MYCBP2 1951-2950 did not change significantly compared to a siGL2-treated control (Figure 12B), reflecting the results obtained in Figure 12A. Considering the above presented results, I can conclude that SKP1 and

SPRYD3 most probably do not interact directly, even though an interaction study with recombinant SPRYD3 and SKP1 would have to be conducted to obtain a solid confirmation. Furthermore, SKP1 does not regulate SPRYD3 protein levels or binding to MYCBP2. The latter is supported by the *in vitro* assays performed in the previous chapter, where I proved a direct physical interaction between MYCBP2 and SPRYD3 (Figure 10B).

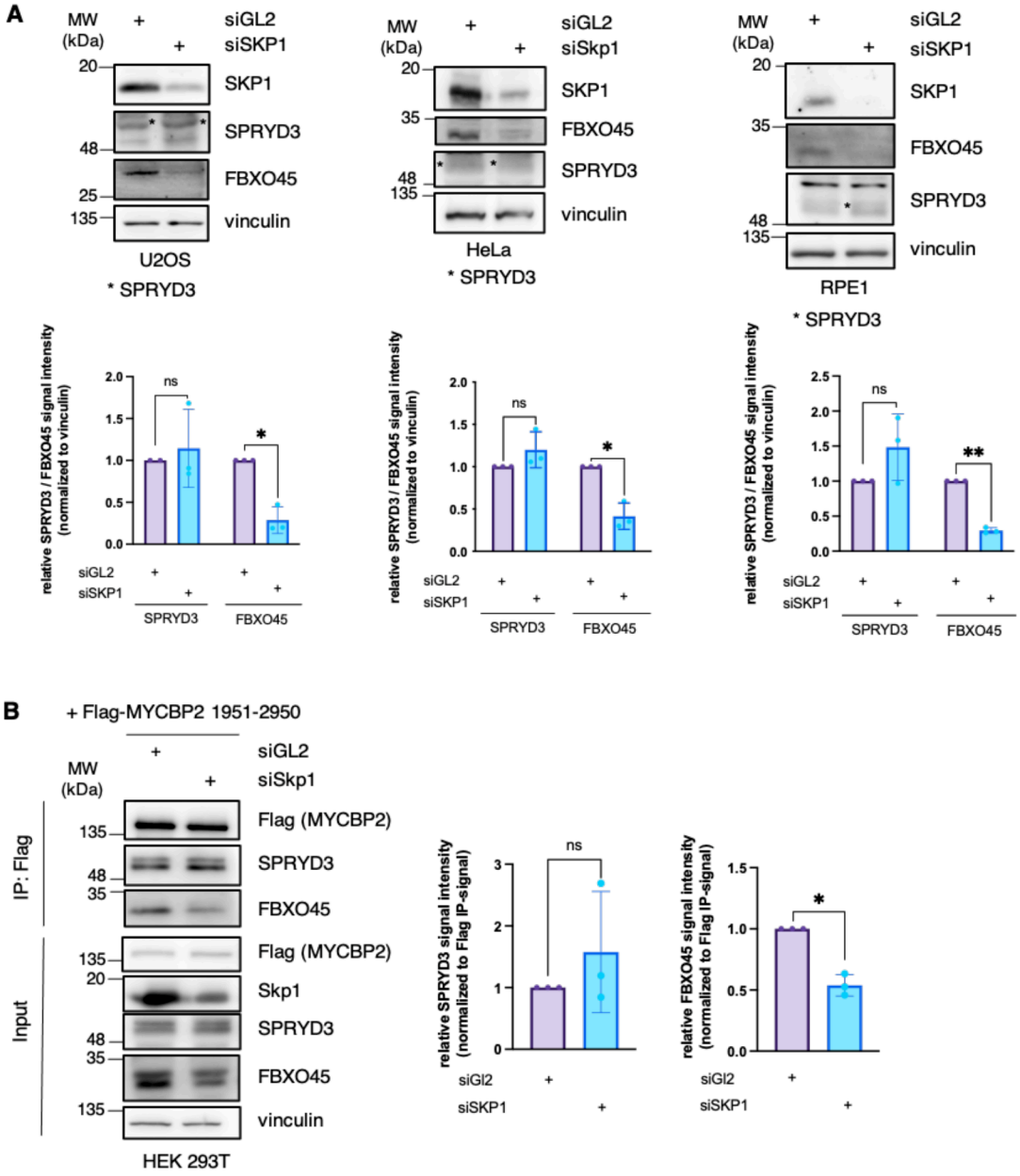


Figure 12: SKP1 does not regulate SPRYD3 protein levels nor mediation of interaction between SPRYD3 and MYCBP2.

(A) U2OS, HeLa or RPE1 cells were transfected twice with 20 nM siRNA targeting GL2 (control) or SKP1. 72h after the first transfection, cells were harvested and protein lysates were subjected to western blot analysis. Graphs depict relative SPRYD3 and FBXO45 western blot signals after normalization with respective vinculin signal. siGl2 served as 100% reference. For statistical analysis, normalized relative values were log-transformed to obtain parametric distribution. Log-transformed values were applied to one sample t and Wilcoxon test, n=3. ns > 0.05, *p < 0.05, **p < 0.01. **(B)** HEK 293T WT cells were transfected twice with 20 nM siRNA targeting GL2 (= control) or SKP1. 48h after the first transfection, Flag-MYCBP2 1951-2950 was transfected and cells were incubated for further

24h. Cells were harvested for Flag-IP. IPs and inputs were subjected to western blot analysis. Graphs depict relative SPRYD3 or FBXO45 western blot signals after normalization and in relation to a siGL2 treated control. Relative values were log-transformed to obtain parametric distribution for statistical analysis. Log-transformed values were applied to one sample t and Wilcoxon test, n=3. ns > 0.05, *p < 0.05;

3.1.4 The MYCBP2-SPRYD3 complex

Taken together, my results gained so far imply that both SPRYD3 and MYCBP2 promote mitotic slippage, respectively (Figure 5). In addition, the two proteins form a complex through direct binding of the SPRYD3 SPRY2-domain to MYCBP2 2550-2825 (Figure 9 and Figure 10B). SPRYD3 and FBXO45 also bind to the MYCBP2-RING domain, but to a far lesser extent compared to their primary binding sites (Figure 8A and 9A). While MYCBP2 can bind both FBXO45 and SPRYD3 at the same time (Figure 10A), complex formation between MYCBP2 and SPRYD3 or MYCBP2 and FBXO45 is still possible in absence of either SPRYD3 or FBXO45, respectively (Figure 8B). Additionally, SKP1 does probably not interact directly with SPRYD3, nor does it seem to regulate its protein levels or binding to MYCBP2 (Figure 11 and 12).

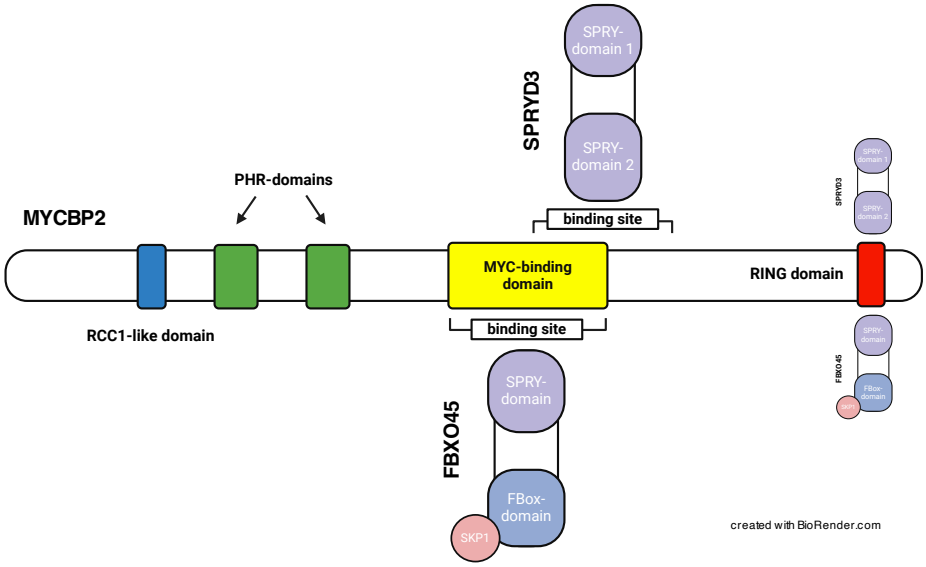


Figure 13: Complex formation of MYCBP2 with FBXO45 and SPRYD3
Schematic overview of potential complex formation consisting of MYCBP2, FBXO45 and SPRYD3 according to so far presented results.

3.1.5 Identification of putative SPRYD3-MYCBP2 interaction partners and substrates

As described previously, MYCBP2 and SPRYD3 form a complex through direct interaction. Next, in order to assess whether the MYCBP2-SPRYD3 complex exhibits ubiquitylation activity, I aimed at identifying potential interactors and substrates by

using again a combined IP-MS analysis approach. I ectopically expressed Flag-SPRYD3 in HEK 293T WT cells and immunoprecipitated Flag-SPRYD3 using Flag-beads. MS-analysis was performed by the DKFZ proteomics facility. In the resulting MS-screen, proteins such as MYCBP2, FBXO45, RAE1, SKP1 and FBXW7 were significantly enriched (Figure 14A) thus validating my approach as MYCBP2 and SPRYD3 were previously identified as binding partners of FBXO45 (Figure 4A) (Desbois et al., 2018; Saiga et al., 2009). All afore-mentioned proteins interacted with Flag-SPRYD3 in HEK 293T cells (Figure 14B). My aim was the identification of MYCBP2-SPRYD3 interactors and/or substrates that are involved in regulation of mitotic cell fate, thus I evaluated, which other proteins reported to regulate mitotic slippage were present in the MS-screen. Interestingly, CHAMP1 and XIAP co-precipitated significantly in the Flag-SPRYD3 MS-screen and interacted with Flag-SPRYD3 in HEK 293T cells (Figure 14A and B). Both XIAP and CHAMP1 were previously reported as regulators of mitotic slippage (Hino et al., 2021; Hou et al., 2017). Therefore, I wondered whether their function in mitotic cell fate decision is regulated by MYCBP2-SPRYD3-mediated ubiquitylation. I decided to explore this hypothesis by investigating the function of MYCBP2-SPRYD3 in regard to CHAMP1 and XIAP through interaction experiments and ubiquitylation assays.

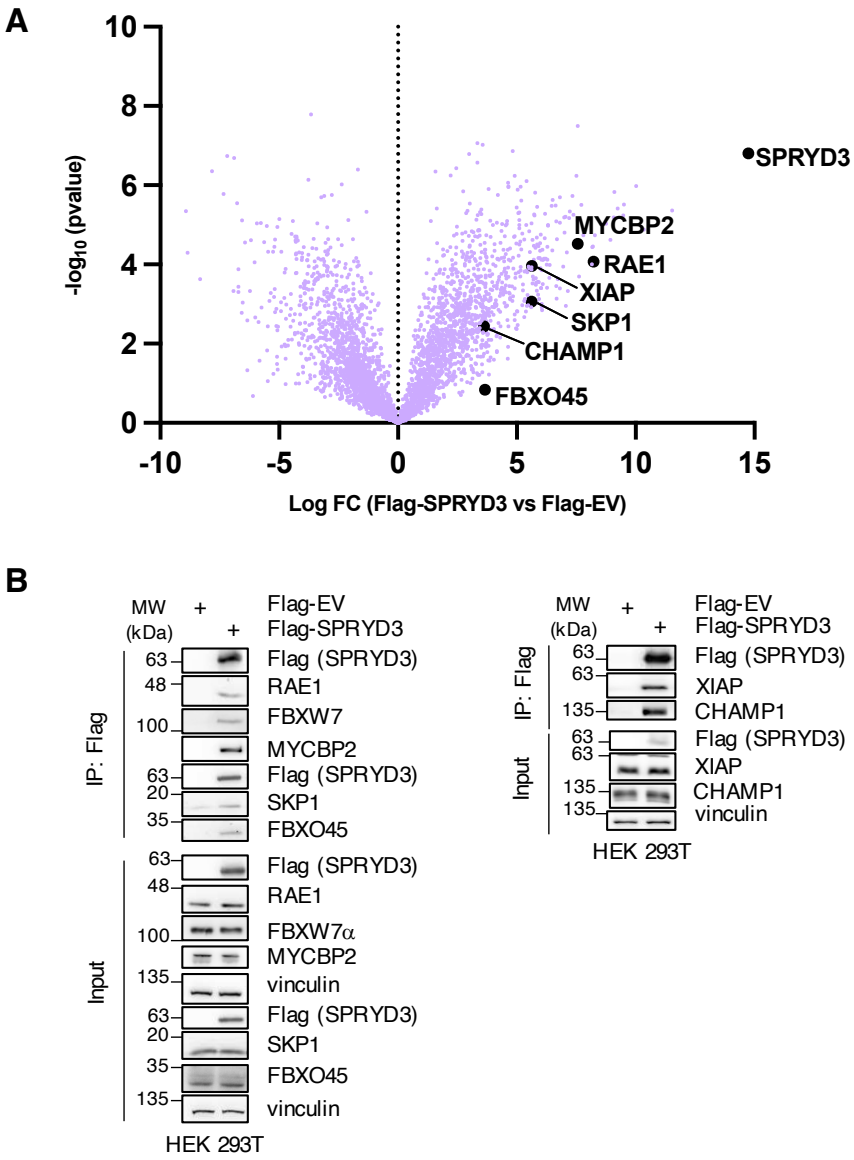


Figure 14: CHAMP1 and XIAP are new interactors of SPRYD3.
(A) Volcano plot showing significantly enriched putative interactors after combined IP-MS approach. Flag-SPRYD3 was overexpressed in HEK 293T WT cells and IPs were subjected to MS analysis for identification of potential interactors. n=4. **(B)** Flag-SPRYD3 was ectopically expressed in HEK 293T cells for 24h. Cells were harvested for Flag-IP. IPs were subjected to western blot analysis.

3.2 Validation of CHAMP1 as a potential SPRYD3 interaction partner

The scope of my thesis was to validate MYCBP2-SPRYD3 as a new E3 ligase complex that regulates a substrate in the context of mitotic cell fate decision. I decided to investigate the two SPRYD3-interactors CHAMP1 and XIAP, since their function in mitotic slippage regulation is reported (Hino et al., 2021; Hou et al., 2017). I first set out to investigate CHAMP1 and its relationship with MYCBP2-SPRYD3 by performing various interaction experiments and ubiquitylation assays.

3.2.1 CHAMP1 and SPRYD3 interact both in asynchronous and mitotic cells

I performed reciprocal Flag-co-IPs to validate an interaction between CHAMP1 and SPRYD3 in cells. I ectopically expressed Flag-SPRYD3 and GFP-CHAMP1 or Flag-CHAMP1 and MYC-SPRYD3 in HEK 293T WT cells and confirmed a reciprocal interaction (Figure 15).

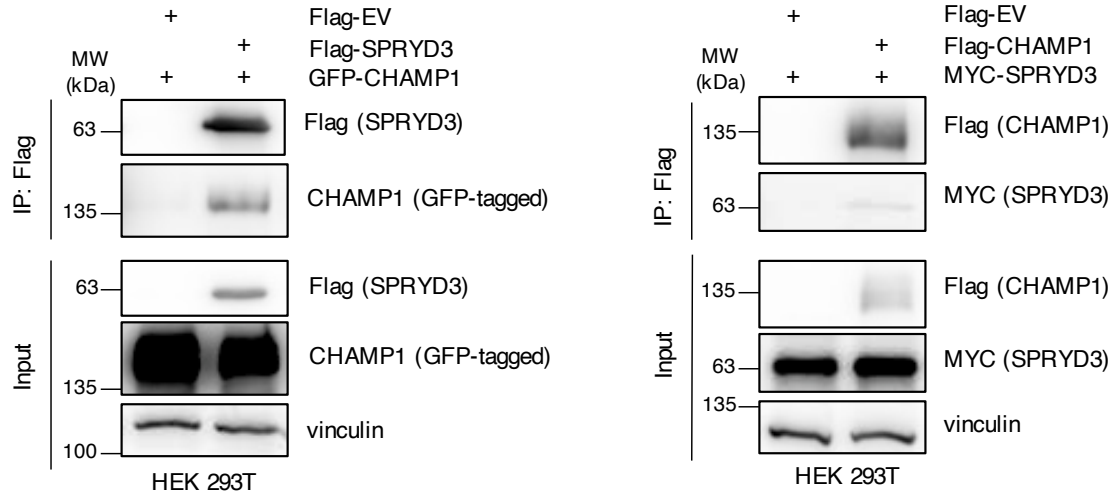


Figure 15: Interaction between CHAMP1 and SPRYD3.
Flag-SPRYD3 and GFP-CHAMP1 or Flag-CHAMP1 and MYC-SPRYD3 were co-transfected as indicated into HEK 293T WT cells and overexpressed for 24h. Cells were harvested for Flag-IP. IPs and inputs were subjected to western blot analysis.

Since both proteins regulate mitotic cell fate, I hypothesized that CHAMP1 and SPRYD3 might interact stronger in mitosis compared to asynchronous cells. I ectopically expressed Flag-SPRYD3 in HEK 293T WT cells for 24h. In order to obtain a mitotic cell population, I treated cells with 100 ng/ml nocodazole for approximately 17h prior to harvest. Asynchronous cells were left untreated. Interestingly, CHAMP1 co-precipitated with Flag-SPRYD3 in asynchronous and mitotic cells, but the interaction in asynchronous cells was stronger (Figure 16A). CHAMP1 is phosphorylated during mitosis (Itoh et al., 2011) and perhaps, this phosphorylation might alter the interaction pattern between SPRYD3 and CHAMP1, leading to its disruption. Further experiments would be needed to assess this hypothesis. Interestingly, when treating Flag-SPRYD3-overexpressing HEK 293T cells with proteasome inhibitor MG132, CHAMP1 co-precipitation significantly increased compared to an untreated control (Figure 16B). This is characteristic for ubiquitylation substrates destined for proteasomal degradation. I therefore hypothesized that CHAMP1 could be a substrate of the MYCBP2-SPRYD3 complex targeted for

ubiquitylation-dependent proteasomal destruction. This would explain the increased interaction between CHAMP1 and SPRYD3 after inhibition of the proteasome.

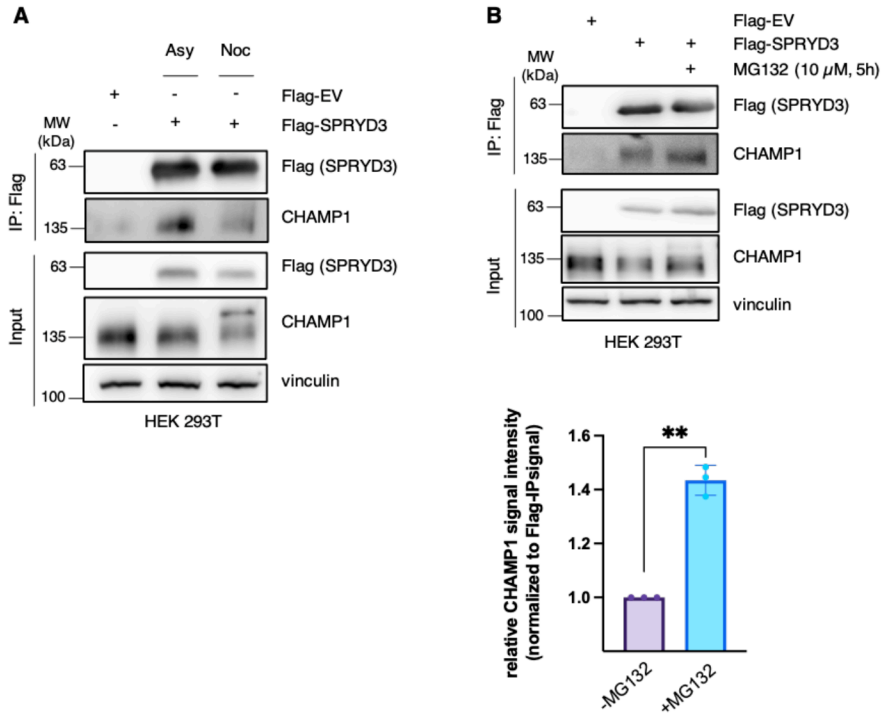


Figure 16: CHAMP1 and SPRYD3 interact in asynchronous and mitotic cells.
(A) Flag-SPRYD3 was ectopically expressed in HEK 293T WT cells for 24h. Asynchronous cells were harvested after 24 hours. Mitotic cells were treated with nocodazole for 17 hours prior to harvest. Flag-IP was performed. IPs and inputs were subjected to western blot analysis. **(B)** Flag-SPRYD3 was transfected into HEK 293T WT cells and overexpressed for 24h. One set of Flag-SPRYD3 transfected HEK 293T cells was treated with MG132 5h before harvest and Flag-IP was performed. Graph depicts relative CHMAMP1 IP western blot signals after normalization and -MG132 treatment was used as 100% reference. Relative values were log-transformed to obtain parametric distribution for statistical analysis. Log-transformed values were applied to one sample t and Wilcoxon test, n=3 independent experiments. $^{**}p < 0.01$.

Lastly, to assess the SPRYD3-domain that mediates interaction with CHAMP1, I ectopically expressed Flag-SPRYD3 deletion mutants together with GFP-CHAMP1 in HEK 293T cells. GFP-CHAMP1 co-precipitated with Flag-SPRYD3 and Flag-SPRYD3ΔSPRY2 (Figure 17), indicating that the SPRYD3 SPRY1-domain mediates interaction with CHAMP1.

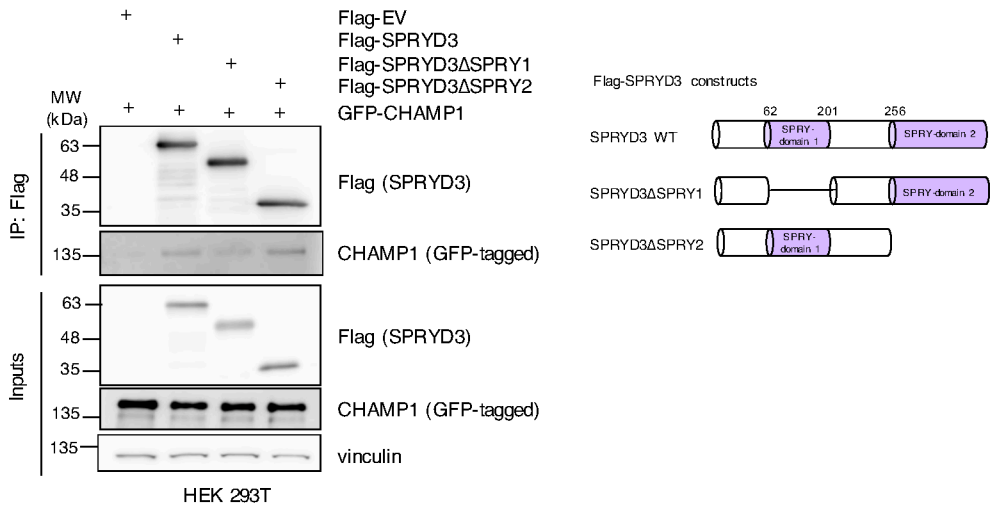


Figure 17: The SPRYD3SPRY1-domain mediates interaction with CHAMP1.
Flag-SPRYD3 constructs and GFP-CHAMP1 were co-transfected into HEK 293T WT cells and overexpressed for 24h. Cells were harvested and Flag-SPRYD3 was immunoprecipitated using Flag-M2 beads. IPs and inputs were subjected to western blot analysis.

3.2.2 MYCBP2-SPRYD3 deubiquitylates CHAMP1

Since the interaction between SPRYD3 and CHAMP1 significantly increased upon proteasome inhibition (Figure 16B), I explored the possibility of CHAMP1 being an ubiquitylation substrate of the potential MYCBP2-SPRYD3 complex destined for proteasomal destruction. I performed various siRNA experiments and ubiquitylation assays in different cell lines. First, I assessed CHAMP1 protein levels after SPRYD3 downregulation. I transfected U2OS and HeLa cells with siRNA targeting either GL2 (control) or SPRYD3 using up to three different siRNAs and performed western blot analysis. Interestingly, CHAMP1 protein levels increased upon SPRYD3 downregulation in both cell lines. The increase was significant for SPRYD3 siRNAs #2 and #3, whereas for SPRYD3 siRNA #1, CHAMP1 protein levels increased without breaching the significance threshold (Figure 18). Nonetheless, these results indicate that SPRYD3 regulates CHAMP1 protein levels negatively, potentially through proteasome directed ubiquitylation.

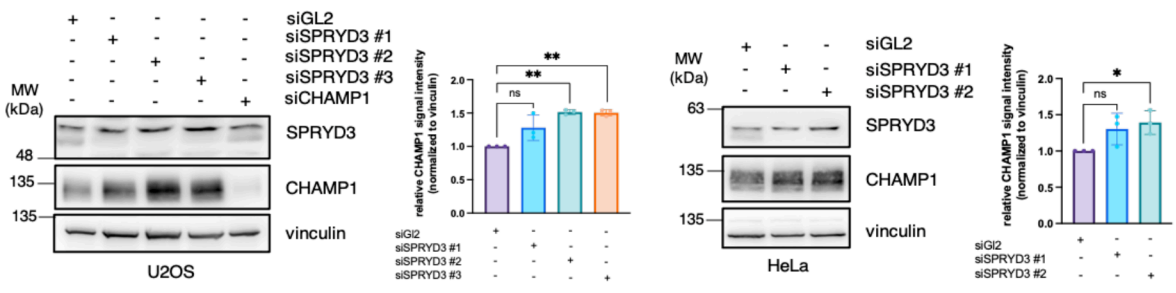


Figure 18: CHAMP1 protein levels are negatively regulated by SPRYD3.

U2OS or HeLa cells were transfected twice with 20 nM siRNA targeting Gl2 (=control), SPRYD3 or CHAMP1. 72h after the first transfection, cells were harvested and protein lysates were subjected to western blot analysis. Graphs depict relative CHAMP1 western blot signals after normalization and in relation to a siGl2 treated control. Relative values were log-transformed to obtain parametric distribution and subjected to a one sample t and Wilcoxon test, n=3 independent experiments. ns > 0.05, *p < 0.05, **p < 0.01.

To test whether MYCBP2-SPRYD3 ubiquitylates CHAMP1, I ectopically expressed GFP-CHAMP1, MYC-SPRYD3 and HA-Ubiquitin in HEK 293T WT or ΔFBXO45 cells and performed GFP pull-down assays. I included the HEK 293T ΔFBXO45 cell line to exclude any function of FBXO45 in regard to CHAMP1. Surprisingly, co-expression of MYC-SPRYD3 resulted in decreased ubiquitylation of CHAMP1 in both cell lines (Figure 19), which stands in contrast to the previously obtained results (Figure 16B and 18). Since the above presented results are rather difficult to interpret, I decided to focus on the next potential interactor identified in the Flag-SPRYD3 MS-analysis screen, XIAP.

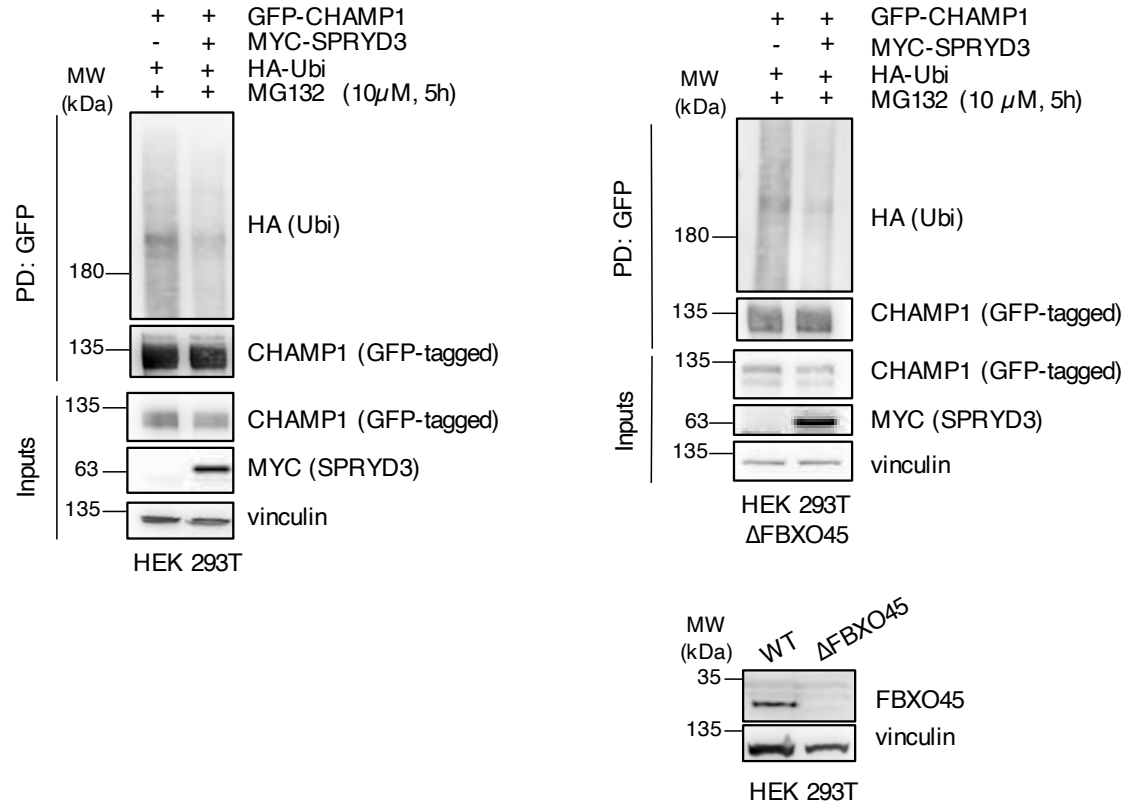


Figure 19: Ectopic expression of SPRYD3 decreases CHAMP1 ubiquitylation levels.
GFP-CHAMP1, MYC-SPRYD3 and HA-Ubiquitin were ectopically overexpressed in HEK 293T WT or ΔFBXO45 for 24h. 5h prior to harvest, cells were treated with MG132. Cells were harvested for GFP pull-down. Pull-downs and inputs were subjected to western blot analysis.

3.3 Validation of XIAP as SPRYD3 interaction partner

XIAP was identified as a potential interaction partner of Flag-SPRYD3 in the MS-screen performed in HEK 293T WT cells (Figure 14). XIAP is reported to have a

function in mitotic cell fate regulation by promoting mitotic slippage after MT-poison treatment (Hou et al., 2017). I hypothesized that the function of XIAP in mitotic slippage could be regulated by the MYCBP2-SPRYD3 complex in an ubiquitylation-dependent manner. I performed multiple interaction experiments and ubiquitylation assays to investigate the role of XIAP as interaction partner and substrate of the MYCBP2-SPRYD3 complex.

3.3.1 XIAP interacts with SPRYD3

In order to validate and characterize the interaction between XIAP and SPRYD3 in more detail, I performed various interaction experiments. Since both SPRYD3 and XIAP promote mitotic slippage, I again wondered whether these two proteins might preferentially interact during mitosis. I ectopically expressed Flag-SPRYD3 in HEK 293T WT cells for 24h and compared the level of interaction between Flag-SPRYD3 and endogenous XIAP in asynchronous and mitotic cells. To obtain a mitotic cell population, cells were treated for approximately 17h with 100 ng/ml nocodazole prior to harvest, whereas asynchronous cells were left untreated. Flag-SPRYD3 bound endogenous XIAP in asynchronous and mitotic cells to similar levels (Figure 20A). Various E3 ligase specificity factors, such as FBXW7, bind their respective substrates in a phosphorylation-dependent manner (Hänle-Kreidler et al., 2022; Hao et al., 2007; Orlicky et al., 2003; Verma et al., 1997). I performed a Flag-SPRYD3 IP assay combined with λ-phosphatase treatment to investigate whether phosphorylation contributes to the interaction between SPRYD3 and XIAP. Interestingly, λ-phosphatase treatment of Flag-SPRYD3 immunoprecipitated complexes significantly reduced the amount of XIAP co-precipitating with Flag-SPRYD3 compared to a non-treated control (20B). Taken together, these results indicate that XIAP interacts with SPRYD3 in asynchronous and mitotic cells and that phosphorylation might play a role in the interaction between SPRYD3 and XIAP.

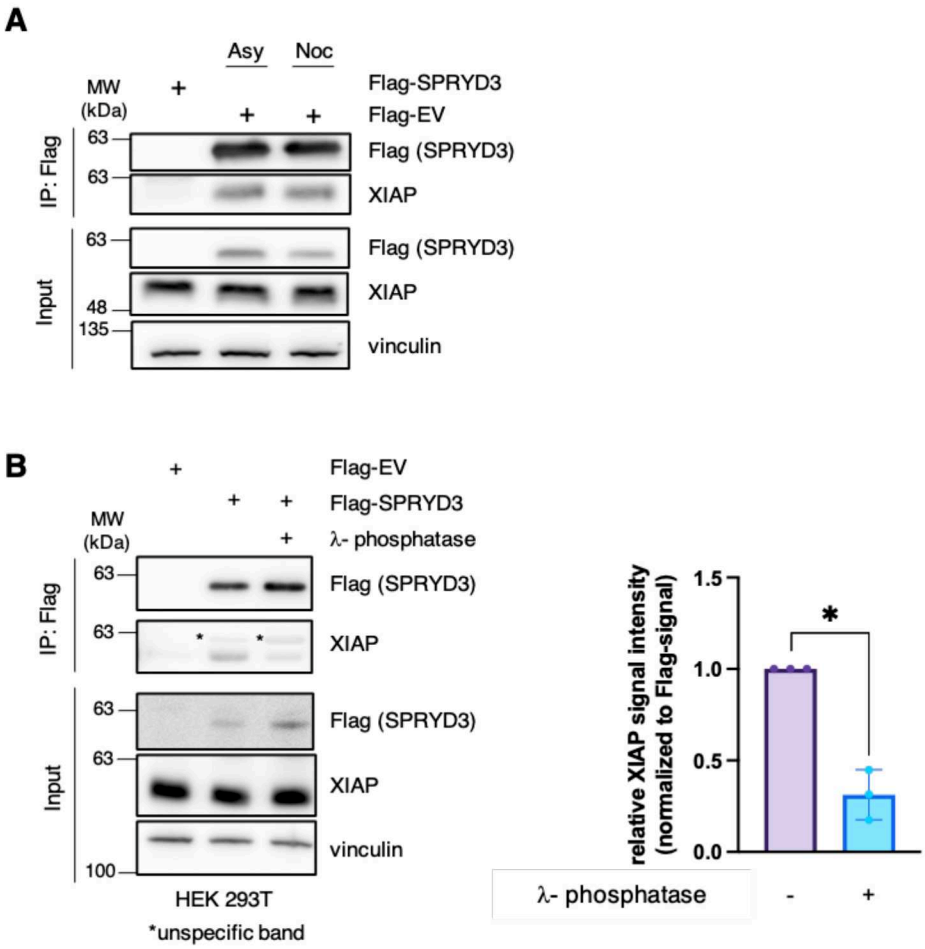


Figure 20: SPRYD3 interacts with XIAP in asynchronous and mitotic cells and the interaction is dependent on phosphorylation.
(A) HEK293T WT cells were transfected with Flag-SPRYD3 and incubated for 24h. 17h previous to harvest, cells were synchronized with nocodazole to obtain a mitotic cell population. Cells were harvested for Flag-IP. IPs were subjected to western blot analysis. **(B)** Flag-SPRYD3 was ectopically expressed in HEK 293T WT cells for 24h. Cells were harvested for Flag-IP. One IP-sample was treated with λ-phosphatase before eluting complexes from Flag-M2 beads. Graph depicts XIAP IP western blot signals previously normalized to respective Flag-SPRYD3 IP signals. Statistical analysis was performed with log-transformed values to obtain parametric distribution. A one sample t and Wilcoxon test was performed, n=3 independent experiments. *$p < 0.05$, * indicates unspecific bands.

3.3.2 The BIR2-BIR3 of XIAP and the SPRY2-domain of SPRYD3 mediate their interaction

In order to characterize the interaction between SPRYD3 and XIAP in more detail, I used XIAP and SPRYD3 deletion mutants to identify the reciprocal binding sites (Figure 21A and B). XIAP is itself an E3 ligase with 5 characterized domains, denoted as BIR1-, BIR2-, BIR3-, UBA- and RING-domain. These domains are essential for different kinds of functions (Figure 21A) (Abbas and Larisch, 2020; Galbán and Duckett, 2010; Vucic, 2018). To asses, which domains are essential for interaction with SPRYD3, I transfected Flag-XIAP truncations into HEK 293T WT cells and immunoprecipitated Flag-XIAP complexes. Endogenous SPRYD3 co-precipitation was

abolished with Flag-XIAP constructs lacking the BIR1- and/or BIR2-domain, indicating that the simultaneous presence of these two domains is necessary for the interaction with SPRYD3 (Figure 21A). Interestingly, the linker region between XIAP BIR1 and BIR2 is also essential for direct binding and inhibition of caspases-3 and -7 (Abbas and Larisch, 2020; Galbán and Duckett, 2010). However, the interaction between SPRYD3 and XIAP with constructs 2 and 3 (Figure 21A), which express the BIR1- and BIR2-domains, but lack the RING-domain, was weaker compared to XIAP constructs expressing all of these three domains simultaneously (Figure 21A). This suggests, that the Flag-XIAP RING-domain further stabilizes the interaction with SPRYD3. Ectopic expression of Flag-SPRYD3 either lacking SPRY1 or SPRY2, revealed that SPRYD3 mediates its interaction with XIAP through the second SPRY-domain (Figure 21B). The SPRYD3 SPRY2-domain was previously shown to be essential for its interaction with MYCBP2 (Figure 9B). The ability of one SPRYD3 SPRY-domain to bind both MYCBP2 and XIAP is similar to FBXO45, as its only SPRY-domain mediates both substrate recruitment and binding to MYCBP2 (Desbois et al., 2018; Saiga et al., 2009).

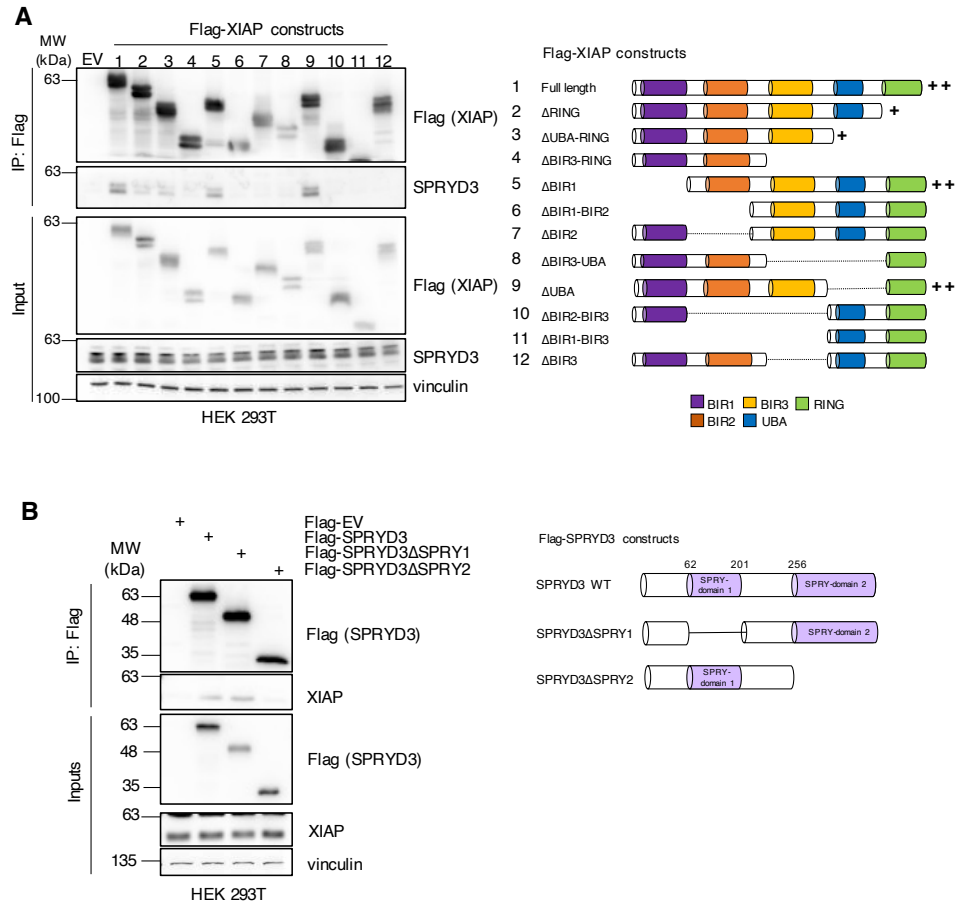


Figure 21: SPRYD3 and XIAP interact through the BIR2-BIR3 and SPRY2-domains, respectively.
(A) Flag-XIAP constructs were transfected into HEK 293T WT cells and overexpressed for 24h. Cells were harvested for Flag-IP. IPs and inputs were subjected to western blot analysis. + indicates interaction of SPRYD3 with Flag-XIAP constructs. **(B)** Flag-SPRYD3 deletion constructs were ectopically expressed in HEK 293T cells for 24h. Cells were harvested for Flag-IP. Follow-up procedures were carried out as described in (A).

3.3.3 MYCBP2-SPRYD3 deubiquitylates XIAP

I next aimed at assessing whether the MYBCP2-SPRYD3 complex exhibits ubiquitylation activity towards XIAP. To do so, I performed siRNA experiments and ubiquitylation assays in different cell lines. I treated U2OS and HeLa cells with siRNA targeting GL2 (control) or SPRYD3 and assessed XIAP protein levels after SPRYD3 knock-down. Interestingly, XIAP protein levels did not change compared to a siGL2-treated control, indicating that potential ubiquitylation of XIAP through SPRYD3 is not linked to proteasomal degradation (Figure 22). However, when performing ubiquitylation assays with ectopically expressed Flag-XIAP and MYC-SPRYD3 or MYC-MYCBP2, I observed decreased ubiquitylation of XIAP compared to a mock-treated control (Figure 23). This was the case in both HEK 293TWT and ΔFBXO45 cells and resembled results obtained for CHAMP1 presented earlier (Figure 19).

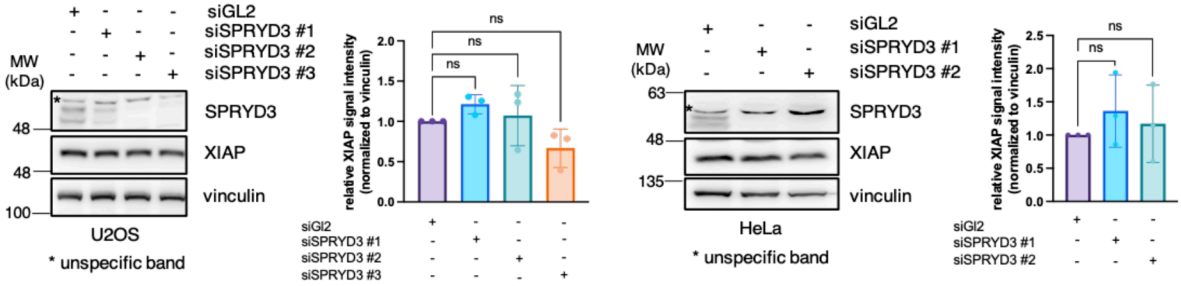


Figure 22: XIAP protein levels are not regulated by SPRYD3.
U2OS or HeLa cells were transfected twice with 20 nM siRNA against GL2 (= control) or SPRYD3. 72h after the first transfection, cells were harvested and protein lysates were subjected to western blot analysis. Graphs depict relative XIAP western blot signals after normalization and in relation to a siGl2 treated control. For statistical analysis, relative values were log-transformed to obtain parametric distribution. Log-transformed values were applied to a one sample t and Wilcoxon test, n=3 independent experiments. ns > 0.05, * indicates unspecific band.

Since ubiquitylation also affects protein fate different from proteasomal degradation, two hypotheses can explain the above presented results: (i) MYCBP2-SPRYD3 degrades an unknown E3 ligase, which under normal conditions is responsible for XIAP degradation-independent ubiquitylation. Therefore, upon ectopic expression of MYCBP2 or SPRYD3, this unknown E3 ligase is degraded resulting in less ubiquitylated XIAP (Figure 23). Since this unknown E3 ligase does not mark XIAP for ubiquitin-mediated destruction, ablation of SPRYD3 does not result in increased XIAP protein levels. (ii) MYCBP2-SPRYD3 regulates a DUB, which enables it to recruit downstream substrates for deubiquitylation. Upon ectopic expression of MYCBP2-SPRYD3, this unknown DUB is increasedly activated and as a result, XIAP is deubiquitylated. Upon reviewing published literature, I considered the second hypothesis to be probable. A study performed by Ma et al. 2014 for example, describes

how the ectopic expression of E3 ligase RNF220 leads to β-catenin deubiquitylation. They explained this observation by identifying that the interaction between the E3 ligase RNF220 and DUB USP7 is responsible for the ability of USP7 to recruit and deubiquitylate its substrate, β-catenin. Consequently β-catenin is stabilized leading to further activation of the Wnt-signaling pathway (Ma et al., 2014). In another study performed by Wu et al. 2016, USP7 was shown to be poly-ubiquitylated in a K63-dependent manner. This polyubiquitylation did not contribute to proteasomal degradation of the DUB, but rather enabled USP7 to recruit, deubiquitylate and stabilize HIF1α, consequently promoting hypoxia-induced EMT and metastasis (Wu et al., 2016). Both of these examples corroborate how E3 ligases and DUBs, although possessing opposing activities, can still form complexes and collaborate. Instead of marking USP7 for proteasomal destruction, the ubiquitylation performed by the E3 ligases described in those studies rather stabilize or activate USP7 so that downstream deubiquitylation events can occur. Further investigation of already published literature revealed that XIAP protein turnover and stability is positively regulated through the deubiquitylation activity of the DUB USP11 (Zhou et al., 2016). USP11 was also reported to deubiquitylate RAE1, a conserved interactor of MYCBP2 (Grill et al., 2012), leading to proper bipolar spindle formation during mitosis (Stockum et al., 2018).

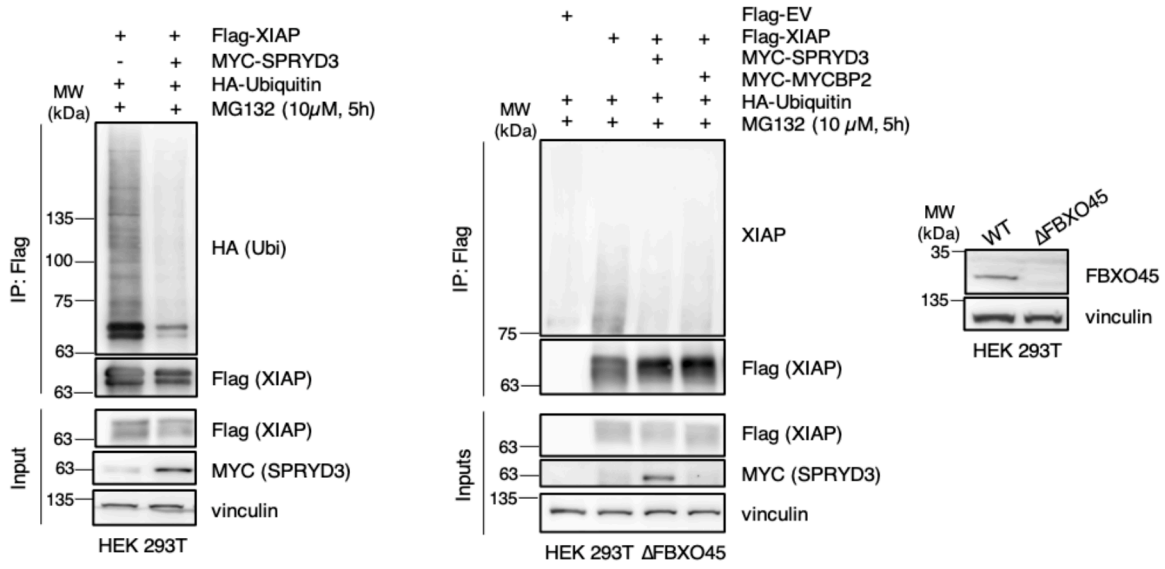


Figure 23: MYCBP2-SPRYD3 overexpression leads to XIAP deubiquitylation.
Flag-XIAP, MYC-MYCBP2 or MYC-SPRYD3 and HA-Ubiquitin were co-transfected into HEK 293T WT or ΔFBXO45 cells and overexpressed for 48h. Cells were treated with MG132 5h prior to harvest and Flag-IP was performed. IPs and inputs were subjected to western blot analysis.

3.4 Characterization of USP11 as a potential substrate of the MYCBP2-SPRYD3 complex

As previously described, XIAP and RAE1 were enriched in the Flag-SPRYD3 MS-screen (Figure 14A) and both interact with ectopically expressed Flag-SPRYD3 (Figure 14B). USP11 was reported to interact with and deubiquitylate both RAE1 and XIAP (Stockum et al., 2018; Zhou et al., 2016). In addition, RAE1 is also a conserved interaction partner of the MYCBP2 E3 ligase (Grill et al., 2012). Thus, I wondered, whether USP11 and MYCBP2-SPRYD3 might collaborate in the deubiquitylation process of XIAP or RAE1 in the same way as it was reported for USP7 and its respective E3 ligases (Ma et al., 2014; Wu et al., 2016). In addition, USP11 is a known tumor promotor (Sun et al., 2019; Zhou et al., 2016) and therefore also might regulate mitotic cell fate. After revising the MS-screen data obtained from Flag-FBXO45 and Flag-SPRYD3 IPs, I encountered USP11 to be positively enriched in both screens (Figure 24). This suggested that USP11 might form part of the MYCBP2-SPRYD3 network and so I decided to explore the possibility of USP11 being regulated by the MYCBP2-SPRYD3 complex in the context of mitotic cell fate decision. In order to validate this hypothesis and characterize the relationship between the MYCBP2-SPRYD3 complex and USP11, I performed various experiments that might help to support my assumption.

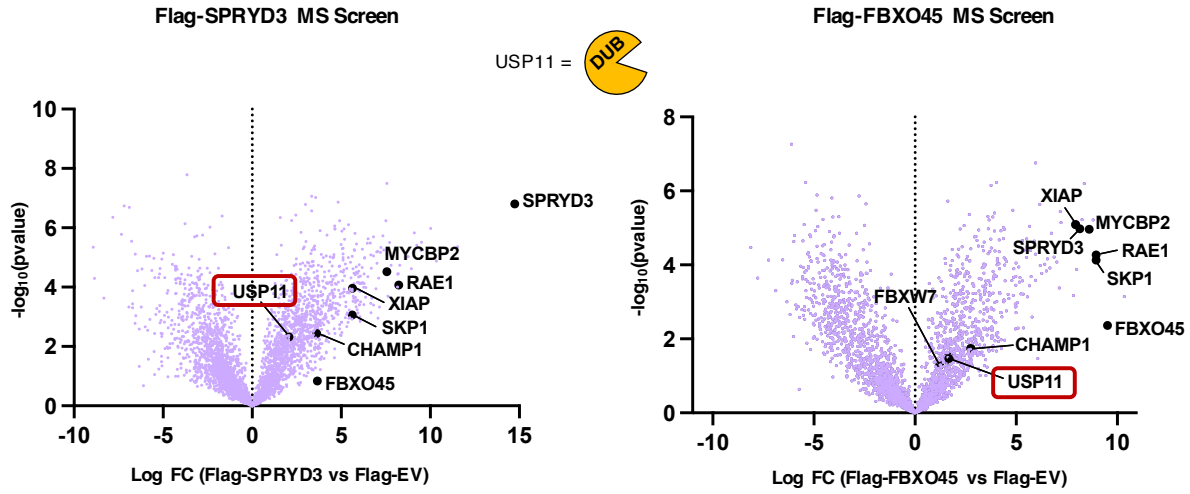


Figure 24: USP11 is a potential interactor of SPRYD3 and FBXO45.
Volcano plot demonstrating enrichment of putative SPRYD3 or FBXO45 interaction partners identified by combined IP-MS analysis approach. n=4 for both screens. Previously obtained data was re-analyzed and USP11 was identified as enriched potential interactor in both screens.

3.4.1 USP11 interacts with MYCBP2 and SPRYD3

Before assessing a putative role of USP11 as an ubiquitylation substrate, I aimed at validating USP11 as an interactor of the MYCBP2-SPRYD3 complex. I ectopically expressed Flag-MYCBP2, Flag-SPRYD3 or Flag-FBXO45 with MYC-USP11 in HEK 293T WT cells and also performed a similar experimental setup in HEK 293T ΔFBXO45 cells to exclude FBXO45 as mediator of interaction. My results show that MYC-USP11 co-precipitated with Flag-MYCBP2 both in HEK 293T WT and ΔFBXO45 cells (Figure 25A). Flag-SPRYD3 and Flag-FBXO45 were both able to co-precipitate MYC-USP11 in HEK 293T WT cells, but in absence of FBXO45, SPRYD3 -USP11 complexes were still able to form (Figure 25B).

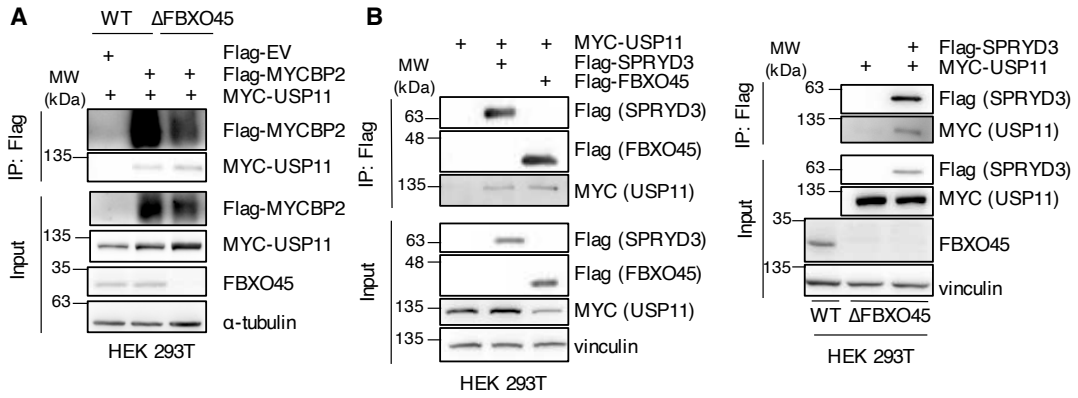


Figure 25: USP11 interacts with MYCPB2 and SPRYD3 independently from FBXO45.
(A) Flag-MYCBP2 and MYC-USP11 were co-transfected into HEK 293T WT or ΔFBXO45 cells and overexpressed for 48h. Cells were harvested for Flag-IP. **(B)** Flag-FBXO45 or Flag-SPRYD3 were co-transfected with MYC-USP11 in HEK 293T WT or ΔFBXO45 cells as indicated and overexpressed for 24h. Cells were harvested for Flag-IP. IPs and inputs were subjected to western blot analysis.

3.4.2 USP11 promotes mitotic slippage in paclitaxel and nocodazole treated cells

Since my aim was the elucidation of how the MYCBP2-SPRYD3 complex regulates mitotic slippage through ubiquitylation of a potential substrate, it was important to investigate the role of USP11 in mitotic cell fate regulation. To show this, I performed live cell imaging experiments in U2OS and RPE1 cells in response to siRNA-mediated downregulation of USP11 in the presence of paclitaxel or nocodazole. Both U2OS and RPE1 cells exhibited significantly higher rates of mitotic cell death in absence of USP11 after paclitaxel and nocodazole treatment compared to a siGL2-treated control (Figure 26), similar to SPRYD3- and MYCBP2-depletion (Figure 5).

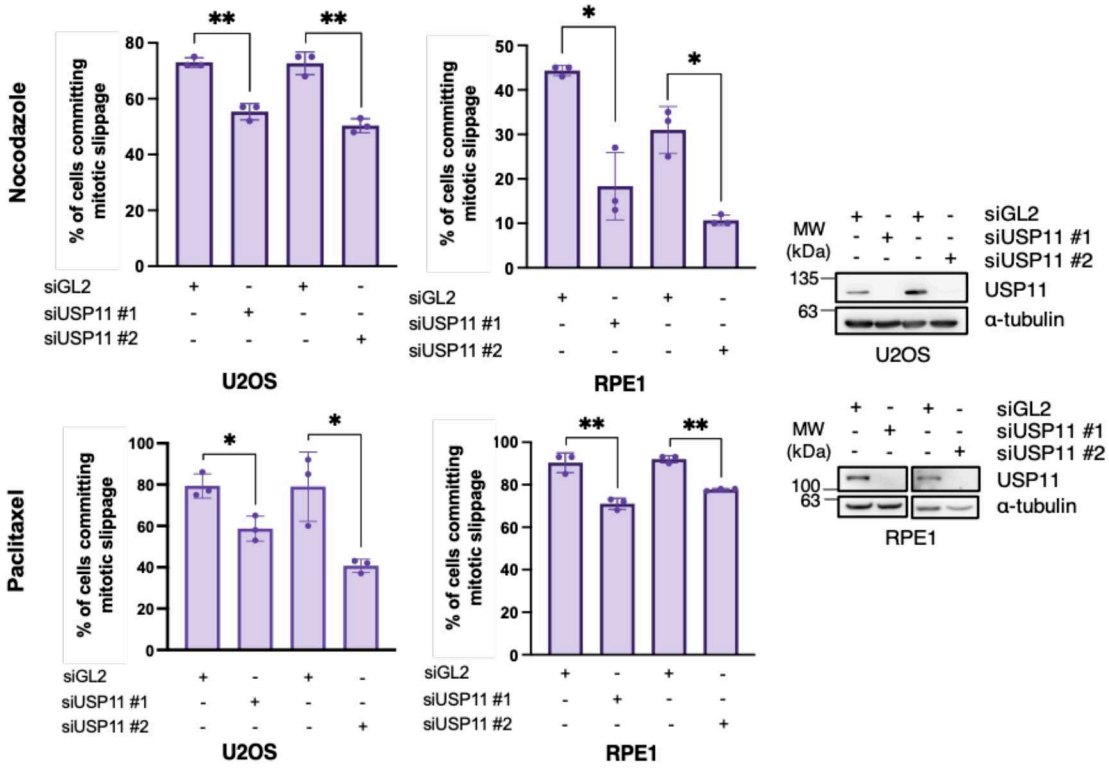


Figure 26: USP11 promotes mitotic slippage in paclitaxel or nocodazole treated U2OS and RPE1 cells. U2OS or RPE1 cells were transfected twice with 20 nM siRNA targeting GI2 (= control) or USP11. 72h after the first transfection, cells were treated with nocodazole or paclitaxel and live cell imaging was performed. Mitotic cell fate of n=60 cells was determined for each experiment. *$p < 0.05$, **$p < 0.01$, one-way ANOVA with Dunette post hoc test, n=3 independent experiments for each cell line and respective drug treatment.

To test whether the effect observed after USP11-depletion is specific for MT-poison presence, I performed live cell imaging in USP11-depleted U2OS and RPE1 cells without prior MT-poison treatment. Similar to MYCBP2- and SPRYD3-depletion in the absence of MT-poisons (Figure 6A), knock-down of USP11 did not alter cell fate in non-drug treated U2OS and RPE1 cells compared to a siGL2-treated control (Figure 27A). Almost 100% of cells underwent normal cell division without significant differences throughout all conditions. Additionally, mitotic timing did not differ between USP11-depleted and control cell populations (Figure 27B). Therefore, I can conclude that the significantly increased percentage of mitotic cell death observed in USP11-depleted cells is specific for MT-poison treatment and does not occur under untreated conditions. These findings resembled previous results obtained with SPRYD3 and MYCBP2 (Figures 5 and 6) and suggested that USP11 might collaborate with MYCBP2-SPRYD3 in promoting mitotic slippage.

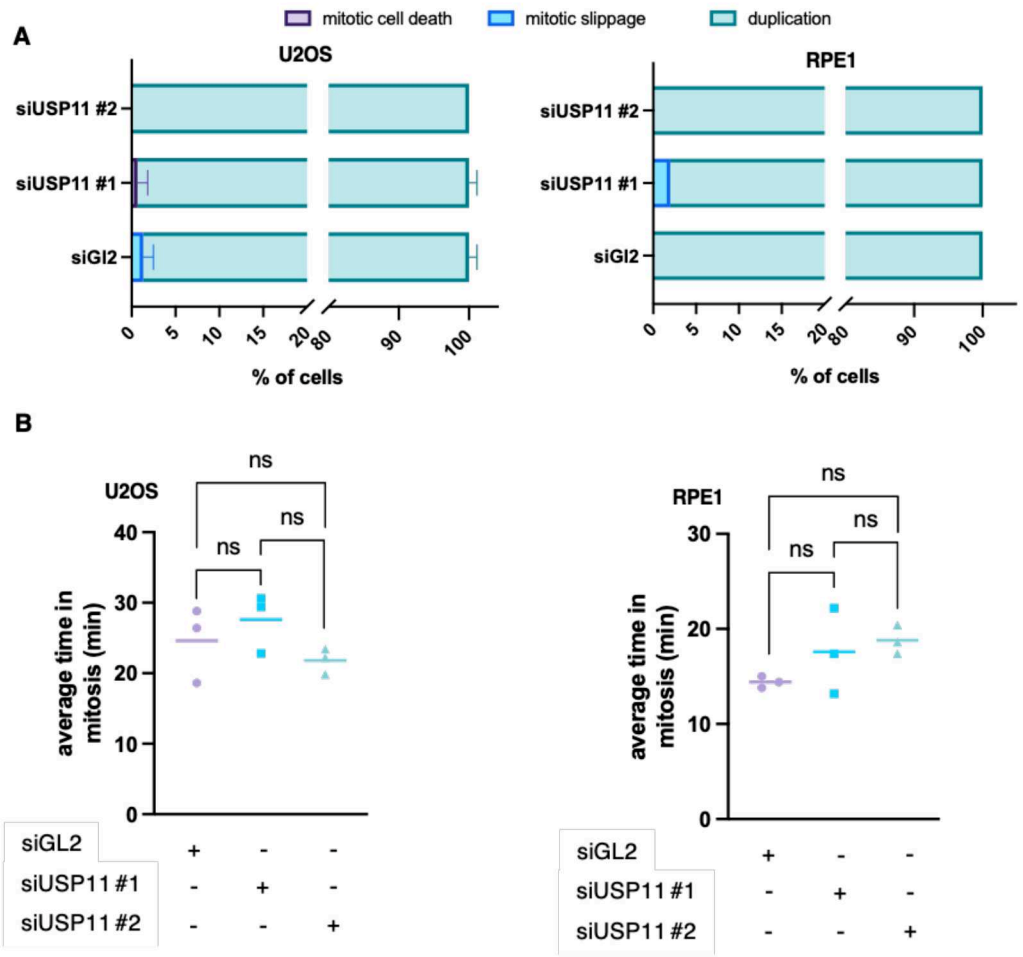


Figure 27: Depletion of USP11 in cycling cells does not alter mitotic cell fate nor timing.
(A) U2OS or RPE1 cells were transfected twice with 20 nM siRNA targeting GL2 (= control) or USP11. 72h after the first transfection, live cell imaging was performed and mitotic cell fate of n=60 cells was determined for each experiment. ns > 0.05, one-way ANOVA with Dunette post hoc test, n = 3 independent experiments for each cell line and drug treatment. **(B)** U2OS or RPE1 cells were transfected twice with 20 nM siRNA targeting GL2 (= control) or USP11. 72h after the first transfection, live cell imaging was performed and time in mitosis for n=60 cells was determined for each experiment. Mitotic timing was determined by visually following cells from roundup (= beginning of mitosis) until cytokinesis (=end of mitosis). ns > 0.05, one-way ANOVA with Dunette post hoc test, n=3 independent experiments for each cell line and drug treatment.

3.4.3 USP11 interacts with the MYCBP2 RCC1-like and MYC-binding domain

To further characterize the relationship between USP11 and the MYCBP2-SPRYD3 complex, I performed additional interaction experiments to elaborate the interaction between USP11 and MYCBP2 or USP11 and SPRYD3 in more detail. First, I ectopically expressed MYC-USP11 with Flag-MYCBP2 constructs previously used for interaction mapping experiments with SPRYD3 (Figure 8A) into HEK 293T WT cells. MYC-USP11 co-precipitated mostly with the Flag-MYCBP2 constructs harboring the RCC1-like domain and the MYC-binding domain, the latter being the construct that also comprises the SPRYD3-binding site (Figure 28A). This indicates that USP11 might have multiple functions regarding MYCBP2 on top of being a potential

ubiquitylation substrate. Furthermore, ectopic expression of Flag-SPRYD3 deletion constructs with MYC-USP11 revealed that USP11 binds throughout the whole protein (Figure 28B).

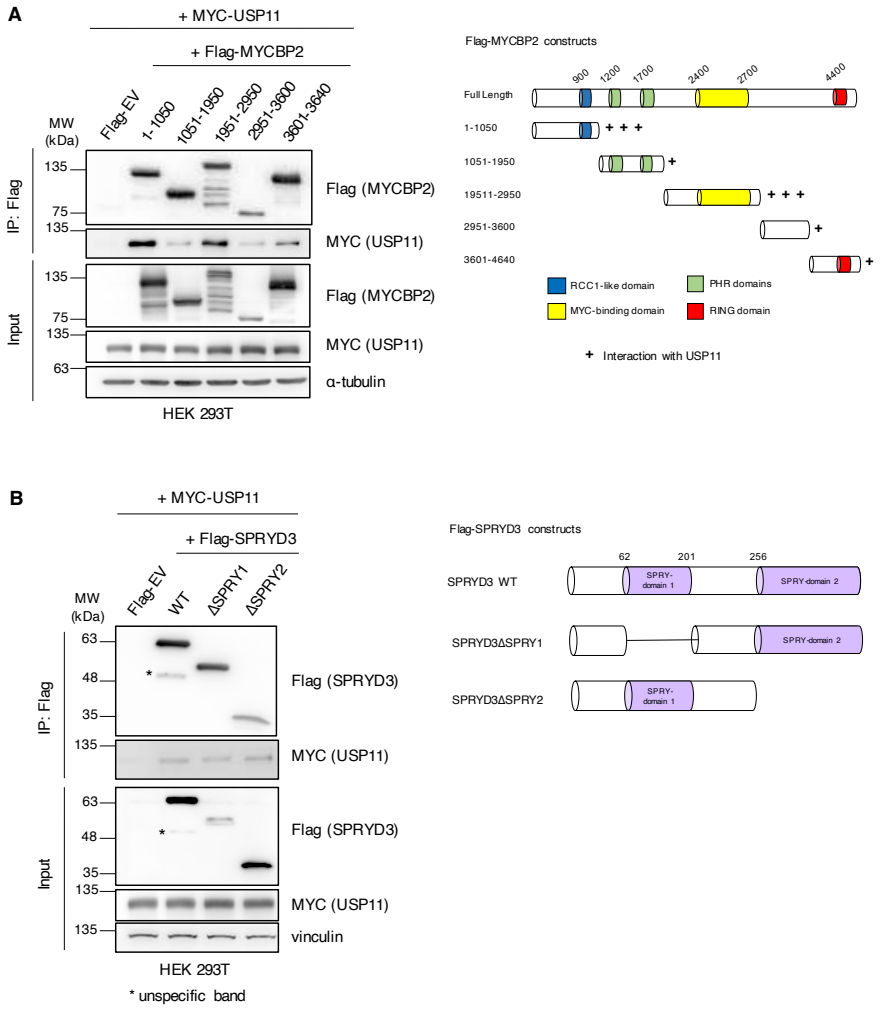


Figure 28: USP11 interacts with the MYCBP2 RCC1-like and MYC-binding domain.
(A) Flag-MYCBP2 constructs and MYC-USP11 were ectopically overexpressed in HEK 293T WT cells for 24h. Cells were harvested for Flag-IP. IPs and inputs were subjected to western blot analysis. **(B)** Flag-SPRYD3 constructs were co-transfected with MYC-USP11 in HEK 293T WT cells and overexpressed for 24h. Follow-up procedures were executed as described in (A).

3.4.4 USP11 interacts with SPRYD3 *in vitro*

Since substrate specificity factors tend to interact with their substrates directly, I wondered, whether SPRYD3, as a potential substrate specificity factor of MYCBP2, directly binds its potential substrate USP11. I recombinantly expressed and purified MBP-SPRYD3 and GST-USP11 from *E. coli* to perform *in vitro* MBP pull-down assays. MBP-SPRYD3 was able to pull down GST-USP11, confirming a direct physical interaction between those two proteins (Figure 29).

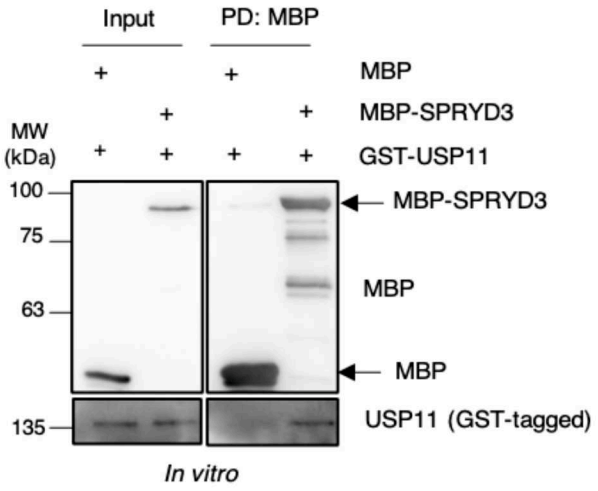


Figure 29: Recombinantly purified USP11 and SPRYD3 interact *in vitro*.
Recombinant MBP or MBP-SPRYD3 was combined with GST-USP11. MBP pull-down was performed.

3.4.5 USP11 is ubiquitylated by the MYCBP2-SPRYD3 E3 ligase complex

The confirmed direct physical interaction between USP11 and SPRYD3 (Figure 29) allows to postulate that USP11 might act as an ubiquitylation substrate of the MYCBP2-SPRYD3 complex. Thus, to assess whether MYCBP2-SPRYD3 possessed ubiquitylation activity towards USP11, I performed *in vivo* and *in vitro* ubiquitylation experiments.

3.4.5.1 SPRYD3-MYCBP2 E3 ligase ubiquitylates USP11

To explore the ability of MYCBP2-SPRYD3 to ubiquitylate USP11, I performed ubiquitylation assays in HEK 293T WT and ΔFBXO45 cells. I ectopically expressed Flag-USP11 with MYC-MYCBP2 or MYC-MYCBP2 C4520S, an E3 ligase dead mutant of MYCBP2 together with HA-Ubiquitin. While co-expression of MYC-MYCBP2 WT increased Flag-USP11 ubiquitylation compared to a control expressing MYC-EV, MYC-MYCBP2 C4250S expression reversed this effect (Figure 30B). I also observed ubiquitylation of Flag-USP11 in HEK 293T ΔFBXO45 cells, confirming that the canonical substrate specificity factor FBXO45 is not involved in USP11 ubiquitylation (Figure 30C). Interestingly, Flag-MYCBP2 3601-4640, which only harbors the RING-domain, was sufficient to drive USP11 ubiquitylation in HEK 293T WT and ΔFBXO45 cells (Figure 30D). This can be explained with the fact that SPRYD3 also binds the MYCBP2 RING-domain as shown previously (Figure 8A) and might mediate USP11 ubiquitylation also from there.

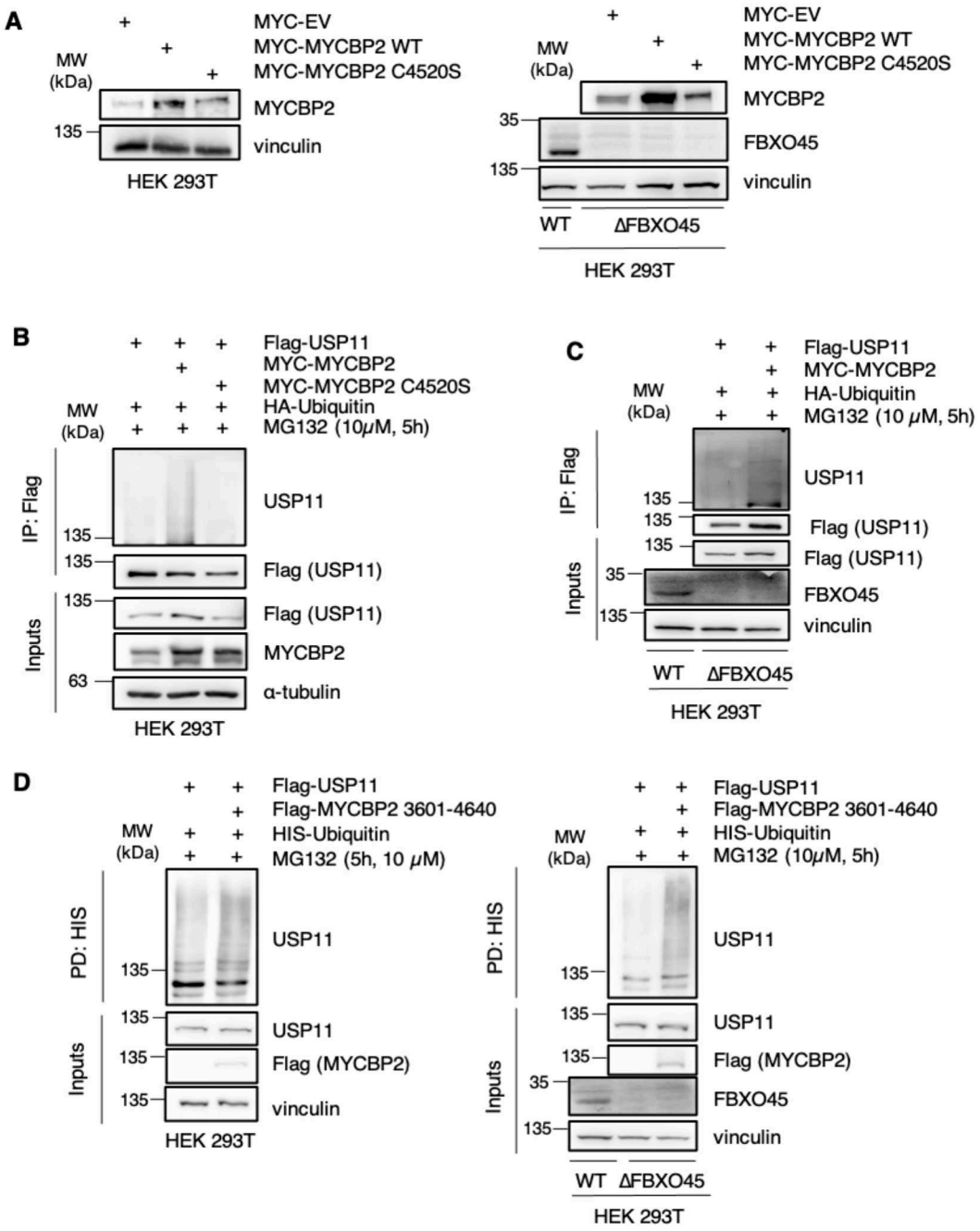


Figure 30: MYCBP2 ubiquitylates USP11 in the absence of FBXO45.
(A) Representative western blots of HEK 293T WT and ΔFBXO45 cell protein lysates for detection of endogenous FBXO45 and overexpression of MYC-MYCBP2 WT and catalytic inactive MYC-MYCBP2 C4520S. DNA was transfected into HEK 293T WT or ΔFBXO45 cells and overexpressed for 48h. **(B)** Flag-USP11, MYC-MYCBP2 or MYC-MYCBP2 C4520S and HA-Ubiquitin were transfected into HEK 293T WT cells and expressed for 48h. 5h prior to harvest cells were treated with MG132. Cells were harvested for Flag-IP. IPs and inputs were subjected to western blot analysis. **(C)** Flag-USP11, MYC-MYCBP2 and HA-Ubiquitin were transfected into HEK 293T ΔFBXO45 cells and overexpressed for 48h. Follow-up procedures were executed as described in (B). **(D)** Flag-USP11, Flag-MYCBP2 3601-4640 and HIS-Ubiquitin were transfected into HEK 293T WT or ΔFBXO45 cells and overexpressed for 24h. Cells were harvested for HIS pull-down. Follow-up procedures were executed as described in (B).

Furthermore, I investigated whether SPRYD3 mediated USP11 ubiquitylation. I ectopically expressed Flag-USP11 with either MYC-SPRYD3 or MYC-FBXO45 and

HA-Ubiquitin in HEK 293T WT or ΔFBXO45 cells. Only MYC-SPRYD3 expression led to Flag-USP11 ubiquitylation in HEK 293T WT cells, while MYC-FBXO45 expression showed no effect (Figure 31A). In HEK 293T ΔFBXO45 cells MYC-SPRYD3 was still capable to perform USP11-ubiquitylation (Figure 31B), suggesting that FBXO45 is not a substrate specifity factor for USP11. Taken together, both MYCBP2 and SPRYD3 are capable of ubiquitylating USP11 independently from FBXO45.

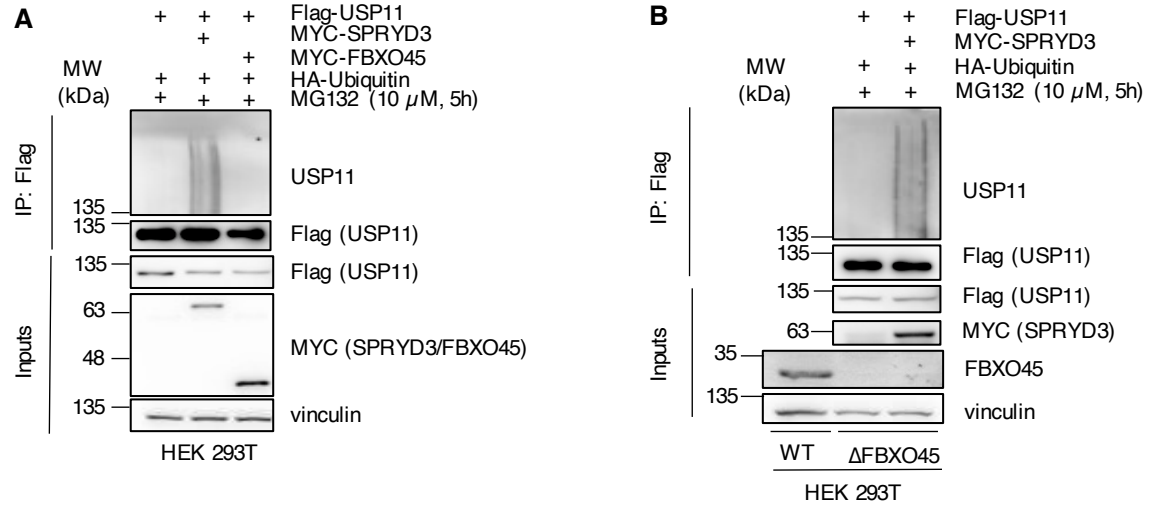


Figure 31: SPRYD3, but not FBXO45, ubiquitylates USP11.
(A) Flag-USP11, MYC-SPRYD3 or MYC-FBXO45 and HA-Ubiquitin were ectopically expressed in HEK 293T WT cells 24h. 5h prior to harvest, cells were treated with MG132. Cells were harvested for Flag-IP. IPs and inputs were subjected to western blot. **(B)** Flag-USP11, MYC-SPRYD3 and HA-Ubiquitin were transfected into HEK 293T ΔFBXO45 cells and overexpressed for 24h. Follow-up procedures were carried out as described in (A).

3.4.5.2 The MYCBP2-SPRYD3 complex ubiquitylates USP11 *in vivo* and *in vitro*

So far, I confirmed that MYCBP2 and SPRYD3 ubiquitylate USP11 separately (Figures 30 and 31). To exclude that MYCBP2 and SPRYD3 might be part of different E3 ligase complexes, I aimed at assessing, whether MYCBP2-SPRYD3 forms a complex to ubiquitylate USP11 in cells and *in vitro*. First, I investigated whether MYCBP2-SPRYD3 was capable of ubiquitylating USP11 as a complex in cells. I used RNAi to deplete HEK 293T WT cells of SPRYD3 or MYCBP2, and additionally co-transfected Flag-USP11 and MYC-MYCBP2 3601-4640 or MYC-SPRYD3 and HIS-Ubiquitin. This would help me to assess whether MYCBP2 and SPRYD3 would still be capable of ubiquitylating USP11 in absence of the other. In both cases, USP11 ubiquitylation decreased in both SPRYD3- and MYCBP2-depleted cells compared to a siGL2-treated control, even though MYC-MYCBP2 3601-4640 or MYC-SPRYD3 were expressed, as indicated (Figure 32A and B). This suggested that the MYCBP2-SPRYD3 complex ubiquitylates USP11. To further confirm these results, I performed another

ubiquitylation assay by co-expressing Flag-USP11 with MYC-SPRYD3 WT or the respective SPRYD3 SPRY-domain deletion mutants. I hypothesized, that while MYC-SPRYD3 WT should ubiquitylate Flag-USP11, MYC-SPRYD3ΔSPRY2 should not be capable to do so, since it cannot recruit MYCBP2 (Figure 9B), and would therefore lack its E3 ligase activity. As expected, MYC-SPRYD3ΔSPRY2 co-expression decreased Flag-USP11 ubiquitylation compared to MYC-SPRYD3 WT expressing cells (Figure 32C). Surprisingly, MYC-SPRYD3ΔSPRY1 was also not capable of ubiquitylating USP11 (Figure 32C). One explanation for this observation could be that MYC-SPRYD3ΔSPRY1 is less stable within the cell compared to Flag-SPRYD3 WT and Flag-SPRYD3ΔSPRY2 (Figure 32C, 3rd input lane), and while SPRYD3ΔSPRY1 is still able to interact with USP11 (Figure 28B), it probably might not be able to recruit as much for ubiquitylation. This further suggests that MYCBP2-SPRYD3 ubiquitylates USP11 as a complex.

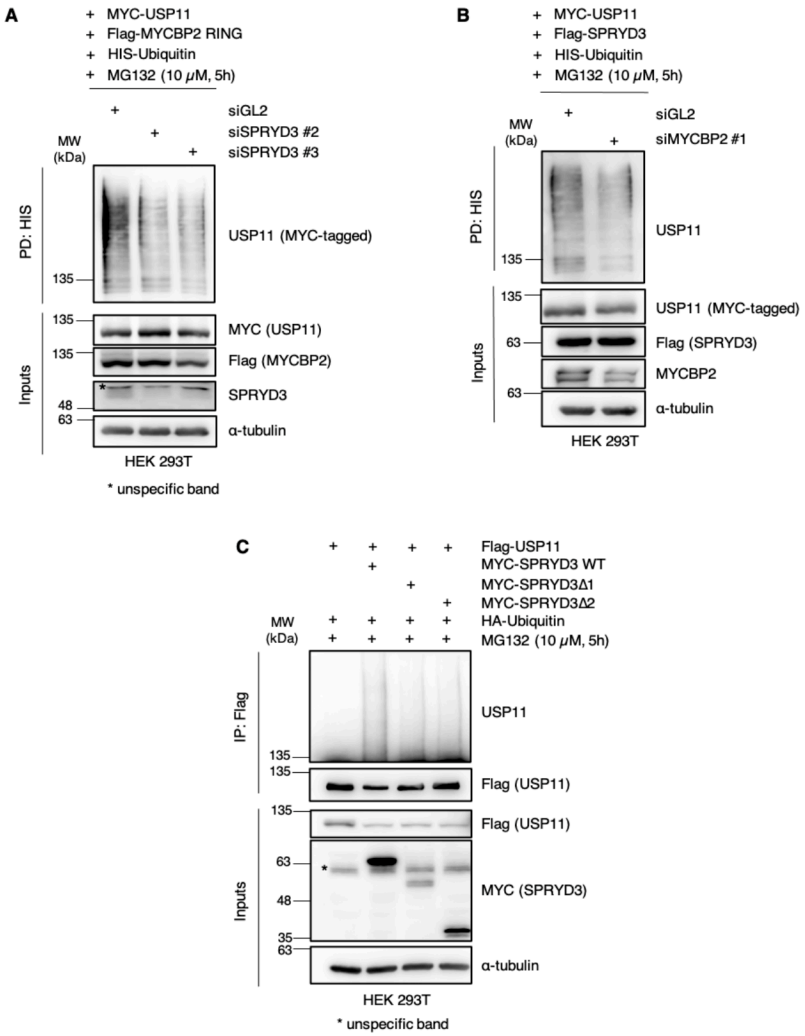


Figure 32: MYCBP2 and SPRYD3 ubiquitylate USP11 as a complex.

(A) HEK 293T WT cells were transfected twice with 20 nM siRNA targeting GL2 (= control) or SPRYD3. 48h after the first transfection, MYC-USP11, Flag-MYCBP2 3601-4640 and HIS-Ubiquitin were transfected and cells were incubated for further 24h. 5h prior to harvest, cell were treated with MG132. Cells were harvested for HIS pull-down. Pull-downs and inputs were subjected to western blot analysis. **(B)** HEK 293T WT cells were transfected twice with 20 nM siRNA targeting Gl2 (= control) or MYCBP2. 48h after the first transfection, MYC-USP11, Flag-SPRYD3 and HIS-Ubiquitin were transfected and cells were incubated for further 24h. Follow-up procedures were executed as described in (A). **(C)** Flag-USP11 was co-transfected with MYC-SPRYD3 constructs and overexpressed for 24h. 5h prior to harvest, cells were treated with MG132. Cells were harvested for Flag-IP. IPs and inputs were subjected to western blot analysis.

To further confirm that MYCBP2-SPRYD3 ubiquitylates USP11 as a complex and this ubiquitylation occurs directly, I performed *in vitro* ubiquitylation assays. Due to the high molecular weight of MYCBP2, I was not able to recombinantly purify full-length MYCBP2 from *E. coli*. Therefore, I precipitated the E3 ligase complex from cells by co-transfecting Flag-SPRYD3 WT and MYC-MYCBP2 WT into HEK 293T WT cells. I included two E3 ligase complex controls consisting of Flag-SPRYD3 WT and MYC-MYCBP2 C4520S or Flag-SPRYD3ΔSPRY2 and MYC-MYCBP2 WT. The first of the control complexes does not exhibit E3 ligase activity as the catalytic inactive mutant MYCB2 C4520S was used. The latter of the control-complexes should not be capable to ubiquitylate USP11 (Figure 32C), since SPRYD3ΔSPRY2 cannot recruit MYCBP2 (Figure 9B). Immunoprecipitated E3 ligase complexes were eluted from Flag-beads and mixed with recombinant HIS-USP11, HIS-Uba1, GST-UbcH5b, Ubiquitin and ATP, incubated for 0 or 1h and applied to western blot analysis. *In vitro* ubiquitylation of USP11 occurred only in presence of the WT E3 ligase complex consisting of Flag-SPRYD3 WT and MYC-MYCBP2 WT, while the E3 ligase complexes containing either MYC-MYCBP2 C2450S or Flag-SPRYD3ΔSPRY2 were unable to ubiquitylate USP11 (Figure 33). Taken together all of the above presented results, it is conceivable that MYCBP2-SPRYD3 forms an active E3 ligase complex that directly targets its substrate USP11 for ubiquitylation.

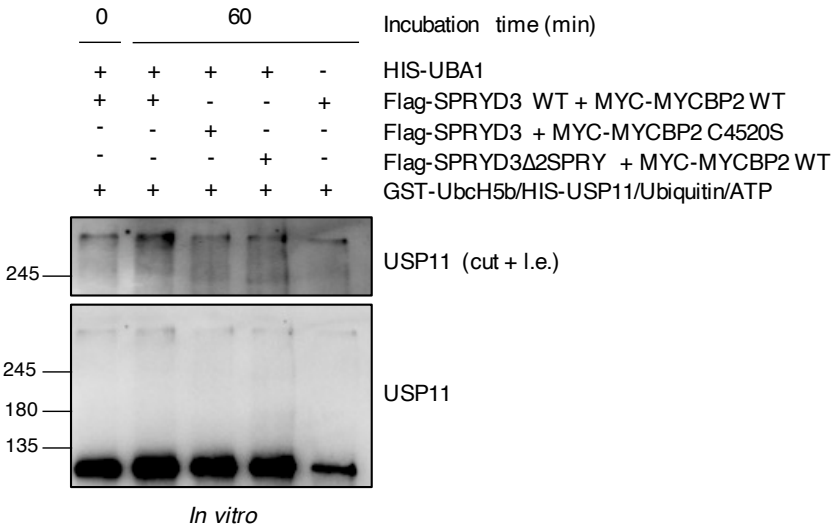


Figure 33: MYCBP2-SPRYD3 ubiquitylates USP11 *in vitro*.
Flag-SPRYD3 WT or Flag-SPRYD3ΔSPRY2 was co-expressed with MYC-MYCBP2 WT or MYC-MYCBP2 C4520S in HEK 293 WT cells for 48h and Flag-IP was performed. *In vitro* ubiquitylation assays were performed using recombinant HIS-Uba1, GST-UbcH5b, Ubiquitin and ATP and Flag-SPRYD3/MYC-MYCBP2 complexes eluted from Flag-M2 beads. The mixtures were incubated for 0 or 60 min at 37 °C.

3.4.6 MYCBP2-SPRYD3 attaches K63-linked ubiquitin chains to USP11

As previously shown, the newly identified E3 ligase complex MYCBP2-SPRYD3 ubiquitylates USP11 in cells and *in vitro* (Figures 30-33). I next aimed at characterizing the Ub-chain type attached to USP11 by MYCBP2-SPRYD3. To create Ub-chains on substrates, substrate-bound Ub is itself ubiquitylated on one of its several internal lysine residues. K48-linked Ub-chains usually mediate proteasomal degradation whereas K63-linked Ub-chains are involved in immune response regulation, DNA repair or scaffold formation (Doil et al., 2009; Sobhian et al., 2007; Wu et al., 2016). To establish which Ub-chain type is attached to USP11 by the MYCBP2-SPRYD3 E3 ligase complex, I performed ubiquitylation assays by ectopically expressing Flag-USP11 with MYC-MYCBP2 and different HA-Ubiquitin variants. While HA-Ubiquitin WT can still form all Ub-chain types, HA-Ubiquitin K48R and HA-Ubiquitin K63R impair chain type formation containing K48- or K63-linkages, respectively. Interestingly, MYC-MYCBP2 was capable of ubiquitylating Flag-USP11 in presence of HA-Ubiquitin WT and K48R, whereas co-expression of HA-Ubiquitin K63R abolished Flag-USP11 ubiquitylation (Figure 34). This suggests that MYCBP2-SPRYD3 links K63-linked Ub-chains to USP11, which probably do not lead to its proteasomal destruction, but rather regulate other protein fates. Since both MYCBP2-SPRYD3 and USP11 promote mitotic slippage, and I hypothesized that they might collaborate in doing so, it would make

sense that MYCBP2-SPRYD3-mediated ubiquitylation does not lead to USP11's proteasomal destruction.

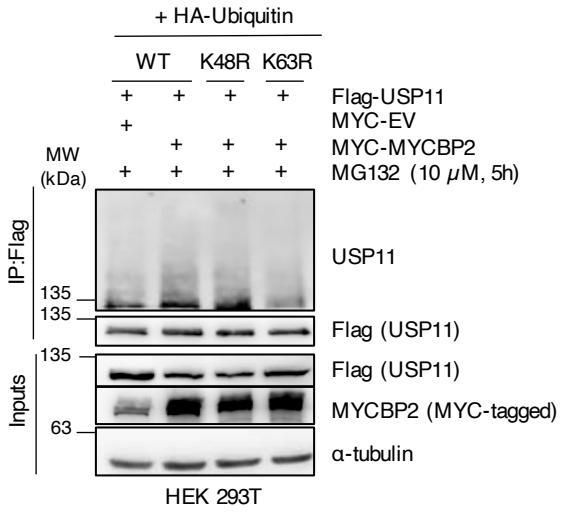


Figure 34: MYCBP2 attaches K63-linked Ub-chains to USP11.
Flag-USP11 was co-transfected with MYC-MYCBP2 and HA-Ubiquitin WT or variants and overexpressed for 48h. MG132 was added to cells 5h prior to harvest. Cells were harvested for Flag-IP. IPs and inputs were subjected to western blot analysis.

3.4.7 MYCBP2-SPRYD3 mediated ubiquitylation of USP11 is not linked to proteasomal degradation

Since both the E3 ligase complex MYCBP2-SPRYD3 and USP11 promote mitotic slippage subsequent to MT-poison treatment, I suspected that MYCBP2-SPRYD3-mediated ubiquitylation of USP11 is not linked to its proteasomal destruction. This was partly confirmed by the fact that USP11 ubiquitylation by MYCBP2-SPRYD3 occurs via K63-linked Ub-chains, which do not necessarily mediate proteasomal degradation (Doil et al., 2009; Sobhian et al., 2007; Wu et al., 2016) (Figure 34). I performed various siRNA experiments and cycloheximide (CHX) chases to monitor USP11 protein level turnover in absence of SPRYD3. CHX treatment stops protein translation by inhibiting polypeptide elongation in the ribosome and thus allows for protein turnover monitoring. I treated U2OS and RPE1 cells with siRNA either targeting GL2 (control) or SPRYD3 and assessed USP11 protein levels (Figure 35A). In U2OS cells, USP11 protein levels were destabilized after SPRYD3 depletion compared to a siGL2-treated control, with the siRNA siSPRYD3 #2 breaching the significance threshold (Figure 35A). In RPE1 cells, the results were less clear, but no significant change of USP11 protein levels after SPRYD3 depletion could be observed. This suggests that ubiquitylation of USP11 mediated by MYCBP2-SPRYD3 does probably not lead to its proteasomal destruction. To confirm this, I performed CHX chases in U2OS cells to stop protein translation and

monitor USP11 protein turnover in absence of SPRYD3 over a specific period of time. USP11 protein levels decayed slightly, but not significantly faster in SPRYD3-depleted U2OS cells compared to a siGL2-treated control (Figure 35B). Again, this points to the idea that proteasomal degradation is not a consequence of MYCBP2-SPRYD3-mediated USP11 ubiquitylation. To corroborate these results, I generated different clones of a doxycycline (Dox) inducible U2OS T-REX MYC-SPRYD3 cell line and induced MYC-SPRYD3 overexpression with Dox for 72h. In all three clones, USP11 protein levels did not change significantly when comparing Dox-treated U2OS cells to a non-treated control (Figure 35C). Additionally, CHX chase in the Dox-treated clone #8 of the U2OS T-REX MYC-SPRYD3 cell line did not show a significant difference in USP11 protein turnover compared to a non-treated control (Figure 35D). Overall, the obtained results indicate that MYCBP2-SPRYD3-mediated ubiquitylation of USP11 does not result in its proteasomal destruction.

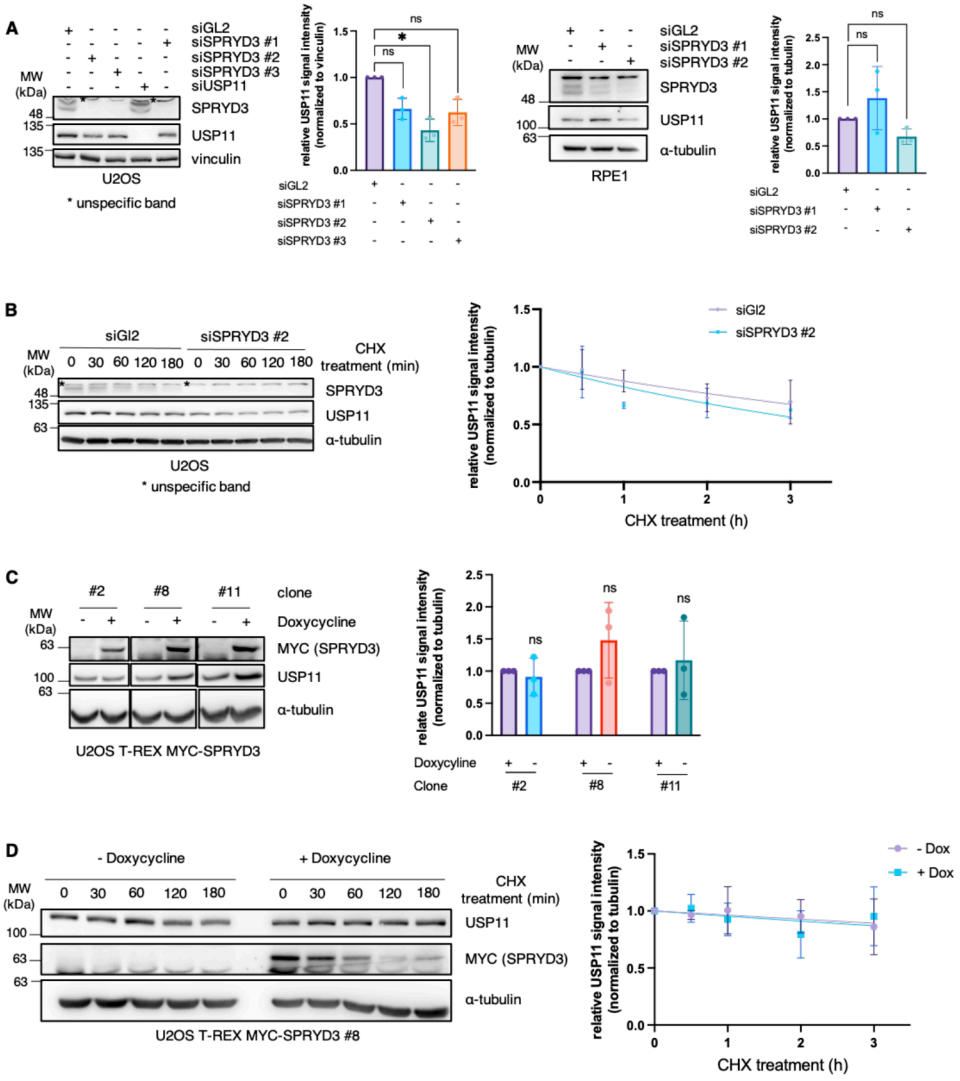


Figure 35: Ubiquitylation of USP11 is not linked to proteasomal destruction.

(A) U2OS or RPE1 cells were transfected twice with 20 nM siRNA targeting GL2 (= control), USP11 or SPRYD3 and harvested after 72h. Protein lysates were subjected to western blot analysis. Graphs depict relative USP11 western blot signals after normalization and in relation to a siGl2 treated control. Relative values were log-transformed to obtain parametric distribution and applied to one sample t and Wilcoxon test, n=3 independent experiments. ns > 0.05, *p < 0.05, * indicates unspecific band. **(B)** U2OS cells were transfected twice with 20 nM siRNA targeting GL2 (= control) or SPRYD3. After 72h, protein synthesis was blocked via CHX treatment for indicated durations prior to harvest. Protein half-lives were determined by fitting to a one-phase decay model, n=3 independent experiments. **(C)** U2OS T-REX MYC-SPRYD3 clones #2, #8 and #11 were treated with -/+ 2 µg/ml Doxycycline and harvested after 72h. Protein lysates were subjected to western blot analysis. Graphs depict relative USP11 western blot signals after normalization and in relation to a siGL2 treated control. Relative values were log-transformed to obtain parametric distribution and applied to one sample t and Wilcoxon test, n=3 independent experiments. ns > 0.05. **(D)** U2OS T-REX MYC-SPRYD3 clone #8 was treated with -/+ 2 µg/ml doxycycline for 72h. Protein synthesis was blocked via CHX treatment for indicated durations prior to harvest. Protein half-lives were determined by fitting to a one-phase decay model, n=3 independent experiments.

3.4.8 MYCBP2-SPRYD3 targets non-canonical USP11 residues for ubiquitylation

MYCBP2 was reported to auto-ubiquitylate itself and NMNAT2 via esterification, preferentially targeting threonines and serines (Mabbitt et al., 2020; Pao et al., 2018). It was suggested that standard buffers used for ubiquitylation assay sample preparation do not allow for observation of non-canonical ubiquitylation sites, since the presence of reducing agents such as β-mercaptoethanol or DTT weakens esterification bonds between Ub and serine, threonine and especially disrupts interactions with cysteine side chains (Song et al., 2009; Vosper et al., 2009). Under standard buffer conditions (2x Laemmli + DTT), I was able to observe MYCBP2-SPRYD3-mediated USP11 ubiquitylation (Figure 30-34). However, the ubiquitylation signal was very weak and a long exposure time was required to detect the ubiquitylation signals in western blot. Due to the preference of MYCBP2 to target threonines and serines (Pao et al., 2018), I wondered whether MYCBP2-SPRYD3 might target non-canonical USP11 side chains for ubiquitylation that could be visualized by using different buffer conditions. I decided to perform a similar experiment as described in Vosper et al., 2009, where ubiquitylation assays were performed under buffer conditions lacking reducing agents (Vosper et al., 2009). I ectopically expressed Flag-USP11 together with MYC-SPRYD3 or MYC-MYCBP2 and HA-Ubiquitin in HEK 293T cells and boiled the IP-samples in 2x Laemmli buffer +/- DTT, as indicated, to compare the USP11 ubiquitylation signals in between conditions (Figure 36A). Surprisingly, when performing western blot analysis with these samples, much stronger ubiquitylation of USP11 by MYC-SPRYD3 or MYC-MYCBP2 was observed when samples were boiled in sample buffer without DTT compared to buffer containing DTT (Figure 36A). When exposing the USP11 ubiquitylation western blot signal for longer time, only a faint ubiquitylation of USP11 in presence of DTT was detectable (Figure 36A). This suggests that MYCBP2-

SPRYD3 does not only target lysine side chains that can be detected under standard buffer conditions, but also modifies non-canonical USP11 side chains for ubiquitylation, which remain undetected when using standard buffer (2x Laemmli +DTT). Next, I wanted to determine the USP11 ubiquitylation sites targeted by MYCBP2-SPRYD3 and performed a combined IP-MS screen. A ubiquitylation assay was performed by over-expressing Flag-USP11 together with MYC-MYCBP2 or MYC-SPRYD3 and HA-Ubiquitin in HEK 293T cells to allow ubiquitylation of USP11 in the cell. Flag-USP11 was immunoprecipitated and IP samples were denatured in 2x Laemmli with or without DTT in order to determine potential canonical and non-canonical ubiquitylation sites of USP11. IP samples were handed over to the DKFZ proteomics facility, which analyzed ubiquitylated USP11 residues through MS. Only USP11-residues modified in both MYC-MYCBP2 and MYC-SPRYD3 co-expressing conditions were considered. Under +DTT conditions, residues USP11^{K107}, USP11^{K355}, USP11^{K714} and USP11^{K840} were identified as potential ubiquitylation sites after MYC-SPRYD3 or MYC-MYCBP2 co-expression with USP11 (Figure 36B, highlighted in green). Under -DTT conditions, residues USP11^{S530} and USP11^{K531} were found to be ubiquitylated (Figure 36B, highlighted in red). In order to assess whether any of these identified USP11 residues could play a role in MYCBP2-SPRYD3-mediated ubiquitylation, all of these 6 residues were point-mutated to an alanine residue, resulting in the Flag-USP11^{6A} mutant. USP11^{C318} is important for USP11 deubiquitylation activity and its exchange to a serine abolishes its ability to deubiquitylate substrates senataxin (SETX) or tau (Jurga et al., 2021; Yan et al., 2022) (Figure 36B, highlighted in purple). On top of assessing the ability of MYCBP2-SPRYD3 to ubiquitylate Flag-USP11^{6A}, I decided to generate and include the catalytic inactive mutant Flag-USP11^{C318S}, to investigate whether C318 might also be important for USP11 ubiquitylation. Interestingly, when analyzing expression levels in HEK 293T cells, Flag-USP11^{6A} and Flag-USP11^{C318S} were less expressed compared to Flag-USP11^{WT}, with Flag-USP11^{C318S} breaching the significance threshold (Figure 36C). This indicates, that Flag-USP11^{C318S} and Flag-USP11^{6A} might be less stable compared to Flag-USP11^{WT}. Next, I performed ubiquitylation assays in HEK 293T cells to assess the importance of these USP11 residues for MYCBP2-SPRYD3-mediated ubiquitylation. I ectopically expressed Flag-USP11^{WT}, Flag-USP11^{C318S} or Flag-USP11^{6A} with either MYC-MYCBP2 or MYC-SPRYD3 and HA-Ubiquitin in HEK 293T cells and performed western blot analysis by denaturing IP samples in -DTT buffer. Surprisingly, neither MYC-MYCBP2 nor MYC-

SPRYD3 were able to ubiquitylate Flag-USP11^{C318S} or Flag-USP11^{6A} (Figure 36D). This suggested that USP11^{C318} and one or several residues mutated in the Flag-USP11^{6A} mutant might be targeted by MYCBP2-SPRYD3 for ubiquitylation. Surprisingly, I observed that MYCBP2-SPRYD3 seems to target USP11^{C318} for ubiquitylation, since point mutating this residue to a serine abolishes USP11 ubiquitylation (Figure 36D). Non-canonical ubiquitylation on internal substrate cysteines has been reported before (Carvalho et al., 2007; Kelsall et al., 2019; Okumoto et al., 2011), and it is known that MYCBP2 preferentially targets non-canonical side chains, such as threonines and serines for ubiquitylation (Pao et al., 2018). The fact that MYCBP2-SPRYD3 seems to target USP11 lysines and/or serines and specifically cysteine 318 (Figure 36D), points out the mechanistic versatility of MYCBP2 in ubiquitylating and thus regulating its substrates.

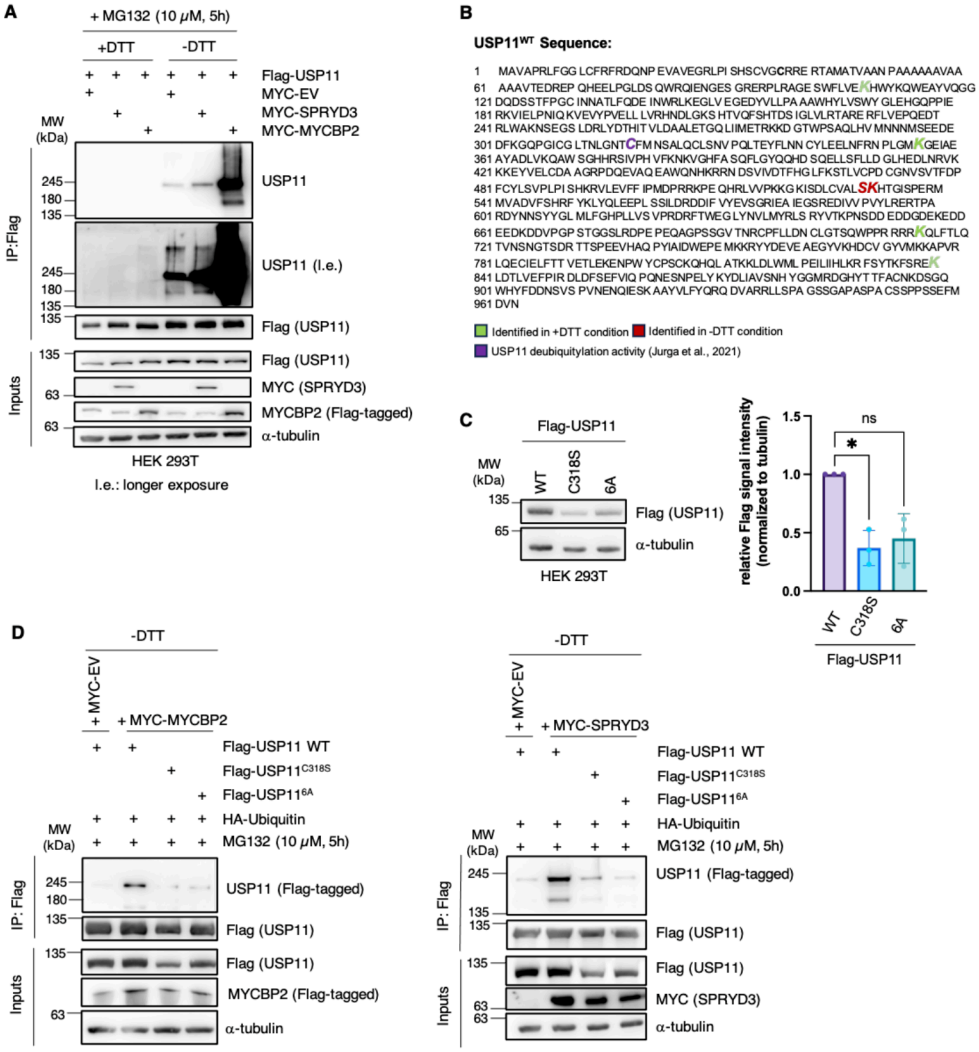


Figure 36: MYCBP2-SPRYD3 ubiquitylates non-canonical USP11 residues.
(A) Flag-USP11 was co-expressed with MYC-SPRYD3 or MYC-MYCBP2 and HA-Ubiquitin in HEK 293T WT cells and overexpressed for 24h. 5h prior to harvest, cells were treated with MG132. Cells were harvested for Flag-IP. IPs were boiled in 2x Laemmli buffer with or without DTT (+/-DTT) as indicated in the figure. IPs and inputs were subjected to western blot analysis. **(B)** USP11^{WT} sequence with highlighted potential ubiquitylation sites (green/red)

identified in IP-MS approach after Flag-USP11 and MYC-MYCBP2 or MYC-SPRYD3 co-expression in HEK 293T WT cells. Cysteine 318, responsible for USP11 deubiquitylation activity (Jurga et al., 2021; Yan et al., 2022) is highlighted in purple.**(C)** Flag-USP11^{WT}, Flag-USP11^{C318S} or Flag-USP11^{6A} was transfected into HEK 293T WT cells and over-expressed for 24h. Cells were harvested and protein lysates were subjected to western blot analysis. Graphs depict relative Flag western blot signals after normalization and Flag-USP11^{WT} was used as 100% reference. Relative values were log-transformed to obtain parametric distribution and applied to one sample t and Wilcoxon test, n=3 independent experiments. ns > 0.05, *p < 0.05. **(D)** Flag-USP11^{WT}, Flag-USP11^{C318S} or Flag-USP11^{6A} was co-transfected with either MYC-MYCBP2 (left WB blot) or MYC-SPRYD3 (right WB blot) and HA-Ubiquitin into HEK 293T WT cells and incubated for 24h. 5h prior to harvest, MG132 was added to cells. Cells were harvested and Flag-IP was performed. IPs were boiled in 2x Laemmli buffer without DTT (-DTT).

3.4.9 MYCBP2-SPRYD3-mediated ubiquitylation of USP11 is essential for bipolar spindle formation

As shown previously, MYCBP2-SPRYD3-mediated ubiquitylation of USP11 does not result in its proteasomal destruction (Figure 35). I hypothesized that instead, USP11 ubiquitylation might lead to its activation or ability to recruit a downstream substrate for deubiquitylation. A study published by Stockum et al. 2018 reported that USP11 regulates bipolar spindle formation through deubiquitylation of RAE1 and thus, USP11 deubiquitylation activity is important for this process (Stockum et al., 2018). Depletion of USP11 or RAE1 leads to spindle multipolarity in U2OS cells treated with nocodazole (Stockum et al., 2018). Interestingly, multipolar spindles are a possible consequence of MT-poison treatment, which can result in mitotic cell death (Abal et al., 2001; Zhou et al., 2023). RAE1 is a known and conserved interactor of MYCBP2 (Grill et al., 2012) and USP11 a newly identified ubiquitylation substrate of the MYCBP2-SPRYD3 E3 ligase. It therefore seemed conceivable that MYCBP2-SPRYD3, USP11 and RAE1 might collaborate in regulating bipolar spindle formation. Similar to K63-ubiquitylation of USP7, which is essential for its ability to recruit and deubiquitylate its substrate HIF1α (Wu et al., 2016), MYCBP2-SPRYD3-mediated ubiquitylation of USP11 might regulate RAE1 recruitment, deubiquitylation and thus promotion of bipolar spindle formation. In order to investigate this, I performed immunofluorescence experiments combined with RNA interference or plasmid overexpression. To test whether SPRYD3 and MYCBP2 influence bipolar spindle formation, I treated U2OS and RPE1 cells with siRNAs either targeting GL2 (control), SPRYD3 or MYCBP2 and subsequently treated them with nocodazole for 24h. I included USP11 knock-down as a positive control (Stockum et al., 2018). After a total of 72h of siRNA downregulation, I released the cells from mitotic block into medium containing 5 µM proteasome inhibitor MG132 for another 90 minutes (Stockum et al., 2018). Cells were fixed and stained with centrin and α-tubulin antibodies to visualize centrosomes and mitotic spindles. Similar to

USP11 knock-down, siRNA-mediated depletion of SPRYD3 and MYCBP2 exhibited a significantly higher number of mitotic cells with aberrant spindles compared to a siGL2-treated control in both U2OS and RPE1 cells (Figure 37). By analyzing the number of mitotic U2OS or RPE1 cells containing either ≤ 4 or >4 centrin dots, I realized that more than half of mitotic cells containing aberrant spindle pole numbers only exhibited 4 or less centrin signals throughout all conditions. While in some mitotic cells with aberrant spindle pole number, spindle poles exhibited one centrin dot instead of two, in other cases, centrin signal was completely absent (Figure 37, white arrows; single centrin signal not shown). This suggests that aberrant spindles did not arise from centrosome amplification, but rather result from centrosome disengagement or MT-spindle breakage and following formation of an acentrosomal pole. This phenomenon dramatically increased in SPRYD3-, MYCBP2- or USP11-depleted U2OS or RPE1 cells compared to siGL2-treated cells (Figure 37).

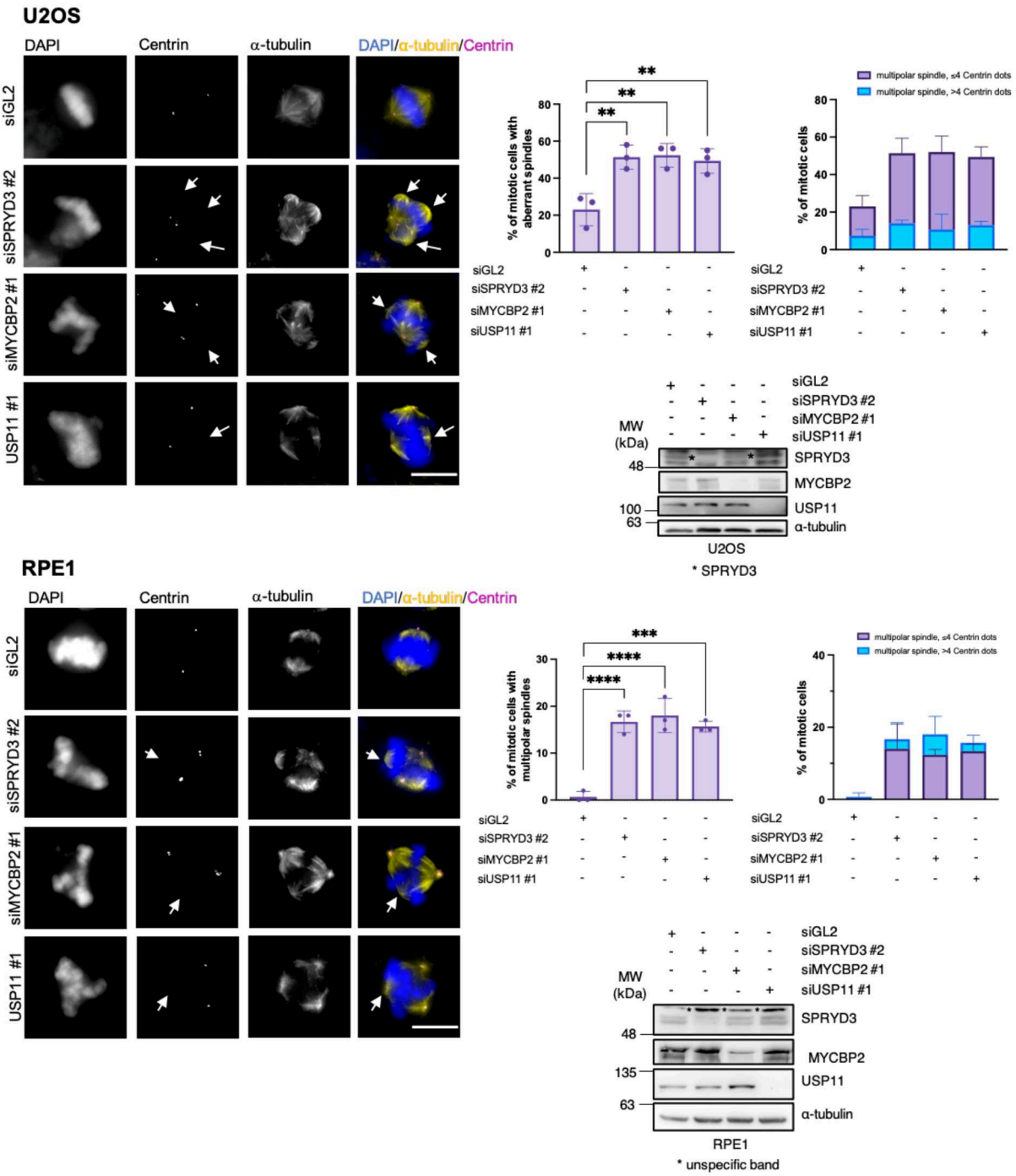


Figure 37: USP11-, SPRYD3- and MYCBP2-depletion cause multipolar spindle formation in nocodazole-treated RPE1 or U2OS cells.
U2OS or RPE1 cells were transfected twice with 50 nM siRNA targeting GL2 (= control) or SPRYD3, MYCBP2 or USP11. 48h after the first transfection, cells were treated with nocodazole and incubated for further 24h. After 24h, cells were treated for additional 90 min with MG132. Cells were fixed and stained for centrin, α-tubulin and DNA. For each experiment, 55 (U2OS) or 65 (RPE1) mitotic cells per condition were analyzed for mitotic spindle number. Results were subjected to one-way ANOVA with Dunette post hoc test, n=4 independent experiments (U2OS) and n=3 independent experiments (RPE1). $**p < 0.01$, $***p < 0.001$, $****p < 0.0001$. White arrows indicate the absence of centrin-signal. Scale bar = 10 µm.

To explore whether MYCBP2-SPRYD3-mediated ubiquitylation of USP11 plays a role in the ability of USP11 to promote proper mitotic spindle formation through

deubiquitylation, I performed a similar experiment as described above. I co-transfected U2OS cells with Flag-EV or Flag-USP11 and MYC-EV or MYC-MYCBP2 C4520S or MYC-SPRYD3ΔSPRY2, treated the cells with nocodazole for 24h and released them into medium containing 5 μM MG132 for additional 90 min (Stockum et al., 2018). Co-expression of Flag-USP11 and MYC-EV significantly decreased the number of mitotic cells exhibiting aberrant spindles compared to control cells co-expressing Flag-EV and MYC-EV (Figure 38A). Co-expression of Flag-USP11 with the E3 ligase dead mutant MYC-MYCBP2 C4520S or deletion mutant MYC-SPRYD3ΔSPRY2 reversed this effect and significantly increased the number of mitotic cells carrying aberrant spindles compared to cells overexpressing Flag-USP11 and MYC-EV (Figure 38A). This suggested that ubiquitylation of USP11 exerted by a functional MYCBP2-SPRYD3 E3 ligase complex is important for its catalytic and thus, deubiquitylation activity and function in bipolar spindle formation. To confirm this result, I performed an additional IF experiment by using the Flag-USP11 mutants identified previously, which carry point mutations that abolish MYCBP2-SPRYD3-mediated USP11-ubiquitylation (Figure 36D). Briefly, I transfected U2OS cells with Flag-EV, Flag-USP11^{WT}, Flag-USP11^{C318S} or Flag-USP11^{6A} and treated the cells with 200 ng/ml nocodazole for 24h. After nocodazole wash-out, cells were released into medium containing 5 μM MG132 for 90 minutes (Stockum et al., 2018). Cells were fixed and stained for α-tubulin and DNA. Ectopic expression of Flag-USP11^{WT} decreased the number of cells exhibiting multipolar spindles after nocodazole treatment compared to a control transfected with Flag-EV (Figure 38B). Interestingly, the Flag-USP11^{C318S} mutant exhibited significantly more multipolar spindle carrying cells compared to Flag-USP11^{WT} expressing cells, while the Flag-USP11^{6A} mutant behaved similar to Flag-USP11^{WT} (Figure 38B). Both Flag-USP11^{C318S} and Flag-USP11^{6A} mutants cannot be ubiquitylated by the E3 ligase MYCBP2-SPRYD3, thus indicating that these USP11 residues are the ubiquitylation target sites (Figure 36D). However, USP11^{C318} seems to be the residue, whose ubiquitylation is important for the function of USP11 in bipolar spindle formation (Figure 38B). One or more of the other six residues mutated in the USP11^{6A} mutant might be important for MYCBP2-SPRYD3-mediated USP11 ubiquitylation, but its ubiquitylation seems to regulate other functions than bipolar spindle formation. To finally confirm that ubiquitylation of USP11^{C318} by MYCBP2-SPRYD3 is responsible for the function of USP11 in bipolar spindle formation, I performed a final IF experiment by depleting USP11 from U2OS cells and transfect them with WT or siRNA-resistant DNA-plasmids

Flag-USP11 $^{WT / WT siRes}$ or Flag-USP11$^{C318S / C318S siRes}$. Cells were transfected with siRNA targeting either GL2 or USP11 and additionally transfected with Flag-USP11 plasmids as indicated in Figure 38C. Depletion of USP11 together with Flag-EV overexpression increased the number of cells carrying aberrant spindles compared to a siGL2 + MYC-EV transfected control (Figure 38C), reflecting the results obtained in Figure 37. Combined USP11-depletion and Flag-USP11^{WT} overexpression resulted in a slight, but not significant decrease of multipolar spindle carrying cells compared to USP11-depleted cells overexpressing MYC-EV. The slight, but non-significant decrease observed, can be described with the fact that some residual Flag-USP11^{WT} is still left after siUSP11 treatment, potentially contributing to a slight repression of the multipolar spindle phenotype (Figure 38C, western blot, 3rd lane). Transfection of USP11-depleted U2OS cells with Flag-USP11$^{WT siRes}$ rescued the multipolar spindle phenotype, by significantly decreasing the number of mitotic cells with aberrant spindle pole numbers compared to USP11-depleted cells expressing MYC-EV. Transfection of Flag-USP11^{C318S} or Flag-USP11$^{C318S siRes}$ into USP11-depleted U2OS cells caused no significant change compared to USP11-depleted cells overexpressing MYC-EV (Figure 38C). This confirmed that ubiquitylation of USP11^{C318} is essential for USP11's function in bipolar spindle formation, since the siRNA-resistant Flag-USP11$^{C318S siRes}$ was uncapable to rescue the multipolar spindle phenotype observed in mitotic cells caused by USP11-depletion. Taken together the above presented results, I can conclude that MYCBP2-SPRYD3-mediated ubiquitylation of USP11 on residue C318 is essential for the function of USP11 in bipolar spindle formation in mitotic U2OS cells.

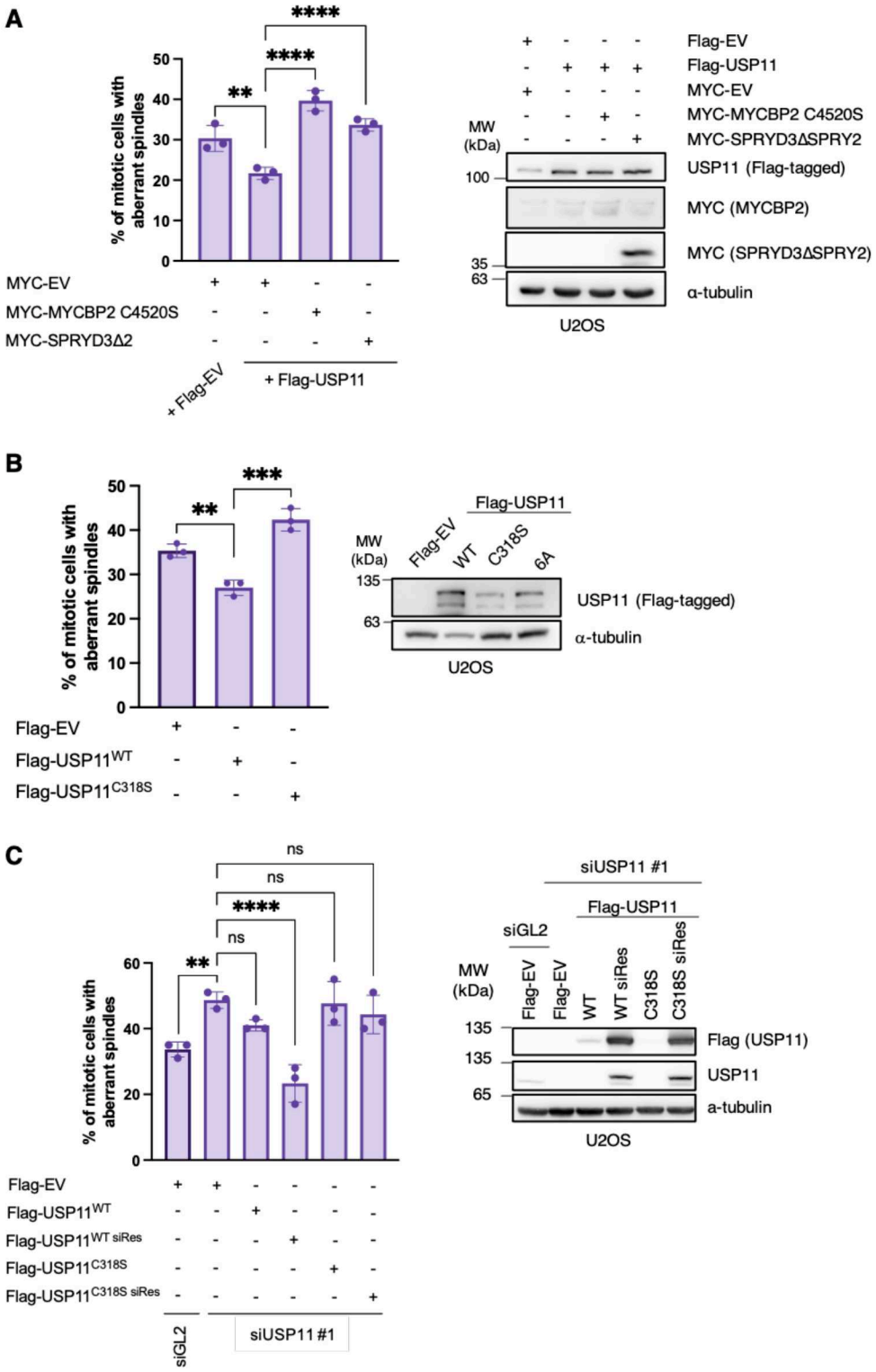


Figure 38: MYCBP2-SPRYD3 mediated ubiquitylation of USP11^{C318} leads to bipolar spindle formation. **(A)** U2OS cells were transfected with 2 µg in total of indicated DNA. 24h after transfection, cells were treated with nocodazole and incubated for further 24h. After completed incubation time, cells were released from mitotic block into medium containing MG132 for additional 90 min (Stockum et al., 2018). Cells were fixed and stained for α-tubulin and DNA. For each replicate, 65 mitotic cells per condition were analyzed for mitotic spindle number. Results were subjected to one-way ANOVA with Dunette post hoc test, n=3 independent experiments. $^{**}p < 0.01$. **(B)** U2OS cells were and transfected with 2 µg of Flag-EV, Flag-USP11^{WT}, Flag-USP11^{C318S} or Flag-USP11^{6A}. 24h after transfection, cells were treated with nocodazole for additional 24h. After nocodazole wash-out, cells were treated with MG132 for 90 min (Stockum et al., 2018). Cells were fixed and stained for α-tubulin and DNA. For each replicate, 65 mitotic cells per condition were analyzed for mitotic spindle pole number. Results were subjected to one-way ANOVA with Dunette post hoc test, n=3. *ns* > 0.05, $^{**}p < 0.0$. **(C)** U2OS cells were transfected twice with

50 nM siRNA targeting GL2 (control) or USP11. 24h after the first siRNA transfection, U2OS cells were transfected with Flag-USP11$^{WT\ /\ WT\ siRes}$ or Flag-USP11$^{C318S\ /\ C318S\ siRes}$ as indicated. Cells were treated with nocodazole and MG132 as indicated in (A) after incubation of 24h. Subsequent to fixation and staining, 65 mitotic cells per condition were analyzed for mitotic spindle pole number. Results were subjected to one-way ANOVA with Dunette post hoc test, n=3. *ns* > 0.05, *p < 0.05, **p < 0.01.

3.4.10 MYCBP2-SPRYD3 and USP11 promote mitotic slippage through bipolar spindle formation

As described in the previous chapter, MYCBP2-SPRYD3-mediated ubiquitylation of USP11^{C318} promotes bipolar spindle formation after nocodazole treatment (Figure 38). Additionally, both the E3 ligase MYCBP2-SPRYD3 and the DUB USP11 promote mitotic slippage after nocodazole or paclitaxel treatment (Figures 5 and 26). Interestingly, multipolar spindles are not only a potential consequence of MT-poison treatment, but can also lead to mitotic cell death to avoid aberrant cell division (Abal et al., 2001; Zhou et al., 2023). I wondered whether bipolar spindle formation regulated through MYCBP2-SPRYD3-mediated USP11 ubiquitylation is the mechanism underlying mitotic slippage after MT-poison treatment. In order to assess this hypothesis, I performed live cell imaging by transfecting U2OS cells with Flag-EV, Flag-USP11^{WT}, Flag-USP11^{C318S} or Flag-USP11^{6A} and subsequently treated them with nocodazole or paclitaxel. While ectopic expression of Flag-USP11^{WT} increased the percentage of cells undergoing mitotic slippage compared to a control expressing Flag-EV, Flag-USP11^{C318S} counteracted this effect (Figure 39). Ectopic expression of Flag-USP11^{C318S} exhibited a significantly lower percentage of mitotic cells undergoing slippage compared to Flag-USP11^{WT}, almost reaching the same levels as Flag-EV expressing cells (Figure 39). However, Flag-USP11^{6A} overexpression behaved similar to Flag-USP11^{WT} expressing cells (Figure 39). This suggests that bipolar spindle formation mediated through ubiquitylation of USP11^{C318} by the E3 ligase MYCBP2-SPRYD3 contributes to mitotic slippage, whereas the abolishment of this cascade sensitizes cells for mitotic cell death in presence of MT-poisons. Ubiquitylation of residues of one or more USP11 residues mutated in the Flag-USP11^{6A} mutant by MYCBP2-SPRYD3 seems to regulate other processes than bipolar spindle formation and consequent mitotic slippage.

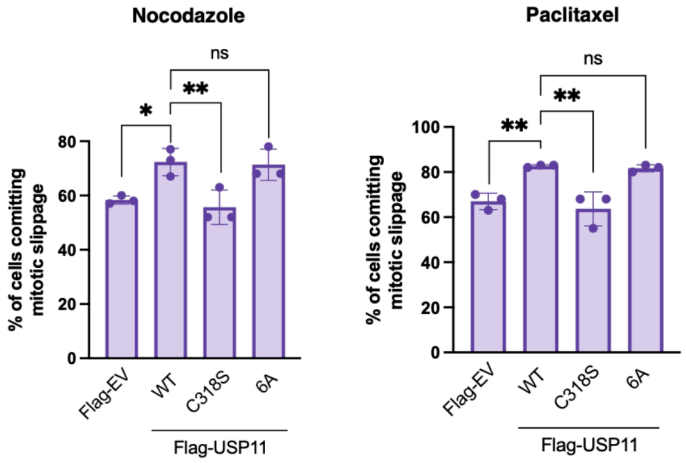


Figure 39: Ectopic expression of Flag-USP11^{C318S} increases mitotic slippage in MT-poison treated cells. U2OS cells were transfected with Flag-EV, Flag-USP11^{WT}, Flag-USP11^{C318S} or Flag-USP11^{6A}, and treated with nocodazole 48h after transfection. Live cell imaging was performed and mitotic cell fate of 60 cells was determined for each experiment. *p < 0.05, **p < 0.01, one-way ANOVA with Dunette post hoc test, n = 3 for each cell line and respective drug treatment.

3.4.11 MYCBP2-SPRYD3-mediated ubiquitylation of USP11^{C318} is required for USP11-RAE1 interaction

USP11 promotes bipolar spindle formation through RAE1 deubiquitylation (Stockum et al., 2018). RAE1 is an important regulator of mitotic spindle formation and collaborates with SMC1 and NuMA to ensure proper MT-spindle bundling (Wong, 2010; Wong et al., 2006). Disruption of the NuMA/RAE1 or SMC1/RAE1 balance as well as abolishment of RAE1 deubiquitylation by USP11 promotes multipolar spindle formation (Stockum et al., 2018; Wong, 2010; Wong et al., 2006). USP7 was described to deubiquitylate its substrate HIF1α only after K63-mediated ubiquitylation (Wu et al., 2016). I hypothesized that MYCBP2-SPRYD3, USP11 and RAE1 might collaborate in promoting bipolar spindle formation in a similar manner. As described in previous chapters, MYCBP2-SPRYD3 promotes bipolar spindle formation through ubiquitylation of USP11 (Figure 38). I wondered whether MYCBP2-SPRYD3-mediated ubiquitylation of USP11^{C318} might enable USP11 to recruit and deubiquitylate RAE1, thus resulting in bipolar spindle formation. I set out to explore this possibility by performing ubiquitylation assays and various interaction experiments. First, I co-transfected GFP-RAE1, with MYC-SPRYD3 or MYC-MYCBP2 and HA-Ubiquitin into HEK 293T WT cells and pulled down GFP-RAE1 to analyze its ubiquitylation status. Interestingly, GFP-RAE1 was less ubiquitylated in presence of both MYC-SPRYD3 or MYC-MYCBP2 compared to a control overexpressing GFP-RAE1 together with MYC-EV (Figure 40A). This supports the hypothesis that overexpression of an active MYCBP2-

SPRYD3 E3 ligase complex enhances the activity of a DUB, probably USP11, which consequently results in enhanced RAE1 deubiquitylation. To investigate, whether USP11 is the DUB regulating this process, I analyzed the interaction between Flag-USP11 and HA-RAE1 in presence or absence of MYCBP2 ubiquitylation activity. I co-expressed Flag-USP11 and HA-RAE1 together with MYC-MYCBP2 WT or MYC-MYCBP2 C4520S and immunoprecipitated Flag-USP11 to analyze HA-RAE1 co-precipitation. Interestingly, co-expression of MYC-MYCBP2 WT significantly increased the interaction between Flag-USP11 and HA-RAE1 compared to a control co-expressing MYC-EV. Co-expression of catalytically inactive MYC-MYCBP2 C4502S reversed this effect and significantly decreased co-precipitation of HA-RAE1 compared to cells co-expressing MYC-MYCBP2 WT (Figure 40B). This indicates that the interaction between USP11 and RAE1 requires MYCBP2 ubiquitylation activity. To corroborate this result, I co-expressed Flag-EV, Flag-USP11^{WT}, Flag-USP11^{C318S} or Flag-USP11^{6A} with GFP-RAE1 and immunoprecipitated Flag-tagged proteins. While Flag-USP11^{WT} and Flag-USP11^{6A} interacted with HA-RAE1 similarly, the interaction between Flag-USP11^{C318S} and HA-RAE1 significantly decreased compared to Flag-USP11^{WT} expressing cells (Figure 40C). This confirms that the interaction between RAE1 and USP11 relies on MYCBP2-SPRYD3-mediated ubiquitylation of USP11^{C318}, probably resulting in bipolar spindle formation and promotion of mitotic slippage.

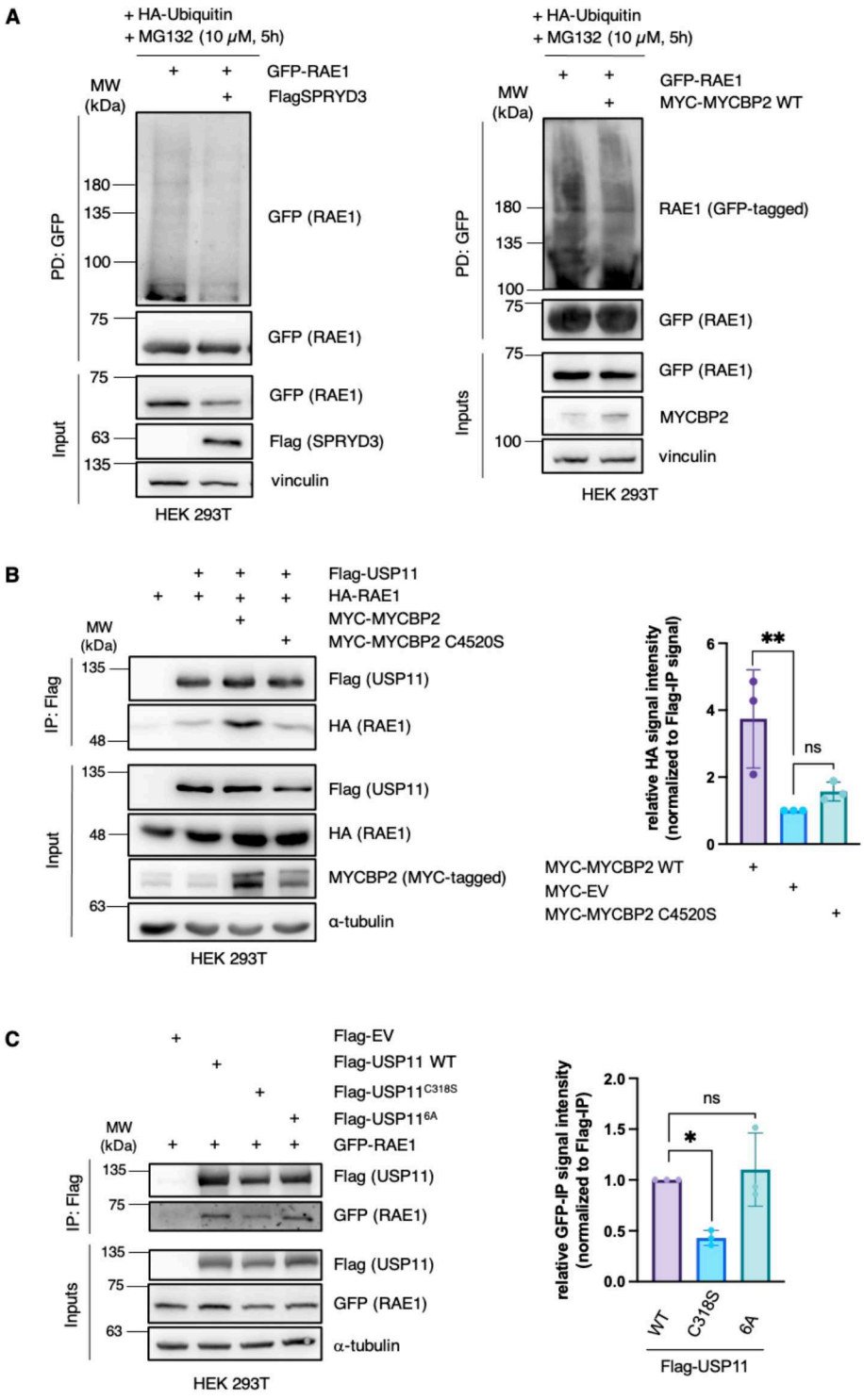


Figure 40: MYCBP2-SPRYD3-mediated ubiquitylation of USP11^{C318} is important for USP11/RAE1 interaction. **(A)** GFP-RAE1, MYC-SPRYD3 or MYC-MYCBP2 and HA-Ubiquitin were co-transfected into HEK 293T WT cells as indicated and overexpressed for 24h. MG132 was added 5h prior to harvest. Cells were harvested for GFP pull-down. **(B)** Flag-USP11 was co-transfected with HA-RAE1 and MYC-MYCBP2 or MYC-MYCBP2 C4520S into HEK 293T WT cells and overexpressed for 48h. Cells were harvested for Flag-USP11 IP. IPs and inputs were subjected to western blot analysis. Graph demonstrates relative HA-signal after normalization to respective Flag-IP signal. Sample with MYC-EV expression was set as reference. Statistical analysis was performed with log-transformed values to obtain parametric distribution. ns > 0.05, $^{**}p < 0.01$, one-way ANOVA with Dunette post hoc test, n=3. **(C)** GFP-RAE1 was ectopically co-expressed with Flag-USP11^{WT}, Flag-USP11^{C318S} or Flag-USP11^{6A} in HEK 293T WT for 24h. Cells were harvested and Flag-IP was performed. Graph depicts GFP-IP western blot signal after normalization to respective Flag-IP signal. Sample expressing Flag-USP11WT was used as reference. Statistical

analysis was performed using log-transformed relative values to obtain parametric distribution. ns > 0.05, *p < 0.05, one-way ANOVA with Dunette post hoc test, n=3.

3.4.12 RAE1 promotes mitotic slippage

In the previous chapter I demonstrated that the interaction between USP11 and RAE1 is dependent on MYCBP2-SPRYD3-mediated ubiquitylation of USP11^{C318}. This suggests that the function of RAE1 in bipolar spindle formation is dependent on the ubiquitylation status of USP11^{C318}. MYCBP2-SPRYD3-mediated ubiquitylation of USP11 results in an increased percentage of cells that perform mitotic slippage after MT-poison treatment. If RAE1 deubiquitylation is the downstream target of this cascade, its depletion should have a similar phenotype compared to USP11-, MYCBP2- or SPRYD3-depleted cells. RAE1 has already been reported to inhibit apoptosis in presence of paclitaxel, suggesting that its bipolar spindle promoting function helps cells to evade mitotic arrest induced by MT-poisons (Kobayashi et al., 2021). I decided to corroborate this result by performing live cell imaging in RAE1-depleted U2OS or RPE1 cells treated with either nocodazole or paclitaxel. Interestingly, both cell lines exhibited a significant decrease in mitotic slippage in absence of RAE1 compared to a siGL2-treated control after nocodazole or paclitaxel treatment (Figure 41). This confirmed that RAE1 works in the same pathway as USP11 and MYCBP2-SPRYD3, since abolishment of USP11^{C318} ubiquitylation mediated by MYCBP2-SPRYD3 results in a significant decrease of USP11-RAE1 interaction and increases multipolar spindles as well as mitotic cell death after MT-poison treatment.

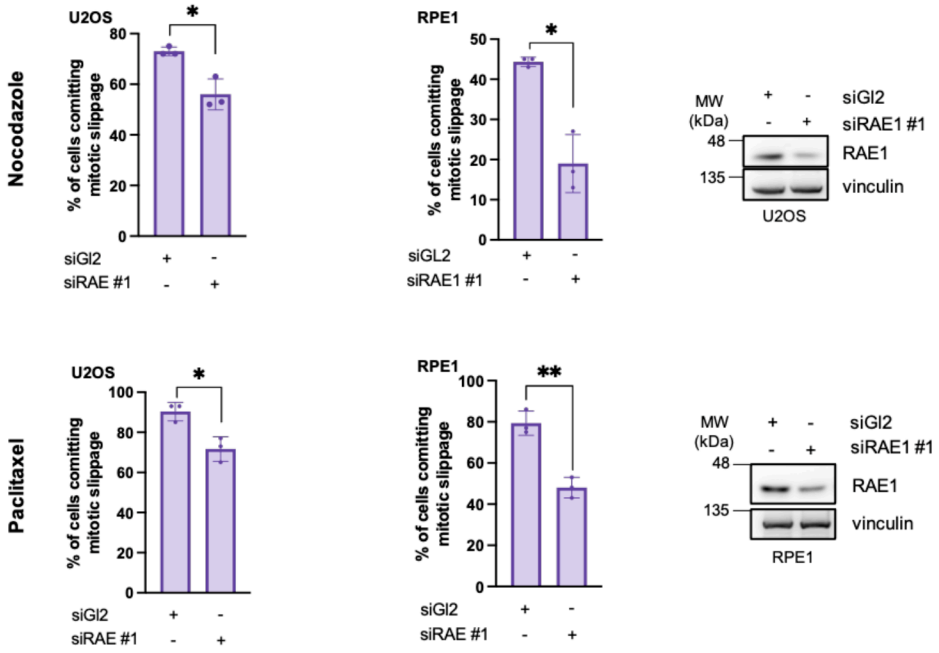


Figure 41: RAE1 promotes mitotic slippage in nocodazole or paclitaxel treated U2OS and RPE1 cells.

U2OS or RPE1 cells were transfected twice with 20 nM siRNA targeting GL2 (control) or RAE1. 72h after the first transfection, cells were treated with nocodazole or paclitaxel. Live cell imaging was performed and mitotic cell fate of n=60 cells was determined for each experiment. *$p < 0.05$, **$p < 0.01$, Student *t*-test with Welch correction.

4. Discussion

Apoptotic evasion represents a major issue in cancer therapy and jeopardizes the use of MT-poisons, such as taxanes and vinca alkaloids. Mitotic slippage, a potential apoptotic evasion mechanism, enables cancer cells to escape MT-poison induced mitotic arrest by allowing them to acquire an interphasic state without previous completion of anaphase and cytokinesis (Rieder and Maiato, 2004). Consequently, tetraploidy and genomic instability is generated, with the possibility of producing MT-poison resistant and more aggressive tumors (Chan et al., 2012; Cheng and Crasta, 2017; Ganem et al., 2007; McGranahan et al., 2012). Indeed, mitotic slippage is considered as one of the main contributors to chemoresistance development after MT-poison treatment (Chan et al., 2012).

MT-poisons alter MT-dynamics during mitosis and thus interfere with correct spindle formation, inducing a sustained SAC and mitotic arrest (Brito and Rieder, 2006; Musacchio and Salmon, 2007). Several attempts have been made to develop drugs targeting non-MT proteins, such as mitotic kinesins Eg5 and CENPE or kinases PLK1 and Aurora A/B, to induce mitotic arrest. Unfortunately, only some exceptions have shown efficacy *in vivo*, with the majority of drugs underscoring classical MT-poisons (Chan et al., 2012; Huszar et al., 2009; Manchado et al., 2012; Salmela and Kallio, 2013). Thus, elucidating the mechanisms leading up to mitotic slippage is of great importance, in order to elaborate new strategies that allow continued use of MT-poisons, which have proven efficacious in treatment of solid and hematological cancers (Jordan and Wilson, 2004).

MYCBP2 (PAM) as well as its substrate specificity factor FBXO45 were discovered as important regulators of neuronal development (Desbois et al., 2018; Grill et al., 2016; Saiga et al., 2009). Both FBXO45 and MYCBP2 protein expression alterations have been connected to various neurological pathologies and disorders such as autism, intellectual disability or corpus callosum defects (AlAbdi et al., 2023; Mulle et al., 2010; Quintero-Rivera et al., 2010; Willatt et al., 2005). However, the involvement of the conserved MYCBP2-FBXO45 E3 ligase complex in oncogenesis was soon determined (Chen et al., 2014; Lin et al., 2021; Richter et al., 2020; Tricoli et al., 2018; Xu et al., 2015). MYCBP2-FBXO45 controls the activity (Lin et al., 2021) and proteasomal turnover of a subset of proteins in a ubiquitylation-dependent manner, resulting in hepatocellular tumorigenesis (Lin et al., 2021), regulation of EMT (Xu et al., 2015) or promotion of cancer cell survival (Chen et al., 2014; Richter et al., 2020). This thesis

builds on the discovery of MYCBP2-FBXO45 promoting mitotic slippage and thus cell survival after MT-poison treatment through proteasomal destruction of tumor suppressor and mitotic cell death promotor FBXW7 (Richter et al., 2020). The aim of this thesis is identifying new interactors and/or ubiquitylation-substrates of the MYCBP2-FBXO45 E3 ligase to further understand its involvement in mitotic slippage regulation.

4.1 SPRYD3 is a new MYCBP2-interacting protein

For the identification of new interactors or substrates of the MYCBP2-FBXO45 E3 ligase, I used an IP-based approach combined with MS-analysis after ectopic expression of Flag-FBXO45 or Flag-FBXO45ΔSPRY as bait. Flag-FBXO45ΔSPRY was used as a negative control to specifically identify SPRY-domain interactors, and hence potential substrates. Ectopic Flag-EV expression served as an internal control to exclude false interacting proteins due to unspecific binding with the Flag-tag. Amongst significantly enriched proteins, I encountered known and/or conserved FBXO45-interacting proteins such as MYCBP2 (Desbois et al., 2018; Saiga et al., 2009), FBXW7 (Richter et al., 2020), SKP1 (Desbois et al., 2018; Saiga et al., 2009) and RAE1 (Huttlin et al., 2015; Richter, 2017) validating the success of my screen (Figure 4A). In addition to the known interactors, I identified SPRYD3, a so far poorly characterized protein (Figure 4A). Interestingly, SPRYD3 was also identified in other interactome screens using MYCBP2 (Sakai et al., 2011), FBXW7 (Kourtis et al., 2015; Richter et al., 2020), SKP1 (Huttlin et al., 2021) or RAE1 (Richter, 2017) as bait, suggesting it to be a part of the MYCBP2-FBXO45 network.

SPRYD3 has a molecular weight of approximately 55 kDa (Figure 4B, D) and similar to FBXO45, which has one SPRY domain, SPRYD3 harbors two SPRY-domains, namely SPRY1 and SPRY2 (Figure 4C). Both FBXO45 and SPRYD3 are members of the SPRY/B30.2 protein family that consists of proteins harboring SPRY-domains (D'Cruz et al., 2013). Interestingly, this protein family also comprises a diverse set of E3 ligases, such as TRIM E3 ligases, but also the HECT E3 ligase HERC1 (D'Cruz et al., 2013). SPRY-domains are important mediators of protein-protein interactions and can function as substrate recognition domains of E3 ligases (D'Cruz et al., 2013; Mei et al., 2021; Saiga et al., 2009). In fact, FBXO45 mediates substrate recruitment and binding to MYCBP2 via its only SPRY-domain (Desbois et al., 2018; Richter et al., 2020; Saiga et al., 2009). Another example is represented by TRIM25, which binds

and mediates direct ubiquitylation of its substrate RIP3 via its SPRY-domain (Mei et al., 2021).

Except for its predicted function in surface receptor signaling and cytoskeleton organization (Alliance of Genome Resources), as well as its reported co-upregulation with MYCBP2-FBXO45 in mice lacking FKBP5 expression (Gebru et al., 2024), SPRYD3 protein function remains mostly unknown. Due to affiliation to the same protein family and similar protein architecture to FBXO45, it seemed conceivable to me that SPRYD3 may exert a similar function as FBXO45 within the MCYBP2 E3 ligase complex. I hypothesized that SPRYD3 might act as an additional substrate specifity factor of MYCBP2, thus forming a new E3 ligase complex targeting substrates for ubiquitylation. I decided to follow up on this hypothesis by investigating whether a new E3 ligase complex consisting of MYCBP2-SPRYD3 exists, and whether it plays a role in mitotic cell fate regulation.

It is not uncommon for E3 ligases to engage and interchange substrate specificity factors or express multiple substrate-binding domains to broaden their target scope (Sherpa et al., 2022). In fact, the *Saccharomyces cerevisiae* Ubr1 E3 ligase complex contains three substrate specificity domains that recognize different types of substrates (Baker and Varshavsky, 1991; Bartel et al., 1990; Xia et al., 2008) and furthermore, two of those domains are predicted to overlap (Xia et al., 2008). The CUL4B-based E3 ubiquitin ligase was shown to engage with the two substrate specifity factors WDR1 and LIS1 in a phospho-specific manner, forming two E3 ligase complexes involved in brain development by regulating actin cortex or spindle positioning, respectively (Baxi and Werner, 2023; Stier et al., 2023). CRL4 interacts with substrate receptors Rep-ID and RBBP7 in a sequential and cell cycle specific manner to promote the metaphase to anaphase transition (Jang et al., 2020). And lastly, the multi-subunit E3 ligase complex APC/C interacts with CDC20 or CDH1 to orchestrate cell cycle progression in metaphase and at the M/G1 transition (Greil et al., 2022).

To test the hypothesis of SPRYD3 being a new substrate specificity factor of the MYCBP2 E3 ligase, I characterized the interaction between SPRYD3 and MYCBP2 in more detail. After showing that the two proteins interact from both sides (Figure 7A), I determined that MYCBP2 is important for SPRYD3 protein stability, since its downregulation significantly destabilizes SPRYD3 protein levels (Figure 7B). By using ectopically expressed MYCBP2 truncations harboring its different protein domains (Figure 8 and 9A), I demonstrated that SPRYD3 and FBXO45 have slightly overlapping

binding sites on MYCBP2, resembling the overlapping substrate binding sites reported for Ubr1 (Xia et al., 2008). Furthermore, similar to FBXO45, SPRYD3 uses a SPRY domain, SPRY2, to directly interact with MYCBP2 (Figure 9B and 10B). Interestingly, when FBXO45 or SPRYD3 are absent, MYCBP2 and SPRYD3 or MYCBP2 and FBXO45 can still form complexes, but complex formation is reduced (Figure 8B), suggesting that the stability of all three proteins is interdependent. To assess whether MYCBP2 forms two independent complexes or exists in a state where SPRYD3 and FBXO45 are bound simultaneously, I co-expressed the Flag-tagged MYCBP2 truncation that was shown to bind both SPRYD3 and FBXO45, together with MYC-SPRYD3 or MYC-FBXO45 and performed two consecutive IPs by first immuno-precipitating Flag-tagged MYCBP2 and then MYC-tagged proteins. As shown in Figure 10A, MYCBP2 can form complexes with FBXO45 and SPRYD3 simultaneously, but the fact that FBXO45 can bind MYCBP2 in SPRYD3-depleted cells and SPRYD3 engages with MYCBP2 in FBXO45 knock-out cells (Figure 8B), suggests that different MYCBP2 complexes can exist within the cell. Additionally, since this experiment was performed in asynchronous cells, it cannot be excluded that the MYCBP2 E3 ligase complex could assemble with different substrate specificity factors during the cell cycle, as it was reported for example for CRL4 (Jang et al., 2020). This could be an interesting point for future investigations as the different complexes might exert distinct functions.

4.2 SPRYD3 promotes mitotic slippage after MT-poison treatment

MYCBP2 and SPRYD3 form a complex that can also exist in absence of FBXO45. The scope of my thesis was to further elucidate the function of MYCBP2 in mitotic slippage regulation. Thus, I performed live cell imaging to assess whether SPRYD3 had a function in mitotic cell fate decisions. Depletion of SPRYD3 significantly increased mitotic cell death in presence of either nocodazole or paclitaxel, similar to MYCBP2-depleted cells, which I included as a positive control (Figure 5) (Richter et al., 2020). Interestingly, double-depletion of both MYCBP2 and SPRYD3 promoted mitotic slippage to similar levels as MYCBP2-depletion alone (Figure 5), suggesting that both proteins work in the same pathway, most likely in the same complex. Besides, similar effects were observed in either U2OS or RPE1 cells, which represent a carcinogenic and a non-carcinogenic cell line, respectively. This suggests, that the functions of MYCBP2 and SPRYD3 in mitotic cell fate decisions might not necessarily be cancer-dependent. However, in order to reach a reliable result, more cell lines of each type

need to be analyzed. Interestingly, neither SPRYD3- nor MYCBP2-depletion had any effect on successful mitosis or mitotic timing in absence of MT-poison treatment (Figure 6A and B), suggesting that their function becomes relevant only during mitotic arrest. Again, this applied to both U2OS and RPE1 cells. How exactly SPRYD3 and MYCBP2 become relevant only during mitotic arrest, remains an interesting point for future investigations.

4.3 CHAMP1 and XIAP are deubiquitylated upon ectopic SPRYD3 expression

With the intention of identifying ubiquitylation substrates of the MYCBP2-SPRYD3 complex, I performed an IP-MS approach by ectopically expressing Flag-SPRYD3 in HEK 293T cells as bait. As previously described for the Flag-FBXO45 IP-MS screen (Figure 4A), Flag-EV expression served as an internal control. Interestingly, proteins such as FBXO45, MYCBP2, SKP1, FBXW7 and RAE1 were identified in the Flag-SPRYD3 screen (Figure 14A). This reinforced the idea of SPRYD3 being a part of the MYCBP2 E3 ligase complex, since afore-mentioned proteins also appeared in the Flag-FBXO45 MS screen (Figure 4A). I confirmed my results by *in vivo* interaction studies between endogenous FBXO45, RAE1, FBXW7, MYCBP2 and SKP1 with ectopically expressed Flag-SPRYD3 (Figure 14B).

I used the Flag-SPRYD3 IP-MS data that I generated to search for significantly enriched proteins that could act as potential interactors and/or ubiquitylation substrates of the newly identified MYCBP2-SPRYD3 complex. I searched for proteins with a confirmed function in mitosis and/or mitotic slippage regulation, since my objective was to investigate the role of MYCBP2-SPRYD3 in this process. Two significantly enriched candidates were CHAMP1 and XIAP with reported functions in mitosis and mitotic slippage (Hino et al., 2021; Hou et al., 2017). I validated their interaction with SPRYD3 by ectopically expressing SPRYD3 in HEK 293T cells (Figure 14B).

CHAMP1 promotes mitotic slippage after MT-poison treatment by stabilizing anti-apoptotic factor MCL-1 (Hino et al., 2021). Interestingly, CHAMP1 interacted with SPRYD3 in both asynchronous and mitotic cells, although the interaction was weaker during mitosis (Figure 16A). Phosphorylated forms of CHAMP1 during mitosis have been reported (Itoh et al., 2011) and the decrease in SPRYD3-CHAMP1 interaction could be attributed to this phosphorylation. For example, in the case of the E3 ligase $CRL4^{PRL1}$, its ATR-mediated phosphorylation inhibits ubiquitylation of its substrate ribonucleotide reductase (RNR2) (Bao et al., 2023). Thus, it would be interesting to

assess whether abolishment of CHAMP1-phosphorylation during mitosis would restore CHAMP1-SPRYD3 interaction levels to the level observed in asynchronous cells.

To assess the role of CHAMP1 as a MYCBP2-SPRYD3 ubiquitylation substrate, I investigated its protein stability and ubiquitylation status after modulation of SPRYD3 protein levels. siRNA-mediated SPRYD3-depletion increased CHAMP1 protein levels in a partially significant manner in both U2OS and HeLa cells (Figure 18), possibly implying that SPYRD3 may target CHAMP1 for ubiquitylation-dependent proteasomal degradation. This was further confirmed by the fact that inhibiting the proteasome using MG132 significantly increased the interaction between Flag-SPRYD3 and CHAMP1 in HEK 293T cells (Figure 16B). However, when assessing CHAMP1 ubiquitylation-status after ectopic expression of MYC-SPRYD3 in HEK 293T WT or ΔFBXO45 cells, I observed less ubiquitylated CHAMP1 in MYC-SPRYD3 overexpressing cells compared to mock-treated controls (Figure 19). These results stand in contrast with CHAMP1 proteins levels increasing after siRNA-mediated depletion of SPRYD3 (Figure 18). Thus, the question as to how and why SPRYD3 regulates CHAMP1 remains open for further investigations.

Next, I assessed the role of XIAP as a potential interactor and ubiquitylation substrate of MYCBP2-SPRYD3. I used a similar approach as for CHAMP1 to address a possible function of XIAP as a ubiquitylation substrate of MYCBP2-SPRYD3. Flag-SPRYD3 and XIAP interacted in both asynchronous and mitotic cell populations at similar levels (Figure 20A), suggesting that the interaction might not be cell cycle regulated. Furthermore, treatment with λ-phosphatase reduced the interaction significantly (Figure 20B), indicating a partial importance of phosphorylation for establishment of an interaction. Phosphorylation-mediated interaction between substrates and respective E3 ligases have been reported widely. For example, glycogen synthase kinase-3β (GSK3β) promotes phosphorylation-dependent interaction of FBXW7 and its substrate WDR5 (Hänle-Kreidler et al., 2022). Interestingly, Flag-SPRYD3 engaged with XIAP via its second SPRY-domain (Figure 21B), which is also important for MYCBP2-binding. This resembles FBXO45, which uses its only SPRY-domain for substrate binding and binding to MYCBP2 (Desbois et al., 2018; Richter, 2017; Saiga et al., 2009).

XIAP protein stability remained unaffected after SPRYD3-depletion (Figure 22), suggesting that if SPRYD3-mediated ubiquitylation of XIAP occurs, it is not linked to proteasome degradation. Surprisingly, ectopic expression of MYC-SPRYD3 or MYC-

MYCBP2 in HEK 293T WT or ΔFBXO45 cells, resulted in less ubiquitylated XIAP compared to controls overexpressing MYC-EV (Figure 23). These results are similar to those obtained with CHAMP1. XIAP was reported to be deubiquitylated and thus stabilized by USP11 (Zhou et al., 2016). Additionally, USP11 was reported to promote bipolar spindle formation by interacting and deubiquitylating RAE1 (Stockum et al., 2018). The fact that both XIAP and RAE1 are associated with USP11, but are also validated interactors of SPRYD3 (Figure 14B) and in case of RAE1, a conserved interactor of MYCBP2 (Tian et al., 2011), lead me to hypothesize that USP11 could collaborate with MYCBP2-SPRYD3 to regulate XIAP or RAE1 deubiquitylation. The only point speaking against this hypothesis is the fact that SPRYD3 depletion leaves XIAP levels unchanged (Figure 22), while USP11 depletion was reported to destabilize XIAP protein levels (Zhou et al., 2016). Thus, how MYCBP2-SPRYD3 regulates XIAP remains an open question for future investigations.

4.4 USP11 is a substrate of the MYCBP2-SPRYD3 E3 ligase

Even though the hypothesis of MYCBP2-SPRYD3 regulating USP11 resulting in deubiquitylation of a downstream substrate might not apply for XIAP, I still considered this to be possible for RAE1. USP11 is reported to deubiquitylate RAE1 (Stockum et al., 2018) to mediate bipolar spindle formation. RAE1 is a validated interactor of SPRYD3 (Figure 14), and a conserved interactor of MYCBP2 (Tian et al., 2011). When revising the Flag-FBXO45 and Flag-SPRYD3 IP-MS data, I indeed identified USP11 amongst enriched proteins in both screens (Figure 24). FBXO45 (Sowa et al., 2009), SPRYD3 (Sowa et al., 2009; Stockum et al., 2018), as well as MYCBP2 (Sowa et al., 2009) were enriched in independent interactome screens using USP11 as bait, validating its presence in my MS screens.

I hypothesized that MYCBP2-SPRYD3 might ubiquitylate USP11, resulting in its ability to deubiquitylate RAE1. The need for DUBs to be ubiquitylated by an E3 ligase for substrate-recruitment and consequent deubiquitylation has been reported in various cases. For example, K63-mediated ubiquitylation of the DUB USP7 is crucial for its function in hypoxia-induced metastasis and EMT (Wu et al., 2016). K63-mediated ubiquitylation of USP7 promotes interaction with and deubiquitylation of HIF1α, as well as H3K56 acetylation on the HIF1α promoter (Wu et al., 2016). In another example, the E3 ligase RNF220 mediates ubiquitylation of USP7, which is required for β-catenin deubiquitylation and subsequent activation of WNT-signaling (Ma et al., 2014).

I validated the interaction between ectopically expressed MYCBP2-SPRYD3 and USP11 in HEK 293T WT cells and confirmed their interaction in FBXO45 knock-out cells (Figure 25). Furthermore, I confirmed a direct interaction between recombinant SPRYD3 and USP11 (Figure 29) which strongly suggests that the two proteins directly bind to each other. Before assessing the potential role of USP11 as ubiquitylation substrate of MYCBP2-SPRYD3, I performed live cell imaging experiments in USP11-depleted U2OS or RPE1 cells to assess its function in mitotic cell fate regulation after nocodazole or paclitaxel treatment. Similar to SPRYD3 and MYCBP2, the absence of USP11 decreased mitotic slippage in both cell lines (Figure 26), suggesting that USP11 could act together with MYCBP2-SPRYD3 in the same pathway. In non-drug treated U2OS or RPE1 cells, depletion of USP11 had neither an effect on mitotic cell fate nor on mitotic timing (Figure 27). Thus, these results are in agreement with those obtained with MYCBP2 and SPRYD3.

Various ubiquitylation assays performed in HEK 293T WT and ΔFBXO45 cells confirmed that MYCBP2-SPRYD3 ubiquitylates USP11 *in vivo* and *in vitro* and suggest that FBXO45 does not function in this process (Figures 30-33). Interestingly, ectopic expression of the MYCBP2 RING-domain was sufficient to catalyze USP11 ubiquitylation (Figure 30D). This could be explained with the fact that SPRYD3 also binds the same region (Figure 8) and therefore might mediate USP11 recruitment.

4.5 MYCBP2-SPRYD3 targets USP11^{C318} for proteasome-independent ubiquitylation

I determined that MYCBP2-SPRYD3 generates K63-linked Ub-chains on USP11 (Figure 34). K63-linked Ub-chains are not primarily connected to proteasomal degradation, but regulate other processes such as immune regulation or DNA-repair (Doil et al., 2009; Sobhian et al., 2007). Interestingly, in a recent study, MYCBP2-FBXO45 was reported to modify the oncogene IGF2BP1 via K63-linked ubiquitylation, leading to its activation instead of proteasomal destruction. Similarly, RNAi and CHX chases confirmed that MYCBP2-SPRYD3 ubiquitylation does not lead to proteasomal destruction of USP11 (Figure 35), suggesting a similar role as described for MYCBP2-FBXO45 and IGF2BP1.

I observed weak MYCBP2-SPRYD3-mediated ubiquitylation of USP11 under normal buffer conditions. MYCBP2 is able to target serines and threonines for ubiquitylation (Mabbitt et al., 2020; Pao et al., 2018), but oxyester-linkages are not very stable under

standard buffer conditions used for sample preparation in ubiquitylation assays (Song et al., 2009; Vosper et al., 2009). I therefore modified buffer conditions by leaving out DTT, a known reducing agent that weakens oxyester-, but also abolishes thioester-linkages. Surprisingly, in absence of DTT, USP11-ubiquitylation mediated by MYCBP2-SPRYD3 was much stronger compared to samples prepared with buffer containing DTT (Figure 36A), suggesting the targeting of either serine, threonine or cysteine ubiquitylation sites on USP11.

I determined 6 potential USP11 ubiquitylation-sites in presence of MYCBP2-SPRYD3 through an IP-MS based approach (Figure 36B) and generated a USP11^{6A} mutant by exchanging those residues to alanines and assess their importance in MYCBP2-SPRYD3-mediated ubiquitylation. I also included the catalytic inactive USP11 mutant, USP11^{C318S}, reported to abolish SETX (Jurga et al., 2021) as well as tau (Yan et al., 2022) deubiquitylation. Surprisingly, both USP11 mutants, USP11^{6A} and USP11^{C318S}, abolished MYCBP2-SPRYD3-mediated ubiquitylation (Figure 36D), suggesting those residues as potential ubiquitylation sites.

While the ability of MYCBP2 targeting serines or threonines for ubiquitylation has been described (Mabbitt et al., 2020; Pao et al., 2018), the fact that it targets USP11^{C318} for ubiquitylation is a new finding. Considering that E1, E2 and to some extent E3 enzymes undergo transient complex formation with a Ub-moiety via thioester linkages to cysteines, it seemed conceivable that MYCBP2 might promote cysteine ubiquitylation on its substrate USP11. The necessity of ubiquitylation-mediated activation of DUBs has been reported for the DUB ataxin-3 (AT3) (Todi et al., 2009), and similar to this, MYCBP2-SPRYD3-mediated ubiquitylation of USP11^{C318} might contribute to its catalytic activity and consequent deubiquitylation of SETX (Jurga et al., 2021), tau (Yan et al., 2022) or other known substrates such as RAE1 (Stockum et al., 2018). Furthermore, thioester-linkages are more reactive than amide-bonds, making them important for quick transient modifications during processes where fast alterations are necessary (Kelsall, 2022). Due to its function in mitosis, the MYCBP2-SPRYD3 E3 ligase might require fast transient reactions such as ubiquitylation of USP11^{C318}.

4.6 MYCBP2-SPRYD3, USP11 and RAE1 act in the same pathway to regulate bipolar spindle formation

SPRYD3 has postulated functions in cytoskeleton organization (Alliance of Genome Resources) and links between PHR proteins and MTs have been reported previously (Lewcock et al., 2007; Tian et al., 2011). For example, mouse Phr1 was shown to associate and promote MT-stability and cytoskeletal polarization during neurite growth through ubiquitylation-dependent degradation of kinase DLK (Lewcock et al., 2007). Furthermore, PHR protein function is mediated through the association with the MT-binding protein RAE1 in invertebrate cells (Tian et al., 2011). These findings support the potential role of MYCBP2 and SPRYD3 in bipolar spindle formation. Previously reported interactome screens with either RAE1, MYCBP2, SPRYD3 or USP11 as bait (Huttlin et al., 2015; Richter, 2017; Stockum et al., 2018) (Figure 14), suggested that all of these proteins might form part of the same network and collaborate in bipolar spindle formation.

As I demonstrated in various experiments, MYCBP2-SPRYD3-mediated ubiquitylation of USP11 regulates bipolar spindle formation by promoting its interaction and probably deubiquitylation of RAE1 (Figures 37, 38 and 40). As mentioned previously, the $USP11^{C318S}$ and $USP11^{6A}$ mutants abolished MYCBP2-SPRYD3-mediated ubiquitylation, suggesting that these sites might function as potential ubiquitylation target sites (Figure 36D). I confirmed that MYCBP2-SPRYD3-mediated ubiquitylation of $USP11^{C318}$ is relevant for bipolar spindle formation, while the residues mutated in the $USP11^{6A}$ mutant do not seem to play a role in this process (Figure 38). This indicates that MYCBP2-SPRYD3 and USP11 might additionally cooperate in the regulation of other cellular pathways apart from bipolar spindle formation and it would be interesting for the future to explore this hypothesis.

I confirmed that MYCBP2-SPRYD3-mediated ubiquitylation of USP11 promotes its interaction with RAE1 since in presence of the catalytic inactive mutant MYCBP2 C4250S, the interaction is significantly decreased (Figure 40B). This was further confirmed by the observation that $USP11^{C318S}$ interacted significantly less with RAE1 compared to $USP11^{WT}$ or $USP11^{6A}$ (Figure 40C). Considering that MYCBP2-SPRYD3 applies K63-linked polyubiquitin chains to USP11 (Figure 34) and that MYCBP2 has already been reported to activate IGF2BP1 via K63-mediated polyubiquitylation (Lin et al., 2021), it is possible that similar processes might underlie the MYCBP2-SPRYD3/USP11/RAE1 pathway.

4.7 Bipolar spindle formation regulated by the MYCBP2-SPRYD3/USP11/RAE1 axis promotes mitotic slippage in presence of MT-poisons

Bipolar spindle formation is essential for successful cell division. A failure to build a proper spindle by altering its dynamics or bipolarity can lead to apoptosis in order to avoid aberrant cell division (Jordan and Wilson, 2004). It has been reported that MT-poisons can induce multipolar spindles in cells and that this eventually contributes to mitotic cell death (Abal et al., 2001; Zhou et al., 2023). The fact that MYCBP2-, SPRYD3-, USP11-, RAE1-depletion (Figures 5, 26 and 41) (Stockum et al., 2018) or ectopic expression of USP11^{C318S} (Figure 39) further sensitizes cells for mitotic cell death in presence of MT-poisons and induces multipolar spindles (Figure 37 and 38B and C) suggests a connection between bipolar spindle formation and mitotic slippage. Indeed, RAE1 has been postulated to contribute to cell survival after MT-poison treatment due to its function in positively promoting bipolar spindle formation (Kobayashi et al., 2021).

The competing-threshold model (Gascoigne and Taylor, 2008) might serve as an explanation as to how mitotic slippage might be connected to bipolar spindle formation. Mitotic arrest is an unnatural state that eventually ends in mitotic cell death, if errors triggering mitotic arrest cannot be resolved (Jordan and Wilson, 2004). While stuck in mitotic arrest, gradual Cyclin B1 degradation continues (Brito and Rieder, 2006), while at the same time, apoptotic stimuli accumulate due to intrinsically or extrinsically generated signals that led to mitotic arrest in the first place. Depending on which threshold is breached first, the cell either undergoes mitotic slippage or mitotic cell death. Multipolar spindles might represent an additional apoptotic stimulus to eliminate the cell and avoid aberrant cell division. Bipolar spindles however, might generate less apoptotic stimuli compared to multipolar spindles, enabling Cyclin B1 degradation to breach the threshold for mitotic slippage, before apoptotic stimuli can sufficiently accumulate.

Multipolar spindles upon MYCBP2-, SPRYD3- or USP11-depletion seem to be generated due to centrosome disengagement or microtubule breakage, since more than half of multipolar cells contain spindles with only one or no centrin signal (Figure 37). Acentrosomal spindle poles have been variously reported (Maiato and Logarinho, 2014) and it would be interesting to assess whether pericentriolar proteins are present at these acentrosomal poles. RAE1 regulates spindle bundling and bipolar spindle formation through its interaction with NuMA (Wong et al., 2006) and SMC1 (Wong and

Blobel, 2008). Abolishment of RAE1 deubiquitylation via USP11 due to absence of MYCBP2-SPRYD3-mediated ubiquitylation might affect the interaction between RAE1 and NuMA and/or SMC1, thus resulting in defective bundling and spindle breakage and formation of new acentrosomal spindle poles.

Whereas overexpression of $USP11^{WT}$ or $USP11^{6A}$ promotes mitotic slippage, $USP11^{C318S}$ reverses this effect, by sensitizing cells towards mitotic cell death in presence of MT-poisons (Figure 39). The fact that $USP11^{C318S}$ cannot be ubiquitylated by MYCBP2-SPRYD3 which consequently results in multipolar spindle formation, but at the same time promotes mitotic cell death in presence of MT-poisons, points to a possible link between proper bipolar spindle formation and the ability to undergo mitotic slippage.

5. Working model

The RCR E3 ligase MYCBP2-FBXO45 promotes mitotic slippage and cell survival by targeting FBXW7 and PAR-4 for proteasomal degradation. Mitotic slippage contributes to acquisition of chemoresistance against MT-poisons. Therefore, the elucidation of mechanisms underlying mitotic slippage is an important issue. Its various roles in oncogenesis suggest that on top of afore-mentioned targets, other substrates might be regulated by the MYCBP2-FBXO45 E3 ligase in context of mitotic slippage.

In the presented thesis, I screened for new interactors and/or substrates of the MYCBP2-FBXO45 E3 ligase and identified SPRYD3 as new substrate specificity factor of MYCBP2. I demonstrated that MYCBP2 and SPRYD3 form an active E3 ligase complex independent of FBXO45 and characterized the DUB USP11 as its first direct ubiquitylation substrate. MYCBP2-SPRYD3 ubiquitylates a non-canonical substrate residue, namely USP11 cysteine 318, which is important for USP11 catalytic activity (Jurga et al., 2021; Yan et al., 2022). This ubiquitylation might contribute to USP11 catalytic activation and consequently, USP11 interacts and deubiquitylates RAE1. This in turn promotes bipolar spindle formation and mitotic slippage in presence of MT-poisons. The working model is summarized in Figure 42.

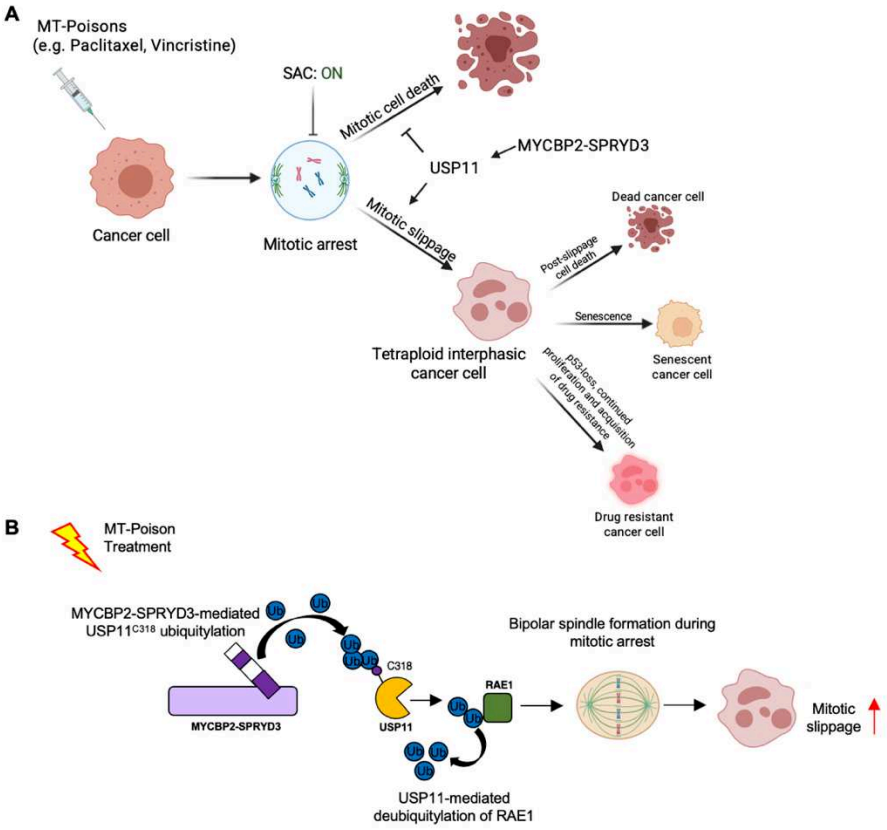


Figure 42: MYCBP2-SPRYD3 ubiquitylates USP11^{C318} to promote interaction with and deubiquitylation of RAE1 and consequent bipolar spindle formation and mitotic slippage in response to MT-poisons.

(A) MT-poison treatment of cancer cells induces prolonged mitotic arrest through sustained activation of the spindle assembly checkpoint (SAC). Depending on various factors, cancer cells either undergo apoptosis in form of mitotic cell death or exit mitosis without previous cytokinesis via mitotic slippage, resulting in interphasic tetraploid cells. These tetraploid cells can undergo post-mitotic cell death or enter growth arrest in form of senescence. Depending on their p53 mutation status, cancer cells can escape these two post-mitotic fates and continue proliferation as genetically instable cells, eventually giving rise to MT-poison resistance mechanisms. MYCBP2-SPRYD3 ubiquitylates USP11 independent of proteasomal degradation and promotes mitotic slippage in presence of MT-poisons. **(B)** MYCBP2-SPRYD3 ubiquitylates the catalytic aa residue $USP11^{C318}$ which leads to interaction with and deubiquitylation of RAE1. Consequently, deubiquitylation of RAE1 promotes bipolar spindle formation, which induces mitotic slippage in presence of MT-poisons.

6. Future perspectives

In my thesis, I elucidated a new mechanism by which MYCBP2 promotes mitotic slippage in presence of spindle poisons. MYCBP2-SPRYD3-mediated ubiquitylation of USP11 promotes bipolar spindle formation, which consequently helps cells to overcome mitotic arrest and slip back into interphase. Since this was only shown in cultured cells, the next step would be to explore whether a combination of suppressing this pathway plus spindle poison treatment sensitizes cancers towards mitotic cell death *in vivo*, such as in mammalian model organisms or organoids.

The USP11^{6A} and USP11^{C318S} mutants both abolish MYCBP2-SPRYD3-mediated ubiquitylation. While ubiquitylation of USP11^{C318} is relevant for its interaction with RAE1 as well as its function in bipolar spindle formation and mitotic slippage, USP11^{6A} did not play a role in these processes. This suggests that additionally to their collaboration in mitotic cell fate regulation and bipolar spindle formation, MYCBP2-SPRYD3 and USP11 regulate other cellular processes. This together with the identification of the exact residue/s mutated in the USP11^{6A} mutant that are targeted by MYCBP2-SPRYD3, remain interesting questions for future investigations.

The fact that MYCBP2-SPRYD3 ubiquitylates USP11^{C318}, the reported catalytic aa residue important for deubiquitylation activity of USP11, leads to further interesting questions for future studies. In case of RAE1, I showed that ubiquitylation of USP11^{C318} promotes its interaction with and probably deubiquitylation by USP11. Taking into account other known USP11 substrates, such as SETX (Jurga et al., 2021) or tau (Yan et al., 2022), it would be interesting to explore whether a similar mechanism is relevant for their regulation. Interestingly, tau is a MT-stabilizing protein, and its deregulation plays an important role in tau pathology. While USP11^{WT} deubiquitylates and thus stabilizes tau, leading to its accumulation in the brain, the catalytic inactive mutant USP11^{C318S} has no impact (Yan et al., 2022). MYCBP2 has reported roles in neuronal development and neurodevelopmental disorders, and the fact that it ubiquitylates USP11^{C318}, raises challenging questions if there could exist a collaboration between the MYCBP2-SPRYD3 E3 ligase and USP11 in tau accumulation.

7. References

Abal, M., Souto, A.A., Amat-Guerri, F., Acuña, A.U., Andreu, J.M., Barasoain, I., 2001. Centrosome and spindle pole microtubules are main targets of a fluorescent taxoid inducing cell death. Cell Motil. 49, 1–15. https://doi.org/10.1002/cm.1016

Abbas, R., Larisch, S., 2020. Targeting XIAP for Promoting Cancer Cell Death—The Story of ARTS and SMAC. Cells 9, 663. https://doi.org/10.3390/cells9030663

AlAbdi, L., Desbois, M., Rusnac, D.-V., Sulaiman, R.A., Rosenfeld, J.A., Lalani, S., Murdock, D.R., Burrage, L.C., Undiagnosed Diseases Network, Billie Au, P.Y., Towner, S., Wilson, W.G., Wong, L., Brunet, T., Strobl-Wildemann, G., Burton, J.E., Hoganson, G., McWalter, K., Begtrup, A., Zarate, Y.A., Christensen, E.L., Opperman, K.J., Giles, A.C., Helaby, R., Kania, A., Zheng, N., Grill, B., Alkuraya, F.S., 2023. Loss-of-function variants in *MYCBP2* cause neurobehavioural phenotypes and corpus callosum defects. Brain 146, 1373–1387. https://doi.org/10.1093/brain/awac364

Babu, J.R., Jeganathan, K.B., Baker, D.J., Wu, X., Kang-Decker, N., Van Deursen, J.M., 2003. Rae1 is an essential mitotic checkpoint regulator that cooperates with Bub3 to prevent chromosome missegregation. J. Cell Biol. 160, 341–353. https://doi.org/10.1083/jcb.200211048

Baker, R.T., Varshavsky, A., 1991. Inhibition of the N-end rule pathway in living cells. Proc. Natl. Acad. Sci. 88, 1090–1094. https://doi.org/10.1073/pnas.88.4.1090

Baker, S.T., Opperman, K.J., Tulgren, E.D., Turgeon, S.M., Bienvenut, W., Grill, B., 2014. RPM-1 Uses Both Ubiquitin Ligase and Phosphatase-Based Mechanisms to Regulate DLK-1 during Neuronal Development. PLoS Genet. 10, e1004297. https://doi.org/10.1371/journal.pgen.1004297

Balachandran, R.S., Heighington, C.S., Starostina, N.G., Anderson, J.W., Owen, D.L., Vasudevan, S., Kipreos, E.T., 2016. The ubiquitin ligase CRL2ZYG11 targets cyclin B1 for degradation in a conserved pathway that facilitates mitotic slippage. J. Cell Biol. 215, 151–166. https://doi.org/10.1083/jcb.201601083

Bao, W., Zhang, W., Huang, Y., Zhao, Y., Wu, C., Duan, L., Wang, L., Yan, S., 2023. Protein kinase ATR inhibits E3 ubiquitin ligase CRL4PRL1 to stabilize ribonucleotide reductase in response to replication stress. Cell Rep. 42, 112685. https://doi.org/10.1016/j.celrep.2023.112685

Bartel, B., Wünning, I., Varshavsky, A., 1990. The recognition component of the N-end rule pathway. EMBO J. 9, 3179–3189. https://doi.org/10.1002/j.1460-2075.1990.tb07516.x

Baxi, A., Werner, A., 2023. You can “tail” them apart: paralog-specific functions of CRL4B ubiquitin ligases during mitosis and brain development. EMBO J. 42, e114931. https://doi.org/10.15252/embj.2023114931

Bernardini, J.P., Brouwer, J.M., Tan, I.K., Sandow, J.J., Huang, S., Stafford, C.A., Bankovacki, A., Riffkin, C.D., Wardak, A.Z., Czabotar, P.E., Lazarou, M., Dewson, G., 2019. Parkin inhibits BAK and BAX apoptotic function by distinct mechanisms during mitophagy. EMBO J. 38, e99916. https://doi.org/10.15252/embj.201899916

Brito, D.A., Rieder, C.L., 2009. The Ability to Survive Mitosis in the Presence of Microtubule Poisons Differs Significantly Between Human Nontransformed (RPE-1) and Cancer (U2OS, HeLa) Cells. Cell Motil. Cytoskeleton 66, 437–447. https://doi.org/10.1002/cm.20316

Brito, D.A., Rieder, C.L., 2006. Mitotic Checkpoint Slippage in Humans Occurs via Cyclin B Destruction in the Presence of an Active Checkpoint. Curr. Biol. 16, 1194–1200. https://doi.org/10.1016/j.cub.2006.04.043

Brown, J.A., Bharathi, A., Ghosh, A., Whalen, W., Fitzgerald, E., Dhar, R., 1995. A Mutation in the *Schizosaccharomyces pombe rae1* Gene Causes Defects in Poly(A)+ RNA Export and in the Cytoskeleton (∗). J. Biol. Chem. 270, 7411–7419. https://doi.org/10.1074/jbc.270.13.7411

Cakir, Z., Funk, K., Lauterwasser, J., Todt, F., Zerbes, R.M., Oelgeklaus, A., Tanaka, A., van der Laan, M., Edlich, F., 2017. Parkin promotes proteasomal degradation of misregulated BAX. J. Cell Sci. 130, 2903–2913. https://doi.org/10.1242/jcs.200162

Cardozo, T., Pagano, M., 2004. The SCF ubiquitin ligase: insights into a molecular machine. Nat. Rev. Mol. Cell Biol. 5, 739–751. https://doi.org/10.1038/nrm1471

Carroll, R.G., Hollville, E., Martin, S.J., 2014. Parkin Sensitizes toward Apoptosis Induced by Mitochondrial Depolarization through Promoting Degradation of Mcl-1. Cell Rep. 9, 1538–1553. https://doi.org/10.1016/j.celrep.2014.10.046

Carvalho, A.F., Pinto, M.P., Grou, C.P., Alencastre, I.S., Fransen, M., Sá-Miranda, C., Azevedo, J.E., 2007. Ubiquitination of Mammalian Pex5p, the Peroxisomal

Import Receptor*. J. Biol. Chem. 282, 31267–31272. https://doi.org/10.1074/jbc.M706325200

Chan, K.-S., Koh, C.-G., Li, H.-Y., 2012. Mitosis-targeted anti-cancer therapies: where they stand. Cell Death Dis. 3, e411–e411. https://doi.org/10.1038/cddis.2012.148

Chen, X., Sahasrabuddhe, A.A., Szankasi, P., Chung, F., Basrur, V., Rangnekar, V.M., Pagano, M., Lim, M.S., Elenitoba-Johnson, K.S.J., 2014. Fbxo45-mediated degradation of the tumor-suppressor Par-4 regulates cancer cell survival. Cell Death Differ. 21, 1535–1545. https://doi.org/10.1038/cdd.2014.92

Cheng, B., Crasta, K., 2017. Consequences of mitotic slippage for antimicrotubule drug therapy. Endocr. Relat. Cancer 24, T97–T106. https://doi.org/10.1530/ERC-17-0147

Ciechanover, A., Heller, H., Elias, S., Haas, A.L., Hershko, A., 1980. ATP-dependent conjugation of reticulocyte proteins with the polypeptide required for protein degradation. Proc. Natl. Acad. Sci. U. S. A. 77, 1365–1368. https://doi.org/10.1073/pnas.77.3.1365

Ciechanover, A., Heller, H., Katz-Etzion, R., Hershko, A., 1981. Activation of the heat-stable polypeptide of the ATP-dependent proteolytic system. Proc. Natl. Acad. Sci. U. S. A. 78, 761. https://doi.org/10.1073/pnas.78.2.761

Ciehanover, A., Hod, Y., Rershkol, A., 1978. A heat-stable polypeptide component of an ATP-dependent proteolytic system from reticulocytes. Biochem. Biophys. Res. Commun. 81.

Cubillos-Rojas, M., Amair-Pinedo, F., Tato, I., Bartrons, R., Ventura, F., Rosa, J.L., 2010. Simultaneous electrophoretic analysis of proteins of very high and low molecular mass using Tris-acetate polyacrylamide gels. Electrophoresis 31, 1318–1321. https://doi.org/10.1002/elps.200900657

Dang, F., Nie, L., Wei, W., 2021. Ubiquitin signaling in cell cycle control and tumorigenesis. Cell Death Differ. 28, 427–438. https://doi.org/10.1038/s41418-020-00648-0

D'Cruz, A.A., Babon, J.J., Norton, R.S., Nicola, N.A., Nicholson, S.E., 2013. Structure and function of the SPRY/B30.2 domain proteins involved in innate immunity. Protein Sci. Publ. Protein Soc. 22, 1–10. https://doi.org/10.1002/pro.2185

Desbois, M., Crawley, O., Evans, P.R., Baker, S.T., Masuho, I., Yasuda, R., Grill, B., 2018. PAM forms an atypical SCF ubiquitin ligase complex that ubiquitinates

and degrades NMNAT2. J. Biol. Chem. 293, 13897–13909. https://doi.org/10.1074/jbc.RA118.002176

Deshaies, R.J., Joazeiro, C.A.P., 2009. RING Domain E3 Ubiquitin Ligases. Annu. Rev. Biochem. 78, 399–434. https://doi.org/10.1146/annurev.biochem.78.101807.093809

Dewson, G., Eichhorn, P.J.A., Komander, D., 2023. Deubiquitinases in cancer. Nat. Rev. Cancer 23, 842–862. https://doi.org/10.1038/s41568-023-00633-y

Doil, C., Mailand, N., Bekker-Jensen, S., Menard, P., Larsen, D.H., Pepperkok, R., Ellenberg, J., Panier, S., Durocher, D., Bartek, J., Lukas, J., Lukas, C., 2009. RNF168 Binds and Amplifies Ubiquitin Conjugates on Damaged Chromosomes to Allow Accumulation of Repair Proteins. Cell 136, 435–446. https://doi.org/10.1016/j.cell.2008.12.041

Dörr, A., Pierre, S., Zhang, D.D., Henke, M., Holland, S., Scholich, K., 2015. MYCBP2 Is a Guanosine Exchange Factor for Ran Protein and Determines Its Localization in Neurons of Dorsal Root Ganglia. J. Biol. Chem. 290, 25620–25635. https://doi.org/10.1074/jbc.M115.646901

Dupont, S., Mamidi, A., Cordenonsi, M., Montagner, M., Zacchigna, L., Adorno, M., Martello, G., Stinchfield, M.J., Soligo, S., Morsut, L., Inui, M., Moro, S., Modena, N., Argenton, F., Newfeld, S.J., Piccolo, S., 2009. FAM/USP9x, a Deubiquitinating Enzyme Essential for TGFβ Signaling, Controls Smad4 Monoubiquitination. Cell 136, 123–135. https://doi.org/10.1016/j.cell.2008.10.051

Eckelman, B.P., Salvesen, G.S., Scott, F.L., 2006. Human inhibitor of apoptosis proteins: why XIAP is the black sheep of the family. EMBO Rep. 7, 988–994. https://doi.org/10.1038/sj.embor.7400795

Engeland, K., 2022. Cell cycle regulation: p53-p21-RB signaling. Cell Death Differ. 29, 946–960. https://doi.org/10.1038/s41418-022-00988-z

Ergün, S., Aslan, S., Demir, D., Kayaoğlu, S., Saydam, M., Keleş, Y., Kolcuoğlu, D., Taşkurt Hekim, N., Güneş, S., 2024. Beyond Death: Unmasking the Intricacies of Apoptosis Escape. Mol. Diagn. Ther. 28, 403–423. https://doi.org/10.1007/s40291-024-00718-w

Galbán, S., Duckett, C.S., 2010. XIAP as a ubiquitin ligase in cellular signaling. Cell Death Differ. 17, 54–60. https://doi.org/10.1038/cdd.2009.81

Ganem, N.J., Storchova, Z., Pellman, D., 2007. Tetraploidy, aneuploidy and cancer. Curr. Opin. Genet. Dev. 17, 157–162. https://doi.org/10.1016/j.gde.2007.02.011

Gascoigne, K.E., Taylor, S.S., 2008. Cancer Cells Display Profound Intra- and Interline Variation following Prolonged Exposure to Antimitotic Drugs. Cancer Cell 14, 111–122. https://doi.org/10.1016/j.ccr.2008.07.002

Gebru, N.T., Guergues, J., Verdina, L.A., Wohlfahrt, J., Wang, S., Armendariz, D.S., Gray, M., Beaulieu-Abdelahad, D., Stevens, S.M., Gulick, D., Blair, L.J., 2024. *Fkbp5* gene deletion: Circadian rhythm profile and brain proteomics in aged mice. Aging Cell 23, e14314. https://doi.org/10.1111/acel.14314

Goldknopf, I.L., Busch, H., 1977. Isopeptide linkage between nonhistone and histone 2A polypeptides of chromosomal conjugate-protein A24. Proc. Natl. Acad. Sci. U. S. A. 74, 864–868. https://doi.org/10.1073/pnas.74.3.864

Goldstein, G., Scheid, M., Hammerling, U., Schlesinger, D.H., Niall, H.D., Boyse, E.A., 1975. Isolation of a polypeptide that has lymphocyte-differentiating properties and is probably represented universally in living cells. Proc. Natl. Acad. Sci. U. S. A. 72, 11–15. https://doi.org/10.1073/pnas.72.1.11

Greil, C., Engelhardt, M., Wäsch, R., 2022. The Role of the APC/C and Its Coactivators Cdh1 and Cdc20 in Cancer Development and Therapy. Front. Genet. 13, 941565. https://doi.org/10.3389/fgene.2022.941565

Grill, B., Chen, L., Tulgren, E.D., Baker, S.T., Bienvenut, W., Anderson, M., Quadroni, M., Jin, Y., Garner, C.C., 2012. RAE-1, a novel PHR binding protein, is required for axon termination and synapse formation in Caenorhabditis elegans. J. Neurosci. Off. J. Soc. Neurosci. 32, 2628–2636. https://doi.org/10.1523/JNEUROSCI.2901-11.2012

Grill, B., Murphey, R.K., Borgen, M.A., 2016. The PHR proteins: intracellular signaling hubs in neuronal development and axon degeneration. Neural Develop. 11, 8. https://doi.org/10.1186/s13064-016-0063-0

Guo, Q., Xie, J., Dang, C.V., Liu, E.T., Bishop, J.M., 1998. Identification of a large Myc-binding protein that contains RCC1-like repeats. Proc. Natl. Acad. Sci. 95, 9172–9177. https://doi.org/10.1073/pnas.95.16.9172

Guo, T., Tang, H., Yuan, Z., Zhang, E., Wang, X., 2022. The Dual Role of USP11 in Cancer. J. Oncol. 2022, 1–8. https://doi.org/10.1155/2022/9963905

Hanahan, D., Weinberg, R.A., 2011. Hallmarks of Cancer: The Next Generation. Cell 144, 646–674. https://doi.org/10.1016/j.cell.2011.02.013

Hanahan, D., Weinberg, R.A., 2000. The Hallmarks of Cancer. Cell 100, 57–70. https://doi.org/10.1016/S0092-8674(00)81683-9

Hänle-Kreidler, S., Richter, K.T., Hoffmann, I., 2022. The SCF-FBXW7 E3 ubiquitin ligase triggers degradation of histone 3 lysine 4 methyltransferase complex component WDR5 to prevent mitotic slippage. J. Biol. Chem. 298, 102703. https://doi.org/10.1016/j.jbc.2022.102703

Hao, B., Oehlmann, S., Sowa, M.E., Harper, J.W., Pavletich, N.P., 2007. Structure of a Fbw7-Skp1-Cyclin E Complex: Multisite-Phosphorylated Substrate Recognition by SCF Ubiquitin Ligases. Mol. Cell 26, 131–143. https://doi.org/10.1016/j.molcel.2007.02.022

Harper, S., Gratton, H.E., Cornaciu, I., Oberer, M., Scott, D.J., Emsley, J., Dreveny, I., 2014. Structure and catalytic regulatory function of ubiquitin specific protease 11 N-terminal and ubiquitin-like domains. Biochemistry 53, 2966–2978. https://doi.org/10.1021/bi500116x

Heckman, K.L., Pease, L.R., 2007. Gene splicing and mutagenesis by PCR-driven overlap extension. Nat. Protoc. 2, 924–932. https://doi.org/10.1038/nprot.2007.132

Hempel, M., Cremer, K., Ockeloen, C.W., Lichtenbelt, K.D., Herkert, J.C., Denecke, J., Haack, T.B., Zink, A.M., Becker, J., Wohlleber, E., Johannsen, J., Alhaddad, B., Pfundt, R., Fuchs, S., Wieczorek, D., Strom, T.M., van Gassen, K.L.I., Kleefstra, T., Kubisch, C., Engels, H., Lessel, D., 2015. De Novo Mutations in *CHAMP1* Cause Intellectual Disability with Severe Speech Impairment. Am. J. Hum. Genet. 97, 493–500. https://doi.org/10.1016/j.ajhg.2015.08.003

Hershko, A., 1985. Occurrence of a Polyubiquitin Structure in Ubiquitin-Protein Conjucates. Biochem. Biophys. Res. Commun. 128.

Hershko, A., Ciechanover, A., Heller, H., Haas, A.L., Rose, I.A., 1980. Proposed role of ATP in protein breakdown: conjugation of protein with multiple chains of the polypeptide of ATP-dependent proteolysis. Proc. Natl. Acad. Sci. U. S. A. 77, 1783–1786. https://doi.org/10.1073/pnas.77.4.1783

Hershko, A., Eytan, E., Ciechanover, A., Haas, A.L., 1982. Immunochemical analysis of the turnover of ubiquitin-protein conjugates in intact cells. Relationship to the breakdown of abnormal proteins. J. Biol. Chem. 257, 13964–13970.

Hershko, A., Heller, H., Elias, S., Ciechanover, A., 1983. Components of ubiquitin-protein ligase system. Resolution, affinity purification, and role in protein breakdown. J. Biol. Chem. 258, 8206–8214.

Hino, M., Iemura, K., Ikeda, M., Itoh, G., Tanaka, K., 2021. Chromosome alignment-maintaining phosphoprotein CHAMP1 plays a role in cell survival through regulating Mcl-1 expression. Cancer Sci. 112, 3711–3721. https://doi.org/10.1111/cas.15018

Hoege, C., Pfander, B., Moldovan, G.-L., Pyrowolakis, G., Jentsch, S., 2002. RAD6-dependent DNA repair is linked to modification of PCNA by ubiquitin and SUMO. Nature 419, 135–141. https://doi.org/10.1038/nature00991

Hou, Y., Allan, L.A., Clarke, P.R., 2017. Phosphorylation of XIAP by CDK1–cyclin-B1 controls mitotic cell death. J. Cell Sci. 130, 502. https://doi.org/10.1242/jcs.192310

Hough, R., Pratt, G., Rechsteiner, M., 1986. Ubiquitin-lysozyme conjugates. Identification and characterization of an ATP-dependent protease from rabbit reticulocyte lysates. J. Biol. Chem. 261, 2400–2408. https://doi.org/10.1016/S0021-9258(17)35950-1

Huszar, D., Theoclitou, M.-E., Skolnik, J., Herbst, R., 2009. Kinesin motor proteins as targets for cancer therapy. Cancer Metastasis Rev. 28, 197–208. https://doi.org/10.1007/s10555-009-9185-8

Huttlin, E.L., Bruckner, R.J., Navarrete-Perea, J., Cannon, J.R., Baltier, K., Gebreab, F., Gygi, M.P., Thornock, A., Zarraga, G., Tam, S., Szpyt, J., Gassaway, B.M., Panov, A., Parzen, H., Fu, S., Golbazi, A., Maenpaa, E., Stricker, K., Guha Thakurta, S., Zhang, T., Rad, R., Pan, J., Nusinow, D.P., Paulo, J.A., Schweppe, D.K., Vaites, L.P., Harper, J.W., Gygi, S.P., 2021. Dual proteome-scale networks reveal cell-specific remodeling of the human interactome. Cell 184, 3022-3040.e28. https://doi.org/10.1016/j.cell.2021.04.011

Huttlin, E.L., Ting, L., Bruckner, R.J., Gebreab, F., Gygi, M.P., Szpyt, J., Tam, S., Zarraga, G., Colby, G., Baltier, K., Dong, R., Guarani, V., Vaites, L.P., Ordureau, A., Rad, R., Erickson, B.K., Wühr, M., Chick, J., Zhai, B., Kolippakkam, D., Mintseris, J., Obar, R.A., Harris, T., Artavanis-Tsakonas, S., Sowa, M.E., DeCamilli, P., Paulo, J.A., Harper, J.W., Gygi, S.P., 2015. The BioPlex Network: A Systematic Exploration of the Human Interactome. Cell 162, 425–440. https://doi.org/10.1016/j.cell.2015.06.043

Ideguchi, H., Ueda, A., Tanaka, M., Yang, J., Tsuji, T., Ohno, S., Hagiwara, E., Aoki, A., Ishigatsubo, Y., 2002. Structural and functional characterization of the USP11 deubiquitinating enzyme, which interacts with the RanGTP-associated protein RanBPM. Biochem. J. 367, 87–95. https://doi.org/10.1042/bj20011851

Inuzuka, H., Shaik, S., Onoyama, I., Gao, D., Tseng, A., Maser, R.S., Zhai, B., Wan, L., Gutierrez, A., Lau, A.W., Xiao, Y., Christie, A.L., Aster, J., Settleman, J., Gygi, S.P., Kung, A.L., Look, T., Nakayama, K.I., DePinho, R.A., Wei, W., 2011. SCFFbw7 Regulates Cellular Apoptosis By Targeting Mcl-1 for Ubiquitination and Destruction. Nature 471, 104–109. https://doi.org/10.1038/nature09732

Itoh, G., Kanno, S., Uchida, K.S.K., Chiba, S., Sugino, S., Watanabe, K., Mizuno, K., Yasui, A., Hirota, T., Tanaka, K., 2011. CAMP (C13orf8, ZNF828) is a novel regulator of kinetochore-microtubule attachment: Role of CAMP in chromosome segregation. EMBO J. 30, 130–144. https://doi.org/10.1038/emboj.2010.276

Jang, S.-M., Nathans, J.F., Fu, H., Redon, C.E., Jenkins, L.M., Thakur, B.L., Pongor, L.S., Baris, A.M., Gross, J.M., O'Neill, M.J., Indig, F.E., Cappell, S.D., Aladjem, M.I., 2020. The RepID–CRL4 ubiquitin ligase complex regulates metaphase to anaphase transition via BUB3 degradation. Nat. Commun. 11, 24. https://doi.org/10.1038/s41467-019-13808-9

Jin, J., Cardozo, T., Lovering, R.C., Elledge, S.J., Pagano, M., Harper, J.W., 2004. Systematic analysis and nomenclature of mammalian F-box proteins. Genes Dev. 18, 2573–2580. https://doi.org/10.1101/gad.1255304

Jin, Q., Gutierrez Diaz, B., Pieters, T., Zhou, Y., Narang, S., Fijalkwoski, I., Borin, C., Van Laere, J., Payton, M., Cho, B.-K., Han, C., Sun, L., Serafin, V., Yacu, G., Von Loocke, W., Basso, G., Veltri, G., Dreveny, I., Ben-Sahra, I., Goo, Y.A., Safgren, S.L., Tsai, Y.-C., Bornhauser, B., Suraneni, P.K., Gaspar-Maia, A., Kandela, I., Van Vlierberghe, P., Crispino, J.D., Tsirigos, A., Ntziachristos, P., 2022. Oncogenic deubiquitination controls tyrosine kinase signaling and therapy response in acute lymphoblastic leukemia. Sci. Adv. 8, eabq8437. https://doi.org/10.1126/sciadv.abq8437

Jordan, M.A., Wilson, L., 2004. Microtubules as a target for anticancer drugs. Nat. Rev. Cancer 4, 253–265. https://doi.org/10.1038/nrc1317

Jurga, M., Abugable, A.A., Goldman, A.S.H., El-Khamisy, S.F., 2021. USP11 controls R-loops by regulating senataxin proteostasis. Nat. Commun. 12, 5156. https://doi.org/10.1038/s41467-021-25459-w

Ke, J., Dai, C., Wu, W., Gao, J., Xia, A., Liu, G., Lv, K., Wu, C., 2014. USP11 regulates p53 stability by deubiquitinating p53. J. Zhejiang Univ. Sci. B 15, 1032–1038. https://doi.org/10.1631/jzus.B1400180

Kelsall, I.R., 2022. Non-lysine ubiquitylation: Doing things differently. Front. Mol. Biosci. 9, 1008175. https://doi.org/10.3389/fmolb.2022.1008175

Kelsall, I.R., McCrory, E.H., Xu, Y., Scudamore, C.L., Nanda, S.K., Mancebo-Gamella, P., Wood, N.T., Knebel, A., Matthews, S.J., Cohen, P., 2022. HOIL-1 ubiquitin ligase activity targets unbranched glucosaccharides and is required to prevent polyglucosan accumulation. EMBO J. 41, e109700. https://doi.org/10.15252/embj.2021109700

Kelsall, I.R., Zhang, J., Knebel, A., Arthur, J.S.C., Cohen, P., 2019. The E3 ligase HOIL-1 catalyses ester bond formation between ubiquitin and components of the Myddosome in mammalian cells. Proc. Natl. Acad. Sci. U. S. A. 116, 13293–13298. https://doi.org/10.1073/pnas.1905873116

Kerr, J.F.R., Wyllie, A.H., Currie, A.R., 1972. Apoptosis: A Basic Biological Phenomenon with Wideranging Implications in Tissue Kinetics. Br. J. Cancer 26, 239–257. https://doi.org/10.1038/bjc.1972.33

Kobayashi, Y., Masuda, T., Fujii, A., Shimizu, D., Sato, K., Kitagawa, A., Tobo, T., Ozato, Y., Saito, H., Kuramitsu, S., Noda, M., Otsu, H., Mizushima, T., Doki, Y., Eguchi, H., Mori, M., Mimori, K., 2021. Mitotic checkpoint regulator RAE1 promotes tumor growth in colorectal cancer. Cancer Sci. 112, 3173–3189. https://doi.org/10.1111/cas.14969

Komander, D., Rape, M., 2012. The ubiquitin code. Annu. Rev. Biochem. 81, 203–229. https://doi.org/10.1146/annurev-biochem-060310-170328

Kourtis, N., Moubarak, R.S., Aranda-Orgilles, B., Lui, K., Aydin, I.T., Trimarchi, T., Darvishian, F., Salvaggio, C., Zhong, J., Bhatt, K., Chen, E.I., Celebi, J.T., Lazaris, C., Tsirigos, A., Osman, I., Hernando, E., Aifantis, I., 2015. FBXW7 modulates cellular stress response and metastatic potential through HSF1 post-translational modification. Nat. Cell Biol. 17, 322–332. https://doi.org/10.1038/ncb3121

Kumari, N., Jaynes, P.W., Saei, A., Iyengar, P.V., Richard, J.L.C., Eichhorn, P.J.A., 2017. The roles of ubiquitin modifying enzymes in neoplastic disease. Biochim. Biophys. Acta BBA - Rev. Cancer 1868, 456–483. https://doi.org/10.1016/j.bbcan.2017.09.002

Lee, E.-W., Seong, D., Seo, J., Jeong, M., Lee, H.-K., Song, J., 2015. USP11-dependent selective cIAP2 deubiquitylation and stabilization determine sensitivity to Smac mimetics. Cell Death Differ. 22, 1463–1476. https://doi.org/10.1038/cdd.2014.234

Lewcock, J.W., Genoud, N., Lettieri, K., Pfaff, S.L., 2007. The Ubiquitin Ligase Phr1 Regulates Axon Outgrowth through Modulation of Microtubule Dynamics. Neuron 56, 604–620. https://doi.org/10.1016/j.neuron.2007.09.009

Li, F., Sarangi, P., Iyer, D.R., Feng, H., Moreau, L., Nguyen, H., Clairmont, C., D'Andrea, A.D., 2022. CHAMP1 binds to REV7/FANCV and promotes homologous recombination repair. Cell Rep. 40, 111297. https://doi.org/10.1016/j.celrep.2022.111297

Lin, C.-H., Chang, H.-S., Yu, W.C.Y., 2008. USP11 Stabilizes HPV-16E7 and Further Modulates the E7 Biological Activity. J. Biol. Chem. 283, 15681–15688. https://doi.org/10.1074/jbc.M708278200

Lin, X.-T., Yu, H.-Q., Fang, L., Tan, Y., Liu, Z.-Y., Wu, D., Zhang, J., Xiong, H.-J., Xie, C.-M., 2021. Elevated FBXO45 promotes liver tumorigenesis through enhancing IGF2BP1 ubiquitination and subsequent PLK1 upregulation. eLife 10, e70715. https://doi.org/10.7554/eLife.70715

Liu, Y., Mukherjee, R., Bonn, F., Colby, T., Matic, I., Glogger, M., Heilemann, M., Dikic, I., 2021. Serine-ubiquitination regulates Golgi morphology and the secretory pathway upon Legionella infection. Cell Death Differ. 28, 2957–2969. https://doi.org/10.1038/s41418-021-00830-y

Lorenz, S., 2018. Structural mechanisms of HECT-type ubiquitin ligases. Biol. Chem. 399, 127–145. https://doi.org/10.1515/hsz-2017-0184

Ma, P., Yang, X., Kong, Q., Li, C., Yang, S., Li, Y., Mao, B., 2014. The Ubiquitin Ligase RNF220 Enhances Canonical Wnt Signaling through USP7-Mediated Deubiquitination of β-Catenin. Mol. Cell. Biol. 34, 4355–4366. https://doi.org/10.1128/MCB.00731-14

Mabbitt, P.D., Loreto, A., Déry, M.-A., Fletcher, A.J., Stanley, M., Pao, K.-C., Wood, N.T., Coleman, M.P., Virdee, S., 2020. Structural basis for RING-Cys-Relay E3 Ligase Activity and its Role in Axon Integrity. Nat. Chem. Biol. 16, 1227–1236. https://doi.org/10.1038/s41589-020-0598-6

Maertens, G.N., El Messaoudi-Aubert, S., Elderkin, S., Hiom, K., Peters, G., 2010. Ubiquitin-specific proteases 7 and 11 modulate Polycomb regulation of the

INK4a tumour suppressor. EMBO J. 29, 2553–2565. https://doi.org/10.1038/emboj.2010.129

Maiato, H., Logarinho, E., 2014. Mitotic spindle multipolarity without centrosome amplification. Nat. Cell Biol. 16, 386–394. https://doi.org/10.1038/ncb2958

Manchado, E., Guillamot, M., Malumbres, M., 2012. Killing cells by targeting mitosis. Cell Death Differ. 19, 369–377. https://doi.org/10.1038/cdd.2011.197

McGranahan, N., Burrell, R.A., Endesfelder, D., Novelli, M.R., Swanton, C., 2012. Cancer chromosomal instability: therapeutic and diagnostic challenges. EMBO Rep. 13, 528–538. https://doi.org/10.1038/embor.2012.61

McIntosh, J.R., 2016. Mitosis. Cold Spring Harb. Perspect. Biol. 8, a023218. https://doi.org/10.1101/cshperspect.a023218

Mulle, J.G., Dodd, A.F., McGrath, J.A., Wolyniec, P.S., Mitchell, A.A., Shetty, A.C., Sobreira, N.L., Valle, D., Rudd, M.K., Satten, G., Cutler, D.J., Pulver, A.E., Warren, S.T., 2010. Microdeletions of 3q29 Confer High Risk for Schizophrenia. Am. J. Hum. Genet. 87, 229–236. https://doi.org/10.1016/j.ajhg.2010.07.013

Murphy, R., Watkins, J.L., Wente, S.R., 1996. GLE2, a Saccharomyces cerevisiae homologue of the Schizosaccharomyces pombe export factor RAE1, is required for nuclear pore complex structure and function. Mol. Biol. Cell 7, 1921–1937. https://doi.org/10.1091/mbc.7.12.1921

Musacchio, A., Salmon, E.D., 2007. The spindle-assembly checkpoint in space and time. Nat. Rev. Mol. Cell Biol. 8, 379–393. https://doi.org/10.1038/nrm2163

Newton, K., Strasser, A., Kayagaki, N., Dixit, V.M., 2024. Cell death. Cell 187, 235–256. https://doi.org/10.1016/j.cell.2023.11.044

Okumoto, K., Misono, S., Miyata, N., Matsumoto, Y., Mukai, S., Fujiki, Y., 2011. Cysteine Ubiquitination of PTS1 Receptor Pex5p Regulates Pex5p Recycling. Traffic 12, 1067–1083. https://doi.org/10.1111/j.1600-0854.2011.01217.x

Orlicky, S., Tang, X., Willems, A., Tyers, M., Sicheri, F., 2003. Structural Basis for Phosphodependent Substrate Selection and Orientation by the SCFCdc4 Ubiquitin Ligase. Cell 112, 243–256. https://doi.org/10.1016/S0092-8674(03)00034-5

Otten, E.G., Werner, E., Casado, A.C., Boyle, K.B., Dharamdasani, V., Pathe, C., Santhanam, B., Randow, F., 2021. Ubiquitylation of lipopolysaccharide by RNF213 during bacterial infection. Nature 594, 111. https://doi.org/10.1038/s41586-021-03566-4

Pao, K.-C., Wood, N.T., Knebel, A., Rafie, K., Stanley, M., Mabbitt, P.D., Sundaramoorthy, R., Hofmann, K., van Aalten, D.M.F., Virdee, S., 2018. Activity-based E3 ligase profiling uncovers an E3 ligase with esterification activity. Nature 556, 381–385. https://doi.org/10.1038/s41586-018-0026-1

Peng, J., Schwartz, D., Elias, J.E., Thoreen, C.C., Cheng, D., Marsischky, G., Roelofs, J., Finley, D., Gygi, S.P., 2003. A proteomics approach to understanding protein ubiquitination. Nat. Biotechnol. 21, 921–926. https://doi.org/10.1038/nbt849

Perrin, A.J., Jiang, X., Birmingham, C.L., So, N.S.Y., Brumell, J.H., 2004. Recognition of Bacteria in the Cytosol of Mammalian Cells by the Ubiquitin System. Curr. Biol. 14, 806–811. https://doi.org/10.1016/j.cub.2004.04.033

Peters, J.-M., 2006. The anaphase promoting complex/cyclosome: a machine designed to destroy. Nat. Rev. Mol. Cell Biol. 7, 644–656. https://doi.org/10.1038/nrm1988

Pickart, C.M., 2001. Mechanisms Underlying Ubiquitination. Annu. Rev. Biochem. 70, 503–533. https://doi.org/10.1146/annurev.biochem.70.1.503

Pritchard, C.E.J., Fornerod, M., Kasper, L.H., van Deursen, J.M.A., 1999. RAE1 Is a Shuttling mRNA Export Factor That Binds to a GLEBS-like NUP98 Motif at the Nuclear Pore Complex through Multiple Domains. J. Cell Biol. 145, 237–254. https://doi.org/10.1083/jcb.145.2.237

Quintero-Rivera, F., Sharifi-Hannauer, P., Martinez-Agosto, J.A., 2010. Autistic and psychiatric findings associated with the 3q29 microdeletion syndrome: Case report and review. Am. J. Med. Genet. A. 152A, 2459–2467. https://doi.org/10.1002/ajmg.a.33573

Richter, K., 2017. Identification and characterization of novel regulators of the tumor suppressor and ubiquitin ligase SCF-FBXW7. Ruprecht-Karls-Universität, Heidelberg.

Richter, K.T., Kschonsak, Y.T., Vodicska, B., Hoffmann, I., 2020. FBXO45-MYCBP2 regulates mitotic cell fate by targeting FBXW7 for degradation. Cell Death Differ. 27, 758–772. https://doi.org/10.1038/s41418-019-0385-7

Rieder, C.L., Cole, R.W., Khodjakov, A., Sluder, G., 1995. The checkpoint delaying anaphase in response to chromosome monoorientation is mediated by an inhibitory signal produced by unattached kinetochores. J. Cell Biol. 130, 941–948. https://doi.org/10.1083/jcb.130.4.941

Rieder, C.L., Maiato, H., 2004. Stuck in Division or Passing through: What Happens When Cells Cannot Satisfy the Spindle Assembly Checkpoint. Dev. Cell 7, 637–651. https://doi.org/10.1016/j.devcel.2004.09.002

Sack, L.M., Davoli, T., Li, M.Z., Li, Y., Xu, Q., Naxerova, K., Wooten, E.C., Bernardi, R.J., Martin, T.D., Chen, T., Leng, Y., Liang, A.C., Scorsone, K.A., Westbrook, T.F., Wong, K.-K., Elledge, S.J., 2018. Profound Tissue Specificity in Proliferation Control Underlies Cancer Drivers and Aneuploidy Patterns. Cell 173, 499-514.e23. https://doi.org/10.1016/j.cell.2018.02.037

Saiga, T., Fukuda, T., Matsumoto, M., Tada, H., Okano, H.J., Okano, H., Nakayama, K.I., 2009. Fbxo45 Forms a Novel Ubiquitin Ligase Complex and Is Required for Neuronal Development. Mol. Cell. Biol. 29, 3529–3543. https://doi.org/10.1128/MCB.00364-09

Sakai, Y., Shaw, C.A., Dawson, B.C., Dugas, D.V., Al-Mohtaseb, Z., Hill, D.E., Zoghbi, H.Y., 2011. Protein interactome reveals converging molecular pathways among autism disorders. Sci. Transl. Med. 3, 86ra49. https://doi.org/10.1126/scitranslmed.3002166

Sakurikar, N., Eichhorn, J.M., Chambers, T.C., 2012. Cyclin-dependent Kinase-1 (Cdk1)/Cyclin B1 Dictates Cell Fate after Mitotic Arrest via Phosphoregulation of Antiapoptotic Bcl-2 Proteins. J. Biol. Chem. 287, 39193–39204. https://doi.org/10.1074/jbc.M112.391854

Salmela, A.-L., Kallio, M.J., 2013. Mitosis as an anti-cancer drug target. Chromosoma 122, 431–449. https://doi.org/10.1007/s00412-013-0419-8

Schimmer, A.D., 2004. Inhibitor of Apoptosis Proteins: Translating Basic Knowledge into Clinical Practice. Cancer Res. 64, 7183–7190. https://doi.org/10.1158/0008-5472.CAN-04-1918

Schindelin, J., Arganda-Carreras, I., Frise, E., Kaynig, V., Longair, M., Pietzsch, T., Preibisch, S., Rueden, C., Saalfeld, S., Schmid, B., Tinevez, J.-Y., White, D.J., Hartenstein, V., Eliceiri, K., Tomancak, P., Cardona, A., 2012. Fiji: an open-source platform for biological-image analysis. Nat. Methods 9, 676–682. https://doi.org/10.1038/nmeth.2019

Schlesinger, D.H., Goldstein, G., Niall, H.D., 1975. The complete amino acid sequence of ubiquitin, an adenylate cyclase stimulating polypeptide probably universal in living cells. Biochemistry 14, 2214–2218. https://doi.org/10.1021/bi00681a026

Schoenfeld, A.R., Apgar, S., Dolios, G., Wang, R., Aaronson, S.A., 2004. BRCA2 Is Ubiquitinated In Vivo and Interacts with USP11, a Deubiquitinating Enzyme That Exhibits Prosurvival Function in the Cellular Response to DNA Damage. Mol. Cell. Biol. 24, 7444–7455. https://doi.org/10.1128/MCB.24.17.7444-7455.2004

Schoenheimer, R., Clarke, H.T., 1942. The dynamic state of body constituents, Harvard university monographs in medicine and public health. Harvard University Press, Cambridge, Mass.

Schwanhäusser, B., Busse, D., Li, N., Dittmar, G., Schuchhardt, J., Wolf, J., Chen, W., Selbach, M., 2011. Global quantification of mammalian gene expression control. Nature 473, 337–342. https://doi.org/10.1038/nature10098

Schwickart, M., Huang, X., Lill, J.R., Liu, J., Ferrando, R., French, D.M., Maecker, H., O'Rourke, K., Bazan, F., Eastham-Anderson, J., Yue, P., Dornan, D., Huang, D.C.S., Dixit, V.M., 2010. Deubiquitinase USP9X stabilizes MCL1 and promotes tumour cell survival. Nature 463, 103–107. https://doi.org/10.1038/nature08646

Sharp, P.M., Li, W.-H., 1987. Ubiquitin genes as a paradigm of concerted evolution of tandem repeats. J. Mol. Evol. 25, 58–64. https://doi.org/10.1007/BF02100041

Sherpa, D., Chrustowicz, J., Schulman, B.A., 2022. How the ends signal the end: Regulation by E3 ubiquitin ligases recognizing protein termini. Mol. Cell 82, 1424–1438. https://doi.org/10.1016/j.molcel.2022.02.004

Shevchenko, A., Tomas, H., Havli, J., Olsen, J.V., Mann, M., 2006. In-gel digestion for mass spectrometric characterization of proteins and proteomes. Nat. Protoc. 1, 2856–2860. https://doi.org/10.1038/nprot.2006.468

Sobhian, B., Shao, G., Lilli, D.R., Culhane, A.C., Moreau, L.A., Xia, B., Livingston, D.M., Greenberg, R.A., 2007. RAP80 Targets BRCA1 to Specific Ubiquitin Structures at DNA Damage Sites. Science 316, 1198. https://doi.org/10.1126/science.1139516

Song, J., Wang, J., Jozwiak, A.A., Hu, W., Swiderski, P.M., Chen, Y., 2009. Stability of thioester intermediates in ubiquitin-like modifications. Protein Sci. 18, 2492–2499. https://doi.org/10.1002/pro.254

Sowa, M.E., Bennett, E.J., Gygi, S.P., Harper, J.W., 2009. Defining the human deubiquitinating enzyme interaction landscape. Cell 138, 389–403. https://doi.org/10.1016/j.cell.2009.04.042

Stier, A., Gilberto, S., Mohamed, W.I., Royall, L.N., Helenius, J., Mikicic, I., Sajic, T., Beli, P., Müller, D.J., Jessberger, S., Peter, M., 2023. The CUL4B -based E3

ubiquitin ligase regulates mitosis and brain development by recruiting phospho-specific DCAFs. EMBO J. 42, e112847. https://doi.org/10.15252/embj.2022112847

Stockum, A., Snijders, A.P., Maertens, G.N., 2018. USP11 deubiquitinates RAE1 and plays a key role in bipolar spindle formation. PLoS ONE 13, e0190513. https://doi.org/10.1371/journal.pone.0190513

Sun, H., Ou, B., Zhao, S., Liu, Xueni, Song, L., Liu, Xisheng, Wang, R., Peng, Z., 2019. USP11 promotes growth and metastasis of colorectal cancer via PPP1CA-mediated activation of ERK/MAPK signaling pathway. EBioMedicine 48, 236–247. https://doi.org/10.1016/j.ebiom.2019.08.061

Swanson, D.A., Freund, C.L., Ploder, L., McInnes, R.R., Valle, D., 1996. A Ubiquitin C-Terminal Hydrolase Gene on the Proximal Short Arm of the X Chromosome: Implications for X-Linked Retinal Disorders. Hum. Mol. Genet. 5, 533–538. https://doi.org/10.1093/hmg/5.4.533

Tatham, M.H., Plechanovová, A., Jaffray, E.G., Salmen, H., Hay, R.T., 2013. Ube2W conjugates ubiquitin to α-amino groups of protein N-termini. Biochem. J. 453, 137–145. https://doi.org/10.1042/BJ20130244

Thornberry, N.A., Lazebnik, Y., 1998. Caspases: Enemies Within. Science 281, 1312–1316. https://doi.org/10.1126/science.281.5381.1312

Tian, X., Li, J., Valakh, V., DiAntonio, A., Wu, C., 2011. Drosophila Rae1 controls the abundance of the ubiquitin ligase Highwire in post-mitotic neurons. Nat. Neurosci. 14, 1267–1275. https://doi.org/10.1038/nn.2922

Ting, X., Xia, L., Yang, J., He, L., Si, W., Shang, Y., Sun, L., 2019. USP11 acts as a histone deubiquitinase functioning in chromatin reorganization during DNA repair. Nucleic Acids Res. 47, 9721–9740. https://doi.org/10.1093/nar/gkz726

Todi, S.V., Winborn, B.J., Scaglione, K.M., Blount, J.R., Travis, S.M., Paulson, H.L., 2009. Ubiquitination directly enhances activity of the deubiquitinating enzyme ataxin-3. EMBO J. 28, 372–382. https://doi.org/10.1038/emboj.2008.289

Tricoli, J.V., Boardman, L.A., Patidar, R., Sindiri, S., Jang, J.S., Walsh, W.D., McGregor, P.M., Camalier, C.E., Mehaffey, M.G., Furman, W.L., Bahrami, A., Williams, P.M., Lih, C.-J., Conley, B.A., Khan, J., 2018. A Mutational Comparison of Adult and Adolescent and Young Adult (AYA) Colon Cancer. Cancer 124, 1070–1082. https://doi.org/10.1002/cncr.31136

Tyanova, S., Temu, T., Cox, J., 2016. The MaxQuant computational platform for mass spectrometry-based shotgun proteomics. Nat. Protoc. 11, 2301–2319. https://doi.org/10.1038/nprot.2016.136

Verma, R., Annan, R.S., Huddleston, M.J., Carr, S.A., Reynard, G., Deshaies, R.J., 1997. Phosphorylation of Sic1p by G_1 Cdk Required for Its Degradation and Entry into S Phase. Science 278, 455–460. https://doi.org/10.1126/science.278.5337.455

Vosper, J.M.D., McDowell, G.S., Hindley, C.J., Fiore-Heriche, C.S., Kucerova, R., Horan, I., Philpott, A., 2009. Ubiquitylation on Canonical and Non-canonical Sites Targets the Transcription Factor Neurogenin for Ubiquitin-mediated Proteolysis. J. Biol. Chem. 284, 15458. https://doi.org/10.1074/jbc.M809366200

Vucic, D., 2018. XIAP at the crossroads of cell death and inflammation. Oncotarget 9, 27319–27320. https://doi.org/10.18632/oncotarget.25363

Walsh, C.T., Garneau-Tsodikova, S., Gatto Jr., G.J., 2005. Protein Posttranslational Modifications: The Chemistry of Proteome Diversifications. Angew. Chem. Int. Ed. 44, 7342–7372. https://doi.org/10.1002/anie.200501023

Wang, D., Ma, L., Wang, B., Liu, J., Wei, W., 2017. E3 ubiquitin ligases in cancer and implications for therapies. Cancer Metastasis Rev. 36, 683–702. https://doi.org/10.1007/s10555-017-9703-z

Waxman, L., Fagan, J.M., Goldberg, A.L., 1987. Demonstration of two distinct high molecular weight proteases in rabbit reticulocytes, one of which degrades ubiquitin conjugates. J. Biol. Chem. 262, 2451–2457.

Wenzel, D.M., Lissounov, A., Brzovic, P.S., Klevit, R.E., 2011. UBCH7 reactivity profile reveals parkin and HHARI to be RING/HECT hybrids. Nature 474, 105–108. https://doi.org/10.1038/nature09966

Wertz, I.E., Kusam, S., Lam, C., Okamoto, T., Sandoval, W., Anderson, D.J., Helgason, E., Ernst, J.A., Eby, M., Liu, J., Belmont, L.D., Kaminker, J.S., O'Rourke, K.M., Pujara, K., Kohli, P.B., Johnson, A.R., Chiu, M.L., Lill, J.R., Jackson, P.K., Fairbrother, W.J., Seshagiri, S., Ludlam, M.J.C., Leong, K.G., Dueber, E.C., Maecker, H., Huang, D.C.S., Dixit, V.M., 2011. Sensitivity to antitubulin chemotherapeutics is regulated by MCL1 and FBW7. Nature 471, 110–114. https://doi.org/10.1038/nature09779

Wilkinson, K.D., Urban, M.K., Haas, A.L., 1980. Ubiquitin is the ATP-dependent proteolysis factor I of rabbit reticulocytes. J. Biol. Chem. 255, 7529–7532. https://doi.org/10.1016/S0021-9258(19)43857-X

Willatt, L., Cox, J., Barber, J., Cabanas, E.D., Collins, A., Donnai, D., FitzPatrick, D.R., Maher, E., Martin, H., Parnau, J., Pindar, L., Ramsay, J., Shaw-Smith, C., Sistermans, E.A., Tettenborn, M., Trump, D., de Vries, B.B.A., Walker, K., Raymond, F.L., 2005. 3q29 Microdeletion Syndrome: Clinical and Molecular Characterization of a New Syndrome. Am. J. Hum. Genet. 77, 154–160. https://doi.org/10.1086/431653

Williams, C., van den Berg, M., Sprenger, R.R., Distel, B., 2007. A Conserved Cysteine Is Essential for Pex4p-dependent Ubiquitination of the Peroxisomal Import Receptor Pex5p*. J. Biol. Chem. 282, 22534–22543. https://doi.org/10.1074/jbc.M702038200

Wong, R.W., 2010. Interaction between Rae1 and Cohesin subunit SMC1 is required for proper spindle formation. Cell Cycle 9, 198–200. https://doi.org/10.4161/cc.9.1.10431

Wong, R.W., Blobel, G., 2008. Cohesin subunit SMC1 associates with mitotic microtubules at the spindle pole. Proc. Natl. Acad. Sci. U. S. A. 105, 15441–15445. https://doi.org/10.1073/pnas.0807660105

Wong, R.W., Blobel, G., Coutavas, E., 2006. Rae1 interaction with NuMA is required for bipolar spindle formation. Proc. Natl. Acad. Sci. U. S. A. 103, 19783–19787. https://doi.org/10.1073/pnas.0609582104

Wu, H.-T., Kuo, Y.-C., Hung, J.-J., Huang, C.-H., Chen, W.-Y., Chou, T.-Y., Chen, Y., Chen, Yi-Ju, Chen, Yu-Ju, Cheng, W.-C., Teng, S.-C., Wu, K.-J., 2016. K63-polyubiquitinated HAUSP deubiquitinates HIF-1α and dictates H3K56 acetylation promoting hypoxia-induced tumour progression. Nat. Commun. 7, 13644. https://doi.org/10.1038/ncomms13644

Xia, Z., Webster, A., Du, F., Piatkov, K., Ghislain, M., Varshavsky, A., 2008. Substrate-binding Sites of UBR1, the Ubiquitin Ligase of the N-end Rule Pathway*. J. Biol. Chem. 283, 24011–24028. https://doi.org/10.1074/jbc.M802583200

Xu, M., Zhu, C., Zhao, X., Chen, C., Zhang, H., Yuan, H., Deng, R., Dou, J., Wang, Y., Huang, J., Chen, Q., Jiang, B., Yu, J., 2015. Atypical ubiquitin E3 ligase complex Skp1-Pam-Fbxo45 controls the core epithelial-to-mesenchymal transition-

inducing transcription factors. Oncotarget 6, 979–994. https://doi.org/10.18632/oncotarget.2825

Xu, P., Duong, D.M., Seyfried, N.T., Cheng, D., Xie, Y., Robert, J., Rush, J., Hochstrasser, M., Finley, D., Peng, J., 2009. Quantitative Proteomics Reveals the Function of Unconventional Ubiquitin Chains in Proteasomal Degradation. Cell 137, 133–145. https://doi.org/10.1016/j.cell.2009.01.041

Yan, Y., Wang, X., Chaput, D., Shin, M.-K., Koh, Y., Gan, L., Pieper, A.A., Woo, J.-A.A., Kang, D.E., 2022. X-linked ubiquitin-specific peptidase 11 increases tauopathy vulnerability in women. Cell 185, 3913-3930.e19. https://doi.org/10.1016/j.cell.2022.09.002

Yang, C.-S., Jividen, K., Spencer, A., Dworak, N., Ni, L., Oostdyk, L.T., Chatterjee, M., Kuśmider, B., Reon, B., Parlak, M., Gorbunova, V., Abbas, T., Jeffery, E., Sherman, N.E., Paschal, B.M., 2017. Ubiquitin Modification by the E3 Ligase/ADP-Ribosyltransferase Dtx3L/Parp9. Mol. Cell 66, 503-516.e5. https://doi.org/10.1016/j.molcel.2017.04.028

Zhou, A.S., Tucker, J.B., Scribano, C.M., Lynch, A.R., Carlsen, C.L., Pop-Vicas, S.T., Pattaswamy, S.M., Burkard, M.E., Weaver, B.A., 2023. Diverse microtubule-targeted anticancer agents kill cells by inducing chromosome missegregation on multipolar spindles. PLoS Biol. 21, e3002339. https://doi.org/10.1371/journal.pbio.3002339

Zhou, Z., Luo, A., Shrivastava, I., He, M., Huang, Y., Bahar, I., Liu, Z., Wan, Y., 2016. Regulation of XIAP Turnover Reveals a Role for USP11 in Promotion of Tumorigenesis. EBioMedicine 15, 48–61. https://doi.org/10.1016/j.ebiom.2016.12.014

Zhu, X., Ménard, R., Sulea, T., 2007. High incidence of ubiquitin-like domains in human ubiquitin-specific proteases. Proteins Struct. Funct. Bioinforma. 69, 1–7. https://doi.org/10.1002/prot.21546

8. Appendix

8.1 Abbreviations

aa	Amino acid
A	Alanine
APC/C	Anaphase promoting complex/cyclosome
APF1	ATP-dependent proteolysis factor 1
APS	Ammonium peroxodisulfate
AT3	Ataxin-3
ATP	Adenosine triphosphate
bp	Base pair
BAK	bcl-2 homologues antagonist/killer
BIR	Baculovirus IAP repeat
BSA	Bovine serum albumin
BUB1	Budding uninhibited by benzimidazole 1 protein
C	Cysteine
CDC20	Cell division cycle protein 20 homolog
CDK	Cyclin-dependent kinase
CHAMP1	Chromosome alignment maintaining phosphoprotein 1
CHX	Cycloheximide
CKI	Cyclin-dependent kinase inhibitor
CRC	Colorectal cancer
Cul1/CUL1	Cullin 1
Cys	Cysteine
DBS	Doube-strand break
DLK	Dual leucine zipper-bearing kinase
DMEM	Dulbecco’s Modified Eagle’s Medium
DMSO	Dimethyl sulfoxide
DNA	Deoxyribonucleic acid
Dox	Doxycycline
DTT	Dithiothreitol
DUB	Deubiquitylating enzyme
DUSP	Domain present in ubiquitin-specific protease
EDTA	Ethylenediaminetetraacetic acid

EMT	Epithelial-to-mesenchymal transition
FBS	Fetal bovine serum
FBP	F-Box protein
FBXO45	F-box protein 45
FBXW7α	F-box/Wd repeat-containing protein 7
FKBP5	F506 binding protein 5
FSN-1	F-Box synaptic protein 1
G1	Gap 1 (phase)
G2	Gap 2 (phase)
GFP	Green fluorescent protein
GST	Glutathione S-transferase
HECT	Homologous to the E6-associated protein carboxyl terminus
HIF1α	Hypoxia-inducible-factor 1
HIW	Highwire
HR	Homologous repair
HRP	Horseradish peroxidase
IAP	Inhibitor of apoptosis
IF	Immunofluorescence
IP	Immunoprecipitation
IPTG	Isopropyl β-D-thiogalactopyranoside
K	Lysine
kb	Kilobase
kDa	Kilo-Dalton
LB	Lysogeny broth
LCK	Lymphocyte-specific protein tyrosine kinase
LPS	Lipopolysaccharide
Lys	Lysine
M	Mitotic (phase)
MAD2	Mitotic arrest deficient protein 2
MAD2L2	Mitotic arrest deficient 2 like 2
MBP	Maltose-binding protein
MCC	Mitotic checkpoint complex
MCL-1	Myeloid leukemia 1
MDM2	Murine double minute 2

Met	Methionine
MS	Mass spectrometry
MT	Mitcrotubule
MW	Molecular weight
MYCBP2	MYC-binding protein 2
NEM	N-ethylmaleimide
NuMA	Nuclear mitotic apparatus protein
ns	not significant
OD	Optical density
PAGE	Polyacrylamide gel electrophoresis
PAM	Protein associated with MYC
PAR-4	Prostate apoptosis protein 4
PBS	Phosphate buffered saline
PBS-T	Phosphate buffered saline – tween20
PCR	Polymerase chain reaction
PD	Pull-down
PEI	Polyethylenimine
PEX5	Peroxisomal biogenesis factor 5
PHR	PAM/HIW/RPM-1
PPP1CA	Protein phosphatase 1 catalytic subunit α
PRC1	Polycomb repressive complex 1
PTEN	Phosphatase and tensin homologue depleted
RAE1	Ribonucleic acid export 1
pRB	Retinoblastoma protein
RBR	RING-between-RING
RBX1	RING box protein 1
RCC1	Regulator of chromosome condensation
RCR	RING-Cys-Relay
REV7	Revertibility protein 7
RING	Really interesting new gene
RIP3	Receptor-interacting protein kinase 3
ROS	Reactive oxygen species
RPM-1	Regulator of presynaptic morphology 1
RT	Room temperature

S	DNA-synthesis (phase)
SAC	Spindle assembly checkpoint
Ser	Serine
SCF	SKP1-CUL1-F-Box protein complex
SD	Standard deviation
SDS	Sodium dodecyl sulfate
SDS-PAGE	Sodium dodecyl polyacrylamide gel electrophoresis
SETX	senataxin
siRNA	Small interfering RNA
SKP1	S-phase kinase-associated protein 1
SKP2	S-phase kinase-associated protein 2
SKR-1	SKP1-related protein
SMC1	Structural maintenance of chromosomes 1
SPRYD3	SPRY-domain containing protein 3
T	Threonine
TAE	Tris-acetate-EDTA
TEMED	N,N,N',N'-Tetramethylethylenediamine
hTERT	Human Telomerase reverse transcriptase
TF	Transcription factor
Thr	Threonine
TLCK	1-Chloro-3-tosylamido-7-amino-2-butanon
TPCK	1-Chloro-3-tosylamido7-amino-2-heptanon
β-TrCP	Beta-transducin repeat-containing protein
TRIM	Tripartite motif
U	Unit
UBA	Ubiquitin-associated domain
UBL	Ubiquitin-like domain
USP	Ubiquitin-specific protease
USP7	Ubiquitin-specific protease 7
USP11	Ubiquitin-specific protease 11
UCH	Ubiquitin C-terminal hydrolase
UHX1	Ubiquitin hydrolase on the X chromosome
WB	Western blot
WDR5	WD repeat-containing protein 5

WT	Wild-type
XIAP	X-linked inhibitor of apoptosis

8.2 Figures

Figure 1: Schematic overview of the ubiquitylation cascade. 6
Figure 2: Schematic overview of mitotic cell fates after MT-poison treatment. 15
Figure 3: Schematic overview of MYCBP2-FBXO45 E3 ligase complex and its underlying ubiquitylation mechanism. 18
Figure 4: SPRYD3 is a new interactor of FBXO45. 63
Figure 5: SPRYD3 mediates mitotic slippage in nocodazole or paclitaxel treated U2OS and RPE1 cells. 65
Figure 6: Depletion of SPRYD3 or MYCBP2 in untreated cells does not alter mitotic cell fate or timing. 66
Figure 7: SPRYD3 interacts with and is stabilized by MYCBP2. 68
Figure 8: SPRYD3 interacts with the MYCBP2 MYC-binding domain independently of FBXO45. 69
Figure 9: SPRYD3 binds to MYCBP2 via its SPRY2-domain. 70
Figure 10: SPRYD3 directly interacts with MYCBP2. 72
Figure 11: SPRYD3 and SKP1 do not interact directly. 73
Figure 12: SKP1 does not regulate SPRYD3 protein levels nor mediation of interaction between SPRYD3 and MYCBP2. 74
Figure 13: Complex formation of MYCBP2 with FBXO45 and SPRYD3 75
Figure 14: CHAMP1 and XIAP are new interactors of SPRYD3. 77
Figure 15: Interaction between CHAMP1 and SPRYD3. 78
Figure 16: CHAMP1 and SPRYD3 interact in asynchronous and mitotic cells. 79
Figure 17: The SPRYD3SPRY1-domain mediates interaction with CHAMP1. 80
Figure 18: CHAMP1 protein levels are negatively regulated by SPRYD3. 80
Figure 19: Ectopic expression of SPRYD3 decreases CHAMP1 ubiquitylation levels. 81
Figure 20: SPRYD3 interacts with XIAP in asynchronous and mitotic cells and the interaction is dependent on phosphorylation. 83
Figure 21: SPRYD3 and XIAP interact through the BIR2-BIR3 and SPRY2-domains, respectively. 84
Figure 22: XIAP protein levels are not regulated by SPRYD3. 85

Figure 23: MYCBP2-SPRYD3 overexpression leads to XIAP deubiquitylation. 86
Figure 24: USP11 is a potential interactor of SPRYD3 and FBXO45. 87
Figure 25: USP11 interacts with MYCPB2 and SPRYD3 independently from FBXO45. 88
Figure 26: USP11 promotes mitotic slippage in paclitaxel or nocodazole treated U2OS and RPE1 cells. 89
Figure 27: Depletion of USP11 in cycling cells does not alter mitotic cell fate nor timing. 90
Figure 28: USP11 interacts with the MYCBP2 RCC1-like and MYC-binding domain. 91
Figure 29: Recombinantly purified USP11 and SPRYD3 interact *in vitro*. 92
Figure 30: MYCBP2 ubiquitylates USP11 in the absence of FBXO45.....93
Figure 31: SPRYD3, but not FBXO45, ubiquitylates USP11. 94
Figure 32: MYCBP2 and SPRYD3 ubiquitylate USP11 as a complex. 95
Figure 33: MYCBP2-SPRYD3 ubiquitylates USP11 *in vitro*.....97
Figure 34: MYCBP2 attaches K63-linked Ub-chains to USP11. 98
Figure 35: Ubiquitylation of USP11 is not linked to proteasomal destruction.....99
Figure 36: MYCBP2-SPRYD3 ubiquitylates non-canonical USP11 residues. 102
Figure 37: USP11-, SPRYD3- and MYCBP2-depletion cause multipolar spindle formation in nocodazole-treated RPE1 or U2OS cells. 105
Figure 38: MYCBP2-SPRYD3 mediated ubiquitylation of USP11^{C318} leads to bipolar spindle formation.....108
Figure 39: Ectopic expression of Flag-USP11^{C318S} increases mitotic slippage in MT-poison treated cells. 110
Figure 40: MYCBP2-SPRYD3-mediated ubiquitylation of USP11^{C318} is important for USP11/RAE1 interaction.....112
Figure 41: RAE1 promotes mitotic slippage in nocodazole or paclitaxel treated U2OS and RPE1 cells. 113
Figure 42: MYCBP2-SPRYD3 ubiquitylates USP11^{C318} to promote interaction with and deubiquitylation of RAE1 and consequent bipolar spindle formation and mitotic slippage in response to MT-poisons. 127

8.3 List of Tables

Table 1: Chemicals and reagents 25

Table 2: Laboratory equipment 28
Table 3: Buffers 29
Table 4: Primary antibodies 34
Table 5: Secondary antibodies 35
Table 6: Small interfering RNAs 35
Table 7: Primers 36
Table 8: Provided plasmids 37
Table 9: Plasmids generated during this thesis 38
Table 10: Bacterial strains 40
Table 11: Cell lines 40
Table 12: Kits 41
Table 13: Antibiotics 41

9. Acknowledgements

I would like to express my thanks to Prof. Dr. Ingrid Hoffmann for giving me the opportunity to join her lab and to work on this interesting project.
I would also like to thank Dr. Aurélie Ernst and Prof. Dr. Sebastian Schuck for being part of my thesis advisory committee and for their time, expertise and helpful scientific input. Additionally, I thank Prof. Dr. Sylvia Erhardt for joining my thesis defense examination committee and being the second examiner. I also thank Prof. Dr. Martin Müller and Prof. Dr. Gislene Pereira for joining my thesis defense examination committee.
I want to express my thanks to all of the past lab members of the Hoffmann lab, who provided a nice working environment, as well as giving advice and support: Bettina Dörr, Dr. Simon Hänle-Kreidler, Dr. Vesna Zivanovic, Dr. Kübra Gürkaslar, Dr. Josina Großmann, Claudia Dang, Seher Aksu, Sophia Grossi-Mayer, Jolanta Nickel and Antonia Rost. I am happy to have met you and to have shared nice moments. Special thanks go out to Dr. Kübra Gürkaslar, who supported me mentally and with good counsel throughout the good and especially bad times and stuck with me until the end. Thank you very much, I wish you all the best for your future.
I would like to thank the DKFZ Light Microscope Facility, especially Manuela Brom for introducing me to the system, and the DKFZ Proteomics Facility, especially Dr. Dominic Helm and Dr. Martin Schneider, for their support and expertise.
Special thanks go out to my whole family, especially my mother Antonia, my father Victor and my aunt Lina, for their never-ending support during the good and hard times of this journey, their trust in me and their understanding and love throughout the entire process. Furthermore, I want to thank my friends and my room mates, and especially my partner Hannah for her patience, support and love, as well as encouraging words she provided me with throughout this whole time. I love you.
I could not have succeeded in this without any of the people mentioned here. Thank you.